Technische Universität München

Fakultät Wissenschaftszentrum Weihenstephan für Ernährung, Landnutzung und Umwelt

Lehrstuhl für Systembiologie der Pflanzen

Interaction of *Arabidopsis* AMSH proteins with ESCRT-III and their role in intracellular membrane trafficking

Anthi Katsiarimpa

Vollständiger Abdruck der von der Fakultät Wissenschaftszentrum Weihenstephan für Ernährung, Landnutzung und Umwelt der Technischen Universität München zur Erlangung des akademischen Grades eines

Doktors der Naturwissenschaften

genehmigten Dissertation.

Vorsitzender: Univ.-Prof. Dr. W. Liebl
Prüfer der Dissertation: 1. Univ.-Prof. Dr. C. Schwechheimer
2. Univ.-Prof. Dr. B. Poppenberger-Sieberer
3. Univ.-Prof. Dr. K. Schneitz

Acknowledgements

First I would like to recognize the scientific direction of my PhD supervisor Dr. Erika Isono. I would like to thank her for giving me the opportunity to join her research group of such an interesting project, for her guidance, enthusiasm and encouraging advice throughout this time.

I convey my gratitude to my co-supervisor Prof. Dr. Claus Schwechheimer, who first sponsored me when I was a graduate student and kept encouraging me all the way through my PhD.

I would like to acknowledge my thesis committee members Prof. Dr. Wolfgang Liebl and Prof. Dr. Brigitte Poppenberger.

I would like to express my gratitude to Prof. Dr Marie-Theres Hauser, Dr. Corina Weis, Dr. Maya Ostertag and Prof. Dr. Ralph Hückelhoven, for the material, the data and their work, that contributed to my project.

Many thanks to Dr. Balaji Enugutti and Dr. Prasad Vaddepalli for the regular scientific discussion and help they provided me. I am greatful to all the members of the Departments of Plant Developmental Biology and Botany for their technical support and for sharing devices.

I am thankful to Petra Wick and Rita Kaindl for their support and help in administration matters.

Last, I would like to express my *heartfelt* thanks to each of all, past and present members of our Department, Dr. Isabel Müller, Dr. Björn C. Willige, Dr. Esther M.N. Dohmann, Dr. Melina Zourelidou, Dr. René Richter, Soumya Ghosh, Jana Hakenjos, Carola Nill, Siv Ahlers, Dr. Carina Behringer, Quirin Ranftl, Inês Catarina Barbosa, Julia Mergner, Ulrich Lutz, Benjamin Weller, Emmanouil Bastakis, Ourania Lantzouni, Jutta Elgner,Marie-Kristin Nagel, Cornelia Kolb, Kamila Kalinowska and Franziska Anzenberger, for their support and their help, for encouraging me through this time and for creating such a pleasant working atmosphere. During these years some of them have become real friends, a very special thanks to them, since friends are one of the most precious things in my life.

Anthi

"We especially need imagination in science. It is not all mathematics, nor all logic, but it is somewhat beauty and poetry."

Maria Mitchell

Table of contents

Katsiarimpa et al., 2011

Katsiarimpa and Kalinowska et al., 2013

Lebenslauf

Abstract

Ubiquitination is a post-translational modification that regulates a variety of cellular processes. Ubiquitination can be reversed by the activity of deubiquitinating enzymes (DUBs). While the function of many ubiquitinating enzymes is well understood, the regulation of biological processes by DUBs is not yet well explored. ASSOCIATED MOLECULE WITH THE SH3 DOMAIN OF STAM (AMSH), is a DUB that belongs to the Jab1/Mov34/Mpr1 Pad1 N-terminal+ (MPN+)domain protein family. The *Arabidopsisthaliana* genome encodes three AMSH proteins, named AMSH1, AMSH2 and AMSH3. This study focuses on the functional characterization of *Arabidopsis* AMSH1 and AMSH3, and on elucidating the pathways that are regulated by these enzymes. At the beginning of this study, we had shown that AMSH3 isan active DUB, essential for vacuole biogenesis and plant development (Isono et al., 2010).

This work shows that AMSH3 interacts with two ENDOSOMAL SORTING COMPLEX REQUIRED FOR TRANSPORT (ESCRT)-III core subunits, vacuolar protein sorting (VPS) 2.1 and VPS24.1. Interrupting this interaction leads to accumulation of ubiquitinated conjugates. It is further demonstrated that AMSH3, VPS2.1 and VPS24.1 co-localize in class E compartments when the disassembly of ESRT-III is inhibited. This study provides evidence that AMSH3 is implicated in the ESCRT-III mediated endocytotic pathway.

The DUB activity of AMSH3 and proper endosomal trafficking is likely also a prerequisite in optimal nutrient recycling through the autophagy pathway. Plants expressing the inactive AMSH3 or a dominant negative (DN) form of VPS2.1 display accelerated senescence to artificial carbon starvation, as observed for autophagy deficient mutants.

Besides AMSH3, AMSH1 interacts also with VPS2.1 and *amsh1-1* mutants display enhanced sensitivity to carbon limiting conditions. In *amsh1-1* as well as in plants expressing the DN VPS2.1 the autophagy marker AUTOPHAGIC PROTEIN 8 (ATG8) is accumulated and fewer autophagosomes are observed in the vacuoles, indicating defects in the autophagy pathway.

The findings of this study suggest that efficient deubiquitination activity of AMSH3 and AMSH1 regulates certain steps in endocytosis and autophagy and, moreover, that these two pathways might be linked.

Zusammenfassung

Ubiquitinierungist einepost-translationale Modifikation, die eine Vielzahlvon zellulären Prozessereguliert. Die Ubiquitinierung kanndurch die Aktivität vonDeubiquitinasen (DUBs) rückgängig gemacht werden. Obwohl dieFunktion vielerEnzyme des Ubiquitinierungssystemsausführlich untersuchtworden ist, ist noch wenig über dieRegulierungbiologischer ProzessedurchDUBsbekannt. ASSOCIATED MOLECULE WITH THE SH3 DOMAIN OF STAM (AMSH) ist ein DUB,das zur Familie der Proteine mit einer Jab1/Mov34/Mpr1Pad1N-terminal+ (MPN+) Domäne gehört. DasGenom von *Arabidopsis thaliana*kodiert für dreiAMSHProteine, genannt AMSH1, AMSH2undAMSH3. Diese Studiekonzentriert sich auf diefunktionelle Charakterisierung von*Arabidopsis*AMSH1undAMSH3als auchaufdie Aufklärung derSignalwege, diedurch diese Enzymereguliert werden. Für AMSH3 war von uns gezeigt worden, dass es ein aktivesundessentielles DUB fürdie Biogenese der Vakuole und die Pflanzenentwicklung ist (Isono etal., 2010).

Diese Arbeit zeigt nun, dass AMSH3 mit zwei ENDOSOMAL SORTING COMPLEX REQUIRED FOR TRANSPORT (ESCRT)-III Kern-Untereinheiten, VACUOLE PROTEIN SORTING (VPS) 2.1 und VPS24.1 interagiert. Das Blockieren dieser Interaktion führt zu Akkumulation von ubiquitinierten Konjugaten. Es wird des Weiteren gezeigt, dass AMSH3, VPS2.1 und VPS24.1 in sogenannten Klasse E Kompartimenten kolokalisieren, wenn die Dissoziation des ESCRT-III gehemmt wird. Diese Studie liefertHinweise darauf, dassAMSH3 an der ESCRT-III abhängigen Endozytose beteiligt ist.

Die DUB Aktivität von AMSH3 und der ordnungsgemäße endosomale Transport ist wahrscheinlich eine Voraussetzung für das optimale Recyceln von Kohlenhydraten durch Autophagie. Pflanzen, die ein inaktives AMSH3 oder eine dominant-negative (DN) Form von VPS2.1 exprimieren, zeigen beschleunigte Seneszenz bei künstlichem Kohlenhydratmangel, ähnlich wie es auch bei Autophagiemutanten beobachtet worden war.

Außer AMSH3 interagiert auch AMSH1 mit VPS2.1 und *amsh1-1* Mutanten zeigen eine erhöhte Empfindlichkeit gegenüber Kohlenhydratmangel. Sowohl in *amsh1-1* als auch in Pflanzen, die das DN VPS2.1 exprimieren, akkumuliert der Autophagiemarker AUTOPHAGIC PROTEIN 8 (ATG8) und in der Vakuole können weniger Autophagosomen beobachtet werden, was auf Defekte in der Autophagie

hinweist.

Die Ergebnisse dieser Studie deuten darauf hin, dass die effiziente DUB-Aktivität von AMSH3 und AMSH1 bestimmte Schritte in der Endozytose und der Autophagie reguliert und darüberhinaus, dass diese beiden Wege miteinander verbunden sein könnten.

List of Figures

List of Tables

List of Abbreviations

2,4-D	2,4-Dichlorophenoxyacetic acid
AAA	ATPase Associated with various cellular activities
AGO1	ARGONAUTE 1
Amp	ampicillin
AMSH	ASSOCIATEDMOLECULE WITH THE SH3 DOMAIN OF STAM
APS	ammonium peroxydisulphate
ATG	AUTOPHAGIC PROTEIN
ATP	adenosine triphosphate
AUX1	AUXIN-RESISTANT 1
Bar	bialaphos resistance
BOR1	HIGH BORON REQUIRING 1
BRCC36	BRCA1-BRCA2-CONTAINING COMPLEX SUBUNIT 36
BRO1	BCK1-LIKE RESISTANCE TO OSMOTIC SHOCK
CaR	CALCIUM SENSING RECEPTOR
CBB	Coomassie Brilliant Blue
cDNA	complementaryDNA
CHC	CLATHRIN HEAVY CHAIN
CHMP	CHROMATIN MODIFYING PROTEINS/ CHARGED MULTIVESICULAR BODY PROTEIN
Co-IP	Co-immunoprecipitation assay
COP9	CONSTITUTIVE PHOTOMORPHOGENESIS 9
CSN5	COP9 SIGNALOSOME SUBUNIT 5
Cyt b5	Cytochrome b5
dATP	desoxy-adenosine triphosphate
dCTP	desoxy-cytidine triphosphate
dGTP	desoxy-guanosine triphosphate
DMF	N,N-dimethylformamid
DMSO	dimethyl sulfoxide
dNTPs	desoxy-ribonucleoside triphosphate
DTT	dithiothreitol
dTTP	desoxy-thymidine triphosphate
DUBs	deubiquitinating enzymes
EGFR	EPIDERMAL GROWTH FACTOR RECEPTOR
EHD2	EH-DOMAIN-CONTAINING PROTEIN
ELC	ELCH
ESCRT	ENDOSOMAL SORTING COMPLEX REQUIRED FOR TRANSPORT
FAT10	HUMAN LEUKOCYTE ANTIGEN F-ASSOCIATED
FUB1	FAUUBIQUITIN-LIKE PROTEIN

FYVE	Fab-1, YGL023, Vps27, and EEA1
GAD	GAL4 DNA activation domain
GAT	GGA and Tom1
GBD	GAL4 DNA binding domain
GFP	green fluorescent protein
GLUE	pleckstrin homology GRAM-like ubiquitin-binding in EAP45
GM	growth medium
GST	glutathioneS-transferase
HA	hemagglutinin
HECT	homologous to the E6AP carboxyl terminus
His	histidine
HRP	horseradish peroxidase
HRS	HGF-REGULATED TYROSINE KINASE SUBSTRATE
HSE1	HEAT SHOCK ELEMENT 1
Hyg	hygromycine B
ILV	intralumenal vesicles
IPTG	isopropyl β-D-1-thiogalactopyranoside
IRT1	IRON-REGULATED TRANSPORTER 1
ISG15	INTERFERON-STIMULATED GENE-15
IST1	*INCREASED SODIUM TOLERANCE 1*
JOSD1	JOSEPHIN DOMAIN-CONTAINING PROTEIN 1
K	lysine
Kan	kanamycin
KcA3.1	CA^{2+}-ACTIVATED K^+ CHANNEL
L	leucine
LC3	MICROTUBULE-ASSOCIATED PROTEIN 1 LIGHT CHAIN 3
L*er*	Landsberg *erecta*
Leu	leucine
MDC	monodansylcadaverine
MES	2-(N-morpholino)ethanesulfonic acid
Met1	methionine 1
MIM1	MIT interacting motif 1
MIT	microtubule interacting and trafficking domain
MJDs	MACHADO-JOSEPH DISEASE PROTEIN DOMAIN PROTEASES
MPN+/JAM	Jab1/Mov34/Mpr1 Pad1 N-terminal+
MPND	MPN DOMAIN-CONTAINING PROTEIN
mRNA	messengerRNA
MS	Murashige & Skoog medium
MUB	MEMBRANE-ANCHORED UBL
MVB12	MULTIVESICULAR BODY SORTING FACTOR OF 12kDa
MVB	multivesicular body
MYSM1	Myb-like, SWIRM and MPN domain 1

NBR1	NEIGHBOR OF BRCA1 GENE1
NEDD8	NEURONAL-PRECURSOR-CELL-EXPRESSED DEVELOPMENTALLY DOWNREGULATED PROTEIN-8
NF-κB	nuclear factor kappa-light-chain-enhancer of activated B cells
NLS	nuclear localization signal
OTU	OVARIAN TUMOR PROTEASE
PAGE	polyacrylamide gel electrophoresis
PCR	polymerase chain reaction
PEG4000	polyethylene glykol 4000
PI3P	phospatetidylinositol 3-phosphate
PIN2	PIN-FORMED 2
POH1	26S PROTEASOME-ASSOCIATED PAD1 HOMOLOGUE 1
pps	protoplasts
PRPF8	PRE-MRNA-PROCESSING SPLICING FACTOR 8
PTA	pTA7002
RFP	red fluorescent protein
RING	REALLY INTERESTING NEW GENE
RPN11	REGULATORY PARTICLE NON-ATPASE 11
Sal1	supernumerary aleurone layers 1
SD	synthetic complete drop-out
SDS	sodium dodecyl sulfate
SH3	SRC-HOMOLOGY DOMAIN-3
SKD1	SUPPRESSOR OF K+ TRANSPORT GROWTH FACTOR 1
SNARE	N-ETHYLMALEIMIDE-SENSITIVE FUSION (NSF) ATTACHMENT PROTEIN RECEPTOR
SNF7	SUCROSE NON-FERMENTING 7
sqRT-PCR	semiquantitative real time-PCR
STAM	SIGNAL TRANSDUCING ADAPTOR MOLECULE
SUMO	SMALL UBIQUITIN-LIKE MODIFIER
T-DNA	transferDNA
TEMED	tetramethylethylenediamine
TGN	*trans*-Golgi network
Trp	tryptophane
TSG101	TUMOR SUSCEPTIBILITY GENE 101
Ub	ubiquitin
UBD	ubiquitin binding domain
UBL5	UBIQUITIN-LIKE PROTEIN-5
UBL	UBIQUITIN-LIKE PROTEIN
UBPY	UBIQUITIN-SPECIFIC PROTEASE Y
UBQ	UBIQUITIN
UCH	UBIQUITIN C-TERMINAL HYDROLASE
UEV	E2 variant domain

UFM1	UBIQUITIN FOLD-MODIFIER-1
URM1	UBIQUITIN-RELATED MODIFIER-1
USP	UBIQUITIN-SPECIFIC PROTEASE
VAMP8	VESICLE-ASSOCIATED MEMBRANE PROTEIN 8
VCL1	VACUOLESS1
VPS	VACUOLAR PROTEIN SORTING
VTA1	VESICLE AMINE TRANSPORT 1
W	tryptophane
WT	wild type
X-Gal	5-Bromo-4-chloro-3-indolyl β-D galactopyranoside
Y2H	yeast two-hybrid
YFP	yellow fluorescent protein

1. Introduction

1.1 Ubiquitin system

1.1.1 Ubiquitination and deubiquitination

Ubiquitin is a small modifier protein that consists of 76 amino acids and that is highly conserved in all eukaryotes. Post-translational modification of proteins by ubiquitin is referred to as ubiquitination. Ubiquitination is a fundamental mechanism for regulating protein function and stability and serves as a signal for many cellular processes. Although the best-characterized function of ubiquitination is in the context of targeting substrates for degradation by the 26S proteasome (reviewed in (Hershko and Ciechanover, 1998)), ubiquitination has also been linked to cell cycle, chromatin regulation, apoptosis, intracellular trafficking, cell signaling, autophagy, transcription, translation and DNA damage response (reviewed in (Husnjak and Dikic, 2012; Komander and Rape, 2012)). The covalent attachment of ubiquitin to proteins is mediated by a cascade of three diverse classes of enzymes called E1, E2 and E3 (Figure 1). E1, an ubiquitin activating enzyme, starts the process of ubiquitination. E1 binds to ubiquitin in an ATP-dependent process and then passes ubiquitin to E2. E2 is an ubiquitin conjugating enzyme that transfers ubiquitin to E3, an ubiquitin ligase. E3 recognizes the substrates and transfers ubiquitin to the substrates by mediating the formation of an isopeptide bond between a lysine residue of the protein substrate and the carboxyl group of the carboxyl terminal glycine of ubiquitin. Proteins may be ubiquitinated on a single or several lysines resulting in mono or multiubiquitination.

Two families of E3 ligases have been characterized until now according to their catalytic domain. One family contains a homologous to the E6-ASSOCIATED PROTEIN (E6AP) carboxyl terminus (HECT) domain and the other a really interesting new gene (RING) finger or a U-box domain (reviewed in (Hershko and Ciechanover, 1998; Komander, 2009)). HECT and RING E3 ligases promote ubiquitination of substrates using different mechanisms. HECT E3 ligases accept first ubiquitin from an E2 and then catalyzes the transfer to the substrate, while the RING finger and U-box E3 ligases bring the E2 enzyme and the substrate to a close proximity to promote substrate ubiquitination.

Ubiquitin contains seven lysines (K6, K11, K27, K29, K33, K48 and K63) that can be subjected to formation of a bond with another ubiquitin molecule. Therefore a ubiquitin molecule bound to a substrate serves as an acceptor for the attachment of another ubiquitin molecule during sequential rounds of ubiquitination, resulting in the formation of polyubiquitin chains. Besides the lysines, the amino terminal methionine 1 (Met1) of ubiquitin can also form a peptide bond with the carboxyl terminal glycine of another ubiquitin. According to which residue is used for the linkages, distinct chain types are formed (reviewed in (Ikeda and Dikic, 2008; Komander, 2009; Komander and Rape, 2012)). Structural analysis of five ubiquitin chains until now, has revealed that Met1 or K63 linkages result in an open (linear) chain conformation, while K48, K6 and K11 to more compact chains (reviewed in (Kulathu and Komander, 2012)).

The different chain types regulate the destiny of the substrates for different pathways. In yeast and mammals, K48- and K11-linked chains, the most abundant in the cells, mediate the degradation of the proteins by the proteasome (Thrower et al., 2000; Xu et al., 2009). K63-linked chains serve as a signal for endocytosis of plasma membrane proteins and are implicated in cell signalling and in the recruitment of DNA repair enzymes (reviewed in (Herrmann et al., 2007; Kerscher et al., 2006)). Met1 chains are associated with activation of nuclear factor kappa-light-chain-enhancer of activated B cells (NF-κB), a protein complex controlling DNA transcription (Iwai et al., 2009). The role of K6, K27, K29 and K33-linked chains is poorly understood until now.

For the formation of polyubiquitin chains another family of enzymes has been characterized in yeast and mammals to be involved, the E4 family (Koegl et al., 1999). E4 is a ubiquitination factor, that drives in combination with E1, E2 and E3 the formation of long ubiquitin chains, which cannot be formed only by the action of E3 ligases.

The versatility of the ubiquitin pathway is determined by the combination of E2 and E3 enzymes. The human genome encodes two E1s, at least 38 E2s and over 600 E3s (reviewed in (Ye and Rape, 2009)). The yeast genome encodes one E1, 11 E2s and up to 100 E3s (reviewed in (Finley et al., 2012)). The thousands of E2-E3 enzyme combinations, that can be formed, may specify the chain type assembled on the substrates and thus determine the destiny of the proteins. Although the mechanisms underlying chain specificity is not fully understood, it has been

demonstrated that several E2 enzymes assemble polyubiquitin chains with linkage specificity (reviewed in (Kulathu and Komander, 2012)). Employment of certain E2 enzymes results in the assembly of only K11, or K48 or K63 polyubiquitin chains. E3 enzymes are in charge of recognizing the substrates and determine also the specificity of ubiquitination. The existence of hundreds of different E3 ligases reflects the diversity of the ubiquitin system. While the specificity of ubiquitin chain formation by RING E3 ligases may depend on the E2 enzyme, HECT mediated chain assembly is independent of the E2 encoded linkage specificity. Some HECT E3 enzymes exclusively assemble certain linkages (reviewed in (Kulathu and Komander, 2012)).

Ubiquitin interaction domains present in the substrates can also determine the specificity of their ubiquitination. Ubiquitin binding domains (UBD) are interaction modules with different ubiquitin binding properties (Hurley et al., 2006; Rahighi and Dikic, 2012). To date, almost 20 different families of UBDs are characterizedwith structurally and functionally diverse properties (Rahighi and Dikic, 2012). Although a class of UBDs is shown to bind to polyubiquitin chains without linkage specificity, there are domains exhibiting specificity based on chain linkage pattern (Hurley et al., 2006; Rahighi and Dikic, 2012).

A number of distinct ubiquitin-like proteins (UBLs) have been discovered to function as protein modifiers as well. 20 UBLs have been discovered until now (reviewed in (van der Veen and Ploegh, 2012)) and new members are still being added. Known UBLs include SMALL UBIQUITIN-LIKE MODIFIER (SUMO), INTERFERON-STIMULATED GENE-15 (ISG15), UBIQUITIN-RELATED MODIFIER-1 (URM1), NEURONAL-PRECURSOR-CELL-EXPRESSED DEVELOPMENTALLY DOWNREGULATED PROTEIN-8 (NEDD8), HUMAN LEUKOCYTE ANTIGEN F-ASSOCIATED (FAT10), AUTOPHAGY PROTEIN 8 (ATG8), ATG12, FAU UBIQUITIN-LIKE PROTEIN (FUB1), MEMBRANE-ANCHORED UBL (MUB),UBIQUITIN FOLD-MODIFIER-1 (UFM1) and UBIQUITIN-LIKE PROTEIN-5 (UBL5). Although ubiquitin and UBLs do not share high sequence similarity, they share canonical ubiquitin fold structure and a carboxyl terminal glycine, for the formation of an isopeptide bond with a lysine of the substrates. UBLs are attached to proteins via an ubiquitin like pathway, employing E1, E2 and E3 enzymes or like enzymes. UBLs are involved in distinct cellular pathways including transcription, DNA repair, signal transduction, cell-cycle control and autophagy (reviewed in (Kerscher et al., 2006)).
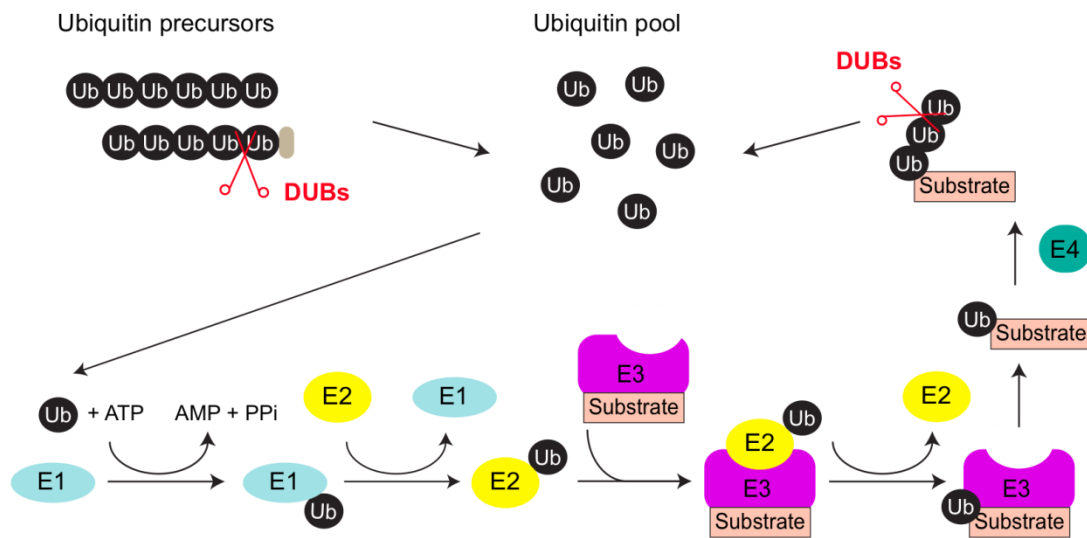
Figure 1: Ubiquitination and deubiquitination.
Ubiquitin (Ub) precursor molecules consisting of several ubiquitin copies or fused to ribosomal proteins are hydrolyzed by deubiquitinating enzymes (DUBs) to monomers. An ubiquitin molecule is activated by an E1 activating enzyme, in an ATP dependent manner and transferred to an E2 conjugating enzyme. Finally an E3 ligase mediates the transfer of ubiquitin from E2 to a lysine of the target protein by forming an isopeptide bond. The substrate can further be ubiquitinated on different lysine residues, resulting in multiubiquitination or on a lysine of the first attached ubiquitin resulting in the assembly of a polyubiquitin chain. E4s, ubiquitin factors, are implicated in the formation of polyubiquitin chains. Ubiquitination can be reversed by DUBs, that hydrolyzes the isopeptide bonds and release the ubiquitin molecules.

Protein ubiquitination events are counter regulated by the activity of a family of isopeptidases, called deubiquitinating enzymes (DUBs). DUBs are proteases that reverse ubiquitination of proteins by counteracting the action of E3 ligases. They hydrolyze the isopeptide bond between the carboxyl terminus of ubiquitin and the lysine of the substrate. The hydrolysis of the isopeptide bonds results in breaking down the ubiquitin chains and releasing the ubiquitin molecules from protein targets (reviewed in (Amerik and Hochstrasser, 2004)) (Figure 1).

Certain DUBs are also in charge of generating free ubiquitin molecules from precursor molecules (Komander, 2010). Ubiquitin genes code either for polyubiquitin precursor proteins or ubiquitin fused to ribosomal proteins (Kimura and Tanaka, 2010) (Figure 1). Single ubiquitin molecules have to be cleaved off from the precursor molecules by DUBs, in order to be recognized by E1s. DUBs are responsible for the maintenance of free ubiquitin pool within the cell, by recycling ubiquitin molecules from substrates. that follow the degradation pathway. DUBs activities include the removal of ubiquitin from proteins, to rescue them from

proteasomal or lysosomal degradation or to influence cell signaling events (Komander, 2009).

Coordinated action of E3 ubiquitin ligases and DUBs enables the regulation of ubiquitin signaling events. DUBs are in this way implicated in cell-cycle, DNA repair, cytokine signaling, apoptosis, endocytosis, regulation of transcription and RNA processing as well as other cellular pathways (Clague et al., 2012). Therefore, it is likely that dysfunction of DUBs may result in cellular phenotypes and pathologies (Komander, 2010; Wilkinson, 2009). Mutational studies of certain DUBs leads to imbalance of protein levels and hence to diseases. DUBs are linked to the development of cancer, since they are responsible for the regulation of NF-kB, the tumor suppressor A20 and other proteins associated to cancer (Komander, 2010; Wilkinson, 2009). Moreover, several mutated DUBs cause inflammation, defects in immune response and neurological disorders (Komander, 2010; Wilkinson, 2009).

The human genome encodes around 100 DUBs. All eukaryotic DUBs are divided into five distinct subfamilies according to their catalytic domain (Nijman et al., 2005; Reyes-Turcu et al., 2009). Four families, the ubiquitin C-terminal hydrolases (UCHs), the ubiquitin-specific proteases (USPs), the Machado-Joseph disease protein domain proteases (MJDs) and the ovarian tumor proteases (OTUs), consist of papain-like cysteine proteases. The last family, the Jab1/Mov34/Mpr1 Pad1 N-terminal+ (MPN+/JAMM) domain family, contains metalloproteases. Cysteine DUBs use catalytic diads or triads of amino acids to catalyze the hydrolysis of the ubiquitin isopeptide bonds. The cysteine residue performs a nucleophilic attack to the bond (Komander, 2010). Metalloproteases coordinate zinc ions to activate water molecules to attack the bonds (Komander, 2010).

DUBs subscribe to the specificity of the ubiquitin system by displaying selectivity for both ubiquitin chain types and substrates. These enzymes have to deal with ubiquitin chains of diverse linkages and lengths. Although limited, structural analysis has shown that certain DUBs, like the OTU enzymes ,display linkage specificity, while USP enzymes do not (Mevissen et al., 2013). There are DUBs hydrolyzing only K63 or K48 linked chains (Rahighi and Dikic, 2012). The catalytic domain as well as UBDs in certain DUBs serve as recognition sites, contributing to their specificity of binding and hydrolyzing specific ubiquitin chains. Specificity of DUBs is also determined by direct affinity to the ubiquitinated protein. Moreover, interaction proteins or adaptor subunits can recruit DUBs to certain substrates.

1.1.2 Ubiquitin system and endocytosis

One of the cellular pathways that are regulated by the ubiquitin system is endocytosis. Endocytosis refers to the biological process, by which cells internalize proteins from the plasma membrane and recycle them back or sort them for degradation by the lysosome/vacuole (Figure 2A). Vacuole in yeast and plant cells is equivalent to lysosome in mammalian cells. In the endocytosis pathway rounds of ubiquitination and deubiquitination events control the homeostasis of plasma membrane receptors.

The endocytosis pathway has mostly been studied in yeast and mammals (Figure 2A). Endocytosis starts with ubiquitination of plasma membrane receptors mediated by an E3 ubiquitin ligase. Monoubiquitination or K63 polyubiquitination triggers endocytosis of marked proteins (reviewed in (Haglund and Dikic, 2012)). It was first shown in yeast that Ste2p, a pheromone G coupled protein receptor, is internalized upon monoubiquitination (Schandel and Jenness, 1994). Many other plasma membrane poteins are shown to be endocytosed upon monoubiquitination (reviewed in (Haglund et al., 2003)). K63 linked polyubiquitin chains target plasma membrane proteins for endocytosis. A number of tyrosine kinase receptors are internalized upon attachment of K63 polyubiquitin chains (Geetha et al., 2005; Haglund and Dikic, 2012; Mosesson et al., 2003).

Ubiquitinated plasma membrane receptors are incorporated into clathrin coated vesicles, internalized from the plasma membrane by inward budding of plasma membrane vesicles (cargos) and sorted on early endosomes. Endosomes are intracellular sorting organelles, playing an important role in the endocytosis of plasma membrane proteins. From early endosomes the proteins can either be recycled back to the plasma membrane or can be retained to the endosomal membrane and selected for lysosomal degradation. When not recycled, the cargos are transported from early to late endosomes. Multiple sorting events on late endosomes initiate the invagination of them into intralumenal vesicles (ILV) to form mature endosomes, the so-called multivesicular bodies (MVBs). MVBs fuse with the lysosome, release the content and the receptors are degraded by lysosomal peptidases (reviewed in (Piper and Katzmann, 2007)).

DUBs are also employed in the endocytosis pathway and regulate the rates of ubiquitinated receptor endocytosis (Figure 2A). DUBs are recruited to the endosomal
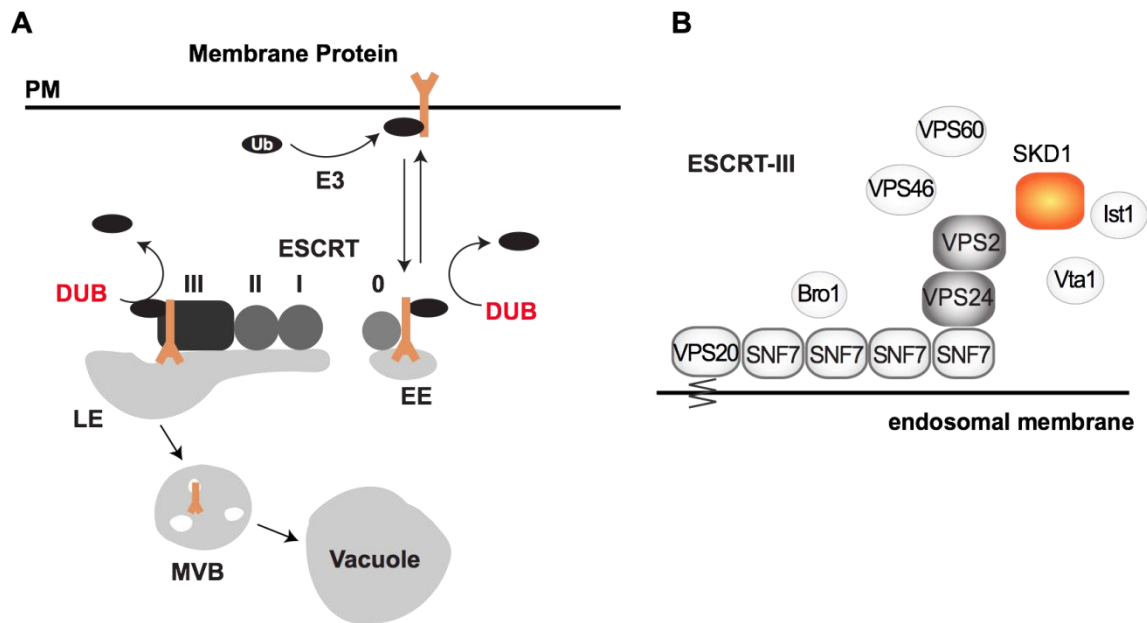
Figure 2: Model of endosomal sorting pathway.
A) Plasma membrane receptors are ubiquitinated by an E3 ligase, internalized and transported to early endosomes (EE) through interaction with ESCRT-0. From here they can recycle back to the membrane or further sorted for degradation. The receptors are recruited by the ESCRT machinery (I, II, III) and invaginated into intraluminal vesicles of late endosomes (LE) to form multivesicular bodies (MVBs). MVBs fuse with the vacuole and their content is degraded by vacuolar peptidases. DUBs can act in this pathway by deubiquitinating the receptors either at early endosomes to contribute to their recycling or at late endosomes for Ub recycling.
B) Formation of ESCRT-III. ESCRT-III subunit SNF7 binds to the membrane bound VPS20 and oligomerizes. SNF7 oligomerization is terminated by VPS24 and VPS2. VPS2 together with VPS46, VPS60 and Ist1 recruit SKD1 and its cofactor VTA1. BRO1 interacts with SNF7 and is implicated in the membrane scission events for MVB biogenesis.

system through interaction with different components of the system and act at different levels. In yeast the deubiquitinating enzyme Doa4p (Papa and Hochstrasser, 1993) acts at the level of late endosomes, where the receptors are already committed to their degradation pathway, and contributes to the recycling of ubiquitin molecules (Swaminathan et al., 1999). Doa4p has also been shown to have additional roles linked to the proteasome (Papa et al., 1999). Deletion of Doa4p causes loss of cell viability due to the reduced levels of free ubiquitin pool within the cell, indicating the important role of deubiquitination during endocytosis (Swaminathan et al., 1999). Moreover, in *doa4Δ* defects in the proteolysis of both proteasomal and vacuolar substrates are demonstrated. The best-characterized DUBs in mammalian cells employed in endocytosis are UBIQUITIN-SPECIFIC PROTEASE Y (UBPY)(Kato et al., 2000), the closest human homologue to Doa4p, and ASSOCIATED MOLECULE WITH THE SH3 DOMAIN OF STAM (AMSH)

(Tanaka et al., 1999). These DUBs are recruited on early and late endosomes via interaction with components of the endocytosis pathway that compromise the ESCRT machinery (Kato et al., 2000; Tanaka et al., 1999). Deubiquitination at the level of early endosomes regulates recycling events of endocytosed receptors back to the plasma membrane, controlling their homeostasis (McCullough et al., 2004). Despite AMSH and UBPY another DUB, JOSEPHIN DOMAIN-CONTAINING PROTEIN 1 (JOSD1), was recently shown *in vitro* to be implicated in endocytosis (Seki et al., 2013). However, the exact role *in vivo* is not elucidated yet.

Besides the deubiquitination of plasma membrane proteins, DUBs may deubiquitinate members of the pathway. Endocytosis components are also ubiquitinated (Shields et al., 2011). It has been shown in yeast that deubiquitination of receptors or components of the pathway is essential for sorting events into MVBs (Nikko and Andre, 2007). Deletion of UBPY results in accumulation of receptors on endosomes, blocks the degradation of cargos by the lysosome and increases the number and size of MVBs (Row et al., 2006). Moreover, there have been studies revealing the importance of deubiquitination for proper transport to the lysosome. For example, a plasma membrane protein, Ca^{2+}-ACTIVATED K^+ CHANNEL (KcA3.1), follows the endocytosis pathway upon polyubiquitination (Balut et al., 2011). However, the transport to the vacuole is not completed when it is not deubiquitinated by UBPY (Balut et al., 2011).

Further studies have to reveal other DUBs that are implicated in endocytosis. Elucidating the exact function and role of these enzymes will help to understand the mechanism, with which the ubiquitin system controls the rates of protein degradation by the lysosome and cell signalling via endocytosis.

1.2 ESCRT machinery

Protein endosomal sorting and MVB formation require the ESCRT machinery, a class of well-conserved proteins, called the class E VACUOLAR PROTEIN SORTING (VPS) proteins. They were first indentified in the yeast *Saccharomyces cerevisiae* by observing yeast mutants defective in sorting a soluble vacuolar protein to the vacuole
(Piper et al., 1995; Raymond et al., 1992; Rieder et al., 1996). Class E *vps* mutants accumulate endocytosed receptors in abnormal late endosomal structures, named

class E compartments (Babst et al., 1997; Raymond et al., 1992; Rieder et al., 1996).The class E Vps counterparts in animal cells are called CHROMATIN MODIFYING PROTEINS/CHARGED MULTIVESICULAR BODY PROTEINS (CHMPs). These Vps/CHMP proteins are recruited from the cytoplasm to endosomes and are assembled into four heteromeric endosomal sorting complexes required for transport (ESCRT), named ESCRT-0, ESCRT-I, ESCRT-II and ESCRT-III, that compose the ESCRT machinery (Figure 2A). Ubiquitinated receptors are recognized by subunits of ESCRT-0 and together with the subsequent action of ESCRT-I and ESCRT-II are sorted on the endosomal membrane. The receptors are then interacting with ESCRT-III, sorted into MVBs and in the end degraded in the lysosome/vacuole. Many ESCRT members contain UBDs, which provide affinity to ubiquitinated substrates (Alam et al., 2004; Katzmann et al., 2001; Piper and Katzmann, 2007). While ESCRT-0, -I and –II serve to recognize and target the internalized receptors to endosomal mebranes, ESCRT-III is implicated in MVB biogenesis. Members of the ESCRT machinery are working as scaffold proteins for the recruitment of deubiquitinating enzymes in the endocytosis pathway.

Although the ESCRT machinery was first identified to mediate the endosomal sorting of plasma membrane proteins, involvement of the machinery in cytokinesis, viral budding and autophagy has also been described (reviewed in (Henne et al., 2011; Roxrud et al., 2010)).

1.2.1 ESCRT-0

The ESCRT-dependent MVB pathway for membrane protein degradation is employed by ESCRT-0. ESCRT-0 consists of two proteins VPS27/HGF-REGULATED TYROSINE KINASE SUBSTRATE (HRS) and HEAT SHOCK ELEMENT 1 (HSE1)/SIGNAL TRANSDUCING ADAPTOR MOLECULE (STAM) (Asao et al., 1997; Bache et al., 2003; Prag et al., 2007). VPS27/HRS interacts with HSE1/STAM via coiled-coil GGA and Tom1 (GAT) domains forming a heterodimer. ESCRT-0 localizes to early endosomes via binding of HRS to phospatidylinositol 3-phosphate (PI3P) of early endosomes through its Fab-1, YGL023, Vps27, and EEA1 (FYVE) lipid-binding domain. Both subunits of the complex contain UBD and are therefore able to bind ubiquitin moieties attached to internalized membrane proteins. Concentration of ubiquitinated cargos on endosomes is additionally supported by the

interaction of HRS with clathrin, through its clathrin binding box. The ability to bind PI3P, ubiquitin and clathrin enables ESCRT-0 to initiate endocytosis by sorting the proteins on early endosomes. Finally, ESCRT-0 is responsible for recruitment of ESCRT-I on endosomes.

1.2.2 ESCRT-I

ESCRT-I is a hetero-tetrameric complex constisting of VPS23/TUMOR SUSCEPTIBILITY GENE 101 (TSG101), VPS28, VPS37 (Katzmann et al., 2001) and MULTIVESICULAR BODY SORTING FACTOR of 12kDa (MVB12) (Shields et al., 2009). ESCRT-I is located to endosomes through interaction of Vps23 with HRS and with ubiquitinated cargos via an E2 variant domain (UEV) (Katzmann et al., 2003). Anchoring of ESCRT-I to endosomes is orientated also by transient interaction of VPS23 with PI3P. MVB12 contains also an UBD domain and is able of binding ubiquitinated cargos (Shields et al., 2009). At the opposite end of the complex VPS28 binds to ESCRT-II.

1.2.3 ESCRT-II

ESCRT-II is a hetero-tetrameric complex composed of VPS36/ELL-ASSOCIATED PROTEIN (EAP) 45, VPS22/EAP22 and two copies of VP25/EAP20 (Babst et al., 2002; Hierro et al., 2004). VPS36 contains a pleckstin homology GRAM-Like Ubiquitin-binding in EAP45 (GLUE) domain, which interacts with VPS28 of ESCRT-I. This GLUE domain connects ESCRT-II to PI3P of endosomes and provides binding affinity to ubiqutin. Targeting to endosomes is enriched by the lipid domain of VPS22, interacting with PI3P of the membrane (Hurley, 2008; Im and Hurley, 2008). VPS25 interacts with ESCRT-III and initiates the assembly of the complex.

1.2.4 ESCRT-III

ESCRT-III is the last complex of the ESCRT machinery and responsible for the proper internalization of ubiquitinated proteins into MVBs and for MVB biogenesis. VPS proteins compromising ESCRT-III are playing a role in membrane budding and

scission events. ESCRT-III consists of four core subunits VPS20/CHMP6, SUCROSE NON-FERMENTING 7 (SNF7)/VPS32/CHMP4, VPS24/CHMP3 and VPS2/CHMP2 (Figure 2B). The subunits are present in a closed autoinhibitory state in the cytoplasm. Studies in yeast have shown that ESCRT-III is assembled in a highly ordered manner (Teis et al., 2008). Vps20p is recruited through interaction with ESCRT-II to the limiting membrane of endosomes and induces the oligomerization of Snf7p. The oligomerization is terminated upon capping of Snf7p filaments by Vps24p. Vps24p interacts with the last core subunit Vps2p. After the complete assembly of ESCRT-III, Vps4p, an AAA-ATPase, is recruited to the complex. The activity of Vps4p induces the disassembly of Vps polymers from the endosomal membrane allowing the reuse of the subunits (Saksena et al., 2009). Disassembly of ESCRT-III is required for proper endosomal sorting of ubiquitinated receptors and the formation of MVBs. In yeast, when the ATP hydrolysis activity of Vps4p is disrupted, either by deletion or expression of an enzymatic inactive variant of Vps4p (Vps4^{EQ}p), ESCRT-III subunits accumulate on endosomes, MVB formation is defective and receptor endocytosis is inhibited (Babst et al., 1997). These defects cause the formation of aberrant endosomal compartments, named class E compartments (Babst et al., 1997). Except for the core proteins, accessory proteins VPS46/CHMP1 (Nickerson et al., 2006), Vps60/CHMP5 (Yeo et al., 2003), I*NCREASED SODIUM TOLERANCE 1* (IST1) (Scott et al., 2005), VESICLE AMINE TRANSPORT 1(VTA1) (Azmi et al., 2006) and BCK1-LIKERESISTANCETOOSMOTIC SHOCK (BRO1) (Wemmer et al., 2011) participate in recruitment and activation of VPS4 and disassembly of the complex (Figure 2B).

1.3 Ubiquitin system and endocytosis in plants

The ubiquitin system is highly conserved from mammals to plants. However, it appears to be more diversified in plants compared to other organisms. Approximately 6% of the *Arabidopsis* proteins are suspected to have functions related to the ubiquitin system (reviewed in (Downes and Vierstra, 2005; Wang and Deng, 2011)). The *Arabidopsis* genome contains 16 ubiquitin–coding genes, two E1s, at least 37 E2s and more than 1500 E3s. The unusual large number of E3s reveals the complexity of the ubiquitin system in plants. For the deubiquitination enzymes, there are 70 genes identified until now (reviewed in (Vierstra, 2012)). The best-

characterized aspect of ubiquitination in plants, as well as in all eukaryotes, lies in context of protein degradation via the 26S proteasome. The ubiquitin proteasome system affects nearly every aspect of plant growth and development, including cell-cycle, embryogenesis, senescence, defense, environmental responses and hormone signaling (reviewed in (Vierstra, 2009)). Besides the function of ubiquitin in the proteasomal degradation system, several reports indicate that ubiquitin serves as a signal to mediate endocytosis and endosomal trafficking also in plants.

Studies in plants regarding the endosomal sorting pathway and the proteins involved are limited compared to yeast and mammals. A number of plasma membrane proteins in plants are shown to be endocytosed upon ubiquitination. Mono- or diubiquitnation of a boron transporter, *HIGH BORON REQUIRING 1*(BOR1), is required for vacuolar degradation via endocytosis (Kasai et al., 2011). Monoubiquitination of IRON-REGULATED TRANSPORTER 1 (IRT1) triggers its endocytosis (Barberon et al., 2011). For PIN-FORMED 2 (PIN2), an auxin efflux carrier, it was shown that K63-polyubiquitination is required for sorting from early endosomes to the vacuole (Leitner et al., 2012). Characterization of these plasma membrane receptors has shown that in plants endocytosis plays an important role in boron uptake, in iron homeoastasis, in the regulation of auxin transport and overall in embryo differentiation and development.

Although plants share the same basic molecular mechanism for the sorting of plasma membrane receptors to the vacuole with yeast and mammals, they have developed molecular and structural specializations, which are connected with plant specific functions (reviewed in (Otegui and Spitzer, 2008)). With the exception of ESCRT-0, homologues for all major counterparts of the endosomal pathway in yeast and mammals have been identified also in plants. In addition, plants contain some specific homologues (Leung et al., 2008; Richardson et al., 2011; Richardson and Mullen, 2011; Spitzer et al., 2006; Winter and Hauser, 2006). Constituent proteins of the ESCRT complexes in yeast, mammals and *Arabidopsis* are listed with equivalent nomenclature in Table 1. Plant genome encodes proteins, which interact with ESCRT-I and ubiquitin moieties and might thereby contribute in early sorting events of endocytosis and substitute the role of ESCRT-0 (Wang et al., 2010; Winter and Hauser, 2006). Interaction networks seem also to be conserved (Haas et al., 2007; Ibl et al., 2012; Richardson et al., 2011; Shahriari et al., 2010; Spitzer et al., 2009; Spitzer et al., 2006).

Table 1: ESCRT-III subunits in yeast, mammals and *Arabidopsis thaliana*

Subomplex	Yeast	Mammals	Arabidopsis
Core Complex	Vps20p	CHMP6	VPS20.1 VPS20.2 VPS2.3
	Snf7p/Vps32p	CHMP4A CHMP4B CHMP4C	SNF7.1 SNF7.2
	Vps24p	CHMP3	VPS24.1 VPS24.2
	Vps2p	CHMP2A CHMP2B	VPS2.1 VPS2.2 VPS2.3
Accessory proteins	Vps4p	VPS4A VPS4B	SKD1
	Vps60p	CHMP5	VPS60.1 VPS60.2
	Vps46p/Did2p	CHMP1A CHMP1B	CHMP1A/VPS46.1 CHMP1B/VPS46.2
	Bro1p/Vps31p	ALIX/AIP1	BRO1
	Vta1p	VTA1/LIP5	VTA1
	Ist1p	IST1	

The nomenclature of yeast (*Saccharomyces cerevisiae*), mammalian (human) and plant (*Arabidopsis thaliana*) ESCRT-III and ESCRT-III associated proteins is based on those previously published (Leung et al., 2008; Richardson et al., 2011; Richardson and Mullen, 2011; Spitzer et al., 2006; Winter and Hauser, 2006).

Overall, few of the plant endosomal components have been functionally characterized until now. Studies in *Arabidopsis thaliana* have shown that ELCH (ELC)/VPS23, an ESCRT-I subunit, interacts with ubiquitin and other *Arabidopsis* homologues of ESCRT-I, it localizes to endosomes and *elc* mutants exhibit cytokinesis

defects (Spitzer et al., 2006). Knockout of ESCRT-III accessory proteinsCMHP1A and CHMP1B, causes in *Arabidopsis* plants inhibition of endocytosis (Spitzer et al., 2009). In *chmp1a/chmp1b* mutants proteins involved in auxin transport, AUXIN-RESISTANT1 (AUX1) and PIN2, auxin influx and efflux carrier, respectively, are not properly endocytosed. As a result no proper auxin gradients are established and *chmp1a/chmp1b* mutants are compromised in embryo development (Spitzer et al., 2009). Characterization of the plant homologue of yeast Vps4p, AtSKD1, revealed that an inactive version of the ATPase leads in *Arabidopsis* to accumulation of class E compartments, enlarged MVBs, inhibition of vacuolar trafficking, defects in cytokinesis and formation of fragmented vacuoles (Haas et al., 2007; Shahriari et al., 2010). CHMP1 homologues in *Zea mays*, SUPERNUMERARY ALEURONE LAYERS 1 (SAL1)(Shen et al., 2003), as well as in *Nicotiana benthamiana*(Yang et al., 2004), have been shown to play a role in endocytosis. In rice functional characterization of the VPS22, an ESCRT-II component, revealed that the knockout mutant shows seedling lethality and impaired the grain appearance (Zhang et al., 2013). SKD1 from the halophyte ice plant *Mesembryanthemum crystallinum* was also shown to be involved in intracellular trafficking (Jou et al., 2006).

Structural differences between plant and yeast or mammal endosomal system have been observed (Otegui and Spitzer, 2008). Although MVBs have been observed in plants (Tanchak and Fowke, 1987; Tse et al., 2004), the tubulo-vesicular early endosomes, as known from yeast or mammals are not present in plant cells (reviewed in (Otegui and Spitzer, 2008)). Different studies have shown that the trans-Golgi network (TGN) or TGN derivatives are acting as early endosomes (Dettmer et al., 2006; Otegui and Spitzer, 2008; Viotti et al., 2010). Differences in the plant endocytotic system may represent the higher complexity in the organization and trafficking events of the endosomal system (reviewed in (Otegui and Spitzer, 2008; Robinson et al., 2008)).

Further analysis of plant ESCRT components is required to understand the dynamics of the endocytosis pathway in plants. Endocytosis and endosomal trafficking are of paramount importance for key cellular processes. Understanding of the coordinated action of the ESCRT complexes will provide information for the regulation of different developmental aspects of plants.

1.4 Autophagy

Autophagy is another major catabolic process in eukaryotic cells for the degradation of intracellular debris, such as cytoplasmic protein aggregates, large macromolecular complexes and damaged organelles, through the lysosomal/vacuolar machinery (reviewed in (Bassham, 2009; Klionsky and Ohsumi, 1999; Mizushima, 2007; Thompson and Vierstra, 2005)). Autophagy is induced under nutrient starvation conditions and allows the clearance of unneeded proteins in order to recycle and reuse their amino acids. Cells perform an internal quality control and degrade the damaged proteins or organelles through autophagy. Moreover, autophagy acts as an immune mechanism, since it is linked with the elimination of intracellular pathogens. Thus autophagy is important for regulating cellular homeostasis and survival. In mammalian cells dysfunction of this pathway is linked to pathological conditions, such as neurodegeneration and cancer (reviewed in (Levine and Kroemer, 2008; Xie and Klionsky, 2007)).

Two main mechanisms have been characterized in this pathway, micro and macroautophagy (Figure 3A). In microautophagy cytoplasmic material is engulfed by the vacuolar membrane. The material is invaginated and a so-called autophagic body is formed and released in the inner vacuolar lumen and degraded. The resulting macromolecules are released in the cytosol and reused. In macroautophagy, the major autophagic pathway*referred to as autophagy* hereafter, cytoplasmic components are engulfed into cup-shaped membranes, which expand, surround the cytoplasmic components and fuse together to form a double membrane vesicle, called autophagosome. The outer membrane of autophagosomes fuses with the vacuolar membrane, releasing an inner membrane structure, called autophagic body, into the vacuolar lumen for degradation by vacuolar proteases (reviewed in (Bassham, 2007; Thompson and Vierstra, 2005; Yoshimoto et al., 2004)).

Studies in yeast have revealed a group of over 30 autophagic proteins (Atg) involved in the autophagy pathway (reviewed in (Klionsky and Emr, 2000; Ohsumi, 2001; Suzuki and Ohsumi, 2007)). These proteins are participating in two ubiquitin-like conjugation systems, including two main ubiquitin fold proteins ATG8 and ATG12 (Figure 3B). ATG8 has to be first processed to the mature form by ATG4, a DUB. An E1 enzyme, ATG7, associates in an ATP-dependent mechanism to the mature form of ATG8 and ATG12. From ATG7 they are transferred to E2 conjugating enzymes
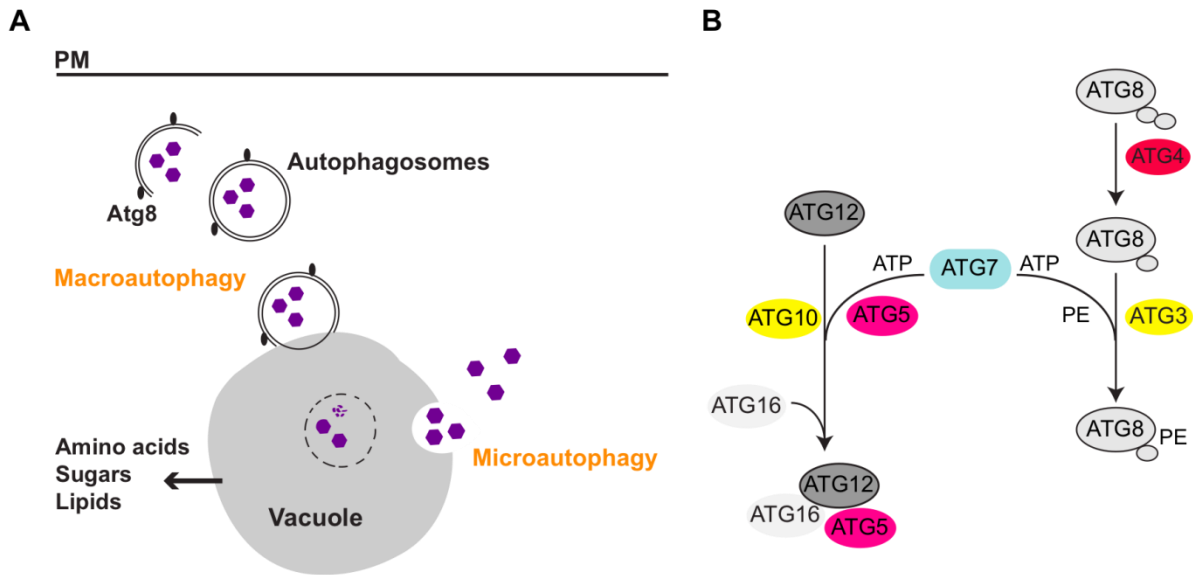
Figure 3: Morphological and biochemical steps during macro- and microautophagy.
A) In macroautophagy cytoplasmic components are sequestered into double membrane structures, the autophagosomes. Autophagosomes fuse with the vacuole and release an autophagic body. In microautophagy, cytoplasmic components are engulfed directly by the vacuolar membrane. An autophagic body is formed and released within the vacuole. The bodies are degraded by hydrolases and simple compounds are recycled to the cytosol.
B) Two ATP dependent Ub-like conjugation systems employ ATG8 and ATG12 for autophagosome formation. ATG8 and ATG12 are activated by ATG7 and are then associated with the conjugating enzymes ATG3 and ATG10, respectively. ATG8 has to be processed prior to activation by the protease ATG4. ATG3 and ATG10 mediate the conjugation of ATG8 and ATG12 to PE and ATG5, respectively. ATG16 binds to ATG12-ATG5 and participates in the incorporation of AT8-PE into autophagosomes.

ATG3 and ATG10, respectively, which in turn transfer them to their targets the lipid phospatidylethanolamine (PE) and ATG5, respectively. The ATG12-ATG5 adduct associates with ATG16 to promote the formation of an ATG8-PE adduct. Both adducts play a role in the formation of autophagosomes, and especially ATG8-PE is incorporated in the membranes of autophagosomes.

Plants contain an orthologous autophagic system to the yeast. The *Arabidopsis* genome encodes one gene for *ATG7*, *ATG3*, *ATG10* and *ATG5*, two genes for *ATG4* and *ATG12* and nine for *ATG8* (Doelling et al., 2002; Hanaoka et al., 2002; Phillips et al., 2008; Suttangkakul et al., 2011). In plants autophagy is essential for survival under nutrient limiting conditions, since it is responsible for recycling nitrogen and carbon from internal supplies. During leaf senescence and developmental programmed cell death, autophagy is activated to encourage nutrient remobilization (Doelling et al., 2002; Ishida and Yoshimoto, 2008; Thompson and Vierstra, 2005). Moreover, autophagy promotes survival during pathogen invasion, by participating in the regulation of programmed cell death during hypersensitive response to pathogen infection (Hofius et al., 2009; Lenz et al., 2011; Liu et al., 2005; Yoshimoto et al.,

2009). It is also involved in degradation of oxidized proteins during oxidative stress (Xiong et al., 2007a; Xiong et al., 2007b). Besides the activation under stress conditions, autophagy is also initiated during normal growth conditions and contributes to the degradation of protein aggregates and damaged or misfolded proteins or organelles (Inoue et al., 2006; Xiong et al., 2007a).

Arabidopsis mutants affected in *ATG* genes, such as *atg7-1*(Doelling et al., 2002), *atg9*(Hanaoka et al., 2002), *atg4a4b-1*(Yoshimoto et al., 2004), *atg5*(Thompson et al., 2005), undergo a normal lifecycle under favourable growth conditions, but cause developmental defects. These mutants show reduced growth under short day conditions and are hypersensitive to nitrogen and carbon starvation conditions. Autophagy deficient plants exhibit early senescence indicating that these plants try to sustain pools of free amino acids in the absence of autophagy by upregulating other proteolytic routes. Moreover, programmed cell death is enhanced in these mutants (Phillips et al., 2008).

Autophagy was initially thought to be a non-selective bulk degradation pathway. However, accumulating evidence demonstrates a selective mechanism for autophagic degradation (reviewed in (Xie and Klionsky, 2007)). In selective autophagy ATG8 is acting as an autophagic receptor, that is able to interact with adaptor molecules, that function as scaffolding proteins to connect the cargos targeted for degradation with the autophagic machinery (reviewed in (Behrends and Fulda, 2012)). It has been shown that posttranslational modifications of proteins play a role in selective autophagy (reviewed in (Behreds and Fulda, 2012). Ubiquitination targets proteins not only for degradation by the proteasome but also by autophagy (reviewed in (Elsasser et al., 2005; Kirkin et al., 2009c; Shaid et al., 2013)). Ubiquitinated protein aggregates are recognized by ubiquitin binding adaptors, are coupled to autophagosomes and designated for degradation by the lysosome/vacuole. The best-characterized proteins in mammals that function as adaptors for docking ubiquitinated molecules to autophagosomes are p62 and neighbor of BRCA1 gene1 (NBR1) (Kirkin et al., 2009a; Kirkin et al., 2009b; Lamark et al., 2009; Waters et al., 2009). Their ability to bind ubiquitinated molecules and to interact with ATG8 provides the link for the selective lysosomal degradation of cytoplasmic components via autophagy. The adaptors themselves are also autophagic substrates and are degraded in the lysosome (Kirkin et al., 2009b; Lamark et al., 2009).

Studies in *Arabidopsis* about selective autophagy demonstrate that the *Arabidopsis* homologue of mammalian NBR1, AtNBR1, acts as a functional hybrid adaptor molecule for autophagy of mammalian NBR1 and p62 (Svenning et al., 2011; Zhou et al., 2013). The same was true for the NBR1 homologue in tobacco (Zientara-Rytter et al., 2011). AtNBR1 targets ubiquitinated protein aggregates for autophagic clearance (Zhou et al., 2013). Like in mammals, AtNBR1 interacts with ATG8 homologues and is transported through autophagosomes to the vacuole, where it is degraded (Svenning et al., 2011). In the same study, it was shown that in the autophagy deficient mutant *atg7* instead of the transport of AtNBR1 to the vacuole, AtNBR1 accumulated in the cytosol as aggregates, supporting the fact that degradation of NBR1 is mediated via autophagosomes (Svenning et al., 2011).

Selective autophagy has been demonstrated in plant cells for cytochrome b5 (Cyt b5) (Toyooka et al., 2006). When Cyt b5 is aggregating, it is preferentially selected for degradation by autophagosomes (Toyooka et al., 2006). A stromal portion of chloroplasts has been also demonstrated in *Arabidopsis* to be selectively degraded through autophagy (Ishida and Yoshimoto, 2008). Moreover, selective autophagy is linked in plants to the trafficking of anthocyanin to the vacuole (Pourcel et al., 2010). A novel example of ubiquitinated proteins designated for autophagic degradation in plants is ARGONAUTE 1 (AGO1), a component of the RNA-induced silencing complex (Derrien et al., 2012).

Taken together, autophagy is an important pathway, especially during nutrient limiting conditions, but also under favourable conditions, mediating the degradation of certain proteins. However, the understanding of the mechanistic basis for the important roles of plant autophagy in different biological processes is very limited. Moreover, the importance of selective autophagy for plant cell homeostasis is currently unknown.

1.5 AMSH proteins

AMSH is a DUB, that has been shown to be implicated in endocytosis and is suggested to have also a role in autophagy in mammalian as well as in plant cells. AMSH belongs to the MPN+/JAMM domain protein family (McCullough et al., 2004). The family consists of BRCA1-BRCA2-containing complex subunit 36 (BRCC36), COP9 SIGNALOSOME SUBUNIT 5 (CSN5), 26S PROTEASOME-ASSOCIATED

PAD1 HOMOLOGUE 1 (POH1), MPN DOMAIN-CONTAINING PROTEIN (MPND), Myb-like, SWIRM and MPN domains 1 (MYSM1), PRE-MRNA-PROCESSING SPLICING FACTOR 8 (PRPF8), AMSH and AMSH-LP (reviewed in (Kommander et al., 2009). POH1, also known as REGULATORY PARTICLE NON-ATPASE 11 (RPN11) in yeast, was one of the first characterized members of this family (Verma et al., 2002). RPN11, is a subunit of the 26S proteasome and cleaves ubiquitin from proteasome substrates, as they are processed by the proteasome. The deubiquitination activity of the enzymes compromising this family depends on the MPN+ domain, which resides at the carboxyl terminus (Figure 4A). The proteolytic activity of the enzymes depends on two conserved histidine residues and an asparagine residue, which together coordinate a zinc ion. It has been shown that substitution of these residues leads to inactivity (Gusmaroli et al., 2004; Verma et al., 2002).

Among the members of the family AMSH is unique, since it possesses measurable proteolytic activity as a monomer (McCullough et al., 2004), while the others have to be incorporated in a large multiprotein complex, to which they belong, to display deubiquitination activity. AMSH was first identified in mammalian cells as an adaptor molecule of the SH3 domain of STAM, an ESCRT-0 subunit, while screening a cDNA library from human cells for clones interacting with SH3 using far-Western analysis (Tanaka et al., 1999). The human AMSH, HsAMSH, has the ability to hydrolyze specifically K63- linked ubiquitin chains (McCullough et al., 2004) and the catalytic activity is enhanced in the presence of its binding partner STAM (Kim et al., 2006).

It has been shown that HsAMSH additionally interacts with CLATHRIN HEAVY CHAIN (CHC) through the clathrin binding site (CBS) (McCullough et al., 2006; Nakamura et al., 2006) and with a range of CHMPs of the ESCRT-III complex: CHMP1A, CHMP1B, CHMP2A, and CHMP3 (Agromayor and Martin-Serrano, 2006; Kyuuma et al., 2007; McCullough et al., 2006; Row et al., 2007; Tsang et al., 2006), CHMP4B (Tsang et al., 2006), and IST1 (Agromayor et al., 2009) through the microtubule interacting and trafficking domain (MIT). The human AMSH is located on early endosomes, due to the interaction with CHC (Nakamura et al., 2006) and in the nucleus due to the nuclear localization signal (NLS) (Kikuchi et al., 2003).

The deubiquitination activity towards the K63-linked ubiquitin chains and the interaction with clathrin and several ESCRT components suggest a role of HsAMSH in the endocytosis pathway. It has been proposed that HsAMSH can function in the

early steps of endocytosis, due to the interaction with clathrin and ESCRT-0 or in the later stages due to interaction with ESCRT-III subunits (Clague and Urbe, 2006). It has been shown that deubiquitination of internalized plasma membrane receptors, like the EPIDERMAL GROWTH FACTOR RECEPTOR (EGFR) (McCullough et al., 2004) or the CALCIUM SENSING RECEPTOR (CaR) (Reyes-Ibarra et al., 2007), is required for the proper delivery and degradation of the receptors in the vacuole through the endocytosis pathway.

HsAMSH is also required in cytokinesis, where the function of proteins like VESICLE-ASSOCIATED MEMBRANE PROTEIN 8 (VAMP8), an NSF ATTACHMENT PROTEIN RECEPTORS (SNARE), responsible for vesicle fusion events, requires rounds of ubiquitination and deubiquitination (Mukai et al., 2008). The required activity of AMSH on endosomes or at the central spindle regions is mediated through the interaction with ESCRT proteins. It has been proved that not only the enzymatic activity of AMSH but also the binding capability to its interactors is required for clearance of ubiquitinated receptors (Kyuuma et al., 2007). Moreover, studies have shown that HsAMSH regulates the ubiquitination status of ESCRT-0 components, like its interacting partner STAM, which in turn can influence the ESCRT function (McCullough et al., 2006; Sierra et al., 2010).

The significance of the proper function of AMSH has been shown in mice, since AMSH deficient mice die as a consequence of postnatal growth retardation (Ishii et

MIT: Microtubule Interacting and Transport domain
NLS: Nuclear Localizing Signal
CBS: Clathrin Binding Site
SBM: Stam Binding Motif
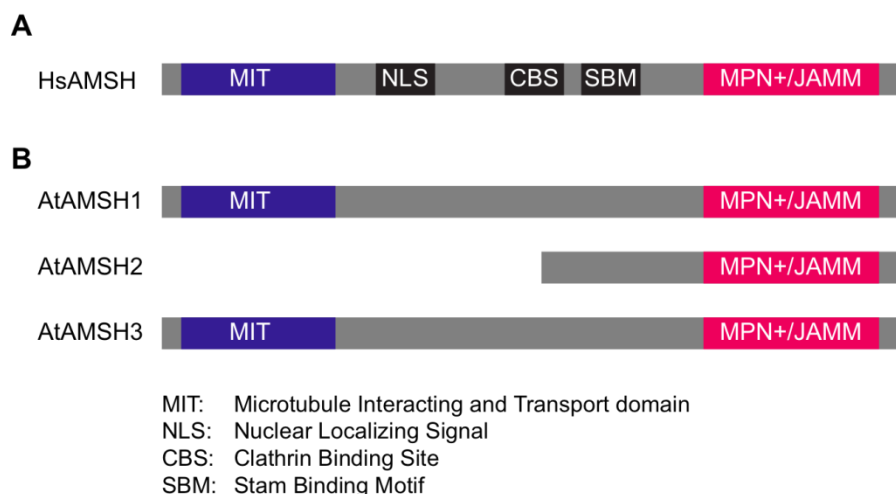
Figure 4: Schematic representation of Human and *Arabidopsis* AMSH proteins.
A) Linear domain diagram of human AMSH. A MPN+/JAMM domain resides in the carboxyl terminus and a MIT domain at the amino terminus. The protein contains also an NLS, a CHC and SBM domain.
B) Linear domain diagram of *Arabidopsis* AMSH1, AMSH2 and AMSH3. All three proteins posses a MPN+/JAMM domain at the C-terminus. AMSH1 and AMSH3 contain also a MIT domain at their amino-terminal part.

al., 2001). However, it is not known how AMSH deficiency results in neuronal damage in brain causing death. Despite the accumulation of ubiquitinated proteins in the absence of AMSH, the autophagic substrate p62 is also accumulated, indicating the requirement of AMSH in the clearance of aggregates via autophagy (Suzuki et al., 2011).

The *Arabidopsis* genome encodes three homologous proteins to the human AMSH (Figure 4B). These proteins are designated as AMSH1, AMSH2 and AMSH3 and show high homology within the catalytic MPN+ domain (Isono et al., 2010). Except AMSH2, which has a shorter amino-terminal part, AMSH1 and AMSH3 possess also a MIT domain at the amino terminus, which is responsible for protein-protein interaction. In contrast to the human AMSH, no other functional domains in the sequence of the *Arabidopsis* AMSH proteins have been characterized yet (Figure 4B).

Arabidopsis AMSH3 is shown to be an active deubiquitinating enzyme(Isono et al., 2010) (Figure 5). In contrast to the human AMSH, it can hydrolyze both K48- and K63- linked ubiquitin chains (Isono et al., 2010) (Figure 5A). Further analysis showed that *Arabidopsisamsh3* null mutants arrest growth at seedling stage and accumulate high amount of ubiquitinated proteins (Isono et al., 2010) (Figure 5B). The same phenotype was observed when an inactive version of AMSH3, AMSH3(AXA) was expressed in plants (Isono et al., 2010). Substitution of the conserved histidine residues to alanine in the catalytic MPN+ domain of AMSH3, named AMSH3(AXA), leads to inactivity *in vitro* (Isono et al., 2010). Moreover, in *amsh3* the formation of the central vacuole is impaired (Isono et al., 2010) (Figure 6A). Interestingly, autophagosomes as well the autophagic marker ATG8 are accumulating in the cells of these mutants (Isono et al., 2010) (Figure 6B). In addition, different trafficking pathways were impaired. The trafficking of protein storage vacuole cargo

Figure 5: *Arabidopsis* AMSH3 is an essential deubiquitinating enzyme (Isono et al., 2010).
A) Phenotypes of 7 days old *amsh3-1* mutants in comparison to wild type (Col-0) of the same age.
B) Immunoblot analysis of total protein extract from seedlings shown in (A) using anti-Ubiquitin and anti-AMSH3 antibod. CDC2 is used as loading control.

SP:GFP:CT24 from the Golgi apparatus to the vacuole and the endocytosis of PIN2 are inhibited (Figure 6B,C) (Isono et al., 2010).

Taken together, AMSH3 is a major deubiquitinating enzyme playing a vital role for plant growth. The proper function of AMSH3 is required in endocytosis and might be also implicated in autophagy. However, the exact function and the regulation of AMSH3 dependent mechanisms in endocytosis and autophagy as well as in vacuole biogenesis had not been characterized. The identification of AMSH3 substrates and interaction proteins is necessary to determine how AMSH3 deubiquitination activity contributes to plant endosomal sorting pathway and autophagy, in order to understand why it is essential for plant development.
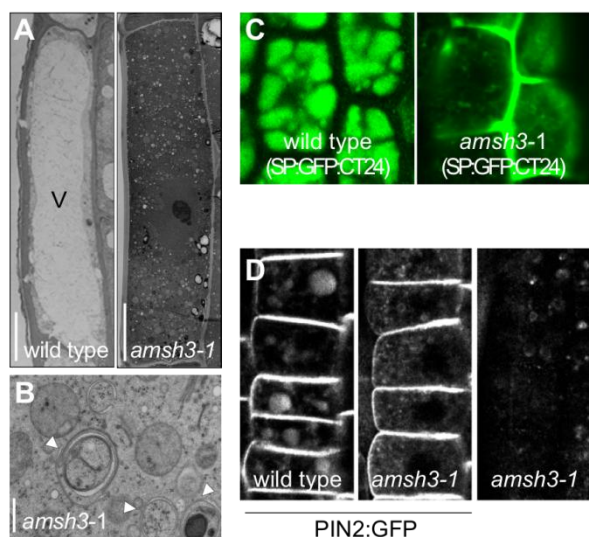
Figure 6: The *amsh3-1* mutant lacks a central vacuole, accumulates autophagosomes and is defective in transport of a model vacuolar cargo and of the plasma membrane protein PIN2 (Isono et al., 2010).
A) and **B)** TEM micrographs of root epidermal cells of wild type and *amsh3-1* seedlings. (A) V, vacuole. Scale bars: 5 µm (wild type), 10 µM (*amsh3-1*). (B) Arrowheads indicate autophagosomes in *amsh3-1*. Scale bar: 0.5 µM.
C) and **D)** Confocal microscopy images of wild type and *amsh3-1* of SP:GFP:CT24 in walking stick-stage embryos (C) and of PIN2-GFP in seedlings after dark treatment (D).

1.6 Aims and objectives of the project

As there was accumulating evidence for the implication of deubiquitination in the plant vacuolar degradation pathways, the primary aim of this study was to gain knowledge about the potential role of the *Arabidopsis* DUBs AMSH3 and AMSH1 in the endosomal trafficking and autophagic pathways. To gain functional data of AMSH3`s role in autophagy, physiological assays were performed with AMSH3(AXA) expressing *Arabidopsis* plants (Isono et al., 2010).

One of the objectives was to identify interactors of AMSH3, implicated in endocytosis and autophagy, using a yeast two-hybrid screen. Elucidating the domains, that are responsible for the interaction using yeast two-hybrid and biochemical assays, provided information about the mechanism of interaction. The overall objective wass to verify these interactions *in vivo* and investigate the biological significance of the interaction. The subcellular localization of these interactors and their co-localization with AMSH3 was observed using fluorescently tagged proteins. Through the generation and characterization of transgenic plants that contain an AMSH3 variant lacking the interaction domains the importance of these interactions was further validated.

This study also aimed to characterize knockout mutants of the interactors. The analysis of proteins known to be degraded in the vacuole through the endosomal or autophagy pathway provided information about the putative defects of these mutants in endocytosis or autophagy.

The role of deubiquitination in endocytosis and autophagy was further assessed in this work by resolving the functional role of the DUB AMSH1. Therefore, AMSH1 was tested for interaction with endosomal components that interacted with AMSH3. Along with these interaction studies, analysis of AMSH1 loss-of-function mutants was required to inspect whether and at which step the two catabolic pathways were affected by the dysfunction of AMSH1.

2. Materials and Methods

2.1 Materials

2.1.1 Chemicals

Table 2: Chemicals used in this study.

Name	Supplier
2,4-Dichlorophenoxyacetic acid (2,4-D)	Sigma-Aldrich, Munich
3-Amino-1,2,4-triazole	Sigma-Aldrich, Munich
5-Bromo-4-chloro-3-indolyl β-D galactopyranoside (X-Gal)	Applichem, Darmstadt
Acetic acid	Roth, Karlsruhe
Acrylamid Rotiphorese Gel 30 (37, 5:1)	Roth, Karlsruhe
Agar, bacteriological	Applichem, Darmstadt
Agarose	Peqlab Biotechnologie, Erlangen
Ammonium nitrate	Applichem, Darmstadt
Ammonium peroxydisulphate (APS)	Roth, Karlsruhe
Ammonium sulfate	Applichem, Darmstadt
Ampicillin	Roth, Karlsruhe
Basta	Meyer, Langenau
Boric acid	Roth, Karlsruhe
Bromophenol blue	Roth, Karlsruhe
Calcium chloride	Applichem, Darmstadt
Calcium hypochloride	Roth, Karlsruhe
Calcium phosphate dibasic	Roth, Karlsruhe
Cellulase "ONOZUKA" R-10	Yacult Pharmaceutical Ind. Co., LTD, Japan
Chloramphenicol	Roth, Karlsruhe
Chloroform	Roth, Karlsruhe
Coomassie Brilliant Blew R-250	Applichem, Darmstadt
Copper(II) sulfate-5-hydrate	Applichem, Darmstadt
D-Mannitol	Applichem, Darmstadt
D(+)-Xylose	Roth, Karlsruhe
Dansylcadaverine	Sigma-Aldrich, Munich
Desoxyribonucleoside triphosphate (dNTPs)	Fermentas, St. Leon-Rot
Dexamethasone (DEX)	Sigma-Aldrich, Munich

Dinatrium hydrogen phosphate	Roth, Karlsruhe
Dimethyl sulfoxide (DMSO)	Roth, Karlsruhe
Disodium phosphate (dihydrate)	Applichem, Darmstadt
Dithiothreitol (DTT)	Sigma-Aldrich, Munich
E64-d	Santa-Cruz, Heidelberg
Ethanol	Roth, Karlsruhe
Ethanolamine	Sigma-Aldrich, Munich
Ethidium bromide	Roth, Karlsruhe
Ethylene diamine tetraacetic acid	Applichem, Darmstadt
FM4-64	Invitrogen, Darmstadt
Formaldehyde	Roth, Karlsruhe
Gentamycin sulfate	Duchefa, Haarlem, Netherlands
Glycerol	Applichem, Darmstadt
Glycine	Applichem, Darmstadt
Glucose	Applichem, Darmstadt
Hydrochloric acid	Sigma-Aldrich, Munich
Hygromycine B	Sigma-Aldrich, Munich
Imidazole	Roth, Karlsruhe
Isopropanol (2-Propanol, IPA)	Roth, Karlsruhe
Isopropyl β-D-1-thiogalactopyranoside (IPTG)	Applichem, Darmstadt
Kanamycine	Applichem, Darmstadt
L-Glutathione	Sigma-Aldrich, Munich
L-Histidine	Sigma-Aldrich, Munich
L-Leucine	Sigma-Aldrich, Munich
L-Tryptophan	Sigma-Aldrich, Munich
Lithium acetate	Roth, Karlsruhe
Macerozyme R-10	Yacult Pharmaceutical Ind. Co., LTD, Japan
Magnesium sulfate	Applichem, Darmstadt
Magnesium chloride	Applichem, Darmstadt
MES monohydrate	Roth, Karlsruhe
Methanol	Roth, Karlsruhe
Murashige & Skoog Medium	Duchefa, Haarlem, Netherlands
Myo-Inositol	Applichem, Darmstadt
Monosodium phosphate (monohydrate)	Applichem, Darmstadt
N,N-Dimethylformamid (DMF)	Roth, Karlsruhe
Polyethylene glykol 4000 (PEG4000)	Applichem, Darmstadt
Phenol	Roth, Karlsruhe

Phosphinothricine (PPT)	Duchefa, Haarlem, Netherlands
Plant agar	Duchefa, Haarlem, Netherlands
Potassium acetate	Roth, Karlsruhe
Potassium chloride	Applichem, Darmstadt
Potassium hydrogen phosphate	Applichem, Darmstadt
Potassium hydroxide	Applichem, Darmstadt
Potassium iodide	Roth, Karlsruhe
Potassium nitrate	Applichem, Darmstadt
Powdered milk	Applichem, Darmstadt
Rifampicine	Duchefa, Haarlem, Netherlands
Salmon sperm DNA	Sigma-Aldrich, Munich
Sodium carbonate	Roth, Karlsruhe
Sodium chloride	Roth, Karlsruhe
Sodium dodecyl sulfate (SDS)	Applichem, Darmstadt
Sodium phosphate	Roth, Karlsruhe
Silwet L-77	Roth, Karlsruhe
Spectinomycine	Duchefa, Haarlem, Netherlands
Tetramethyl ethylene diamine (TEMED)	Roth, Karlsruhe
Tetracycline	Duchefa, Haarlem, Netherlands
Thiamine (Vit B1)	Duchefa, Haarlem, Netherlands
Tris	Applichem, Darmstadt
Triton X100	Applichem, Darmstadt
Trypton/Pepton	Applichem, Darmstadt
Tween 20	Applichem, Darmstadt
Uracil	Sigma-Aldrich, Munich
Yeast extract	Roth, Karlsruhe
Yeast nitrogen base with amino acids	Sigma-Aldrich, Munich
Yeast nitrogen base without amino acids	Sigma-Aldrich, Munich
Yeast Synthetic drop-out medium (-Leu,- Trp, -Ura)	Sigma-Aldrich, Munich
Yeast Synthetic drop-out medium (-Leu, -Trp)	Sigma-Aldrich, Munich
Zinc sulfate (Heptahydrate)	Roth, Karlsruhe
β-Mercaptoethanol	Roth, Karlsruhe

2.1.2 Other materials and enzymes

Table 3: Materials and enzymes used in this study.

Name	Supplier
Benchmark Protein Ladder	Invitrogen, Darmstadt
Bio-Rad Protein Assay	Bio Rad Laboratories, Munich
BP Clonase II Enzyme Mix	Invitrogen, Darmstadt
Complete EDTA free inhibitor cocktail	Roche, Mannheim
Cre Recombinase	New England Biolabs, Frankfuhrt
Expand High Fidelity PCR System	Roche, Mannheim
GeneRuler 1 kb DNA ladder	Fermentas, St. Leon-Rot
Glutathione Sepharose 4B	GE Healthcare, Munich
Hi-Trap Protein A HP	GE Healthcare, Munich
Hi-Trap Protein G HP	GE Healthcare, Munich
Hi-Trap activated HP	GE Healthcare, Munich
Klenow polymerase	Fermentas, St. Leon-Rot
LR Clonase II Enzyme Mix	Invitrogen, Darmstadt
M-MulV Reverse Transcriptase	Fermentas, St. Leon-Rot
Ni Sepharose High Performance	GE Healthcare, Munich
NucleoSpin RNA Plant Kit	Macherey-Nagel, Düren
PageRuler Plus Prestained Protein Ladder	Fermentas, St. Leon-Rot
PreScission Protease	GE Healthcare, Munich
Primers	Sigma-Aldrich, Munich
PVDF membrane	Merck Millipore, Darmstadt
rDNase	Macherey-Nagel, Düren
Restriction enzymes	Fermentas, St. Leon-Rot
RNaseA	Roth, Karlsruhe
Super Signal West Femto Max. Sens. Substrate	Thermo Fisher Scientific, Bonn
T4 DNA Ligase	Fermentas, St. Leon-Rot
Whatmann paper (3 or 5 mm)	Roth, Karlsruhe
Wizard SV Gel and PCR Clean-Up System	Promega, Mannheim

2.1.3 Vectors

Table 4: Vectors used in this study.

Vectors	Description	Reference
	Entry clones	
pDONR207	Gateway DONR, Kan^R	Invitrogen
pUNI151	Cre-recombinase pUNI, Kan^R	ABRC
	Plant expression vectors	
pGreenII RPS5a	RPS5a promoter, Kan^R, Bar^R	D. Weijers, Wageningen, Netherlands
35S-GW-GFP	Gateway C-terminal GFP fusion vector, 35S promoter, Amp^R, Kan^R	J. Parker, Cologne, Germany
pExtag-YFP-GW	Gateway N-terminal YFP fusion vector, 35S promoter, Amp^R, Bar^R	J. Parker, Cologne, Germany
35S-intron-HA	Gateway C-terminal HA fusion vector, 35S promoter, Amp^R, Kan^R	J. Parker, Cologne, Germany
pGWB560	Gateway C-terminal mCherry fusion vector, 35S promoter, Spec^R, Hyg^R	Nakagawa et al., 2007
pNIGEL7	Cre-recombinase N-terminal YFP fusion vector, UBQ10 promoter, Kan^R, Bar^R	Geldner et al., 2009
pNIGEL17	Cre-recombinase N-terminal mCherry fusion vector, UBQ10 promoter, Kan^R, Bar^R	Geldner et al., 2009
pTA7002	DEX inducible 35S promoter, Kan^R, Hyg^R	Aoyama and Chua, 1997
	Protein expression vectors	
pGEX-6P1	GST fusion vector, TAC promoter, Amp^R	GE Healthcare
pDEST17	Gateway 6xHis fusion vector, T7 promoter, Amp^R	Invitrogen
	Yeast two-hybrid vectors	
pGBKT7	GAL4BD fusion vector, ADH1 promoter, Kan^R, Trp^R	Clontech
pGADT7	GAL4AD fusion vector, ADH1 promoter, Amp^R, Leu^R	Clontech

2.1.4 Plasmids

Table 5: Plasmids used in this study.

Name	Description	Vector
AK1	ADH1:BD-AMSH1	pGBKT7
AK3	ADH1:BD-AMSH3	pGBKT7
AK6	ADH1:BD-AMSH3axa	pGBKT7
AK18	ADH1:AD-AMSH3	pGADT7
AK23	ADH1:AD-AMSH3axa	pGADT7
AK88	ADH1:AD-AMSH3(ΔMIT)	pGADT7
AK85	ADH1:AD-AMSH3(ΔMPN)	pGADT7
AK54	ADH1:AD-AMSH3 (MIT)	pGADT7
AK64	ADH1:AD-AMSH3 (N102)	pGADT7
AK82	ADH1:AD-AMSH3 (N154)	pGADT7
AK26	ADH1:BD-EHD2	pGBKT7
	ADH1:BD-VPS2.1 (Marie-Theres Hauser)	pGBKT7
	ADH1:BD-VPS2.2 (Marie-Theres Hauser)	pGBKT7
	ADH1:BD-VPS2.3 (Marie-Theres Hauser)	pGBKT7
	ADH1:BD-VPS20.1 (Marie-Theres Hauser)	pGBKT7
	ADH1:BD-VPS24.1 (Marie-Theres Hauser)	pGBKT7
	ADH1:BD-VPS46.2 (Marie-Theres Hauser)	pGBKT7
	ADH1:BD-VPS60.1 (Marie-Theres Hauser)	pGBKT7
	ADH1:BD-SNF7.1 (Marie-Theres Hauser)	pGBKT7
EI3	TAC:GST-AMSH3 (Erika Isono)	pGEX-6P1
EI6	TAC:GST-AMSH3(AXA) (Erika Isono)	pGEX-6P1
AK99	TAC:GST-AMSH3(ΔMIT)	pGEX-6P1
AK7	TAC:GST-VPS2.1	pGEX-6P1
AK8	TAC:GST-VPS2.2	pGEX-6P1
AK9	TAC:GST-VPS2.3	pGEX-6P1
AK55	TAC:GST-VPS24.1	pGEX-6P1
AK56	TAC:GST-VPS60.1	pGEX-6P1
AK33	TAC:GST-VPS2.1(mut)	pGEX-6P1
AK35	TAC:GST-VPS2.3(mut)	pGEX-6P1
AK36	TAC:GST-VPS2.1(MIM1)	pGEX-6P1
AK84	T7:6xHis-SKD1	pDEST17
AK19	VPS2.1(cDNA)	pUNI51
AK28	UBQ10:YFP-VPS2.1	pNIGEL07
AK29	UBQ10:mCherry-VPS2.1	pNIGEL17

EI151	35S:HA-SKD1 (Erika Isono)	pJaWohl 2B HA
EI149	35S:HA-SKD1(EQ) (Erika Isono)	pJaWohl 2B HA
EI36	AMSH3:YFP-AMSH3 (Erika Isono)	pGreen0229
AK94	35S:DEX:AMSH3(ΔMIT)	pTA7002
AK89	RPS5a:VPS2.1	pGreenII RPS5
AK34	VPS2.2(cDNA)	pUNI51
AK38	UBQ10:YFP-VPS2.2	pNIGEL07
AK30	VPS2.1(cDNA) (-STOP)	pDONR207
AK49	35S:VPS2.1-GFP	35S-GW-GFP
AK117	35S:VPS2.1-mCherry	pGWB560
AK52	35S:YFP-VPS2.3	pExtag-YFP-GW
AK72	VPS24.1(cDNA) (-STOP)	pDONR207
AK73	35S:VPS24.1-GFP	35S-GW-GFP
AK74	35S:VPS24.1-HA	35S-intron-HA
AK76	VPS24.1(cDNA)	pDONR207
AK101	35S:VPS24.1	35S-intron-HA
EI35	35S:3xHA-AMSH3 (Erika Isono)	pJaWohl 2B GW
EI36	35S:3xHA-AMSH3(AXA) (Erika Isono)	pJaWohl 2B GW
EI37	35S:YFP-AMSH3(AXA) (Erika Isono)	pExtag-YFP-GW
EI163	VPS20.1(cDNA) (Erika Isono)	pDONR207
EI164	35S:VPS20.1-RFP (Erika Isono)	pGWB560

2.1.5 Primers

Table 6: Primers used in this study.

Primers used for the creation of the constructs		
Name	**Description**	**Sequences 5´- 3´**
AKA	GW adaptor fw	GGGGACAAGTTTGTACAAAAAAGCAGGCT
AKB	GW adaptor rv	GGGGACCACTTTGTACAAGAAAGCTGGGT
AK0	AMSH3 fw BamHI	TCGGGGATCCGTATGAAGATTGATCTGAAC
AK1	VPS2.1 fw XhoI	AAGGCTCGAGATGATGAATTCAATCTTCGG
AK2	VPS2.1 rv SalI	AAGGGTCGACTCACATTTTTCTAAGGTTAT
AK3	VPS2.3 fw EcoRI	AAGGGAATTCATGAACATCTTCACTAAG
AK4	VPS2.3 rv SalI	AAGGGTCGACCTATCTAAGCGCCGCCAA
AK7	EHD2 fw BamHI	AAGGGGATCCATATGGAGACTTCATCG
AK8	EHD2 rv XhoI	AAGGCTCGAGTTAATTATCATAAGG
AK21	VPS2.1 fw SfiI	CAGGCCGTCAAGGCCTATGATGAATTCAATC
AK22	VPS2.1 rv NotI	CAGCGGCCGGCTCACATTTTTCTAAG

AK34	VPS2.1 GW fw	AAAAAGCAGGCTCCATGATGAATTCAATCTTCGG
AK35	VPS2.1 GW rv (-STOP)	AGAAAGCTGGGTACATTTTTCTAAGGTTATCCAAC
AK44	VPS2.1 D212N fw	ACAGTGGAGGTATAAACAGTGACCTTCAAGC
AK45	VPS2.1 D212N rv	GCTTGAAGGTCACTGTTTATACCTCCACTGT
AK46	VPS2.1 MIM1 fw	AAGGGGATCCGGAGGTATAGATAGTGAC
AK47	VPS2.3 I199D fw	TTGGCAGTTCTGGAGATGATGAACTGGAGAA
AK48	VPS2.3 I199D rv	TTCTCCAGTTCATCATCTCCAGAACTGCCAA
AK51	AMSH3(MIT) rv SalI	AAGGGTCGACTAACAGCTTATCCACTAG
AK66	VPS24.1 fw BamHI	AAGGGGATCCATGGAGAGAGTGATGAAC
AK67	VPS24.1 rv SalI	TTGGGTCGACTTAGGATCTAACTTTAGC
AK68	VPS60.1 fw BamHI	AAGGGAATCCATGAGGAGAGTTTTCGG
AK69	VPS60.1 rv SalI	TTGGGTCGACTTAACCCCGGAGAGAAG
AK70	AMSH3(MIT) fw BamHI	AAGGGGATCCAGAATCGTATTCCTCTCCGT
AK77	VPS2.2 fw EcoRI	AGGAATTCATATGAACATTTTCAAGAAG
AK78	VPS2.2 rv SalI	AGGTCGACTCAGATTCGTCGTAGCGA
AK88	AMSH3(ΔMIT) fw XhoI	AAGGCTCGAGATGAGGATGAATCCCGTCAGG
AK89	AMSH3 rv SpeI	AAGGACTAGTTTAGCGGAGATCGAGGAC
AK90	VPS24.1 GW fw	AAAAAGCAGGCTCCATGGAGAGAGTGATGAAC
AK91	VPS24.1 GW rv (+STOP)	AGAAAGCTGGGTATTAGGATCTAACTTTAGCGAG
AK92	VPS24.1 GW rv (-STOP)	AGAAAGCTGGGTAGGATCTAACTTTAGCGAGCC
AK97	AMSH3(-N154) rv SalI	AAGGGTCGAGTTACGTCCAGGATGGTTGAG
AK104	AMSH3(ΔMIT) fw XhoI	AAGGCTCGAGATGGATGAATCCCGTCAGGAT
DD1	AMSH3(ΔMIT) fw BamHI	AAGGGGATCCGAGGATGAATCCCGTCA
DD2	AMSH3(ΔMIT) rv NotI	AAGGGCGGCCGCTTAGCGGAGATCGAGGA
EI9	AMSH1 fw BamHI	AAGGGGATCCATGGGGTCGTCTTTTGAGC
EI10	AMSH1 rv SalI	AAGGGTCGACCTATCTGAGATCAATGACATC
EI14	AMSH3 rv SalI	AAGGGTCGACTTAGCGGAGATCGAGGACTT
	AtAMSH3 rv	AAGGGTCGACGCTGCCCTCTTTTCCT

Primers used for genotyping

Name	Description	Sequences 5´- 3´	T-DNA	Alleles
	GABI	ATAACGCTGCGGACATCTACA		GABI-Kat
	LBb3.1	ATTTTGCCGATTTCGGAAC		Salk
	Ds3.1	ACCCGACCGGATCGTATCGG		CSHL
AK71	VPS2.1 fw	ACTCGAAATCTACACAAGCGA		*vps2.1*
AK2	VPS2.1 rv	AAGGGTCGACTCACATTTTTCTAAGG TTAT	GABI	
AK73	VPS2.2 fw	TTGCCTCTGACATCATCTC		*vps2.2*
AK74	VPS2.2 rv	CAACTTACAAGGAAGCCGTG	LBb3.1	
EI154	VPS2.3 fw	ATTTGCTGCGATCACGTTTGAAGC		*vps2.3*
EI155	VPS2.3 rv	CTATTACTGATAAGGAATGCTTGA	LBb3.1	
	AMSH1 fw	AACATTGAGGATTGGATGGGATTTTC		*amsh1-1*
	AMSH1 rv	CTAGGCTGGTCTTCTGCCGTGAAAC	Ds3.1	

Primers used for RT-PCR

Name	Description	Sequences 5´- 3´
	Oligo dT primer	TTTTTTTTTTTTTTTTTTVN
AK77	VPS2.2 fw EcoRI	AGGAATTCATATGAACATTTTCAAGAAG
AK78	VPS2.2 rv SalI	AGGTCGACTCAGATTCGTCGTAGCGA
AK3	VPS2.3 fw E.coRI	AAGGGAATTCATGAACATCTTCACTAAG
AK4	VPS2.3 rv SalI	AAGGGTCGACCTATCTAAGCGCCGCCAA
	ACT8 fw	ATTCAGATGCCCAGAAGTCTTGTTC
	ACT8 rv	GCAAGTGCTGTGATTTCTTTGCTCA

Primers used in the analysis of yeast two-hybrid clones

Description	Sequences5´- 3´
pACT rv	GATGCACAGTTGAAGTGAACTTG
GAL4-AD	CTATTCGATGATGAAGATACCCCACCAAACC

2.1.6 Antibodies

Table 7: Antibodies used in this study.

Primary antibodies

Name	Dilution	Origin	Reference
anti-AMSH3	1:1000	Rabbit	Isono et al., 2010
anti-AMSH1	1:1000	Rabbit	Katsiarimpa and Kalinowska et al., 2013

anti-ATG8a	1:2000	Rabbit	Thompson et al., 2005
anti-CDC2	1:4000	Rabbit	Santa Cruz, Heidelberg
anti-GAL4BD	1:2000	Mouse	Santa Cruz, Heidelberg
anti-GFP	1:3000	Rabbit	Invitrogen, Darmstadt
anti-GST	1:4000	Goat	GE Healthcare, Munich
anti-HA-HRP	1:2000	Mouse	Sigma-Aldrich, Munich
anti-His-HRP	1:1000	Mouse	Sigma-Aldrich, Munich
anti-NBR1	1:2000	Rabbit	Svenning et al., 2011
anti-PIN2	1:3000	Chicken	Men et al., 2008; Agrisera
anti-VPS2.1	1:1000	Rat	In this study
anti-VPS24.1	1:1000	Rabbit	In this study

Secondary antibodies

Name	Dilution	Origin	Reference
anti-Rabbit HRP	1:10000	Goat	Sigma-Aldrich, Munich
anti-Mouse-HRP	1:1000	Rabbit	Thermo Fisher Scientific, Bonn
anti-Rat-HRP	1:1000	Rabbit	Sigma-Aldrich, Munich
anti-Goat-HRP	1:8000	Rabbit	Sigma-Aldrich, Munich
anti-Chicken-HRP	1:6000	Rabbit	Sigma-Aldrich, Munich

2.1.7 *Arabidopsis* lines

Table 8: Trangenic and mutant plants used is this study.

Arabidopsis wild type

Col-0

L*er*

Arabidopsis Mutant lines

Name	Locus	Reference
amsh1-1 (CSHL_ET8678)	AT1G48790	In this study
amsh3-1 (WiscDsLox412D09)	AT4G16144	Isono et al., 2010
atg7-2	AT5G45900	Thompson et al, 2005
pin2 (Salk_042899)	AT5G57090	Willige et al., 2011
vps2.1 (GABI_670D06)	AT2G06530	Katsiarimpa et al., 2011
vps2.2 (SALK_059274)	AT5G44560	Katsiarimpa et al., 2011
vps2.3 (SALK_127119)	AT1G03950	Katsiarimpa et al., 2011

***Arabidopsis* transgenic lines**	
Description	**Reference**
DEX:35S:AMSH3(WT)	Isono et al., 2010
DEX:35S:AMSH3(AXA)	Isono et al., 2010
DEX:35S:AMSH3(AXA) / UBQ10:YFP-VPS2.1	In this study
DEX:35S:AMSH3(ΔMIT)	In this study
35S:VPS2.1-GFP	In this study
35S:VPS24.1-HA	In this study
vps2.1 / RPS5a:VPS2.1	In this study
vps2.2 / UBQ10:YFP-VPS2.2	In this study
vps2.3 / 35S:YFP-VPS2.3	In this study

2.1.8 Bacterial strains

The *Esherichia coli* strains used in the present study were DH5α (Genotype: F-Φ80*lacZ*ΔM15 Δ(*lacZYA-arg*F) U169 *rec*A1 *end*A1 *hsd*R17 (rK-, mK-) *pho*A *sup*E44 λ-*thi*-1 *gyr*A96 *rel*A1; Bethesda Research Laboratories, 1986) for cloning and propagation of plasmids, DB3.1 (Genotype: F- *gyr*A462 *end*A1 Δ(sr1-*rec*A) *mcr*B *mrrhsd*S20(rB-, mB-) *sup*E44 *ara*-14 *gal*K2 *lac*Y1 *pro*A2 *rps*L20(Smr) *xyl*-5 λ-*leumtl*1; Hartley et al., 2000) for propagation of Gateway vectors and Rosetta (DE3) strain (Genotype: F⁻*ompT hsd*S$_B$ (r$_B^-$ m$_B^-$) *gal dcm* (DE3) pRARE (Cam^R); Merck Chemicals) for the expression of recombinant proteins.

The *Agrobacterium tumafeciens* strains GV3101 (pMP90, pMP90RK, pMP90:pSoup; Koncz and Schell, 1981) were used for the *Arabidopsis* transformation.

The yeast strain used to perform the yeast two-hybrid screen and yeast two-hybrid assays was Y190 (Genotype: *MATa gal4 gal80 his3 trp1-901 ade2-101 ura3-52 leu2-3,-112*; Clontech).

2.2 Methods

2.2.1 Methods for plant analysis

2.2.1.1 Sterilization of seeds and growing conditions

Arabidopsis seeds were first incubated in a saturated calciumhypochlorid solution supplemeted with 1% Silwet L-77, for 10 min, then shortly sterilized with 70% Ethanol and subsequently washed four times with sterile water supplemented with 1% Silwet L-77. The seeds were stratified at 4°C for 2 days. In case of *vps2.1* mutants, the seeds were stratified for 5 days. Seeds were plated on growth medium (GM: 4,3 g/l Murashige & Skoog Medium, 10 g/l Sachharose, 0.5 g/l MES, 5.5 g/l Plantagar (pH 5.8)) and grown under continuous light (110 to 150 µmol m^{-2} s^{-1}) at 21 °C. For the experiments regarding autophagy, seeds were platted on ½ MS medium (2.15 g/l Murashige & Skoog Medium, 0.5 g/l MES, 6.5 g/l Plantagar (pH 5.8)) and grown under long day conditions (16 hours light and 8 hours dark) or under short day conditions (8 hours light and 16 hours dark). For adult plants, 7 days old seedlings were transferred on soil and grown under continuous light, under short or long day conditions, depending on the individual experiments.

2.2.1.2 *Agrobacterium tumefaciens*-mediated transformation of *Arabidopsis thaliana*

The transformation of *Arabidopsis* was performed using the standard Floral Dip method (Clough and Bent, 1998). The expression of different constructs in *Arabidopsisthaliana*, was achieved by inserting the corresponding constructs into the appropriate Agrobacterium strain with electroporation. The strains used were GV301 pMP90, GV301 pMP90RK and GV301 pMP90 pSoup. The strain GV301 pMP90 contains a selection marker for Gentamycin (20 µg/ml) and Rifampicin (50 µg/ml), GV301 pMP90RK contains additional a marker for Kanamycin (50 µg/ml) selection and GV301 pMP90 pSoup one additional for Tetracyclin (5 µg/ml). After the transformation of the corresponding strain with the construct, the strains were selected on LB medium (10 g/l Trypton, 5 g/l Yeastextract, 10 g/l NaCl, pH 7 (adjusted with NaOH)) supplemented with the appropriate antibiotics for the strain

and the construct. Bacteria of a 500 ml liquid culture, grown at 30°C, were collected and resuspended in a transformation buffer (2.2 g/l Murashige & Skoog Medium, 50 g/l Glucose, 0.5 g/l MES, 50 µl/l 6-BA (1 mg/ml), 500 µl/l Silwet L-77). Inflorescences from whole Col-0 or L*er* plants were incubated in this suspension for 2 min. Dipped plants were placed under a cover to maintain humidity and left overnight at room temperature to maintain humidity. Plants were placed back to optimal light and temperature conditions for seeding. The obtained seeds from this generation are selected on GM medium with the appropriate antibiotics, depending on the transformed construct. The positive plants were subsequently genotyped using specific primers.

2.2.1.3 PEG mediated transformation of *Arabidopsis* protoplasts

3 to 4 days after subculturing, *Arabidopsis* suspension-cultured cells were collected by centrifugation at 300 g. Cells were resuspended into a WD solution (8 mM $CaCl_2$-$2H_2O$, 0.4 M Mannitol) supplemented with 1 % Cellulase and 0,25 % Macerozym and incubated under gentle agitation at room temperature (20 °C – 25 °C) in the dark. The digestion rate and the formation of protoplats (pps) were observed under a light microscope (Olympus, Bx61). After 3 to 4 hours of incubation, the formed pps were collected by centrifugation at 100 g for 1 min. The pps were washed one time with WD and one time with W5 solution (154 mM NaCl, 125 mM $CaCl_2$, 5 mM KCl, 5 mM Glucose). The pps were resuspended in W5 solution and incubated on ice for 30 min. The pps were afterwards collected by centrifugation at 100 g for 1 min. The supernatant was discarded and the pellet carefully resuspended in MMM solution (15 mM $MgCl_2$, 0.1 % MES, 0.5 M Mannitol) to a density of 0.5 x 10^6 pps/ml. 20 mg of the construct of interest was transformed into 200 µl of protoplasts by the addition of 200 µl PEG solution (40% PEG, 0.4 M Mannitol, 0.1 M $CaCl_2$). The suspension was incubated on ice for 25 min. Protoplasts were collected by the addition of 700 µl W5 solution and centrifugation at 100 g for 2 min. Transformed pps were washed again with W5 and resuspended in K3 solution (for 10 ml K3: 1 ml macro stock (1.5 g $NaH_2PO_4.H_2O$, 9 g $CaCl_2.2H_2O$, 25 g KNO_3, 2.5 g NH_4NO_3, 1.34 g $N_2H_8SO_4$, 2.5 g $MgSO_4.7H_2O$, up to 1 litter with H_2O), 0.01 ml micro stock (75 mg KI, 300 mg H_3BO_3, 1 g $MGSO_4.7H_2O$, 200 mg $ZnSO_4.7H_2O$, 25 mg $Na_2MoO_4.2H_2O$, 2.5 mg $CuSO_4.5H_2O$, 2.5 mg $CoCl_2.6H_2O$, up to 100 ml with H_2O), 0.01 ml vitamin stock

(100 mg Nicotinacid, 100 mg Pyridoxin/HCl, 1 g Thiamin/HCl, up to 100 ml with H_2O), 0.05 ml EDTA stock (7.46 g EDTA, 5.56 g FeIISO$_4$.7 H_2O, up to 1 l with H_2O), 0.1 ml Ca-Phospate stock (1.26 g CaHPO$_4$.2H$_2$O up to 200 ml with H_2O, pH=3 with HCl), 1 mg Myo-Inositol, 2.5 mg D(+)-Xylose, 1.37 g Sucrose (pH=5,6)). Transformed pps were incubated for 16 to 20 hours at room temperature in dark prior to observation by the confocal scanning microscope (Olympus).

2.2.1.4 Chlorophyll content measurement

In order to determine the chlorophyll content, approximately 20 seedlings, after exposure to carbon limiting conditions, were incubated in 1 ml *N,N*-dimethylformamide at 4°C under agitation in the dark. After 24 hours of incubation, the absorbance of the supernatant was measured at 664 and 647 nm. Subsequently total chlorophyll content was calculated according to total Chl = ((OD664*7,04) + (OD647*20,27)) / fresh weight (Porra et al., 1998).

2.2.1.5 Root length measurement

For monitoring differences in the root length of *vps2* mutants, seedlings were grown vertically on GM (4.3 g/l Murashige & Skoog, 10 g/l Sucrose, 0.5 g/l MES, 5,5 g/l Plant agar (pH 5.8)) plates at continuous light for 7 days. The plates were scanned with an Epson Perfection V750 pro scanner and the root length was measured with the help of ImageJ64 software. The mean (± SE) of 20 to 30 seedlings was calculated and *P* values were analyzed by Student's *t*-test.

2.2.2 Molecular biology methods

2.2.2.1 Plasmid purification from E.*coli*

Alkaline lysis based method was used for the purification of plasmids from bacteria. For mini scale purification, one colony from the selection plate containing the putative plasmid was inoculated in 3 ml liquid culture and incubated overnight at 37°C. The grown bacteria from the culture were harvested by centrifugation and resuspended in 300 µl of Buffer P1 (50 mM Tris/HCl (pH 8.0), 10mM EDTA) for

destabilization of the bacterial cell membrane. The following addition of 300 µl of Buffer P2 (200 mM NaOH, 1% SDS) induced the lysis of the membrane and the release of DNA. The circular plasmid is then renatured by the addition of 300 µl of Buffer P3 (3 M potassium acetate, pH 5.5). The solution was then mixed with 100 µl of Phenol/Chloroform (1:1) and centrifuged for the separation of the hydrophobic and hydrophilic phases, in order to isolate the DNA from proteins and cellular debris. The supernatant was mixed with 700 µl of Isopropanol and centrifuged for the concentration of the DNA in the pellet due to dehydration. The pellet was washed once with 70% Ethanol. The dry pellet was resolved in distilled water, supplemented with RNAase for the destruction of RNA. The RNAase has to be incubated for 30 min at 37 °C to get active.

The JETstar 2.0 Plasmid Purification MIDI Kit (Genomed) was used for the midi scale plasmid purification. The isolation of the DNA was performed according to manufacturers instructions.

2.2.2.2 DNA extraction from *Arabidopsis* plants

For the extraction of genomic DNA from plant material (seedling or leave from adult plant) was grind and suspended in 300 µl of extraction buffer (250 mM NaCl, 200 mM Tris/HCl (pH 7.5), 25 mM EDTA (pH 8.0), 0,5% SDS). The suspension was incubated for 20 min in a 65°C water bath and then mixed with 300 µl Phenol/Chloroform (1:1). The suspension was centrifuged at 13.000 rpm for 5 min at room temperature for the separation of hydrophobic and hydrophilic phases, enabling the isolation of the nucleic acids, which were pelleted by the addition of 200 µl Isopropanol. The pellet was washed with 70% ethanol and resolved in distilled water after drying.

2.2.2.3 *Arabidopsis* PCR genotyping

For identification of the genotypes of plants, PCR was performed with 3 µl 10xPCR Reaction buffer (200 mM Tris-HCl (pH 8.4), 500 mM KCl and 25 mM MgCl$_2$), 3 µl of 100 mM of dNTPs Mix (100 mM of dATP, dTTP, dGTP and dCTP), 0.4 µl of each 50 mM primer and 0.2 µl home-made Taq DNA polymerase and 5 to 10 µl of extracted plant genomic DNA in a total volume of 30 µl. The PCR conditions are an

initial denaturation step at 94°C for 4 min, 35 cycles of denaturation at 94°C for 1 min, annealing at 52°C to 58°C for 1 min and extension at 72°C for 1 min/kb, followed by a final extension step at 72°C for 6 min. The PCR products were analyzed on an agarose gel.

2.2.2.4 RNA extraction from plant material and cDNA synthesis

RNA extraction from plant material was performed according to manufacturers instructions using the NucleoSpin RNA Plant Kit (Macherey-Nagel). The only modification was at the step of the DNA digestion with a DNAase (Macherey-Nagel), at which the incubation time instead of 15 min, it was prolonged for 5 min. Before using the extracted RNA for cDNA synthesis the concentration of RNA was determined using the absorbance at 260 nm measured with the photometer. Purity of RNA preparation was assessed by the ratio of absorbance at 260 nm and 280 nm. Pure RNA has an A260/A280 of 1.8 to 2.1.

For cDNA synthesis, a 10 µl reaction volume containing 2 µg of RNA with 1 µl of oligo-dT-primer (20 mM) was incubated for 10 min at 65°C for the denaturation of the nucleic acids and then cooled for 1 min on ice. 1 µl H2O, 2 µl dNTPs (2.5 mM of dATP, dTTP, dGTP and dCTP), 4 µl 5x reactionbuffer and 2 µl (40 U) M/MuLV Reverse Transcriptase (Fermentas) were added to the reaction and incubated for 70 min at 42 °C. For the inactivation of the Transcriptase the reaction was heated for 10 min at 65 °C. The reaction was cooled on ice and 20 µl of distilled water were added.

2.2.2.5 Semiquantitative real time-PCR (sqRT-PCR)

For sqRT-PCR, a set of PCR primers covering the whole coding sequences for the genes of interest were used. 2.7 µl of the synthsized cDNA were used in a PCR reaction. PCR volume and conditions were the same as used for *Arabidopsis* genotyping. Actin was used as a housekeeping gene for the internal loading control.

2.2.2.6 Cloning

For the generation of the following constructs cDNA or genomic fragments were PCR amplified using the Expand High Fidelity PCR System (Roche). For the Y2H constructs of GBD-AMSH3 and GBD-AMSH3(AXA), *AMSH3* and *AMSH3(AXA)* were subcloned from GST-AMSH3 and GST-AMSH3(AXA) (Isono et al., 2010), respectively into the *Bam*HI-*Sal*I sites of pGBDT7 (Clontech). The N*de*I and S*ma*I sites were subsequently cut, filled in with Klenow polymerase (Fermentas) and religated to obtain the proper reading frame. To yield GAD-AMSH3 and GAD-AMSH3(AXA), wild type and dominant negative *AMSH3* were PCR-amplified with primers AK0 and EI14 using the G67772 clone (ABRC)and GST:AMSH3(AXA) (Isono et al., 2010) as a template, respectively, and cloned into the *Bam*HI-*Sal*I sites of pGADT7 (Clontech). The truncated constructs of AMSH3, GAD-AMSH3(ΔMPN), -(MIT), -(N102) and -(N154) were generated with fragments amplified with AK0 and AtAMSH3 rv, AK70 and AK51, AK0 and AK51 and AK0 and AK97, respectively, and cloned into the *Bam*HI-*Sal*I sites of the pGADT7 vector. For GAD-AMSH3(ΔMIT) the gene fragment was amplified with AK88 and EI14 and cloned into the *Xho*I site of pGADT7. For GBD-AMSH1 the cDNA of *AMSH1* was PCR-amplified with EI9 and EI10 and cloned into the *Bam*HI-*Sal*I sites of pGBKT7 (Clontech), subsequently cut with N*de*I and S*ma*I, filled in with Klenow polymerase (Fermentas) and religated, in order to restore the open reading frame. To obtain GBD-EHD2, *EHD2* was aplified from the U88122 clone (ABRC) using the primers AK7 and AK8 and cloned into the *Bam*HI and *Xho*I sites of pGBDT7 vector.

For GST-VPS2.1, GST-VPS2.3, GST-VPS24.1 and GST-VPS60.1, the corresponding ORFs were PCR-amplified using primers AK1 and AK2, AK3 and AK4, AK66 and AK67 and AK68 and AK69, respectively. The resulting fragments were cloned between the *Xho*I and *Sal*I sites (*VPS2.1*), *EcoR*I and *Sal*I sites (*VPS2.3*) and the *Bam*HI and *Sal*I sites (*VPS24.1* and *VPS60.1*) of pGEX-6P-1 (GE Healthcare). GST-VPS2.2 was obtained by subcloning the *VPS2.2* ORF from the Y2H construct into the pGEX-6P-1 vector between the *EcoR*I and *Sal*I sites. The GST-AMSH3(ΔMIT) was constructed by introducing the amplified fragment with DD1 and DD2 primers into the B*am*HI and N*ot*I sites of pGEX-6P-1.

For GST-VPS2.1(mut) and GST-VPS2.3(mut) constructs, the mutations were introduced using *Dpn*I-based site-directed mutagenesis (Stratagene). GST-VPS2.1

and GST-VPS2.3 constructs were used as template to amplify the mutated versions using primers pairs AK44 - AK45 and AK47 - AK48, respectively. The mutated genes were obtained after the digestion of the parental (methylated) DNA by *Dpn*I.

To generate GST-VPS2.1(MIM1), *VPS2.1(MIM1)* was PCR amplified using the AK2-AK46 primers and cloned into the *Bam*HI-*Sal*I sites of pGEX-6P-1.

For cloning UBQ10:YFP-VPS2.1, UBQ10:YFP-VPS2.2 and UBQ10:mCherry-VPS2.1, pUNI-VPS2.1 and pUNI-VPS2.2 were first generated, by cloning the PCR amplified ORF of *VPS2.1* and *VPS2.2* with primers AK21 and AK22 and AK77 and AK78, respectively, between the *Sfi*I and *Not*I (*VPS2.1*) and *Eco*RI and *Sal*I (*VPS2.2*) sites of the pUNI51 vector (ABRC). pUNI-VPS2.1 and pUNI-VPS2.2 were then recombined with pNIGEL7 and pNIGEL17 (Geldner et al., 2009) for YFP and mCherry fusion, respectively with Cre/Lox recombination system (NEB).

pDONR207, 35S-GW-GFP and 35S-intron-HA (J. Parker, Cologne, Germany) were used for the creation of 35S:VPS24.1-GFP and 35S:VPS24.1-HA, respectively using Gateway technology (Invitrogen). *VPS24.1* was amplified with AK90 and AK92 and Gateway adaptor primers. In the case of 35S:VPS24.1, *VPS24.1* was PCR-amplified using AK90 and AK91 primers, which contain a stop codon, and Gateway adaptor primers and introduced in 35S-intron-HA, using Gateway technology.

For the 35S:YFP-VPS2.3 construct, the *VPS2.3* coding sequence was transferred by Gateway recombination from the G13604 (ABRC) cloneto the pExtag-YFP-GW (J. Parker, Cologne, Germany).

To yield RPS5apro:VPS2.1, the ORF of *VPS2.1* was amplified with primers AK1 and AK2 and cloned into the *Xho*I site of pGreenII BAR RPS5a-tNOS (D. Weijers, Wageningen, The Netherlands).

In order to create 35S:VPS2.1-GFP and 35S:VPS2.1-mCherry, the ORF of *VPS2.1* was PCR-amplified using the primers AK34 and AK35 and Gateway adaptor primers, cloned into pDONR207 and then recombined with 35S-GW-GFP (J. Parker, Cologne, Germany) and pGWB560 (Nakagawa et al., 2007) using Gateway cloning system.

35S:DEX:AMSH3(ΔMIT) was generated by inserting the PCR amplified *AMSH3(ΔMIT)*fragment using the AK89 and AK104 primers into the *Xho*I-*Spe*I sites of pTA7002 (Aoyama and Chua, 1997).

All constructs were confirmed by restriction digestion tests and DNA sequencing.

2.2.2.7 Yeast two-hybrid screen

The yeast two-hybrid (Y2H) screen was performed according to the protocol described in Schwechheimer and Deng, 2002. The yeast strain Y190 containing the bait plasmid pGBKT7-AMSH3(AXA) was grown on synthetic complete drop out (SD) medium lacking tryptophan (W) (SD-W, 6.7 g/l Yeast nitrogen base without amino acids, 20g/l Bacto-agar, 0.1 g/l Leucine, 0.02 g/l Uracil, 0.02 g/l Histidine) for 2 days at 30 °C.

The grown yeast cells were transferred to a 150 ml liquid culture in SD-W medium and were further grown at 30 °C at 180 rpm until the OD600 reached 1.5 to 2. The cells were then collected by centrifugation at 1000 g for 5 min and resuspended in 1 l of fresh SD-W medium. The culture was further grown under the same condition for 3 hours until the OD600 reached 0.6 to 1. The cells were pelleted by centrifugation at 1000 g for 5 min and subsequently washed with 500 ml H_2O. The cells were resuspended in 8 ml 1xTE/1xLiAc (10 µM Tris, 1 µM EDTA (pH 8.0) / 0.1 mM LiAc) and divided in 10 aliquots of 800 µl. In each aliquot 20 µg of prey DNA from each aliquot of the cDNA library (Kim et al., 1997), 200 µl of salmon sperm DNA (10 mg/ml) and 6 ml of 40% PEG were added and mixed gently. The cells were first incubated for 30 min at 30 °C and then heat shocked for 15 min at 42 °C after the addition of 700 µl DMSO. Cells were then collected by centrifugation at 1000 g for 5 min and resuspended in 450 µl of 1xTE. From the suspension 442.5 µl were plated on SD medium lacking leucine (L), W and histidine (H) (SD-LWH), supplemented with 10 mM 3-AT, for the screening and 7.5 µl were plated on SD-LW in order to calculate the efficiency of the transformation by counting the number of transformants. About $2x10^6$ transformants were screened on SD-LWH.

To confirm the interaction for each positive transformant, a second screen was performed by extracting the prey plasmids, propagating them in XL1Blue *E.coli* strain and re-transforming them together with pGBKT7 or pGBKT7-AMSH3(AXA) into Y190 yeast cells. The transformants were tested for auxotrophic growth on SD-LWH and for β-galactosidase activity.

2.2.2.8 β-galactosidase assay

In the β-galactosidaseassay, clones containing prey and bait plasmid were restreaked and grown on SD-LW medium for 2 days at 30 °C. The cells were transferred to a 3mM Whatman paper (Roth) by making a lift from the plate. This filter paper was frozen for 2 min in liquid nitrogen, then let to thaw in room temperature and at least placed with the colonies side up on an other 3 mM Whatman paper, which was soaked in LacZ staining solution (100 ml LacZ buffer (65 mM $Na_2HPO_4.7H_2O$, 40 mM $NaH_2PO_4.H_2O$, 10 mM KCl, 1 mM $MgSO_4.7H_2O$ (pH 7.0)), 0,27 µl β-meracptoethanol, 1,67 ml of 20 mg/ml XGAL in DMF). The positive candidates were sequenced with the GAL4-AD and ACT-rv primers.

2.2.2.9 Yeast two-hybrid assay

For a targeted Y2H assay, the yeast strain Y190 was grown on YPD plates at 30 °C for 1 day. The growing cells were collected, resuspended in 100 µl of 1xLA and incubated at room temperature for 10 min. 5 – 10 µl of each DNA plasmid was added to the cells and mixed with 240 µl 40% PEG solution. The mixture was incubated at 30 °C for 30 min. After the incubation 35 µl DMSO were added and the solution was put for 10 min in a 42 °C water bath for heat shock. Yeast cells were collected by centrifugation at 1000 g for 2 min, washed with sterile water and plated on SD-LW medium. The colonies containing both plasmids were visible after two days growing at 30°C.

2.2.3 Biochemical methods

2.2.3.1 Protein extraction from plants

For the isolation of total plant proteins, plant material was homogenized on ice in Protein Extractionbuffer (50 mM Tris-HCl, pH 7.5, 150 mM NaCl, 0.5% Triton X-100, 0.1 µM Protease Inhibitor Coctail (Sigma-Aldrich). Extracts were centrifuged at 13.000 rpm for 15 min. The concentration of the soluble proteins was determined by a Bradford assay (Bradford, 1976) using the Bio-Rad protein assay reagent (Bio-Rad). The extract was mixed with 5xSDS Loading Sample Buffer (250 mM Tris-HCl

(pH 6.8), 10% SDS, 30% Glycerol, 5% β-mercaptoethanol, 0.02% bromophenol blue), heated at 98°C for 5 min and subjected to immunoblot analysis.

For the isolation and analysis of membrane bound proteins, the material obtained after centrifugation at 9000 rpm for 15 min was subsequently ultracentrifuged at 100.000 g for 1 hour at 4°C using the Sorvall MTX 150 Micro-Ultracentrifuge (Thermo Scientific). The pellet containing the membrane fraction was resuspended in 1 ½x SDS loading buffer and heated at 42°C for 5 min.

For the isolation of total proteins from transformed protoplasts, protoplasts were collected by centrifugation, resuspended in 1xSDS loading buffer and heated at 98°C for 5 min.

2.2.3.2 Recombinant protein purification

For the purification of AMSH3 and GST fused VPS2.1, VPS2.2 and VPS2.3, the correspoding pGEXP1 plasmids were transformed in a *E.coli* Rosetta (DE3) strain and the expression was induced by the addition of 0.2 mM IPTG and further incubation at 18°C for 20 h. The purification was performed according to manufacturers instruction using Glutathione-Sepharose 4B beads (GE Healthcare). The GST fused proteins were eluted with 0,2 M reduced Glutathion. In order to obtain the unfused AMSH3 protein, Prescission Protease (GE Healthcare) was added to the Glutathione-Sepharose 4B beads coupled with GST-AMSH3.

In case of His-SKD1, the corresponding pDEST17 plasmid, containing the ORF of *SKD1*, was transformed in *E.coli* Rosetta (DE3) cells. Ni Sepharose High Performance beads (GE Healthcare) were used and the elution was performed with 250 mM Imidazole. All eluted proteins were dialyzed against Buffer A (50 mM Tris-HCl, 100mM NaCl, 10% Glycerol, (pH 7.5)). Protein concentration was determined after SDS-PAGE and Coomassie Brilliant Blue staining, using the Benchmark Protein Ladder (Invitrogen) as a standard, using the LAS-4000 mini (FUJI Film) and the Multi Gauge (FUJI Film) software.

2.2.3.3 *In vitro* binding assay

In the *invitro* binding assay, Glutathione Sepharose 4B beads (GE Healthcare) were saturated with equal amount (8 µg) of GST fused proteins and GST as a control

for 2 hours and then blocked for 30 min with 200 µl saturated milk solution (milkpowder in Buffer A). The coupled Glutathione Sepharose 4B beads were washed once with ice cold Buffer A and suspended in 20 µl Buffer A. 2 µl of the suspended beads were subjected to SDS-PAGE and Coomasie Brilliant Blue staining for the quantification of the bound material. Equal amounts of coupled GST-fused proteins to Glutathione Sepharose 4B were incubated under agitation with 6 pmol AMSH3 or 0,8 µg His-SKD1 in 100 µl ice cold Buffer A, supplemented with 0,2% Triton X-100, for 30 min or 45 min at 4°C, respectively. The beads were then washed three times with ice cold Buffer A, supplemented with 0,3 % Triton X-100 and 1 mM DTT, and three times further with ice cold Buffer A. The collected beads were resuspended in 1xSDS loading buffer and heated at 98 °C for 5 min. Pulled-down proteins were analyzed by immunoblotting using anti-GST, anti-AMSH3 (Isono et al., 2010) and anti-His-HRP antibodies.

2.2.3.4 *In vitro* competition assay

For performing an *in vitro* competition assay between AMSH3 and SKD1 for binding to VPS2.1 and VPS24.1, AMSH3 was initially incubated with the GST fused proteins, as for the the *in vitro* binding assay, and then 6, 72 or 216 pmol of His-SKD1 were added to each reaction. The samples were incubated for 45 min at 4°C under agitation. Beads were washed twice with ice cold Buffer A, supplemented with 0,3 % Triton X-100, and three times further with ice cold Buffer A. The collected beads were resuspended in 1xSDS loading buffer and heated at 98 °C for 5 min. Pulled-down proteins were analyzed by immunoblotting using anti-GST, anti-AMSH3 (Isono et al., 2010) and anti-His-HRP antibodies.

2.2.3.5 SDS-PAGE

Proteins from total protein extract or membrane fraction were separated by SDS-PAGE (Laemmli, 1970). For the preparation of a SDS-PAGE, a 5% stacking gel (1.2 ml H_2O, 0.5 ml stacking buffer (0.5 M Tris-HCl, pH6.8, 0.5 % (w/v) SDS), 0.3 ml Acrylamid, 25 µl 10% APS, 3 µl TEMED) and a 5 to 12% separation gel (1 to 1.7 ml H_2O, 1 ml separation buffer (1.5 M Tris-HCl, pH 8.8, 0.4 % (w/v) SDS), 1.3 to 2 ml Acrylamid, 25 µl 10% APS, 3 µl TEMED) were used. The running of the SDS gels

was performed in a Mini Protean III Cell (Bio-Rad) filled with SDS running buffer (25 mM Tris, 192 mM Glycin and 0.04% SDS).

2.2.3.6 Coomassie Brilliant Blue staining

For determining the amount of purified proteins or for loading controls, proteins were resolved on a SDS-PAGE, stained with Coomassie Brilliant Blue staining (CBB) (2.5 g Coomassie Brilliant Blue R-250, 500 ml Methanol, 100 ml Acidic acid, 400 ml H_2O) and distained with distaining buffer (500 ml Methanol, 100 ml Acidic acid, 400 ml H_2O).

2.2.3.7 Immunoblot analysis

The transfer of resolved proteins on SDS-PAGE on a PVDF membrane was performed using a Semi-Dry (SD) blotter (peqlab, Biotechnologie GmbH) and SD buffer (25 mM Tris, 192 mM Glycin, 20% Methanol, 1.3 mM SDS, pH 8.3 (regulated through NaOH). The PVDF membrane has to be activated prior use by soaking it in Methanol for 20 sec. After 1 to 2 hours of transfer at 1 mA/cm^2, the membrane is blocked in 10% skim milk in TBST buffer (50 mM Tris, 150 mM NaCl, 1 mM MgCl$_2$.6H$_2$O, pH 7.8 adjusted with HCl and 0.05% Triton-X100) for 30 min at room temperature, probed with the first antibody in 5% skim milk in TBST and washed 3 times of 15 min each with TBST at room temperature. The membrane is then probed with an appropriate secondary antibody conjugated to a horseradish peroxidase (HRP) in TBST for 1 hour at room temperature and subsequently washed 3 times of 15 min each with TBST. The proteins recognized by the antibodies were visualized using Super Signal West Femto Maximum Sensitivity Substrate (Thermo Fisher Scientific) in the Luminescent Image Analyzer LAS-4000 mini series (FujiFilm).

2.2.3.8 Production of antibodies

Antibodies against the full length proteins VPS2.1 and VPS24.1 were raised in rats and rabbits (Eurogentec), respectively. The animals were immunized with 600 µg of the corresponding proteins. The proteins were obtained by expression and

purification of VPS2.1 and VPS24.1 in E.*coli* Rosetta (DE3) strain. The GST moiety was cleaved off prior use for the immunization.

The obtained serums from the rat and the rabbit were purified with a 1 ml Hi-Trap Protein A and Protein G column (GE Healthcare), respectively, according to manufacturers instructions. The serums (pH 7.0) were applied to the individual columns and the IgA or IgG antibody isotypes were selected from the serums through specific binding to Protein A or G. By lowering the pH at 2.5 to 3.0 the isotypes could be eluted. The eluted fractions were neutralized with 1M Tris-HCl (pH 9.0) and analyzed on a Coomasie Brilliant Blue stained SDS-PAGE. The fractions containing the IgAs or IgGs were further purified with a VPS2.1 or VPS24.1-loaded 1 ml NHS-activated HP column (GE Healthcare), respectively. Recombinant VPS2.1 and VPS24.1, used also for the immunization of the animals, were coupled to the NHS activated Sepharose High Performance in the columns through their amines. The coupled proteins serve as antigens for further purification of the antibodies. The selected IgA or IgG containing fraction from the previous purification step are loaded on the antigen-affinity columns and are eluted again by lowering the pH (pH 1.9). The loading of the columns with the VPS proteins as well the purification of the IgG fractions was performed by following the manufacturers instructions. The two antibodies were used in a 1:2000 dilution for immunoblot analysis.

2.2.4 Histochemical methods

2.2.4.1 Microscopy

Fluorescently tagged proteins were imaged with an FV-1000/IX81 confocal laser scanning microscope (Olympus) using a UPlanSApo X20 or X60 (Olympus) objective. YFP signals were visualized using the 515 nm laser line, GFP with the 488 nm laser line and RFP or mCherry signals with the 559 nm laser line. Images were obtained using the Fluoview software (Olympus) at a combination of 600 to 800 high voltage, of 1 gain and of 10-20% offset at a frame averaging of 3 means. The images were processed using Adobe Photoshop and Illustrator.

2.2.4.2 Clearing of *Arabidopsis* seeds

Seeds from wild-type and heterozygous *vps2.1* mutant siliques at different developmental stages were excised and cleared with chloral hydrate solution (3g Glycerol, 20g Chloral hydrate and 9 g H_2O) overnight at 30°C to observe the embryos. Samples were mounted between a slide glass and a cover slip in the same solution and kept at 4°C prior to observation under a Bx61 light microscope (Olympus), equipped with a monochrome fluorescence CCD camera XM10 (Olympus). The obtained DIC images of the embryos were processed with Photoshop CS5 (Adobe).

2.2.5 Stainings and live cell imaging

2.2.5.1 E64-d treatment and MDC staining

Arabidopsis seedlings were grown on ½ MS medium for 7 days at long day conditions and then transferred to complete darkness for 2 or 5 days as indicated in each experiment. After dark treatment seedlings were incubated in liquid ½ MS medium, supplemented with 100 µM E64-d or DMSO as a solvent control, for 1 or 15 hours as indicated for each experiment. For visualization of autophagosomes, seedlings were stained with 50 µM MDC (Sigma) in PBS (1.44 M NaCl, 2.7 mM KCl, 0.15 M Na_2HPO_4 and 18 mM KH_2PO_4) for 10 min at room temperature and then washed twice with PBS to remove excess stain.

MDC signals were visualized using the 405 nm laser line and examined using a FV-1000/IX81 confocal laser scanning microscope (Olympus). For quantification of the area of MDC-signals in the vacuoles after E64-D treatment, images were obtained using the UPlanSApo X60 objective (Olympus) with a 2,6x zoom. These images were analyzed using the Fluoview FV1000 software (Olympus). The average (± SE) of all cells for each line was calculated and *P* values were analyzed by Student's *t*-test.

3. Results

3.1 AMSH3 interacting proteins

3.1.1 Interacting proteins of AMSH3 found in a yeast two-hybrid screen

The characterization of *amsh3* mutants revealed a putative implication of AMSH3 in intracellular protein trafficking and autophagy (Isono et al., 2010). An approach to obtain information about the role of the deubiquitinating activity of *Arabidopsis* AMSH3 in these pathways is the identification of AMSH3 interacting proteins. In order to identify interacting proteins, a Y2H screen was conducted using AMSH3 as bait. A construct, in which wild-type AMSH3 was fused to a GAL4 DNA binding domain (GBD), was used as bait to screen against an *Arabidopsis* cDNA library, fused with a GAL4 DNA activation domain (GAD). Unfortunately, since the GBD-AMSH3 fusion protein showed auto-activation in this system (data not shown), the screen was performed with the inactive variant AMSH3(AXA) fused to a GBD domain. From this screen 117 clones were selected and analyzed by sequencing. Comparison of the query sequences with the *Arabidopsis* database TAIR, revealed 86 genes as listed in Table 9 (Appendix). Two of them were out of frame and two were of unknown function.

Since it was assumed that AMSH3 plays a role in intracellular trafficking and autophagy (Isono et al., 2010), I focused on proteins known to be implicated in one or the other pathway. From the list of interactors found with the Y2H screen, two proteins are known to play a role in intracellular trafficking namely, EHD2 and VPS2.1.

VPS2.1 is the *Arabidopsis* homologue of yeast Vps2p (Winter and Hauser, 2006). Vps2p is a subunit of the multi-protein complex ESCRT-III, that is employed in the endosomal trafficking pathway. Studies in mammals and yeast have shown that the function of CHMP2a/Vps2p is associated with the recruitment of VPS4, an AAA-ATPase, necessary for the function of ESCRT-III and MVB biogenesis. Thus, CHMP2a/Vps2p is important for the endocytosis of plasma membrane proteins by contributing to the proper function of ESCRT-III (Fujita et al., 2004; Raymond et al., 1992; Schmidt and Teis, 2012).
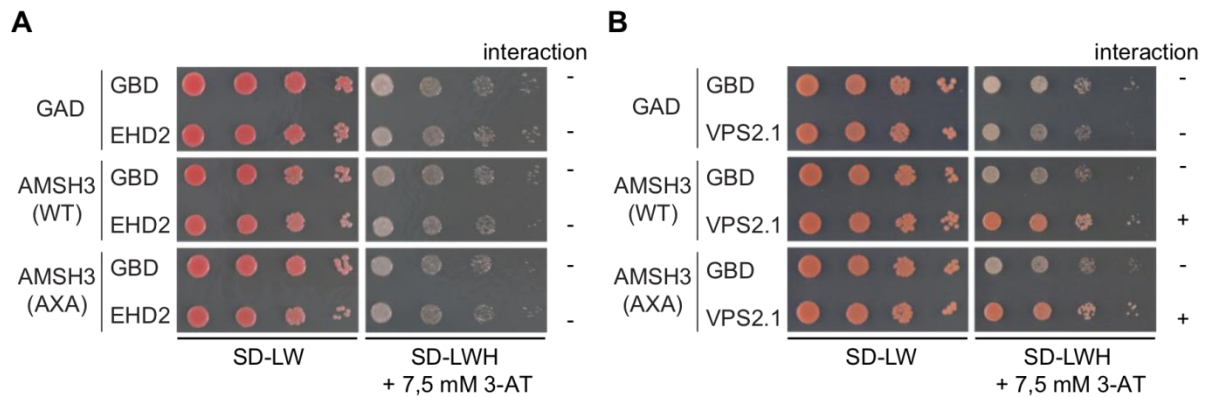
Figure 7: VPS2.1 found as a Y2H interactor of AMSH3.
A) and **B)** Y2H analysis of GAD fused AMSH3 and AMSH3(AXA) with GBD fused EHD2 (A) and VPS2.1 (B). Transformants were plated on synthetic drop out medium lacking leucine and tryptophan (SD-LW) and on SD medium lacking leucine, tryptophan and histidine (SD-LWH), supplemented with 7,5 mM 3-AT to test for their auxotrophic growth. Presence or absence of interaction is indicated.

EPSIN HOMOLOGY (EH)-DOMAIN-CONTAINING PROTEIN 2 (EHD2) is an ATPase, that interacts through the Eps15 homology domain with many endocytotic proteins. EHD2 was shown in plants to be crucial for endocytosis (Bar et al., 2008; Bar and Avni, 2009).

To confirm the interaction of VPS2.1 and EHD2 with AMSH3, the full length ORF of these proteins were cloned into a GBD vector and were tested in a targeted Y2H assay for interaction with GAD-AMSH3 and GAD-AMSH3(AXA) (Figure 7). AMSH3, fused to GAD, shows no auto-activation and was suitable for confirming the results obtained in the Y2H screen. In this assay, the full length VPS2.1 interacted with AMSH3 while the full length EHD2 did not. From the proteins obtained from the screen I continued the validation for the interaction between AMSH3 and VPS2.1.

3.1.2 AMSH3 interacts directly with VPS2.1 and not with VPS2.2 and VPS2.3

The *Arabidopsis* genome contains three homologues to the yeast Vps2p, namely VPS2.1, VPS2.2 and VPS2.3. Since VPS2.1 was found in the screen as an interactor of AMSH3, I set out to verify whether the other two homologues of VPS2.1 are also able to interact with AMSH3. For this purpose, AMSH3 and AMSH3(AXA) fused to GAD were tested in yeast for interaction with GBD fused VPS2 proteins (Figure 8A). Both active and inactive AMSH3 interacted with VPS2.1 but not with VPS2.2 and VPS2.3. To confirm the expression of the different constructs, total protein extract
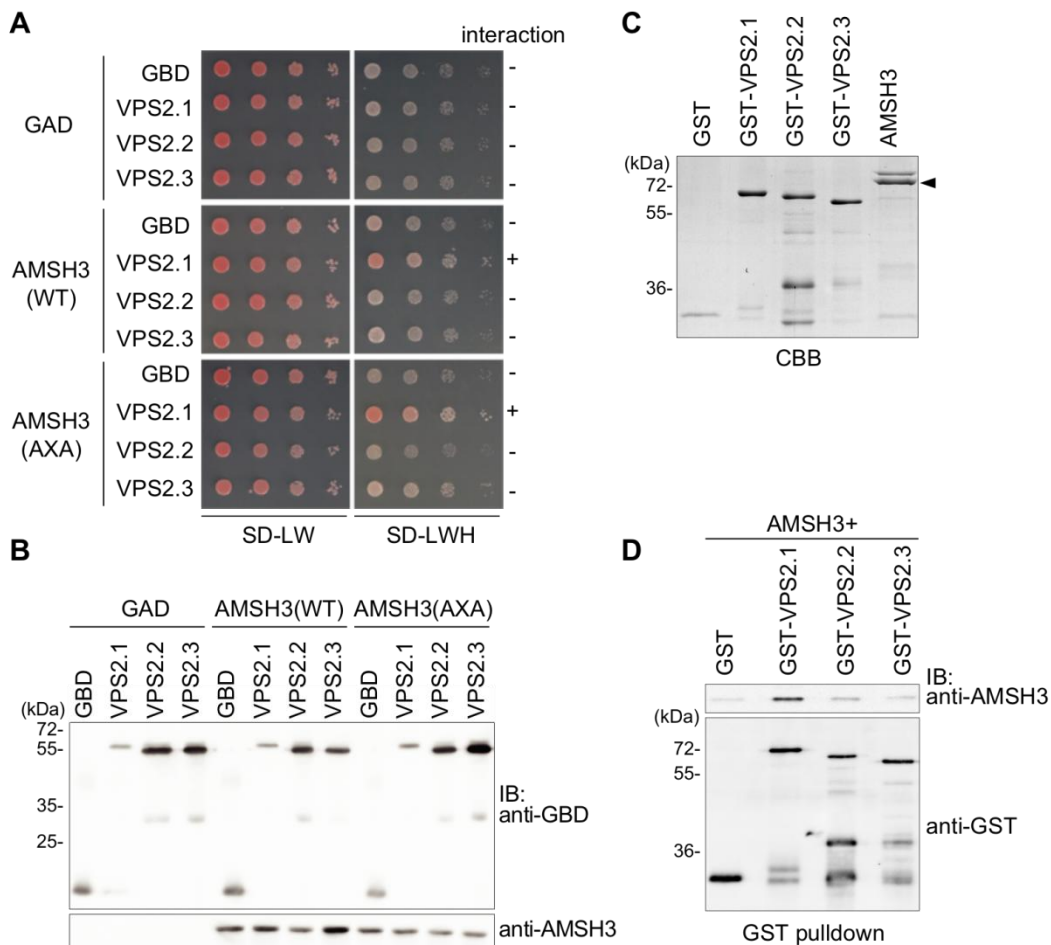
Figure 8: AMSH3 interacts specifically with VPS2.1.
A) Y2H interaction of GAD-AMSH3 or AMSH3(AXA) with GBD fused VPS2 *Arabidopsis* homologs VPS2.1, VPS2.2 and VPS2.3. Transformants containing both plasmids are plated on SD-LW medium and on SD-LWH for their auxotrophic growth test.
B) Protein expression of GAD and GBD constructs shown in (A) is verified by immunoblot using anti-HA and anti-GBD antibodies, respectively.
C) Recombinant GST, GST-VPS2.1, GST-VPS2.2, GST-VPS2.3 and AMSH3 subjected to SDS-page and CBB staining. Arrowhead indicates the right AMSH3 band.
D) Purified proteins from (C) were used in an *in vitro* binding assay, in which AMSH3 was incubated either with GST, or GST-VPS2.1 or GST-VPS2.2 or GST-VPS2.3. GST pulled-down samples were subjected to immunoblot analysis using an anti-AMSH3 and anti-GST antibody.

from the corresponding yeasts were used in immunoblot analysis with an anti-AMSH3 or anti-GAL4GBD antibody (Figure 8B).

Y2H systems do not necessarily select for direct interactions. Indirect interaction can also be scored, in which endogenous yeast proteins serve as bridges. To study whether AMSH3 and VPS2.1 interact directly or indirectly, an *in vitro* binding assay was performed. For this assay, AMSH3, GST-VPS2.1, GST-VPS2.2, GST-VPS2.3 and GST alone were expressed in and purified from E.*coli.* To estimate the purity and to determine the concentration and of the purified proteins, proteins were subjected to SDS-PAGE and detected by CBB staining, (Figure 8C, D). GST-fused proteins or

GST were mounted on GST Sepharose beads and then incubated with AMSH3. GST was used as negative control. The GST pulled-down samples were subjected to immunoblot analysis with anti-GST and anti-AMSH3 antibodies, to detect the GST fused proteins and AMSH3, respectively (Figure 8D). The immunoblot analysis of the GST pulled-down samples revealed that the amount of AMSH3 pulled-down with GST-VPS2.1 was much higher than with GST-VPS2.2 or GST-VPS2.3. The whole assay was repeated three times and the average amount of AMSH3 pulled in each reaction was quantified. The AMSH3 amount pulled-down with GST was set as background and that of VPS2.1 to 100%. The quantification revealed that only 19.8% and 22.6% were bound to VPS2.2 and VPS2.3, respectively.

Both systems the Y2H and the *in vitro* binding assay display interaction of AMSH3 with only one VPS2 homologue. Interaction of AMSH3 with VPS2.1 suggest a specific role of this interaction or a specific role of VPS2.1 in contrast to VPS2.2 and VPS2.3, with which AMSH3 is coupled with.

3.2 AMSH3 interacts with ESCRT-III subunits

3.2.1 AMSH3 interacts with VPS2.1 and VPS24.1

Direct interaction of AMSH3 with VPS2.1 implies interaction of AMSH3 with ESCRT-III. Studies in yeast and mammals regarding the assembly of ESCRT-III have shown that it consists of two main groups of proteins, the core and the accessory proteins as listed in Table 1. Although VPS2.1 was the only ESCRT-III subunit found in the screen, I was interested to analyze whether AMSH3 is able to interact also with other predicted *Arabidopsis* ESCRT-III subunits, listed in Table 1.

For this reason, interaction of AMSH3 was assessed with other ESCRT-III subunits in a Y2H system. I selected for the interaction assay one protein, the closest homologue to each known yeast ESCRT-III core and accessory protein as shown in Table 1. Thus, the core proteins VPS24.1, VPS20.1 and SNF7.1 and two accessory proteins VPS46.1 and VPS60.1 were tested for interaction with AMSH3 in a targeted Y2H assay (Figure 9A). For VPS46.1 interaction with AMSH3 could not be assessed, because of auto-activation when VPS46.1 is fused to GBD (data not shown). Therefore, interaction of VPS46.2 was tested with AMSH3 (Figure 9A). In this assay AMSH3 interacted with VPS24.1 and VPS60.1. The expression of the proteins was

verified by immunoblot analysis. Total protein extracts from the corresponding yeast cells were subjected to immunoblot using an anti-GBD antibody for the GBD fused ESCRT-III subunits and with an anti-AMSH3 antibody for AMSH3 detection (Figure 9B).

To test whether AMSH3 can interact directly with VPS24.1 or VPS60.1, an *in vitro*
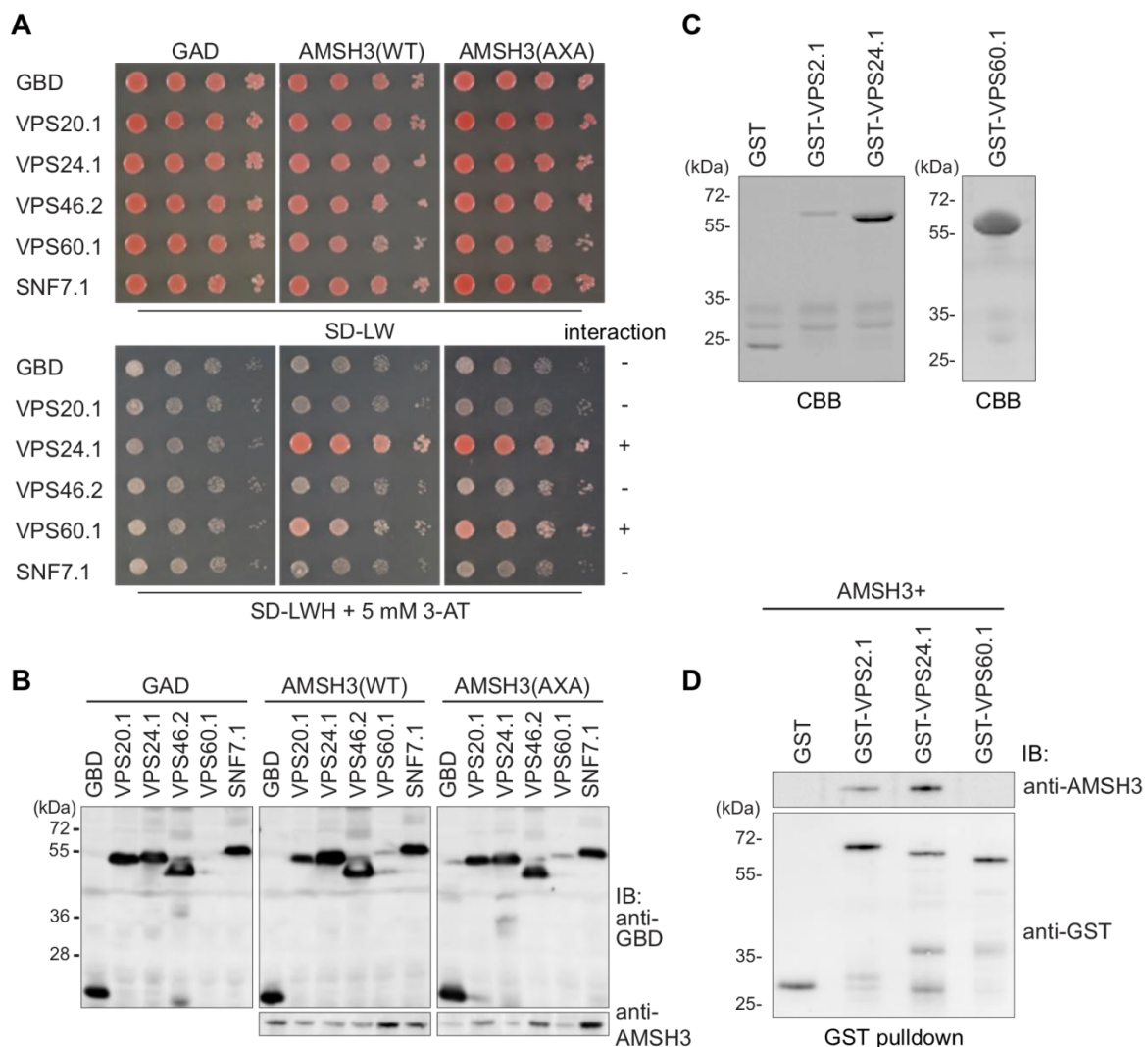
Figure 9: AMSH3 interacts with ESCRT-III subunits VPS2.1, VPS24.1 and VPS60.1.
A) Y2H analysis of GAD-AMSH3 and GAD-AMSH3(AXA) with BD fused ESCRT-III subunits VPS20.1, VPS24.1, VPS46.2, VPS60.1 and SNF7.1. Transformants were spotted on SD-LW medium and on SD-LWH, supplemented with 5 mM 3-AT to test for their auxotrophic growth. Presence or absence of interaction is indicated.
B) Expression analysis of yeast transformants shown in (A). Total proteins from the corresponding yeast cells were extracted and subjected to immunoblot analysis using anti-GBD and anti-AMSH3 antibodies for detection of BD-ESCRT-III and AMSH3, respectively.
C) Recombinant AMSH3, GST, GST-VPS2.1, GST-VPS24.1 and GST-VPS60.1 resolved on SDS-page and stained with CBB.
D) *In vitro* binding assay of AMSH3 with GST, GST-VPS2.1, GST-VPS24.1 and GST-VPS60.1. After incubation, GST pulled-down beads were analyzed on immunoblot using an anti-AMSH3 and anti-GST antibodies.

binding assay was performed. Recombinant AMSH3 was incubated with GST-VPS2.1, GST-VPS24.1, GST-VPS60.1 and GST(Figure 9C). GST-VPS2.1 was used as a positive control. Immunoblot analysis of the GST pulled-down samples revealed that AMSH3 interacts directly with GST-VPS2.1 and GST-VPS24.1 but not with GST-VPS60.1.

According to these data, AMSH3 interacts directly with two predicted ESCRT-III core proteins VPS2.1 and VPS24.1. However, the possibility that the tested proteins are not incorporated in the plant ESCRT-III system cannot be excluded. Therefore, in future the other *Arabidopsis* ESCRT-III homologues, which were not included in this assay, have to be studied for interaction with AMSH3.

3.2.2 AMSH3 interacts with ESCRT-III subunits in a MIT-MIM1 mediated way.

Next step was to gain insight into the mechanism of the interaction between AMSH3 and the two ESCRT-III subunits. Therefore, the domains that are responsible for the interaction were investigated. AMSH3 possess a microtubule interacting and trafficking domain(MIT) at the amino terminus, aligned with different MIT containing proteins (Isono et al., 2010). This was the only functional domain identified in AMSH3 except the catalytic MPN+ domain. The MIT domain is a protein-protein interaction domain.

To address the question whether the MIT domain is responsible for the interaction of AMSH3 with ESCRT-III subunits, different deletion constructs were generated as shown in Figure 10A. These deletion constructs were tested in a Y2H assay for their ability to interact with VPS2.1 and VPS24.1 (Figure 10B). When the MIT domain (amino acids 16 to 102) was deleted (AMSH3(ΔMIT)) the interaction was lost, indicating that the MIT domain is required for interaction. However, the interaction was not impaired when the catalytic site, the MPN domain, was deleted (AMSH3(ΔMPN)), demonstrating that the catalytic domain does not contribute to the interaction with VPS2.1 or VPS24.1. However, the MIT domain alone (AMSH3(MIT)) was not sufficient for interaction with VPS2.1 or VPS24.1, whereas an amino-terminal extension of 16 amino acids (AMSH3(N102)) restored the ability of AMSH3 to interact at least with VPS24.1. In case of VPS2.1, a carboxyl-terminal extension of 52 amino acids after the MIT domain, AMSH3(N154), was still not sufficient for the
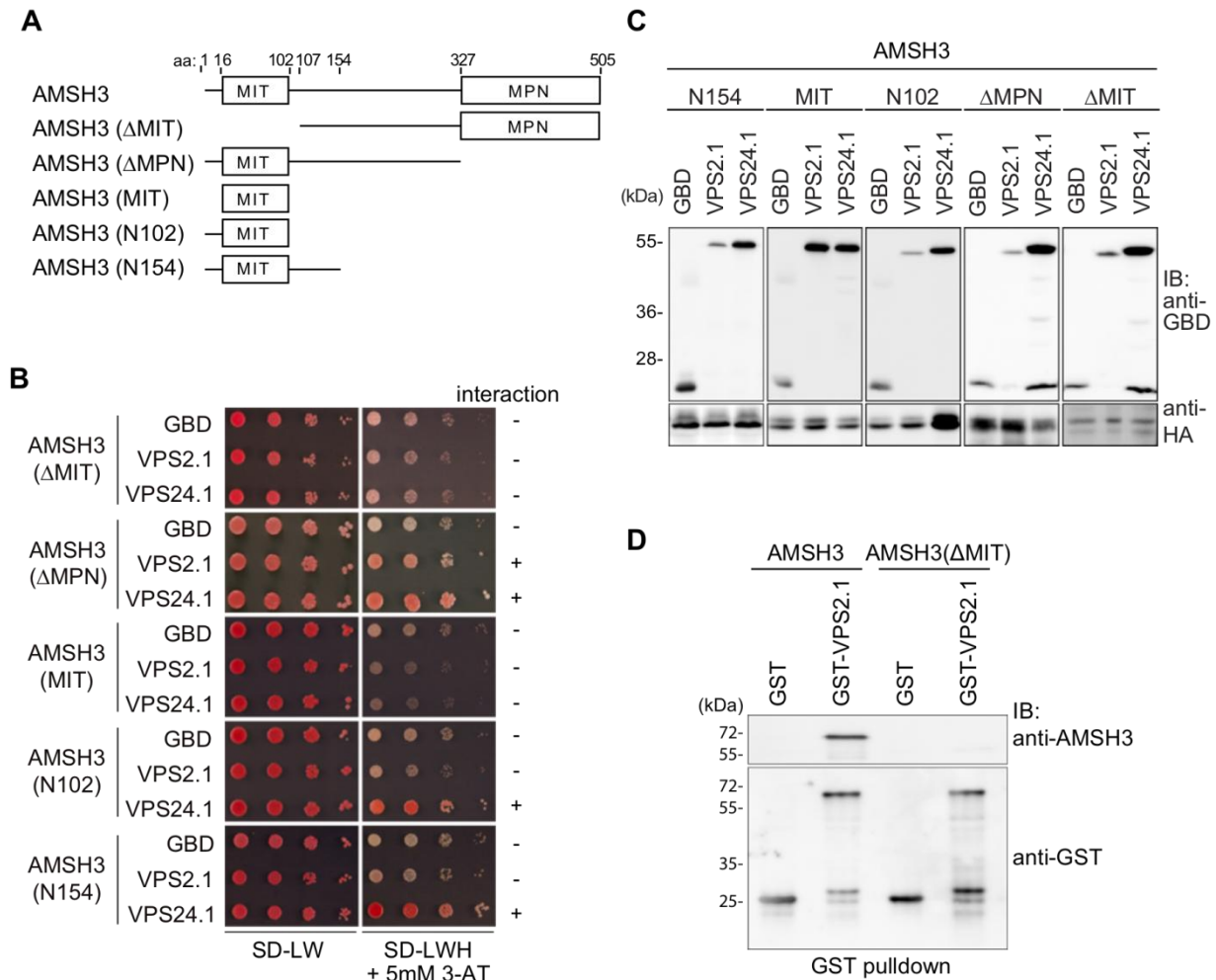
Figure 10: The MIT domain of AMSH3 is necessary for the interaction with VPS2.1 and VPS24.1.
A) Schematic presentation of different truncation constructs of AMSH3.
B) Y2H analysis of AMSH3 truncation constructs depicted in (A) with GBD fused VPS2.1 and VPS24.1. Auxotrophic growth test was performed on SD-LWH plates, supplemented with 5 mM 3-AT. Yeast cells, showing interaction are indicated
C) Immunoblot analysis of total protein extracts from yeast cells in (B) using an anti-HA and anti-GBD antibody for detection of AMSH3 truncated versions and VPS2.1 and VPS24.1, respectively.
D) *In vitro* binding assay of AMSH3 and AMSH3(ΔMIT) with GST and GST-VPS2.1. GST pulled-down samples were analyzed on western blot with an anti-AMSH3 and anti-GST antibody.

interaction. These results show that despite the MIT domain, additional residues are required for interaction with VPS24.1 and VPS2.1. The expression of the different constructs in this Y2H assay was confirmed by immunoblot analyis using an anti-HA and anti-GBD antibody for the detection of GAD and GBD fused proteins, respectively (Figure 10C).

To confirm that the MIT domain is required for the interaction with VPS2.1, an *in vitro* binding assay was performed using recombinant AMSH3(ΔMIT). AMSH3 and AMSH3(ΔMIT) were incubated with GST or GST-VPS2.1. The GST pulled-down samples were analyzed by immunoblotting. The immunoblot revealed that although

the full length AMSH3 was able to bind to GST-VPS2.1, this ability was strongly reduced in case of AMSH3(ΔMIT) (Figure 10D).

Next, the sequence of VPS2.1 was analyzed to find the domain, that is responsible for the interaction with AMSH3. Sequence alignment of *Arabidopsis* VPS2.1 with its counterparts in budding yeast, fruit fly, mouse and human, revealed that VPS2.1 contains a conserved MIT interacting motif 1 (MIM1) domain at the very carboxylterminus (Figure 11A). Studies in yeast have revealed 6 conserved amino acids, compromising the consensus of the MIM1 domain, (D/E)xxLxxRLxxL(K/R) (Kieffer et al., 2008; Obita et al., 2007), present also in *Arabidopsis* VPS2.1. To prove that this MIM1 domain is responsible for the interaction with AMSH3, recombinant GST fused VPS2.1(MIM1) was tested for interaction with AMSH3 in an *in vitro* binding assay (Figure 11B and C). The binding assay revealed that the MIM1 domain of VPS2.1 alone is sufficient for interaction with AMSH3. Sequence alignment of VPS24.1 with its counterparts in yeast, fruit fly, mouse and human revealed that it contains a conserved MIM1 domain (Kieffer et al., 2008) at the very carboxyl terminus (Figure 11D). Therefore it is suggested that VPS24.1 interacts with AMSH3
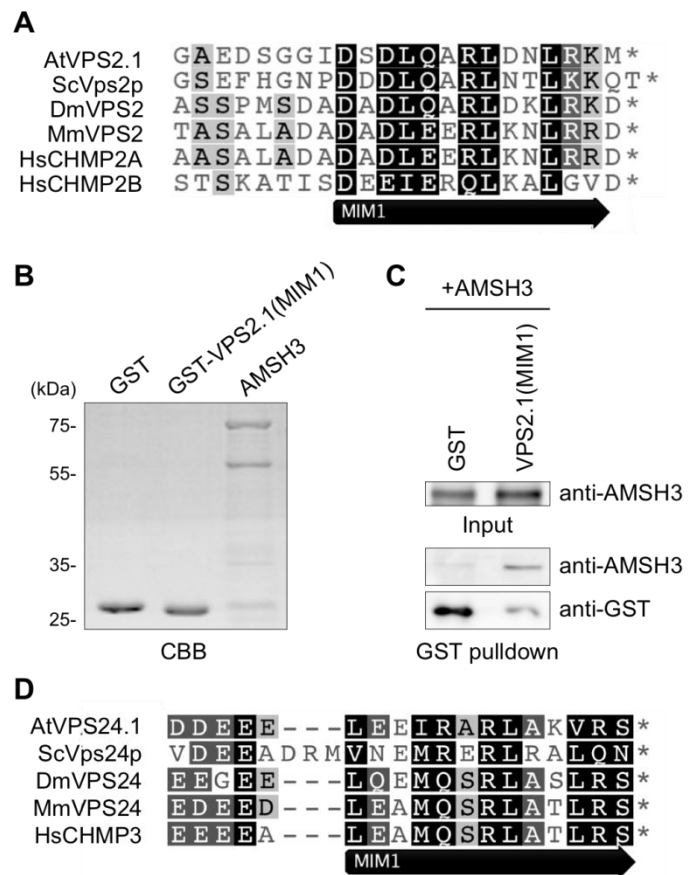
Figure 11: The MIM1 domain of VPS2.1 and VPS24.1 is responsible for interaction with AMSH3.
A) Amino acid alignment of the carboxyl-terminal domain of AtVPS2.1, and its counterparts in budding yeast (ScVps2p), fruit fly (DmVPS2), mouse (MmVPS2) and human (HsCHMP2a, HsCHMP2b), using the MUSCLE algorithm of Geneious software package. The box indicates the MIM1 domain.
B) Recombinant GST, GST-VPS2.1(MIM1) and AMSH3 resolved on SDS page and stained with CBB.
C) *In vitro* binding assay of AMSH3 with GST and GST-VPS2.1(MIM1). Input of AMSH3 (input) and results of pulldown (GST pulldown) are shown on a western blot using an anti-AMSH3 and anti-GST antibody.
D) Amino acid alignment of the carboxyl terminus of AtVPS24.1, and its counterparts in budding yeast, fruit fly, mouse and human using the MUSCLE algorithm of Geneious software package. The MIM1 is indicated

through the MIM1 domain in a MIT-MIM dependent manner.

Taken together, the MIT domain of AMSH3 is necessary for the interaction with the MIM1 motif of VPS2.1 and VPS24.1, presenting a conserved MIT-MIM interaction. Interestingly, besides the sequences compromising the MIT domain of AMSH3, additional residues and different ones are required for interaction with VPS2.1 or VPS24.1, suggesting that they may bind to different interaction surfaces on AMSH3 considering the possibility that VPS2.1 and VPS24.1 are simultaneously binding to AMSH3.

3.2.3 Differences in the MIM1 domain of the VPS2 homologues lead to differential binding affinity to AMSH3

Although the VPS2 proteins share high homology in their amino acid sequences, they have a differential binding affinity towards AMSH3. Characterization of the molecular cause of this differential interaction may provide more detailed information about the interface, where the interaction between AMSH3 and VPS2.1 takes place.

For this reason, the sequences of the MIM1 domain of VPS2.1, VPS2.2 and VPS2.3 were analyzed. Sequence alignment of their amino acids of the carboxyl-terminal part showed that all three proteins contain a MIM1 domain (Figure 12A). However, in case of VPS2.2 and VPS2.3 the spacing between the two first conserved amino acids, the aspartic acid and the leucine, is altered. Instead of two, only one amino acid is present, as indicated by the arrow (Figure 12A). To examine whether this difference in the MIM1 domain is the cause for the non-interaction with AMSH3, mutations were introduced into the MIM1. A mutant variant of VPS2.1 was generated, where the first aspartic acid (D) of MIM1 (D212) was substituted by an asparagine (N) (VPS2.1D212N). For VPS2.3, an additional aspartic acid was inserted between the two first conserved amino acids in the MIM1 domain (Figure 12B). The mutant variants named VPS2.1(mut) and VPS2.3(mut) were fused to GST and expressed in and purified from *E.coli*. The purified proteins were resolved on a CBB gel (Figure 12C). The purified proteins were then used in an *in vitro* binding assay, in order to test their binding affinity to AMSH3 (Figure 12D). The wild-type proteins fused to GST as well GST alone were used as controls. The binding affinity of VPS2.1(mut) was reduced in comparison to VPS2.1. Quantification of the AMSH3 bands from three independent experiments showed a reduction of 65.1 % in the
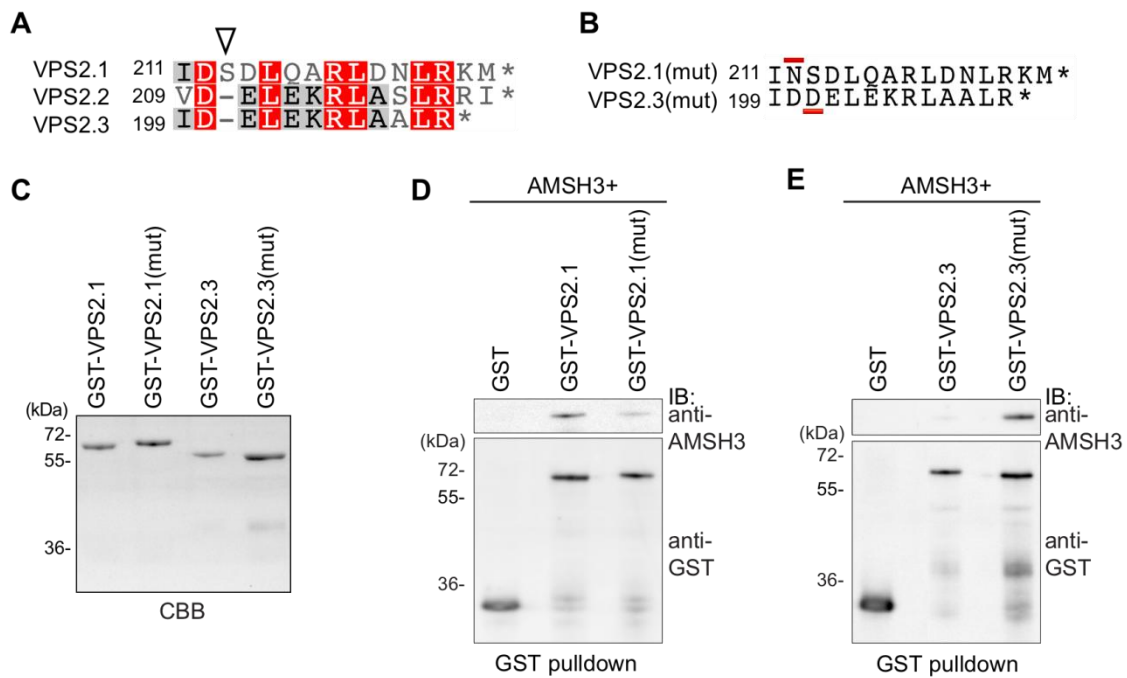
Figure 12: The conserved MIM1 domain in VPS2.1 leads to specific interaction with AMSH3.
A) Amino acid alignment of the MIM1 domain of VPS2.1, VPS2.2 and VPS2.3. Conserved amino acids compromising the MIM1 are highlighted by red boxes. The open arrowhead indicates a gap between the fist two conserved residues in the MIM1 of VPS2.2 and VPS2.3.
B) Mutant variants of VPS2.1 and VPS2.3. In VPS2.1(mut) the first conserved aspartate in the MIM1 (D212) is mutated to an asparagine (N). In VPS2.3(mut) the gab shown in (A) is filled with an aspartate (D). Mutations are indicated by a red line.
C) Recombinant VPS2.1 and VPS2.3, wild type and mutant variants, resolved on SDS-page and stained with CBB. Note, that the mutations within the two VPS2 proteins lead to a slight alteration in their migration pattern on the SDS gel, which might be the result of changes in the disulfide bonds.
D) and **E)** *In vitro* binding assays of AMSH3 with VPS2.1 and VPS2.1(mut) in (D) and VPS2.3 and VPS2.3(mut) in (E). Results are shown on a western blot using anti-AMSH3 and anti-GST antibodies.

binding affinity. Interestingly, in case of VPS2.3, the mutation within the MIM1 domain led to interaction between AMSH3 and VPS2.3(mut) (Figure 12D).

Although all three VPS2 proteins contain a MIM1 domain, these mutational studies in the MIM1 domain of VPS2.1 and VPS2.3 demonstrate that the preferential binding of AMSH3 to VPS2.1 relies on minor differences in the MIM1 domain VPS2.3. The first conserved aspartate and its position in the MIM1 domain are a prerequisite for the binding to the MIT domain of AMSH3. Since the MIM1 domain of VPS2.2 shows the same differences as VPS2.3 compared to VPS2.1, we suggest that VPS2.2 fails to interact with AMSH3 due to the position of the first conserved aspartate in the MIM1 domain.

3.2.4 AMSH3 competes with SKD1 for binding to VPS2.1

Since the differences in the MIM1 domain of VPS2.2 and VPS2.3 imply their binding to AMSH3, it was assessed whether they imply binding to other MIT containing proteins. SKD1 was used to study the binding behaviour of VPS2.1, VPS2.2 and VPS2.3. SKD1 is the *Arabidopsis* homologue of yeast Vps4p and contains a MIT domain (Haas et al., 2007). SKD1 is responsible for the disassembly and the proper function of ESCRT-III. Therefore, I tested whether the wild-type VPS2.1 and VPS2.3 proteins can interact with SKD1. For this purpose recombinant GST, GST-VPS2.1 and GST-VPS2.3 were incubated with His-SKD1 in an *in vitro* binding assay (Figure 13A). The GST pulled-down samples were analyzed on a western blot (Figure 13A). For the detection of His-SKD1, an anti-His antibody was used. The western blot depicts that SKD1 is pulled together with VPS2.1 and VPS2.3, suggesting that SKD1 is able to interact with GST-VPS2.1 and GST-VPS2.3 *in vitro* via its MIT domain.

The analysis was continued with VPS2.1(mut). VPS2.1(mut) was tested for interaction with SKD1 (Figure 13B). The *in vitro* binding assay revealed interaction of SKD1 with VPS2.1(mut). This indicates, that the substitution of the first conserved amino acid of the MIM1 domain could not impair the interaction with SKD1, while it does for AMSH3.

These results demonstrate, that the differences in the MIM1 domain of VPS2.1 and VPS2.3 display an interaction profile specific only for the MIT domain of AMSH3, but not for the MIT domain of SKD1. Moreover, I could show that by mutating the first conserved aspartate of the MIM1 domain of VPS2.1 (VPS2.1(mut)) the binding affinity to AMSH3 is almost eliminated but not to SKD1. These mutational studies show that either the binding affinity of VPS2.1 to SKD1 is stronger than to AMSH3 or that different sites contribute to the binding of the MIM1 domain of VPS2.1.

This poses the question whether SKD1 and AMSH3 can simultaneously bind to VPS2.1 or whether they compete for binding to VPS2.1. To answer this question an *in vitro* competition assay between AMSH3 and SKD1 for binding to VPS2.1 was performed (Figure 13C). In this assay, GST, GST-VPS2.1 and GST-VPS24.1 were first incubated with AMSH3 and then a certain amount of His-SKD1 was added to the reaction. Three reactions with increasing amounts (6 pmol, 72 pmol, 216 pmol) of SKD1 were performed for each GST fused protein. Samples were pulled-down on

GST and analyzed on western blot. Neither AMSH3 nor SKD1 was bound to GST. GST-VPS24.1 was used as negative control for the biding of SKD1, because VPS24.1 binds *in vitro* to AMSH3 (Figure 8D) but not to SKD1 (Figure 13A). In the VPS24.1 reactions, AMSH3 was bound to VPS24.1, independently of the amount of SKD1. Whereas, in the three reactions, in which AMSH3 and SKD1 were incubated with GST-VPS2.1 the amount of AMSH3 bound to GST-VPS2.1 was decreasing when SKD1 was increased. GST-VPS2.1 was also individually incubated with AMSH3 or SKD1 for additional controls. The amount of AMSH3 bound to GST-VPS2.1 was stable in each reaction whereas that of SKD1 was dosage-depended.
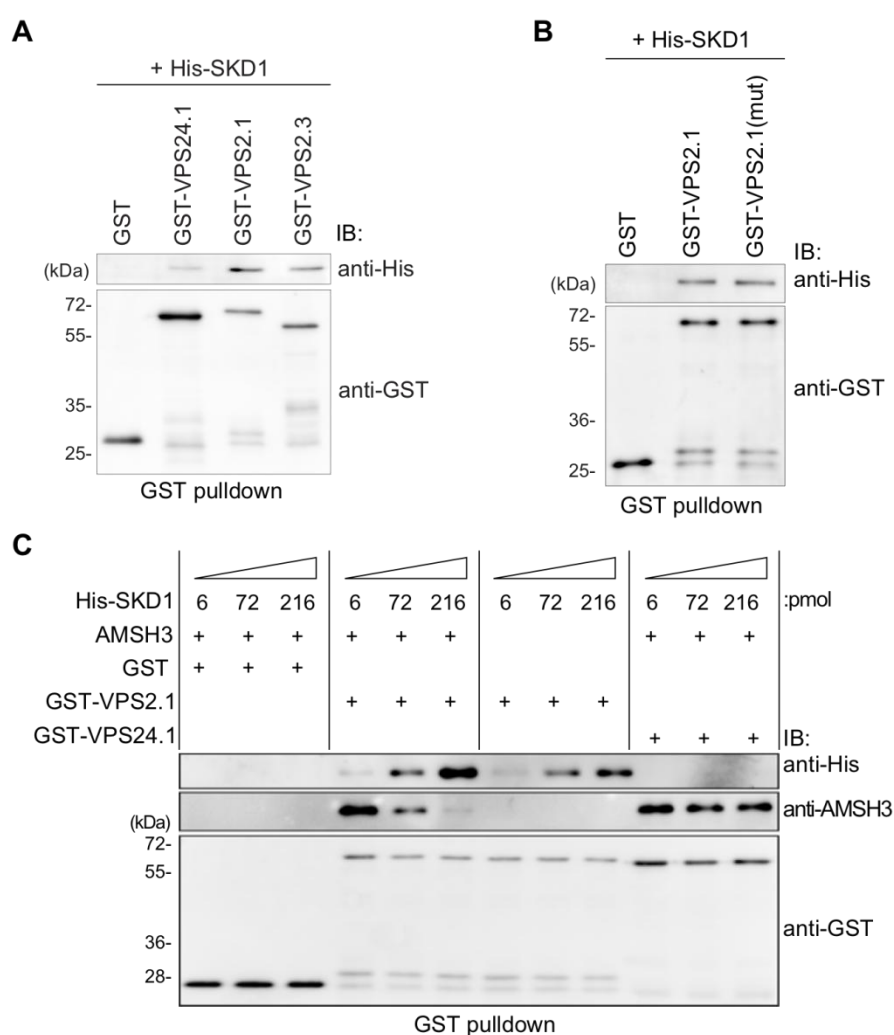
Figure 13: AMSH3 competes with SKD1 for binding to VPS2.1.
A) and **B)** *In vitro* binding assays of His-SKD1 with GST-VPS24.1, GST-VPS2.1 and VPS2.3 in (A) and with GST-VPS2.1 and GST-VPS2.1(mut) in (B). The GST moiety was used as negative control. GST pulled-down samples are analyzed on an immunoblot using anti-His and anti-GST, for the recognition of His-SKD1 and GST fused proteins, respectively.
C) Immunoblot analysis of GST pulled-down samples from an *in vitro* competition assay between AMSH3 and His-SKD1 for binding to GST, GST-VPS2.1 and GST-VPS24.1. In the assay GST fused proteins were incubated with 6 pmol AMSH3 in the presence of 6, 72 or 216 pmol of His-SKD1. Anti-AMSH3, anti-His and anti-GST antibodies were used for the recognition of the different proteins.

VPS2.1 interacts directly with AMSH3 and SKD1 *in vitro*, suggesting a role of VPS2.1 in the recruitment of SKD1 to the complex. AMSH3 and SKD1 compete for binding to VPS2.1. This competition implies a functional regulation between AMSH3 and SKD1 at the level of interaction with VPS2.1 and furthermore at MVB sorting. AMSH3 may regulate the association of SKD1 to ESCRT-III and the following disassembly of the complex, by masking the VPS2.1 binding site. SKD1 in turn associates with VPS2.1 by outcompeting AMSH3 and terminating the further deubiquitination of receptors or ESCRT components by AMSH3.

3.3 *In vivo* interaction of AMSH3 with ESCRT-III

3.3.1 AMSH3 interacts *in vivo* with true ESCRT-III subunits

The *in vitro* data obtained until here support the idea that AMSH3 is involved in the endocytosis pathway through the interaction with VPS2.1 and VPS24.1. To prove a putative function of AMSH3 in context with the two VPS proteins, the interaction has to be confirmed *in vivo*.

Initially I performed a co-immunoprecipitation assay (Co-IP). For this purpose, antibodies against the full-length proteins of VPS2.1 and VPS24.1 were generated. VPS2.1 and VPS24.1 were expressed in and purified from *E.coli* and used for immunization of a rat and a rabbit, respectively, to produce specific antibodies (Figure 14A). The obtained serums were purified using Hi-Trap IgG columns (GE Healthcare) and NHS-activated HP columns (GE Healthcare). The purified antibodies were tested on immunoblot for their ability to recognize the corresponding proteins. The anti-VPS2.1 antibody was tested for its specificity towards VPS2.1, using total protein extract from yeast cells transformed with GBD fused VPS2.1, VPS2.2 and VPS2.3 (Figure 14B). Anti-VPS2.1 could specifically recognize GBD-VPS2.1. VPS2.1 fused to YFP could be detected in total protein extract from UBQ10:YFP-VPS2.1 transgenic seedlings, however, the endogenous protein was not detectable (Figure 14C). The anti-VPS24.1 antibody was tested against total protein extracts from *Arabidopsis* cell culture derived protoplasts, transformed with a 35S:VPS4.1 construct (Figure14D). Protein extracts from untransformed protoplasts were used as control. The overexpressed VPS24.1 could be detected while the endogenous

VPS24.1 in the untransformed cells was hardly detectable. In total protein extract from wild-type (Col-0) plants or 35S:VPS24.1-HA transgenic plants, VPS24.1-HA as well as endogenous VPS24.1 were recognized by the antibody (Figure 14E). Recombinant VPS24.1 was used in the immunoblot as reference for the right height (Figure 14E).

Since the antibodies could specifically recognize VPS2.1 and VPS24.1, they were used in a Co-IP to prove *in vivo* interaction of VPS2.1 or VPS24.1 with AMSH3. After performing an immunoprecipitation assay with the anti-VPS2.1 antibody, VPS2.1 could not be detected, indicating an unstable protein that cannot be used for validating the interaction with AMSH3 through Co-IP. In case of VPS24.1, although the protein could be immunoprecipitated with the anti-VPS24.1 antibody, however, AMSH3 was not co-immunoprecipitated.

The negative result from the Co-IP of VPS24.1 with AMSH3 may indicate that the interaction of AMSH3 with ESCRT-III is transient. Therefore, I resolved their co-
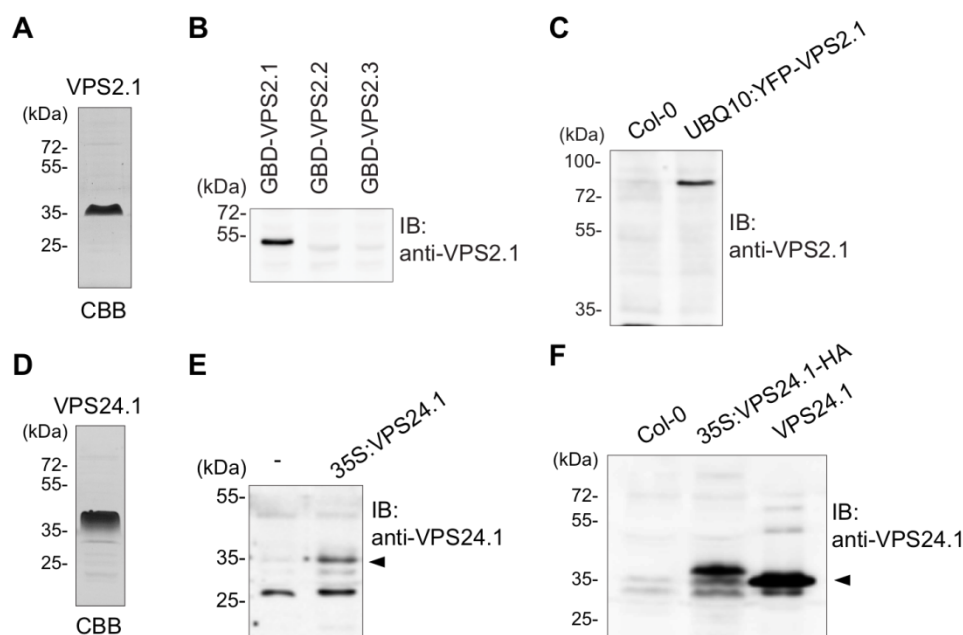
Figure 14: Anti-VPS2.1 and anti-VPS24.1 antibodies recognize specifically the corresponding proteins.
A) and **D)** Recombinant VPS2.1 (A) and VPS24.1 (D) were used for the immunization of a rat and rabbit, respectively. A sample from each recombinant protein was resolved on SDS-page and stained with CBB.
B) and **C)** Immunoblot analysis of total protein extracts from yeast cells transformed with GBD, GBD-VPS2.1, GBD-VPS2.2 and GBD-VPS2.3 (B) and of total protein extracts from wild type (Col-0) and transgenic plants containing UBQ10:YFP-VPS2.1 (C), using the anti-VPS2.1 antibody.
E) and **F)** Immunoblot analysis of total protein extracts from untransformed or transformed *Arabidopsis* protoplasts with 35S:VPS24.1 (E) and of total protein extracts from Col-0 and transgenic plants containing 35S:VPS24.1-HA, compared to recombinant VPS24.1, using the anti-VPS24.1 antibody.

localization in a transient expression system. AMSH3 was fused at the amino terminus with an YFP tag and expressed under its own promoter and VPS2.1 was fused at the amino terminus with a mCherry tag and overexpressed under an UBQ10 promoter. The fusion proteins were co-expressed in *Arabidopsis* cell derived protoplasts and analyzed by a confocal laser-scanning microscope. The confocal analysis showed that both proteins exhibit cytoplasmic localization in the protoplasts (Figure 15A). However, the cytoplasmic localization of the proteins itself does not provide enough evidence about their *in vivo* interaction.

In order to verify their co-localization, I made use of the function of SKD1/VPS4. SKD1/VPS4 is recruited to ESCRT-III through interaction with subunits of the complex (Saksena et al., 2009; Teis et al., 2008). The ATPase activity of SKD1/VPS4 induces the disassembly of the complex and proper invagination of the cargos into MVBs (Saksena et al., 2009). When the activity of SKD1/VPS4 is disrupted by mutations within the catalytic domain, the complex is not disassembled and large endosomal compartments are formed, named class E compartments, visible under the microscope (Babst et al., 1997). In *Arabidopsis* an inactive variant, called SKD1(EQ), results in the formation of class E compartments (Haas et al., 2007; Shahriari et al., 2010). If VPS2.1 and/or VPS24.1 are interacting with AMSH3 *in vivo*, they should both accumulate in class E compartments upon SKD1(EQ) expression, provided that VPS2.1 and VPS24.1 are ESCRT-III subunits acting in the endosomal trafficking pathway.

The behaviour of VPS2.1 upon the expression of SKD1(EQ) was examined UBQ10:YFP-VPS2.1 was co-expressed with 35S:HA-SKD1(EQ) or 35S:HA-SKD1(WT) in protoplasts. 35S:HA-SKD1(WT) was used as a control, to exclude the possibility, that the overexpression of SKD1 itself has an effect on the localization of the proteins. The overexpression of SKD1(WT) did not affect the cytosolic localization of VPS2.1 (Figure 15B). However, when VPS2.1 was co-expressed with SKD1(EQ), the localization of the YFP signal changed and instead of cytosolic localization class E compartments were visible within the cytosol. In 95% of the cells (n=47) YFP-VPS2.1 was relocated to SKD1(EQ) induced class E compartments. When VPS24.1, fused to the carboxyl terminus with a GFP tag under the control of 35S promoter, was expressed in protoplasts it localized in the cytosol (Figure 15C). The cytosolic localization was sustained even after the co-expression of 35S:HA-SKD1(WT). However, when it was co-expressed with 35S:HA-SKD1(EQ), VPS24.1

localized to class E compartments (Figure 15C). VPS2.1 and VPS24.1 co-localized in SKD1(EQ) induced compartments (Figure 15D). The co-localization of them to class E compartments proposes that they belong to the same complex, the ESCRT-III.

The next step was to study the behaviour of AMSH3 towards the expression of SKD1(EQ). AMSH3:YFP-AMSH3 was co-expressed with 35S:HA-SKD1(EQ) and in 31% of the protoplasts (n=45) AMSH3 signals were localized to class E compartments (Figure 16A). AMSH3 reacted to SKD1(EQ) expression but not to the
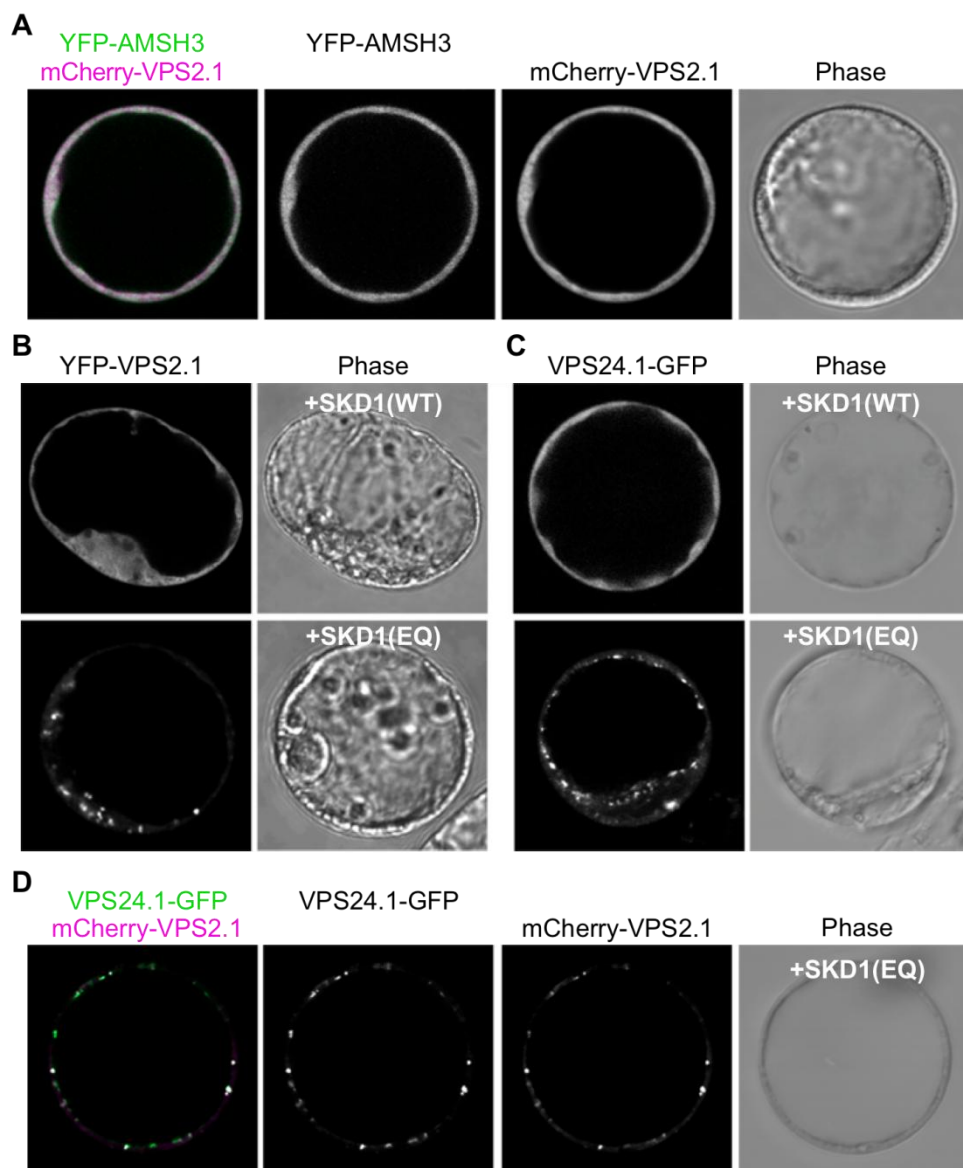
Figure 15: VPS2.1 and VPS24.1 co-localize in SKD1(EQ) induced compartments.
A) UBQ10:mCherry-VPS2.1 co-expressed with AMSH3:YFP-AMSH3 in *Arabidopsis* derived protoplasts and analyzed with a confocal laser scanning microscope.
B) and **C)** Co-expression of 35S:HA-SKD1 or 35S:HA-SKD1(EQ) with UBQ10:YFP-VPS2.1 (B) or 35S:VPS24.1-GFP (C) in *Arabidopsis* protoplasts. Note that the localization of the VPS2.1 and the VPS24.1 signals change after expression of SKD1(EQ) compared to co-expression with SKD1(WT).
D) UBQ10:mCherry-VPS2.1 with 35S:VPS24.1-GFP expressed together with 35S:HA-SKD1(EQ) in protoplasts. VPS2.1 and VPS24.1 signals overlap to SKD1(EQ) induced compartments.
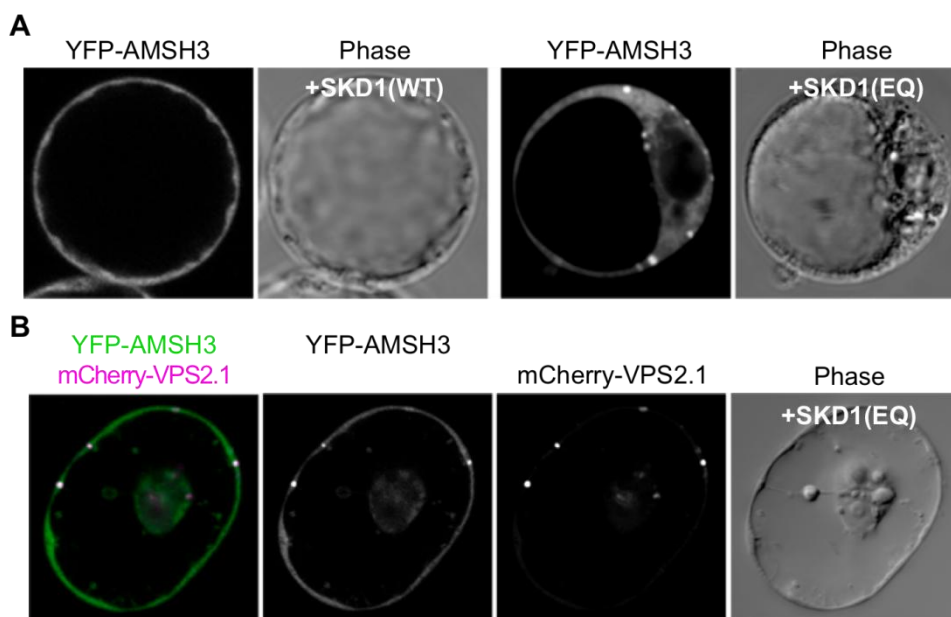
Figure 16: AMSH3 and VPS2.1 co-localize in SKD1(EQ) induced compartments.
A) Confocal analysis of *Arabidopsis* derived protoplasts transformed with AMH3:YFP-AMSH3 and 35S:HA-SKD1(WT) (left panel) or 35S:HA-SKD1(EQ) (right panel). AMSH3 signals are relocated from the cytosol to compartments after SKD1(EQ) expression.
B) Co-localization of AMSH3:YFP-AMSH3 and UBQ10:mCherry-VPS2.1 to SKD1(EQ) induced class E compartments.

same extend as VPS2.1, suggesting that AMSH3 is transiently associated with the endosomal trafficking machinery and/or that AMSH3 has additional interacting partners and is playing a role in other distinct pathways. Transient interaction with ESCRT-III might be the reason for ineffective pulling AMSH3 together with VPS24.1.

Since VPS2.1, VPS24.1 and AMSH3 are re-localized to SKD1(EQ) induced compartments, their co-localization in these compartments was investigated. When AMSH3:YFP-AMSH3 and UBQ10:mCherry-VPS2.1 were co-expressed with SKD1(EQ), AMSH3 and VPS2.1 signals were overlapping to SKD1(EQ) induced compartments (Figure 16B).

From the results obtained from the localization of VPS2.1, VPS24.1 and AMSH3 in *Arabidopsis* derived protoplasts, after the expression of the dominant negative form of SKD1, it can be assumed that VPS2.1 and VPS24.1 are subunits of ESCRT-III working in the endosomal sorting system and that they are interacting *in vivo* with AMSH3.

3.3.2 VPS2.1 is important for plant development and the only VPS2 homologue incorporated in ESCRT-III

Yeast and mammalian VPS2 homologues belong to ESCRT-III and play a role in endocytosis (Babst et al., 2002b; Babst et al., 1998; Bowers et al., 2004; Morita et al., 2010; Teis et al., 2008). For *Arabidopsis* VPS2.1 I could already show that it is relocated upon SKD1(EQ) expression to class E compartments, suggesting a role at the level of MVB formation. The next objective was to inspect the role of VPS2.1 in endocytosis and to address the putative implication of VPS2.2 and VPS2.3 in this pathway.

I first studied the reaction of VPS2.2 and VPS2.3 towards the expression of SKD1(EQ) in protoplasts. VPS2.2 and VPS2.3 were fused at the amino terminus with a fluorescently tag and expressed in protoplasts. The fusion proteins UBQ10:YFP-VPS2.2 and 35S:YFP-VPS2.3 were located in the cytosol (Figure 17A and B, upper panel). The co-expression of 35S:HA-SKD1(WT) did not affect this localization (Figure 17A and B, middle panel). Even after the co-expression of 35S:HA-SKD1(EQ), in most of the expressing protoplasts the cytosolic localization of the proteins was not altered (Figure 17A and B, lower pannel). In contrast to VPS2.1, where 95% of the cells (n=47) showed apparent signal in class E compartments (Figure 15B), only 18% (n=40) and 26% (n=59) of cells accumulated YFP-VPS2.2 and YFP-VPS2.3, respectively to SKD1(WQ) induced class E compartments (Figure 17C). The expression of HA-SKD1(WT) and HA-SKD1(EQ) was verified by western blot using an anti-HA antibody (Figure 17D).

VPS2.1 is the only VPS2 homologue that reacts to the expression of SKD1(EQ) and is located to class E compartments while VPS2.2 and VPS2.3 remain cytosolic. These findings, suggest that only VPS2.1 is incorporated in the classical ESCRT-III. VPS2.2 and VPS2.3 may function in another context and may participate in other pathways with which AMSH3 is not related, since it is not interacting with these two proteins.

To gain information about the function of VPS2.1, I analyzed an *Arabidopsis* mutant of *VPS2.1* and compared it to this of *VPS2.2* and *VPS2.3*. A T-DNA insertion line for each VPS2 homologue was ordered from the stock center and was first analyzed regarding its phenotype. In *VPS2.1* the T-DNA insertion lies in the 4th exon, in *VPS2.2* in the 8th exon and in *VPS2.3* in the 2nd exon (Figure 18A and Figure 19A).

A YFP-VPS2.2 Phase **B** YFP-VPS2.3 Phase

+SKD1(WT)

+SKD1(EQ)

C ■ Compartments ■ No compartments

D

YFP-VPS2.2   YFP-VPS2.3

IB:
anti-HA
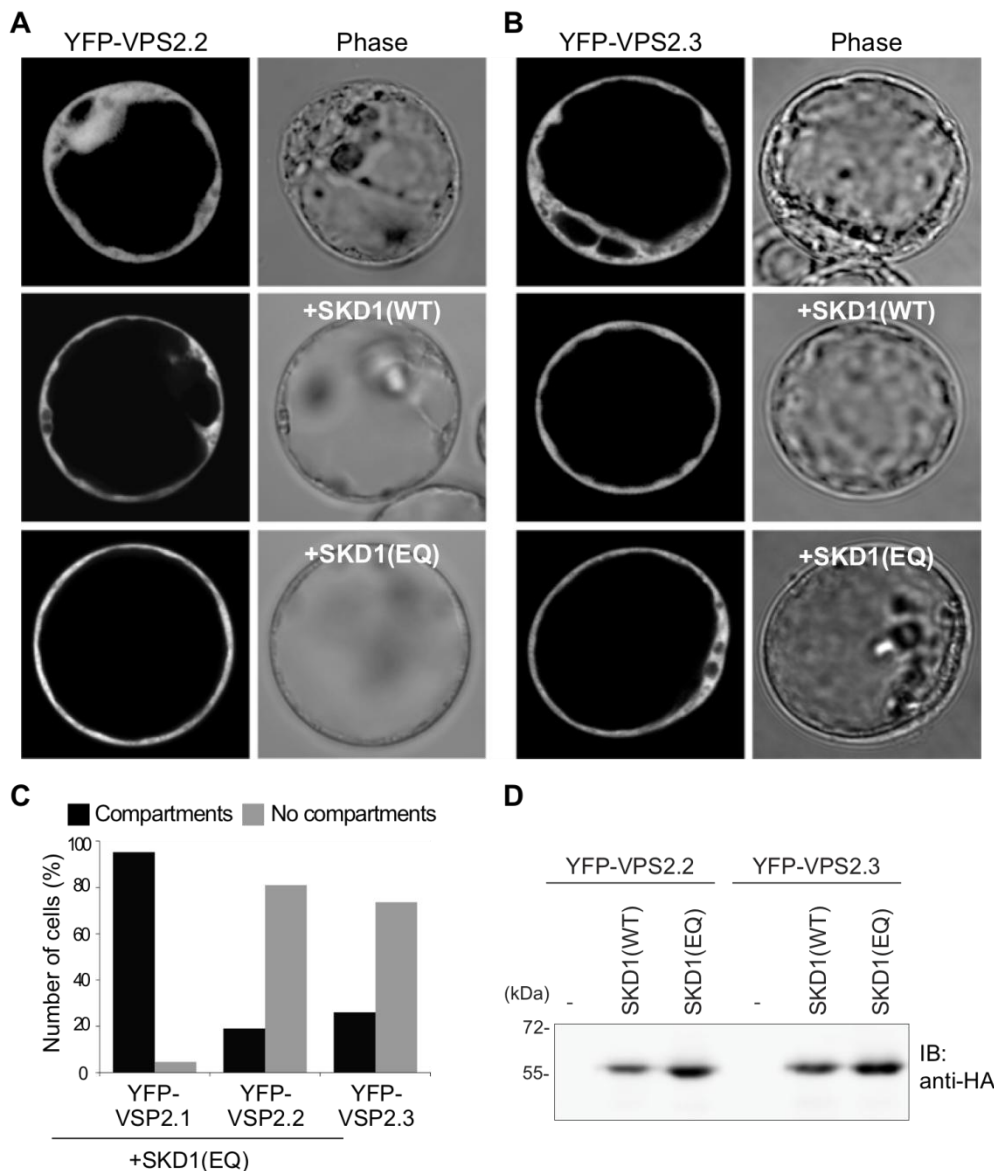
Figure 17: VPS2.2 and VPS2.3 do not localize to SKD1(EQ) induced class E compartments.
A) and **B)** Localization analysis of UBQ10:YFP-VPS2.2 and 35S:YFP-VPS2.3 co-expressed with 35S:HA-SKD1 or 35S:HA-SKD1(EQ) in *Arabidopsis* derived protoplasts.
C) Quantification of *Arabidopsis* protoplasts transformed with UBQ10:YFP-VPS2.1, UBQ10:YFP-VPS2.2 or 35S:YFP-VPS2.3 with 35S:HA-SKD1(EQ) as shown in Figure 15(B), in (A) and in (B), respectively, demonstrating the formation of compartments (solid bars: number of cells with compart-ments; grey bars: number of cells without compartments.
D) For the expression analysis of SKD1(WT) and SKD1(EQ) in the cells shown in (A) and (B), total protein extracts from the corresponding protoplasts were subjected to western blot analysis using an anti-HA antibody.

The insertion site in each gene was confirmed by PCR genotyping using the primers listed in Table 6. In case of *vps2.1*, no homozygous plants could be identified by genotyping. Only heterozygous ones were identified, indicating that the homozygous mutants are embryo lethal. The embryo lethality could be confirmed by

Figure 18: *vps2.1* homozygous mutants are embryo lethal.
A) Schematic representation of the T-DNA insertion site and the primer binding sites in *VPS2.1*. Lines indicate introns and boxes indicate exons (black boxes: coding region, grey boxes: UTRs).
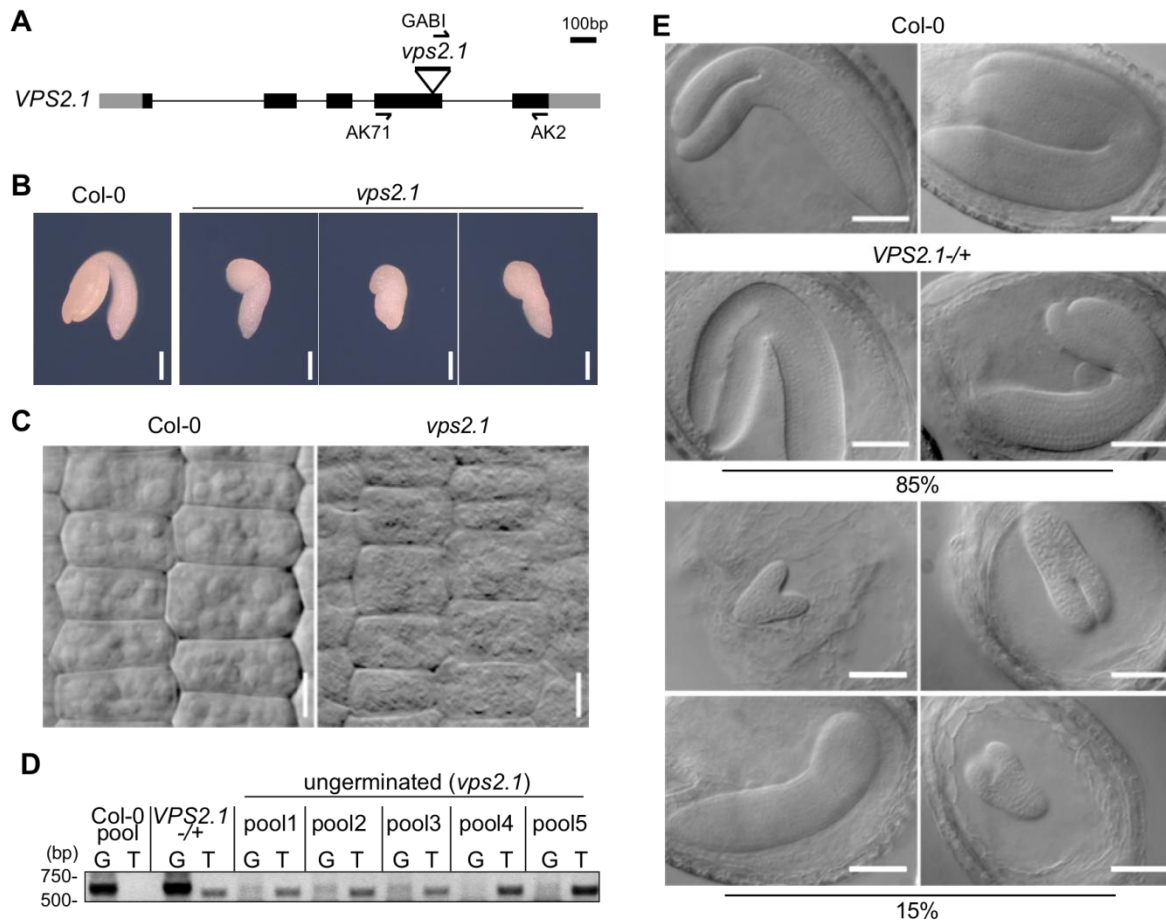**B)** Photographs of wild type (Col-0) and *vps2.1* embryos dissected from dry seeds. Scale bars: 0.2 mm.
C) Confocal microscope images of root epidermal cells from disected embryos from Col-0 and *vps2.1* seeds as shown in (B). Scale Bar: 20 µM.
D) PCR analysis of Col-0 and *vps2.1* embryos as shown in (B). Total DNA was extracted from pools of four embryos. 5 independent pools of embryos dissected from ungerminated seeds of a *VPS2.1-/+* self-pollinated plant were used in the PCR analysis. Genomic DNA from 1 pool of Col-0 embryos and from one *VPS2.1-/+* seedling were used as controls. PCR was performed with either gene specific primers (lanes: G) or a T-DNA left border primer in combination with a gene specific reverse primer (lanes: T). Note that all ungerminated seeds contain embryos homozygous for the T-DNA insertion.
E) Photographs of embryos at walking-stick stage of Col-0 (upper panel) and of a self-pollinated *VPS2.1-/+* (lower panels) plant of the same age. Note that from *VPS2.1-/+* plant 15% of the embryos are delayed in embryogenesis compared to their wild-type looking embryos. Scale bars: 100 µm.

analyzing the progeny of *VPS2.1-/+* heterozygous plants. Within the siliques, 7.2% (n=30) of the seeds were aborted and from the existing seeds 13.7% (n=57) could not germinate after being placed on growth medium. In order to verify whether these ungerminated seeds contain homozygous mutants, the embryos were excised from their seed coat, pooled in a group of four and genomic DNA was extracted, in order to use it for genotyping. Because the yield from one single embryo was not enough, a pool of four was used. Genomic DNA extracted from ungerminated wild-type

seedlings was used as a control. The excised embryos of the ungerminated seeds from a heterozygous *VPS2.1+/-* mutant were smaller than the embryos from wild type and the genotyping revealed that these embryos were homozygous for the insertion (Figure 18B and D). After observing the excised embryos under a confocal scanning microscope, it was obvious that the cells in *vps2.1* homozygous mutants were dead (Figure 18C). In order to find out at which stage the development of the embryos was arrested, embryos from a heterozygous *VPS2.1+/-* mutantplant were examined at different stages and compared to the corresponding embryos from a wild-type plant (Figure 18E). The analysis revealed that 15% of the embryos at the heart or torpedo stagefrom *VPS2.1+/-* mutantplants were delayed compared to the wild type (Table 10), indicating that these delayed embryos are the homozygous *vps2.1* mutants.

For *vps2.2* and *vps2.3*, genotyping revealed homozygous mutant seedlings for both lines. Expression of wild-type *VPS2.2* and *VPS2.3* in *vps2.2* and *vps2.3* mutants, respectively, was verified by semi-quantitative RT-PCR analysis, using gene specific primers for the whole coding region (Figure 19A). Both lines were null
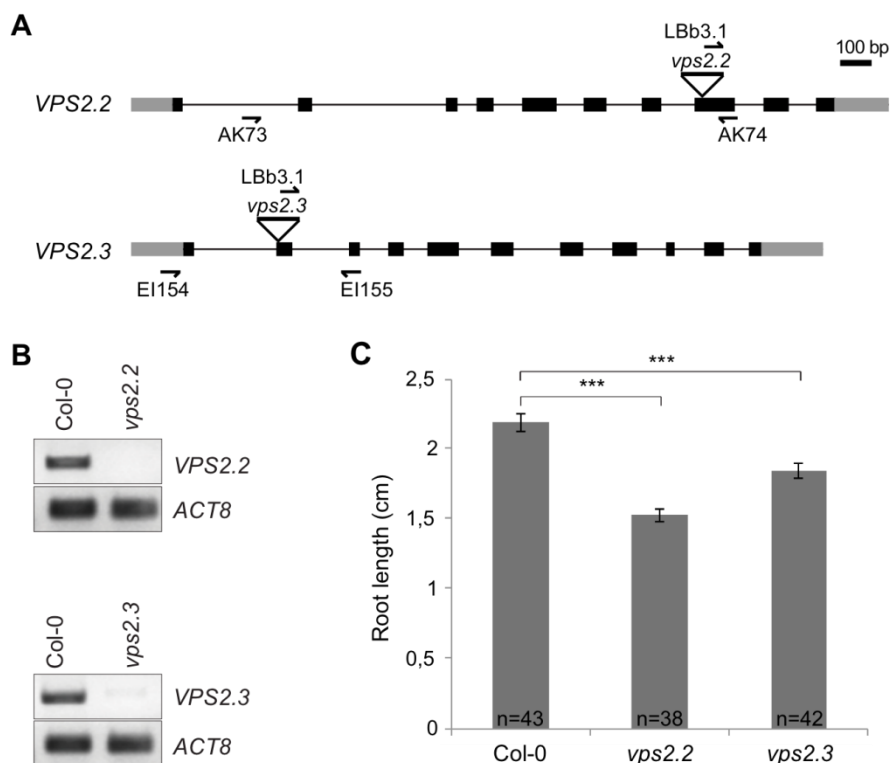
Figure 19: *vps2.2* and *vps2.3* mutants display a reduced root growth phenotype.
A) Schematic representation of the T-DNA insertion site and the primer binding sites in *VPS2.2* and *VPS2.3*. Lines indicate introns and boxes exons (black boxes: coding regions; grey boxes: UTRs).
B) RT-PCR analysis of *VPS2.2* and *VPS2.3* expression in wild type (Col-0) and *vps2.2* (upper panel) and *vps2.3* (lower panel) mutants, respectively. *Actin* (*ACT8*) is used as an internal control.
C) Statistical analysis of root length of 5 days old Col-0, *vps2.2* and *vps2.3* mutant seedlings. Number of seedlings are indicated in each bar. *** indicates significant differences (P<0,001). Erros bars: SE.

mutant lines, since no transcript levels of *VPS2.2* and *VPS2.3* were detectable. Phenotypic analysis of these mutants at seedling stage revealed that the only apparent phenotype of both mutants is the reduced size of the roots compared to wild type of the same age (Figure 19B).

To prove that the phenotypes of the homozygous *vps2.1*, *vps2.2* and *vps2.3* mutants are caused by the knockout of *VPS2.1*, *VPS2.2* and *VPS2.3*, respectively, the mutants were transformed with a wild-type copy of *VPS2.1*, *VPS2.2* and *VPS2.3*, respectively. The short root phenotype observed in *vps2.2* and *vps2.3* mutants could be rescued by the expression of UBQ10:YFP-VPS2.2 and 35S:YFP-VPS2.3, respectively (Figure 20A and B). For the complementation of *vps2.1* mutants, *VPS2.1+/-* heterozygous mutants were first transformed with an UBQ10:YFP-VPS2.1 construct. However, the embryo lethality of the homozygous mutants was not rescued. The failure to complement the lethal phenotype, might depend on the
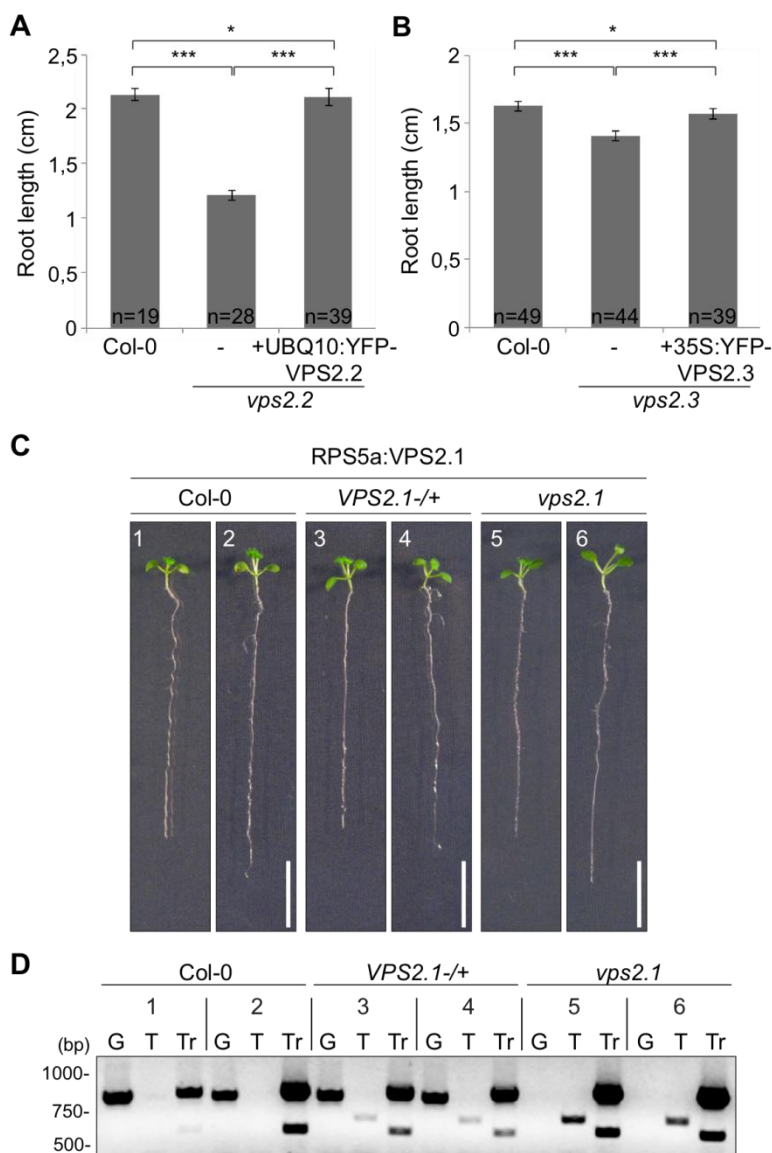
Figure 20: Complementation studies of *vps2.2* and *vps2.3*.
A) and **B)** Complementation of the root growth phenotype of *vps2.2* and *vps2.3* mutants by the expression of UBQ10:YFP-VPS2.2 and 35S:YFP-VPS2.3, respectively. Root length of 5 days old *vps2.2* (A) and 4 days old *vps2.3* (B) mutants compared to those of wild type (Col-0) and mutants seedlings containing the indicated transgenes of the same age. Number of measured seedlings is indicated for each line. * indicates no significant differences (P>0,05) and *** indicates significant differences (P<0,01). Error bars: SE.
C) Photographs of 13 days old Col-0, *VPS2.1+/-* and *vps2.1* mutant seedlings expressing RPS5a:VPS2.1(cDNA). Scale Bar: 1 cm.
D) Genotypic analysis of seedlings shown in (C). PCR was performed with total DNA extracted from the corresponding seedlings with either gene specific primers (lanes: G) or a T-DNA left border primer in combination with the gene specific reverse primer (lanes: T) or a RPS5a forward and a gene specific reverse primer for the transgene (lanes:Tr). * indicates an unspecific band.

UBQ10 promoter, which is not expressed early enough during embryo development, resulting in late expression of VPS2.1. Therefore, *VPS2.1+/-* heterozygous mutants were transformed with a RPS5a:VPS2.1 construct. The RPS5a promoter induces expression already at the stage of two cells stage. After analyzing the progeny of a *VPS2.1+/-* heterozygous mutant containing the RPS5a:VPS2.1 construct, viable homozygous mutants were obtained (Figure 20C).

The phenotype analysis of null mutants of the three VPS2 homologues indicates that VPS2.1 function is not redundant to VPS2.2 and VPS2.3. The embryo lethality of *vps2.1* homozygous mutants suggests that VPS2.1 is already required in embryo development whereas VPS2.2 and VPS2.3 have a slight effect on plant development regarding the root length.

3.3.3 VPS2.1-GFP overexpressing lines are defective in endocytosis

For establishing the role of VPS2.1 in endocytosis, endocytosis dynamics have to be studied in live cells of *vps2.1* mutants. However, *vps2.1* mutants show embryo lethality and are difficult to use, therefore, a dominant negative form of VPS2.1 was generated and introduced in plants. ESCRT-III subunits, as many other VPS proteins, exist as inactive monomers in the cytosol prior to recruitment to the endosomes (Babst et al., 2002a). The autoinhibitory effect, induced by the acidic carboxyl-terminal part of the protein, keeps the proteins in an inactive form (Lata et al., 2008; Shim et al., 2007; Zamborlini et al., 2006). It has been suggested, that interaction with other proteins may release the autoinhibition, so that they can be recruited to the complex. In yeast and mammals it was shown that a large carboxyl-terminal tag, like GFP, leads to the aggregation of VPS proteins, to inhibition of endocytosis and to formation of class E compartments (Howard et al., 2001; Martin-Serrano et al., 2003; Teis et al., 2008; Ward et al., 2005).

Based on this information VPS2.1 was tagged with GFP or mCherry at the carboxyl-terminus under the control of a 35S promoter. The localization and the expression of these fusion proteins were tested in protoplasts. In contrast to the amino-terminal tagged VPS2.1, which exhibited a cytosolic distribution (Figure 15), VPS2.1-GFP localized to cytosolic compartments (Figure 21A). The next step was to examine whether the expression of this construct affects endocytosis. For this end a model cargo, reported to be endocytosed in the *Arabidopsis* protoplast system, was

used. Sven Schellmanns group demonstrated that a plasma membrane ATPase, PMA, is transported to the vacuole through endocytosis, when an ubiquitin molecule is attached to the caroxyl terminus of the protein (Herberth et al., 2012). 35S:PMA-GFP-UB was expressed alone in protoplasts and in 46,9% (n=45) of the cells the signal was visible in the vacuole, while in 44,9% of the cells the GFP signal was located to cytosolic vesicles and in 8,2% of the cells on the tonoplast (Figure 21B). SKD1(EQ) was used as a control for inhibition of endocytosis (Figure 21B). When 35S:GFP-PMA-UB was co-transformed with 35S:HA-SKD1(EQ) only 13,3% (n=15) of the cells showed vacuolar signal, in 80% of the cells GFP-PMA-UB was located to vesicles and in 6,7% on the vacuolar membrane. When PMA-GFP-UB was co-transformed with 35S:VPS2.1-mCherry, PMA was localized to vesicles in 97,9% (n=48) of the cells and in 2,1% on the vacuolar membrane (Figure 21B). The transport of PMA to the vacuole was completely blocked upon expression of 35S:VPS2.1-mCherry, suggesting that VPS2.1-mCherry inhibits endocytosis. Therefore, it can be speculated that VPS2.1 plays an important role in the endosomal trafficking pathway.

Since in the transient system endocytosis was inhibited upon the expression of 35S:VPS2.1-mCherry, a 35S:VPS2.1-GFP construct was transformed into wild-type (Col-0) plants to examine the effects of 35S:VPS2.1-GFP *in planta*. The selected
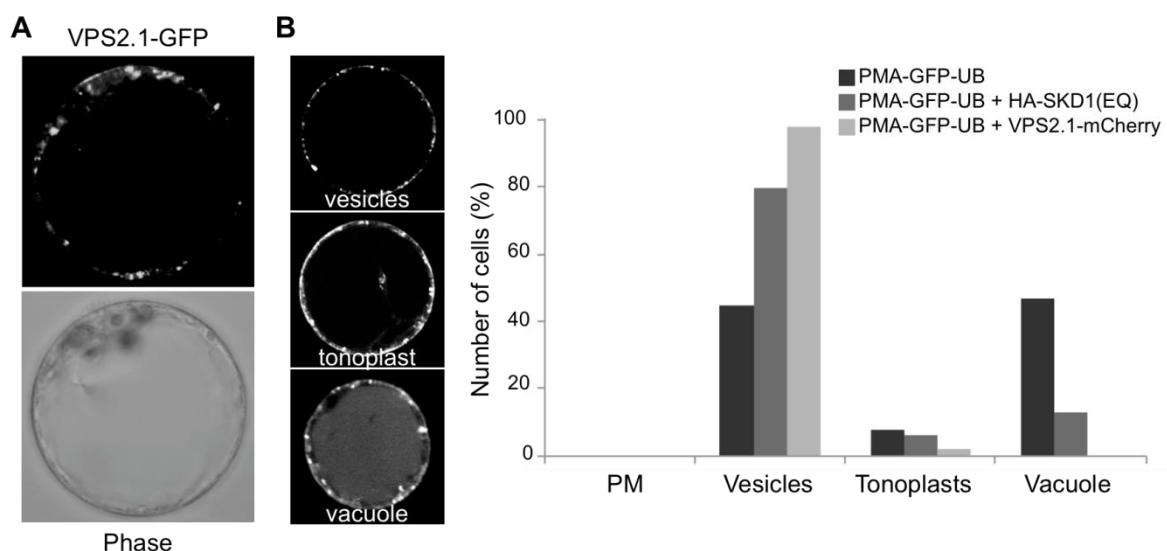
Figure 21: VPS2.1-GFP inhibits the transport of the model cargo PMA-GFP-UB to the vacuole.
A) Confocal image of an *Arabidopsis* cell derived protoplast expressing 35S:VPS2.1-GFP. Note that VPS2.1-GFP is forming cytoplasmic compartments.
B) Statistical analysis of the different localizations of PMA-GFP-UB co-transformed with 35S:HA-SKD1(EQ) or 35S:VPS2.1-GFP in *Arabidopsis* protoplasts (left panel). Pictures of protoplasts displaying the different localizations of PMA-GFP-UB are shown (right panel).

transformants exhibited a dwarf phenotype and had low seed yield (Figure 22A). When VPS2.1-GFP overexpressing seedlings were examined under the confocal microscope, the signal of VPS2.1-GFP was, as in protoplasts, located to cytosolic compartments (Figure 22B). To investigate whether endocytosis was affected in these seedlings, endogenous protein levels of PIN2 were elucidated. PIN2, is an auxin efflux carrier that has been shown in *Arabidopsis* to be endocytosed and degraded in the vacuole (Leitner et al., 2012). Protein extracts from 10 days old seedlings were used for the immunoblot analysis with an anti-PIN2 antibody. As a control for the recognition of the right PIN2 band, membrane fraction from *pin2* mutants (Willige et al., 2011) were used. While comparing the protein levels of PIN2 in VPS2.1-GFP overexpressing and Col-0 seedlings (Figure 22C), PIN2 accumulated in 35S:VPS2.1-GFP seedlings, indicating that degradation of PIN2 by the vacuole is inhibited. This further indicates that endocytosis of PIN2 is impaired in 35S:VPS2.1-GFP lines.

Furthermore, the ubiquitin profile of VPS2.1-GFP containing seedlings was analyzed. Total protein extracts from 7 days old seedlings, grown under continuous light were subjected to immunoblot analysis with an anti-Ubiquitin antibody (Figure
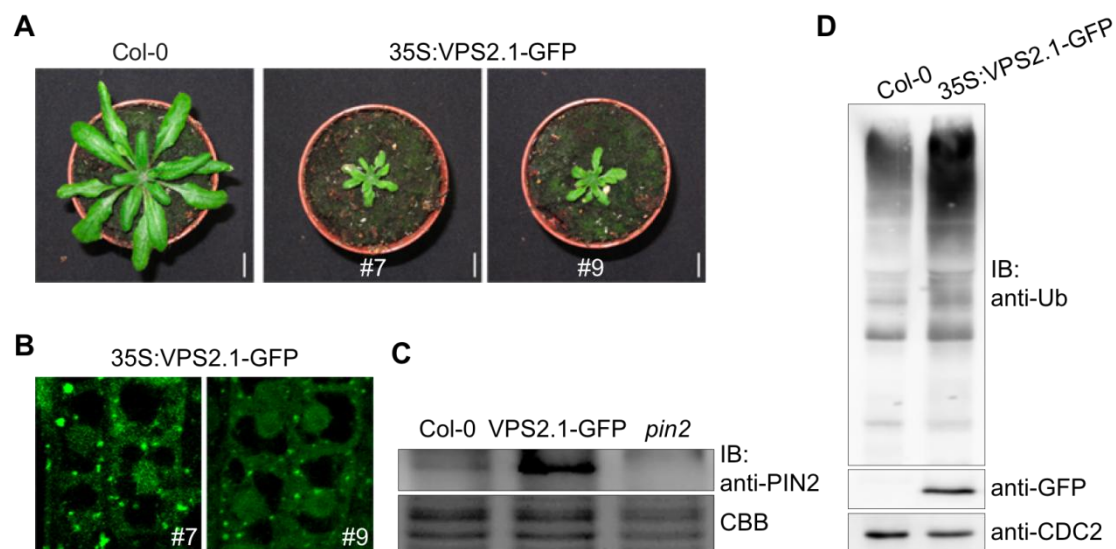
Figure 22: VPS2.1-GFP overexpressing plants are dwarf and accumulate PIN2 and ubiquitinated conjugates.
A) Photographs of VPS2.1-GFP overexpressing plants from two independent lines compared to wild type (Col-0) of the same age. Scale Bar: 1 cm.
B) Confocal microscopy images of VPS2.1-GFP in root epidermal cells of 7 days old seedlings from the two independent lines shown in (A).
C) Membrane protein extracts from roots of 10 days old Col-0 and 35S:VPS2.1-GFP seedlings were subjected to immunoblot analysis using an anti-PIN2 antibody. Membrane protein extracts from *pin2* roots are used as a negative control. CBB stained protein bands are shown as loading control.
D) Ubiquitin profile of 7 days old Col-0 and VPS2.1-GFP overexpressing seedlings. VPS2.1-GFP was detected using an anti-GFP antibody. CDC2 was used as loading control.

22D). The analysis revealed that ubiquitinated conjugates are accumulating in VPS2.1-GFP lines compared to wild type. This accumulation suggests that expression of VPS2.1-GFP results in inhibition of endocytosis resulting in accumulation of ubiquititinated proteins, which are supposed to be degraded in the vacuole following the endosomal trafficking pathway.

These results propose an essential role for VPS2.1 in endocytosis. When the function of VPS2.1 is disrupted endocytosis is inhibited, resulting in developmental defects. However, these defects are not as severe as in *vps2.1* mutants, which might be due to the late expression of VPS2.1-GFP, driven by the 35S promoter, since endogenous VPS2.1 is already expressed in embryo stage.

The interaction of AMSH3 with VPS2.1 implies a role for AMSH3 in endocytosis at least at the level of MVB, where ESCRT-III is located. This fact is supported by the observation that in *amsh3-1* PIN2 is not properly targeted to the vacuole, suggesting endocytosis defects (Isono et al., 2010).

3.3.4 The interaction of AMSH3 with ESCRT-III is important for its function

AMSH3 interacts *in vivo* with two components of ESCRT-III and is implicated in endocytosis. However, the biological significance of this interaction and the exact role of AMSH3 has to be proved. In this line, the first step is to explore whether the function of AMSH3 depends on the interaction with VPS2.1 and/or VPS24.1. To this end, the behaviour of an AMSH3 variant, lacking the ability to interact with ESCRT-III, was examined. Since the MIT domain of AMSH3 is necessary for the interaction with VPS2.1 and VPS24.1, a DEX inducible AMSH3 construct lacking the MIT domain (DEX:35S:AMSH3(ΔMIT)) was generated. This construct was first introduced in Col-0 plants. To investigate wether the deletion of the MIT domain and subsequently the loss of interaction with ESCRT-III subunits affects its deubiquitinating action, the amount of ubiquitinated proteins in the DEX:35S:AMSH3(ΔMIT) plants were analyzed by immunoblot analysis. The ubiquitin profile of DEX:35S:AMSH3(ΔMIT) containing seedlings, grown on GM medium supplemented with DEX, was compared to the ubiquitin profile of seedlings transformed with DEX:35S:AMSH3 or the empty vector pTA7002 (PTA) (Isono et al., 2010), used for the creation of the DEX inducible constructs, and to Col-0 and

amsh3-1 mutants (Isono et al., 2010)(Figure 23B). The DEX:35S:AMSH3(ΔMIT) expressing seedlings accumulated ubiquitinated conjugates compared to AMSH3 overexpressing seedlings, although not to the same extend as in *amsh3-1* mutants (Figure 23B). Interestingly, the DEX:35S:AMSH3(ΔMIT) seedlings were smaller (Figure 23A), suggesting that the overexpression of AMSH3(ΔMIT) acts dominant, even in the presence of endogenous AMSH3, resulting in accumulation of ubiquitinated proteins and subsequently to developmental defects. However, the
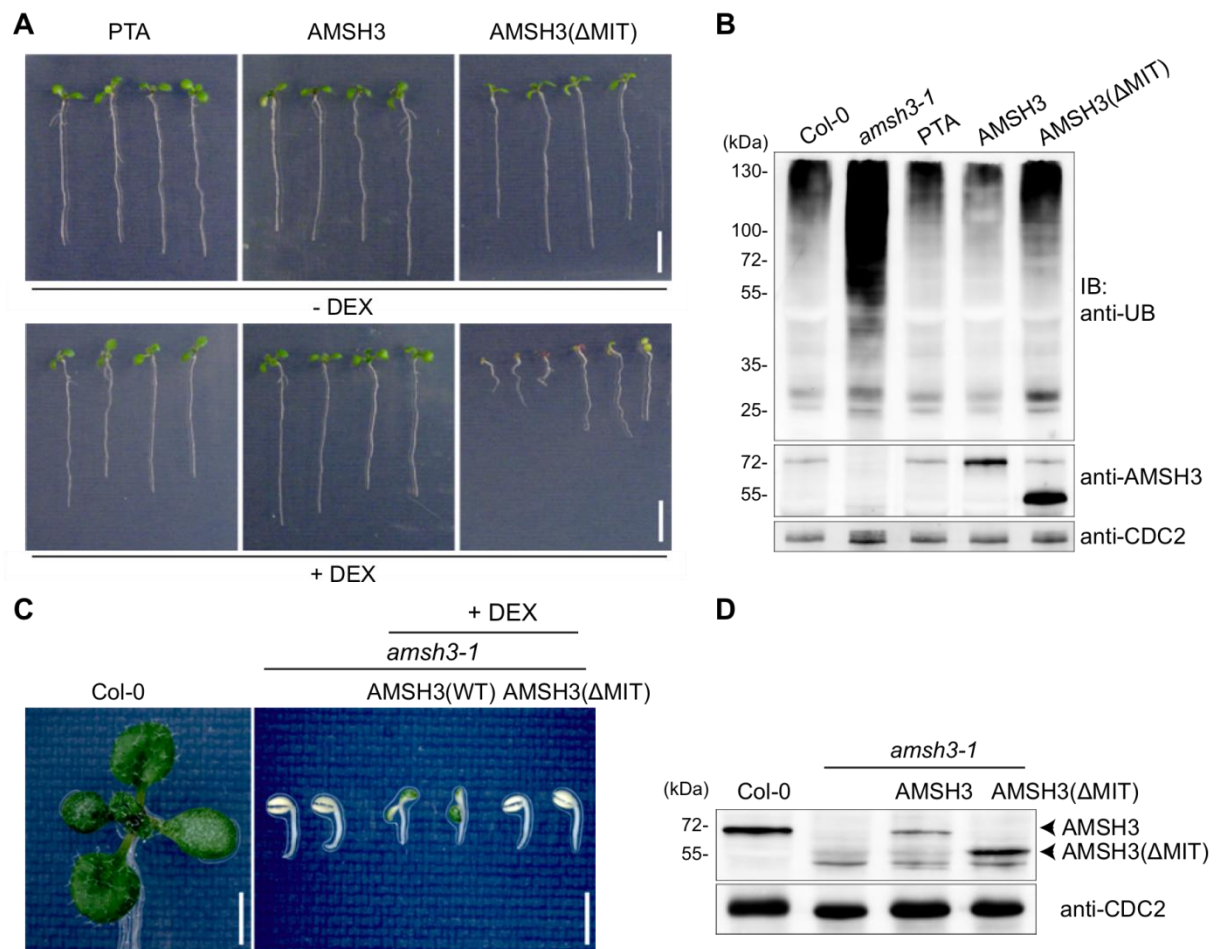
Figure 23: Expression of AMSH3(ΔMIT) leads to developmental defects and is not able to rescue the mutant phenotype.
A) Phenotypic analysis of 7 days old transgenic seedlings expressing DEX:AMSH3(WT), DEX:AMSH3(ΔMIT) or the empty vector (PTA). PTA is used as negative control. Seedlings, that are induced (+DEX; lower panel) or uninduced (-DEX; upper panel), are depicted. Scale Bar: 1 cm.
B) Immunoblot analysis of total protein extracts from DEX induced PTA, AMSH3 and AMSH3(ΔMIT) seedlings shown in (A) using anti-UB and anti-AMSH3 antibodies. Accumulation of ubiquitinated conjugates was compared to protein extract from Col-0 and *amsh3-1*. Note that AMSH3(ΔMIT) overexpressing seedlings accumulate ubiquitinated proteins, but not to the same extend as *amsh3-1*.
C) Phenotype of 7 days old *amsh3-1* mutants, expressing DEX:AMSH3 or DEX:AMSH3(ΔMIT), compared to *amsh3-1* mutant and Col-0 seedlings. Expression was induced by applying 30 μM DEX to the medium. Note that AMSH3 expression leads to green cotyledons. Scale Bar: 2 mm.
D) AMSH3 expression was verified by immunoblot analysis of total protein extracts from seedlings shown in (C) using an anti-AMSH3 antibody. CDC2 is used as loading control.

defects and the accumulation of ubiquitinated proteins in plants overexpressing AMSH3(ΔMIT) imply defects in endocytosis. The way in which AMSH3(ΔMIT) acts dominant as well as the inhibition of endocytosis has to be examined further.

DEX:35S:AMSH3(ΔMIT) was also transformed in *AMSH3+/-* heterozygous mutants, in order to examine the ability of this construct to rescue the seedling lethal phenotype of *amsh3-1* mutants. Transgenic *amsh3-1* mutants with the DEX:35S:AMSH3 contsruct were used as a control. Seedlings were grown on medium containing DEX, in order to induce the expression of the proteins as early as possible (Figure 23C). The overexpression of wild-type AMSH3 partially rescued the *amsh3-1* phenotype. However, AMSH3(ΔMIT) could not rescue the *amsh3-1* seedling lethal phenotype, even not partially. The expression of the transgenes was confirmed by immunoblot analysis (Figure 23D).

AMSH3, lacking the MIT interaction domain induces the accumulation of ubiquitinated proteins and cannot rescue the mutant phenotype, indicating a non-functional protein. Taken together, it is proposed that the interaction of AMSH3 with ESCRT-III provides a candidate recruitment mechanism for AMSH3 to its substrates. When the interaction is lost AMSH3 is not recruited to the substrates, which may need to be deubiquitinated for their proper function or endocytosis, resulting in developmental defects.

3.3.5 The activity of AMSH3 can influence the localization of VPS2.1 and VPS24.1

In order to obtain more information about the biological importance of the interaction between AMSH3 and ESCRT-III subunits, the behaviour of VPS2.1 and VPS24.1 in the presence of enzymatic inactive AMSH3, AMSH3(AXA), was examined.

First, the binding affinity of AMSH3(AXA) to VPS2.1 was essayed with an *in vitro* binding assay. In this assay, recombinant AMSH3 and AMSH3(AXA) were incubated with GST or GST-VPS2.1. After pulling-down on GST, the amount of AMSH3 and AMSH3(AXA) bound to VPS2.1 was compared by immunoblot analysis (Figure 24A). The comparison revealed that AMSH3(AXA) binds stronger to VPS2.1.

Since AMSH3(AXA) binds stronger to VPS2.1 *in vitro*, I explored the localization of VPS2.1 upon the expression of AMSH3(AXA) in protoplasts. When UBQ10:YFP-

VPS2.1 was expressed with 35S:HA-AMSH3, YFP-VPS2.1 was localized in the cytosol. Interestingly, when UBQ10:YFP-VPS2.1 was co-expressed with 35S:HA-AMSH3(AXA), YFP-VPS2.1 formed cytosolic compartments (Figure 24B). The expression of HA-AMSH3 and HA-AMSH3(AXA) was confirmed by immunoblot
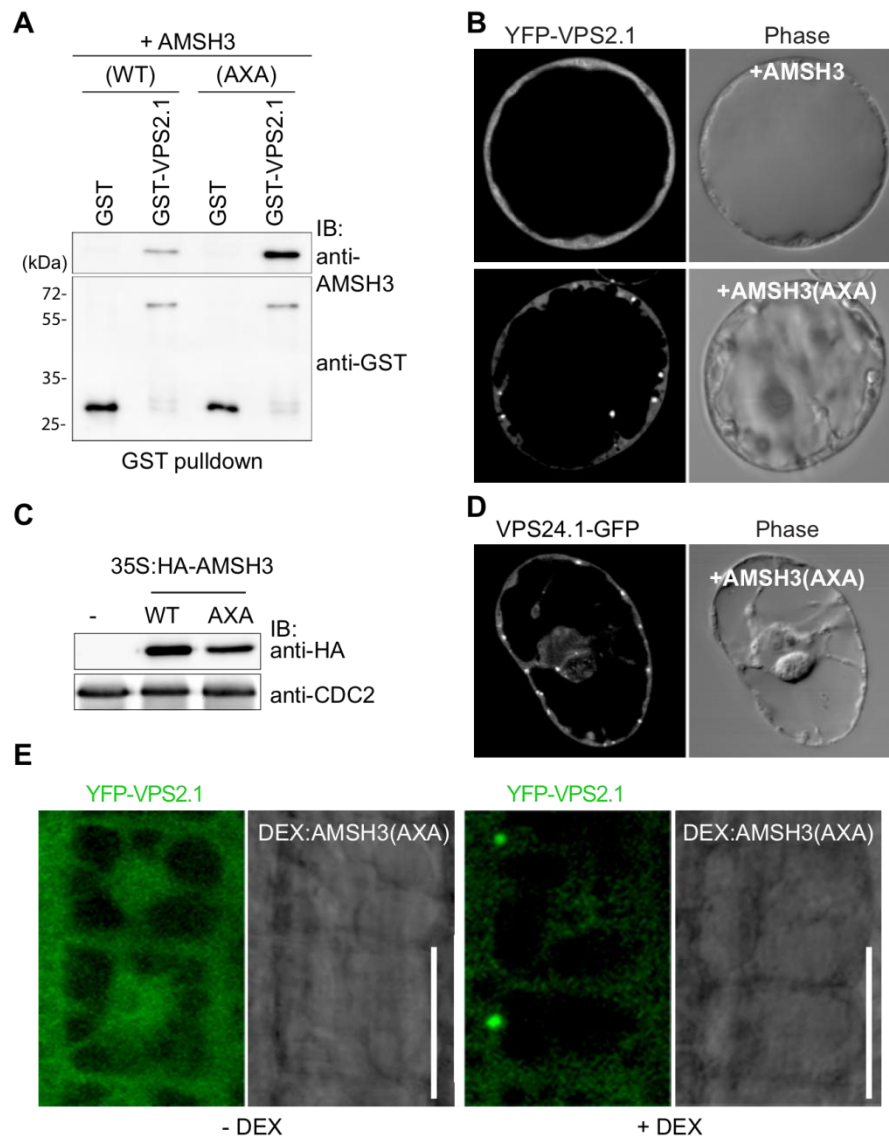
Figure 24: AMSH3(AXA) binds stronger to VPS2.1 and influences the localization of VPS2.1 and VPS24.1.
A) *In vitro* binding assay of AMSH3 and AMSH3(AXA) with GST or GST-VPS2.1. GST pulled-down samples were analyzed on western blot using anti-AMSH3 and anti-GST antibodies.
B) Confocal microscope images of co-transformed *Arabidopsis* derived protoplasts with UBQ10:YFP-VPS2.1 and 35S:HA-AMSH3 or 35S:HA-AMSH3(AXA).
C) To verify the expression of the AMSH3 constructs, total protein extracts from protoplasts shown in (B) were subjected to immunoblot analysis using an anti-HA antibody. CDC2 is used as loading control.
D) Confocal images of an protoplast co-expressing 35S:VPS24.1-GFP and 35S:HA-AMSH3(AXA).
E) 7 days old transgenic seedlings containing DEX:35S:AMSH3(AXA) and UBQ10:YFP-VPS2.1 grown on GM medium supplemented or not with 30 µM DEX, were analyzed by a confocal scanning microscope. Photographs show root epidermal cells. Note the compartments formed after DEX application. Scale Bar: 10 µm.
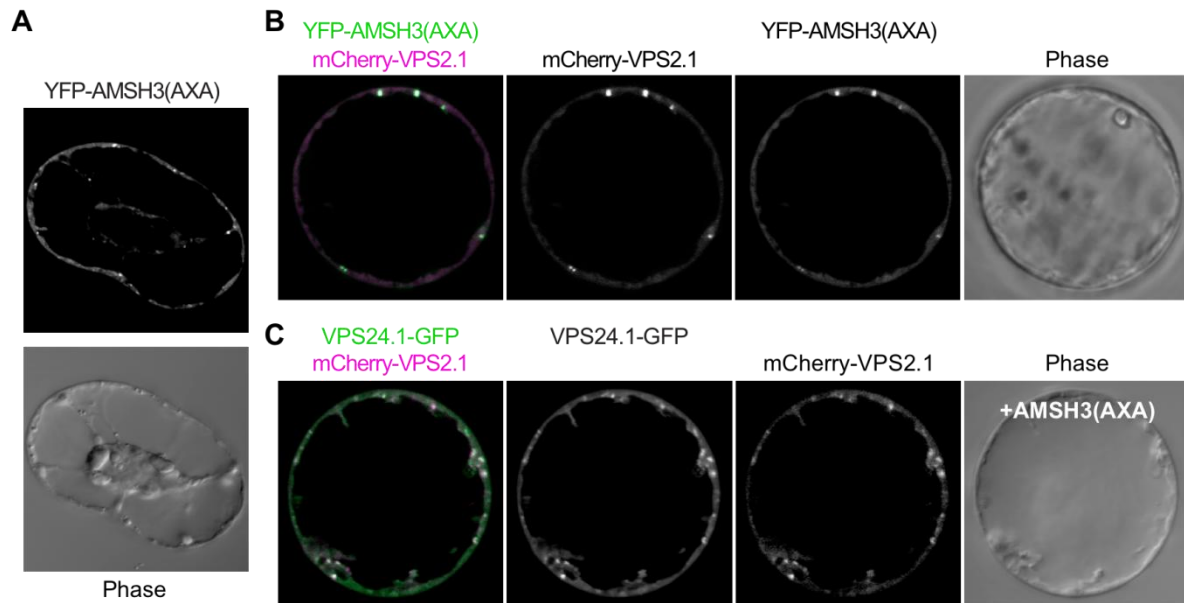
Figure 25: VPS2.1 and VPS24.1 co-localize on AMSH3(AXA) induced compartments.
A) Confocal microscope images of 35S:YFP-AMSH3(AXA) in *Arabidopsis* cell derived proto-plasts. Note that the YFP signal is located to cytosolic compartments.
B) *Arabidopsis* protoplasts co-transformed with 35S:YFP-AMSH3(AXA) and UBQ10:mCherry-VPS2.1. Confocal images show that both signals are co-localizing to cytoplasmic compartments.
C) VPS24.1-GFP and mCherry-VPS2.1 co-localize to cytoplasmic compartments upon the expression of 35S:HA-AMSH3(AXA).

analysis using an anti-HA antibody (Figure 24C). In addition, VPS24.1 was alsorelocated to cytosolic compartments upon expression of AMSH3(AXA) (Figure 24D). To test whether the localization of VPS2.1 is also affected by the expression of inactive AMSH3 *in planta*, UBQ10:YFP-VPS2.1 was transformed in transgenic plants containing a DEX inducible AMSH3(AXA) construct (Isono et al., 2010). To induce the expression of AMSH3(AXA), the transgenic DEX:35S:AMSH3(AXA)/UBQ10:YFP-VPS2.1 seedlings were grown on DEX-supplemented medium and the localization of YFP-VPS2.1 was monitored by a confocal scanning microscope (Figure 24E). VPS2.1 was located in the cytosol in seedlings grown on medium without DEX, but when grown on DEX-supplemented medium VPS2.1 localized to AMSH3(AXA) induced compartments.

Furthermore, the localization of AMSH3(AXA) itself was investigated. 35S:GFP-AMSH3(AXA) was expressed in protoplasts. AMSH3(AXA) did not localize in the cytosol as AMSH3(WT), but was forming big compartments within the cytosol (Figure 25A). These compartments could be the result of mislocalization or aggregation of misfolded AMSH3, due to the mutation within the catalytic domain. When 35S:GFP-AMSH3(AXA) was co-expressed with UBQ10:mCherry-VPS2.1, VPS2.1 was co-

localizing with AMSH3(AXA) in the induced compartments (Figure 25B). Moreover, mCherry-VPS2.1 and VPS24.1-GFP were co-localizing in the AMSH3(AXA) iuced compartments (Figure 25C).

In contrast to VPS2.1 and VPS24.1, the localization of VPS2.3, which is not interacting with AMSH3, was not affected by the expression of AMSH3(AXA) (Figure 26A). When 35S:YFP-VPS2.3, UBQ10:mCherry-VPS2.1 and 35S:HA-AMSH3(AXA) were expressed in protoplats, VPS2.1 localized to the AMSH3(AXA) induced compartments whereas VPS2.3 remained cytosolic (Figure 26A).

From the data obtained so far it can be assumed that the compartments formed by the expression of AMSH3(AXA) are like class E compartments. The stronger binding affinity of AMSH3(AXA) to VPS2.1, as shown in the *in vitro* binding assay, might restrict the recruitment of SKD1 to ESCRT-III and thereby inhibit the disassembly of the complex, so that class E compartments are formed. If this hypothesis is true,
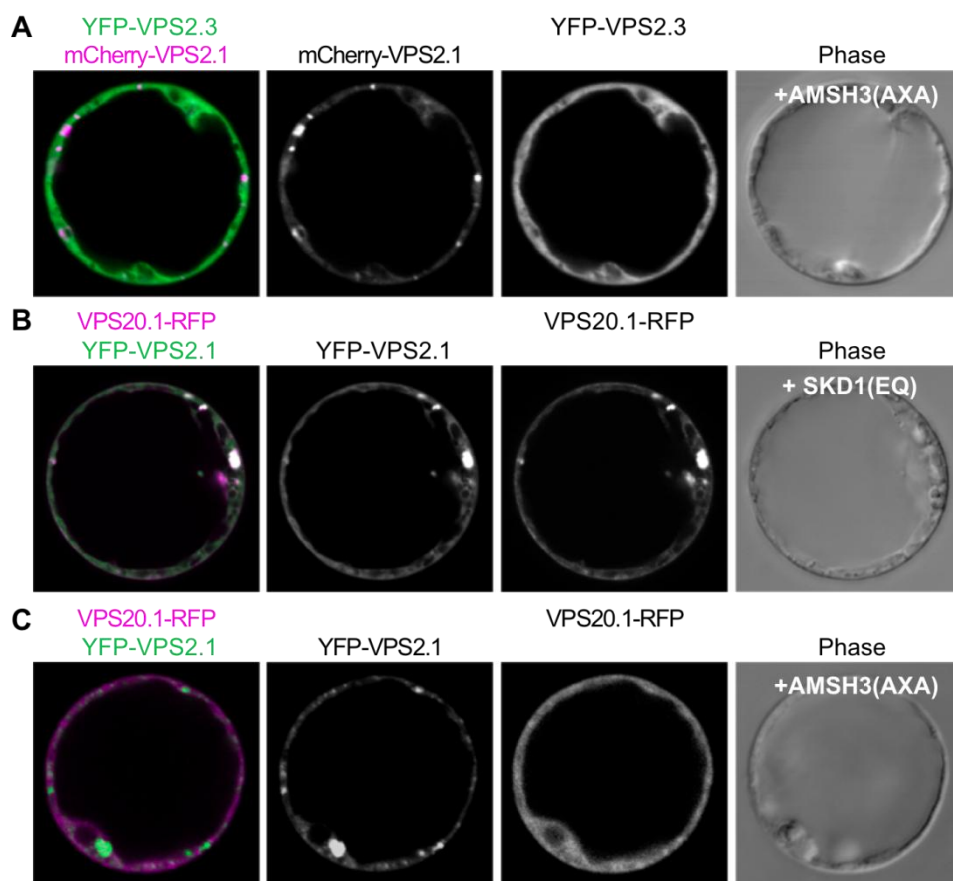
Figure 26: AMSH3(AXA) influences only the localization of its interacting partners.
A), **B)** and **C)** Confocal images of *Arabidopsis* protoplasts expressing 35S:YFP-VPS2.3 with UBQ10:mCherry-VPS2.1 and 35S:HA-AMSH3(AXA) in (A) or 35S:VPS20.1-RFP, with UBQ10:YFP-VPS2.1 and 35S:HA-SKD1(EQ) in (B) or 35S:VPS20.1-RFP with UBQ10:YFP-VPS2.1 and 35S:HA-AMSH3(AXA) in (C). Note that VPS2.3 and VPS20.1 remain cytosolic upon expression of AMSH3(AXA), while VPS2.1 is sequestered into compartments.

other ESCRT-III subunits, which do not interact with AMSH3, should accumulate to the AMSH3(AXA) compartments. Thereforethe behaviour of VPS20.1, another predicted ESCRT-III subunit, was analyzed (Winter and Hauser, 2006). VPS20.1 was fused with a RFP tag at the carboxyl terminus, because a myristoylation site lies at the amino-terminal end (Im et al., 2009), and was expressed under the control of a 35S promoter in protoplasts. The participation of VPS20.1-RFP to endocytosis was assessed by inspecting its reaction towards SKD1(EQ). VPS20.1 was cytosolic in protoplasts, but localized to class E compartments when co-expressed with SKD1(EQ) (Figure 26B). VPS20.1 was co-localizing with VPS2.1 in class E compartments, indicating that VPS20.1 is employed in endocytosis at the level of MVB formation. However, upon the overexpression of HA-AMSH3(AXA), VPS20.1 remained cytosolic, although VPS2.1 was relocated to AMSH3(AXA) induced compartments (Figure 26C).

This observation reveals that the effect of AMSH3(AXA) implies only the localization of VPS2.1 and VPS24.1. Through stronger binding affinity, AMSH3(AXA) sequesters VPS2.1 and VPS24.1 into aggregates and removes them from their usual localization. These results indicate that AMSH3 interacts with VPS2.1 and VPS24.1 in the cytosol before they are recruited to endosomes. Moreover, the expression of AMSH3(AXA) may have an impact on the assembly of ESCRT-III and furthermore to endocytosis, since VPS2.1 and VPS24.1 may not be delivered to endosomes.

3.4 Proposed model of AMSH3 function in endocytosis

Taken all the data into account, I propose a model for the function of AMSH3 in the endocytotic pathway (Figure 27). Plasma membrane receptors like PIN2 are ubiquitinated at the plasma membrane and internalized. The formed cargos are delivered to endosomes through the concerted action of ESCRT-I, ESCRT-II and ESCRT-III. VPS2.1 and VPS24.1, two ESCRT-III core components, interact already with AMSH3 in the cytosol. VPS2.1 and VPS24.1 are then recruited to the endosomes for the assembly of ESCRT-III and AMSH3 is recruited together with them to the endosomal membrane. At the endosomes AMSH3 deubiquitinates the receptors coupled to the ESCRT machinery or components of the machinery itself. Deubiquitination of the receptors contributes to the recycling of free ubiquitin within the cell or might be a prerequisite for the invagination of the receptors into MVBs.

Deubiquitination of ESCRT subunits may also influence their function in endocytosis. Deubiquitination is terminated by SKD1 by outcompeting AMSH3. SKD1 induces the invagination of the receptors into MVBs and the release of ESCRT-III subunits in the cytosol for reuse in new rounds of endocytosis. Formed MVBs fuse with the vacuole to degrade their content.
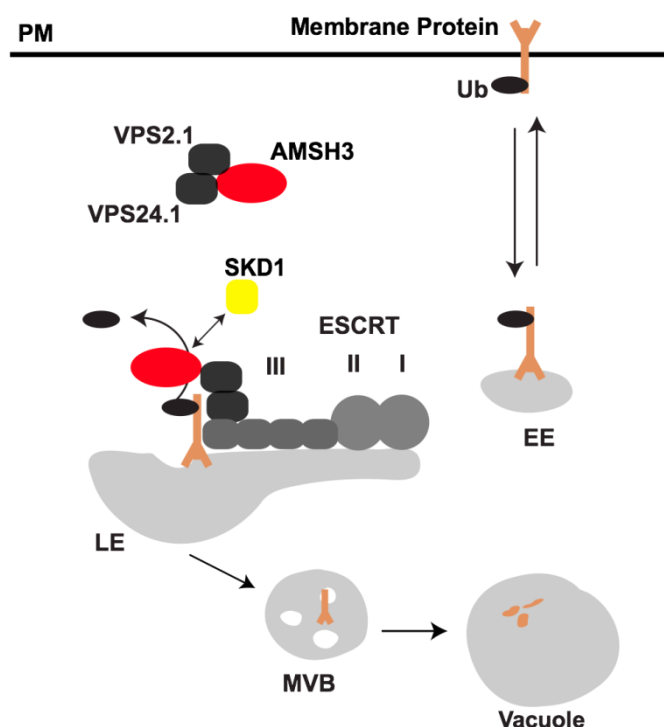
Figure 27: Model of AMSH3 function in the endo-somal sorting system.
In wild-type *Arabidopsis* plants AMSH3 interacts in the cytosol with two ESCT-III subunits VPS2.1 and VPS24.1. Through interaction of VPS24.1 and/or VPS2.1 with other ESCRT-III subunits, anchored on the endosomal membrane, they are together recruited to the endosomal membrane. AMSH3 deubiquitinates the ubiquitinated cargos and is outcompeted by SKD1, which promotes the disassembly of the complex and further sorting events of the cargos to the vacuole for degradation.

3.5 AMSH1 interacts with VPS2.1 and VPS2.2

The closest homologue to AMSH3, AMSH1 possess also a MIT domain at the amino-terminal part (Isono et al., 2010). AMSH1 is shown *in vitro* to be an active deubiquitinating enzyme (Katsiarimpa and Kalinowska et al., 2013), that in contrast to AMSH3 preferentially hydrolyzes K63-linked ubiquitin chains (Katsiarimpa and Kalinowska et al., 2013). Although the sequence identity in the MIT domain of AMSH1 and AMSH3 differs, I examined whether AMSH1 is able to interact with VPS2.1 through its MIT domain.

AMSH1 was tested for interaction with VPS2.1, VPS2.2 and VPS2.3 in a targeted Y2H assay. AMSH1 fused to a GBD domain was transformed together with GAD fused VPS2.1, VPS2.2 and VPS2.3 in yeast. Yeast cells containing both plasmids
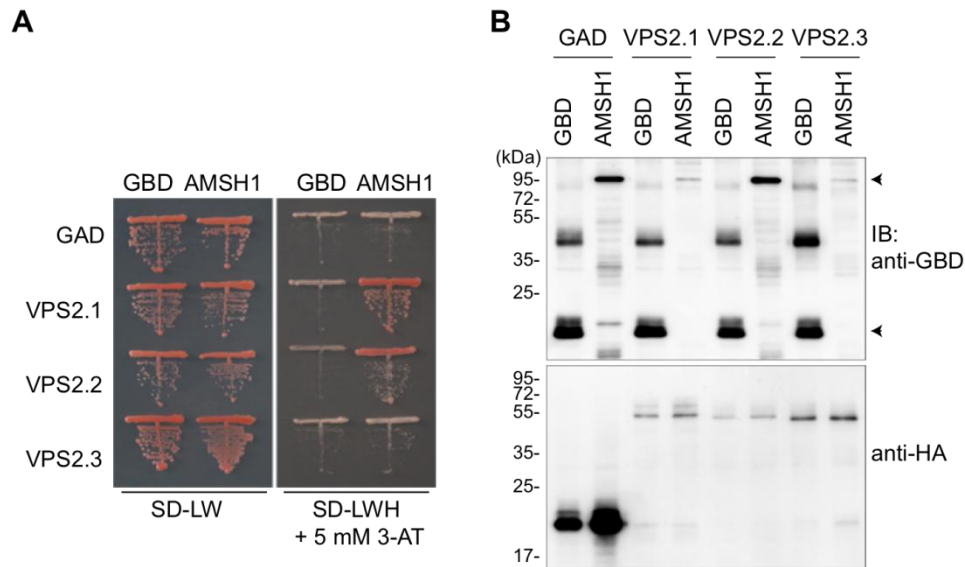
Figure 28: AMSH1 interacts in yeast with VPS2.1 and VPS2.2.
A) Y2H analysis of GBD-AMSH1 with GAD-VPS2.1, GAD-VPS2.2 and GAD-VPS2.3. Transformants were plated on SD-LW and SD-LWH medium, supplemented with 5 mM 3-AT, to test for their auxotrophic growth.
B) Expression of Y2H constructs shown in (A) was verified by immunoblotting of total protein extracts from the corresponding yeast cells, using an anti-GBD and an anti-HA antibody. Upper arrowhead indicates GBD-AMSH1 and lower one GBD.

were tested for interaction on SD-medium lacking histidine and the expression of each protein was verified by western blot (Figure 28A and B). The assay revealed that AMSH1 is able to interact with VPS2.1, suggesting a role in endocytosis. However, AMSH1 interacted also with VPS2.2. The differences in the MIM1 domain of VPS2.2 compared to VPS2.1 affect the binding to the MIT domain of AMSH3 but not to that of AMSH1. AMSH1 might therefore be implicated in distinct pathways than AMSH3.

To investigate the putative implication of AMSH1 in endocytosis, the characterization of *AMSH1* knockout mutants is needed. For this end, an *Arabidopsis* line with a T-DNA insertion in the 5`-UTR of *AMSH1*, in a L*er* background, named *amsh1-1,* was investigated (Figure 29A) (Katsiarimpa and Kalinowska et al., 2013). After verifying the line through genotype PCR, using the primers listed in Table 6, homozygous plants were used for further analysis. The expression of *AMSH1* at the protein level was essayed with immunoblot analysis using an anti-AMSH1 antibody (Katsiarimpa and Kalinowska et al., 2013). The immunoblot revealed, that the T-DNA insertion in the promoter region of *AMSH1* results in reduced protein levels of wild-type protein (Figure 29B). The weak band in *amsh1-1* indicates that the mutant is not

a complete loss-of-function mutant but rather a weak mutant allele with compromised AMSH1 function.

In order to study endocytosis in *amsh1-1*, the levels of a known substrate of this pathway, PIN2 were investigated. An immunoblot analysis with an anti-PIN2 antibody was performed using 10 days old seedlings, grown under long day conditions (LD: 16 hours light and 8 hours dark) (Figure 29C). As control for the recognition of the right PIN2 band, membrane fraction from *pin2* mutants roots was used (Willige et al., 2011). The immunoblot analysis revealed that the levels of PIN2 were not altered in *amsh1-1* compared to wild type, suggesting that the vacuolar degradation of PIN2 is not impaired.

The interaction of AMSH1 with VPS2.1, an ESCRT-III subunit implies a role of AMSH1 in the endocytosis pathways. Although vacuolar degradation of PIN2 is not altered in *amsh1-1*, opposing the theory of AMSH1 working in endocytosis, it can be speculated that the low levels of AMSH1 present in *amsh1-1* are sufficient for endocytosis. Further investigations have to be performed, in order to verify *in vivo* interaction of AMSH1 with ESCRT-III and putative implication in endocytosis.
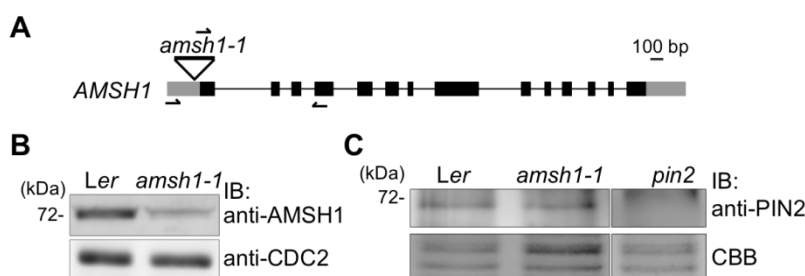
Figure 29: *amsh1-1* mutants do not accumulate PIN2.
A) Schematic representation of the T-DNA insertion site and the primer binding sites in *AMSH1*. Lines indicate introns and boxes exons (black boxes: coding regions; grey boxes: UTRs).
B) Total protein extract from wild type (L*er*) and *amsh1-1* mutants were subjected to western blot and probed with anti-AMSH1 antibody. Note that AMSH1 is reduced in *amsh1-1*. CDC2 is used as loading control.
C) Membrane exacts from roots of 10 days old L*er*, *amsh1-1* and *pin2* seedlings, grown under LD conditions, were analyzed by western blot with an anti-PIN2 antibody. CBB stained protein bands are used as loading control.

3.6 AMSH proteins in the autophagy pathway

3.6.1 The activity of AMSH3 influences the autophagy pathway

While characterizing the *amsh3* mutants, accumulation of autophagosomes by electron microscopy was observed (Isono et al., 2010) (Figure 6B). Immunoblot

analysis using an anti-ATG8 antibody revealed high amount of the autophagy marker ATG8 (Isono et al., 2010). The accumulation of autophagosomes and of the autophagy marker implies defects in the autophagy pathway. To gain knowledge about the reason for the defects in the autophagy pathway in *amsh3* mutants, the ability of plants containing an enzymatic inactive version of AMSH3 to survive under nutrient limiting conditions was examined.

The most typical trigger of autophagy is nutrient starvation. Absence of essential nutrients induces autophagy to recycle nutrients from internal supplies. DEX inducible AMSH3(AXA) plants (Isono et al., 2010) were used to monitor putative defects in the autophagy pathway. Transgenic plants containing the AMSH3(WT) construct or the empty vector PTA were used as negative controls. Seedlings were grown on ½ MS medium supplemented with 30 mM DEX under short day conditions (SD: 8 hours light and 16 hours dark) for 7 days and then transferred to soil and continued to grow under the same light conditions. After transferring them on soil,
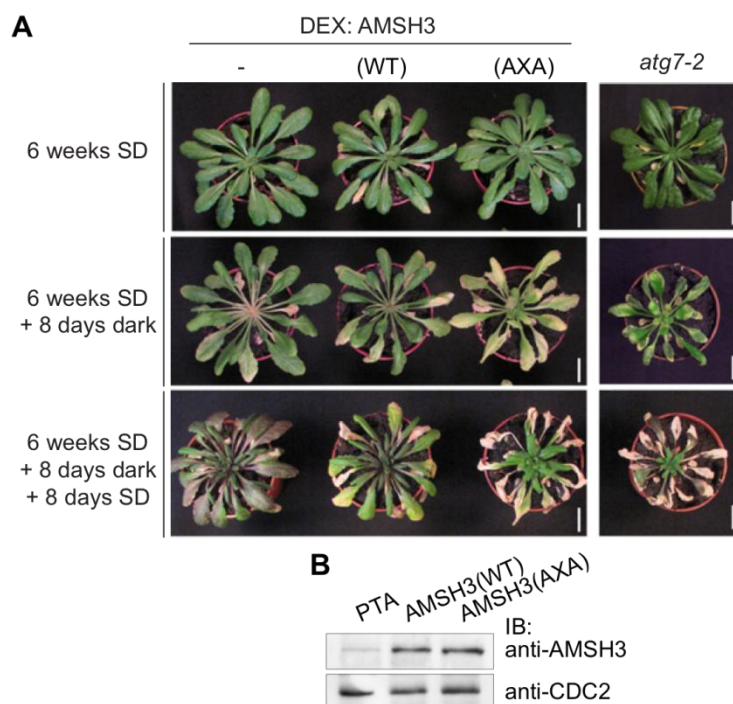
Figure 30: Expression of AMSH3(AXA) in plants results in defective nutrient recycling.
A) Phenotype of 6 weeks old (upper panel) plants expressing DEX:AMSH3(WT) or DEX:AMSH3(AXA), grown under SD conditions. Plants expressing the empty vector (PTA) were used as negative control. Expression was induced by the application of 30 μM DEX. The plants were transferred to complete darkness for 8 days (middle panel) and then transferred back to short day conditions (SD: 8 hours light / 16 hours dark) conditions for 8 days in order to recover (lower panel). Note that the AMSH3(AXA) plants have impaired ability to survive under these conditions. *atg7-2* mutant plants (left panel) grown under the same conditions were used as positive control for nutrient deficiency. Scale Bar: 2 cm.
B) Immunoblot analysis of total protein extracts from the corresponding plants shown in (A), using anti-AMSH3 antibody in order to verify the expression. CDC2 is used as loading control.

plants were treated every fourth day with 30 mM DEX to sustain the expression of the proteins. After 6 weeks of growth, plants (Figure 30A; upper panel) were transferred to continuous dark for 6 days to induce carbon starvation and to activate autophagy. *atg7-2* autophagy deficientmutants, (Hofius et al., 2009) grown under the same conditions, were used as a control for the effects of starvation on plant growth. After dark treatment the plants were placed back to short day conditions and were left to recover for 8 days. Immediately after dark treatment, AMSH3(AXA) overexpressing plants became chlorotic and leaf cell death was induced to a high extent compared to the plants expressing AMSH3(WT) or the empty vector (Figure 30A; middle panel). After 8 days in SD conditions AMSH3(AXA) as well as *atg7-2* plants could not survive, while AMSH3(WT) and PTA plants could recover (Figure 30A; lower panel). This indicates that autophagy was activated to recycle carbon from internal supplies in AMSH3(WT) and PTA plants but not in AMSH3(AXA) plants. The expression of the transgene in each line was verified by western blot using an anti-AMSH3 antibody (Figure 30B).

The accelerated chlorosis and the observed cell death in AMSH3(AXA) overexpressing plants indicate an early onset of senescence and a hypersensitive response to carbon starvation. Hence, plants overexpressing AMSH3(AXA) resemble the phenotype of *atg7-2* mutants and are defective in autophagy, suggesting that the enzymatic activity of AMSH3 is important for this pathway. This result indicates that the accumulation of autophagosomes observed in *amsh3* mutants (Isono et al., 2010) might be a direct consequence of *AMSH3* knockout.

3.6.2 AMSH1 plays a role in autophagy

The sensitivity of plants expressing an enzymatic inactive AMSH3 towards carbon deprivation propose a role of deubiquitination in autophagy. Determining the implication of AMSH3 in autophagy will provide information about the function of AMSH3 and furthermore it will be a large step in understanding autophagy in plants. However, neither *amsh3* mutants nor AMSH3(AXA) plants are appropriate to be used for this purpose. *amsh3* mutants are seedling lethal (Isono et al., 2010) and the expression of AMSH3(AXA) plants is variable depending on the inducible expression system, which may result in variable molecular phenotypes, making these plants inappropriate to be used for molecular analysis.

To reveal the action of deubiquitination in autophagy, I decided to examine whether AMSH1 is implicated in autophagy. To draw conclusions about the relation between AMSH proteins and autophagy, I analyzed *amsh1-1* mutants regarding autophagy. Phenotypic analysis of *amsh1-1* revealed no apparent phenotypic defects at any developmental stage under continuous light or LD conditions (16 hours light and 8 hours dark) (Katsiarimpa and Kalinowska et al., 2013). However, when *amsh1-1* mutants are grown under SD conditions (8 hours light and 16 hours dark), they exhibit an early senescence phenotype compared to wild type (Figure 31A). The early senescence phenotype is one characteristic phenotype of autophagy deficient mutants (Chung et al., 2010; Doelling et al., 2002; Hanaoka et al., 2002; Katsiarimpa and Kalinowska et al., 2013; Thompson et al., 2005; Xiong et al., 2005; Yoshimoto et al., 2004). Based on this obseravation, it was speculated whether *amsh1-1* mutants are defective in autophagy. Therefore, the ability of *amsh1-1* mutants to survive under carbon limiting conditions was examined. Wild type and mutant plants were grown for 4 ½ weeks under SD conditions on soil and then transferred to complete darkness for 8 days. After dark treatment plants were placed back to SD conditions for 5 days in order to recover from nutrient starvation. *amsh1-1* plants could not survive under carbon limiting conditions, while wild type was able to recover (Figure 31B). The hypersensitive response of *amsh1-1* mutants implies defects in autophagy and involvement of AMSH1 in this pathway. To further assess the defects in autophagy, I examined the abundance of an autophagy marker ATG8 (Yoshimoto et al., 2004). Immunoblot analysis of total protein extracts from leaves of *amsh1-1* or L*er* plants prior to dark treatment and direct after dark treatment, using an anti-ATG8a antibody, (Thompson et al., 2005) shows that ATG8 protein levels were highly increased in *amsh1-1* mutants after dark treatment (Figure 31C), confirming that autophagy is impaired in *amsh1-1*.

Since adult plants are more difficult to use for molecular analysis, I further investigated the defects of autophagy in *amsh1-1* mutant seedlings. Nonetheless, I had first to verify that the hypersensitive response of *amsh1-1* mutants after dark treatment is independent of the growth stage. Therefore *amsh1-1* seedlings were grown under LD conditions on ½ MS medium for 12 days or for 7 days at LD conditions and 5 days in complete darkness (Figure 31D). The seedlings kept for 5 days in dark exhibited accelerated chlorosis, proofing defective autophagy. The blot shows that the ATG8 levels in light grown seedlings are comparable between L*er*
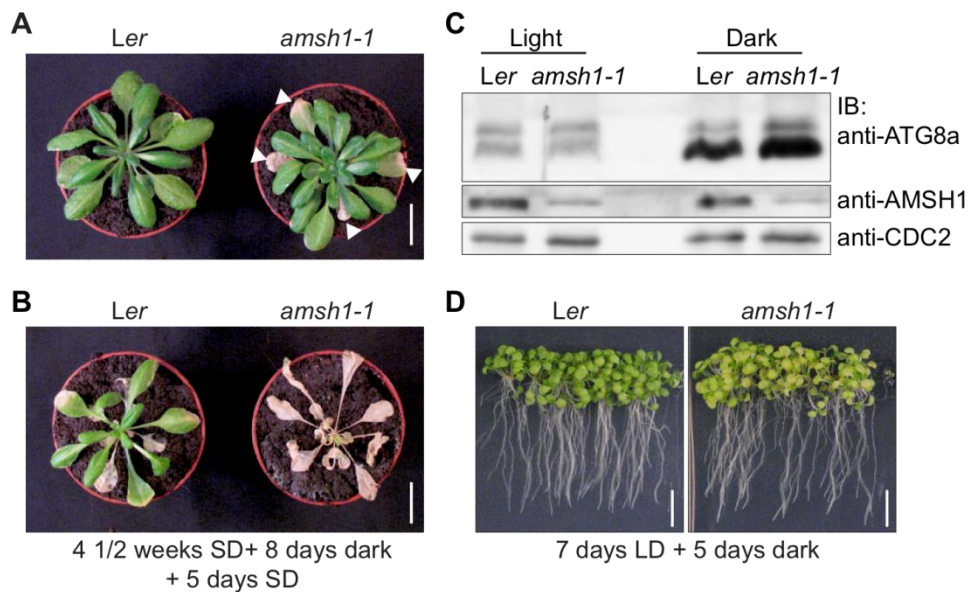
Figure 31: *amsh1-1* mutants display an early senescence phenotype and are defective in autophagy.
A) Photographs of 5 weeks old wild-type (L*er*) and *amsh1-1* mutant plants, grown under SD conditions (SD: 8 hour light / 16 hours dark). Note that *amsh1-1* exhibits early senescence indicated by the arrowheads. Scale bar: 1cm.
B) L*er* and *amsh1-1* plants were grown for 4 ½ weeks under SD conditions, then transferred for 8 days in complete darkness and then for 5 days at SD. Note that in contrast to wild type, *amsh1-1* was unable to survive after dark treatment. Scale Bar: 1 cm.
C) Immunoblot analysis with an anti-ATG8 antibody and an anti-AMSH1 antibody. Total proteins were extracted from leaves of L*er* and *amsh1-1* plants prior and direct after dark treatment. ATG8 accumulates in *amsh1-1* after dark treatment. CDC2 is used as loading control.
D) Photographs of L*er* and *amsh1-1* seedlings grown on ½ MS for 7 days under long day (LD: 16 hours light / 8 hours dark) conditions and then transferred to darkness for 5 days to induce autophagy. Starvation-induced chlorosis is enhanced in *amsh1-1* compared to wild type. Scale Bar: 1 cm.

and *amsh1-1*,while in the dark treated seedlings ATG8 accumulates in *amsh1-1*. The *amsh1-1* mutants have impaired ability to survive under starvation conditions and accumulate the autophagic marker ATG8 under these conditions, indicating defects in the autophagy pathway and proposing a role for AMSH1 in this pathway.

3.6.3 The amount of autophagosomes fused with the vacuole is decreased in *amsh1-1*

Impaired formation of autophagosomes in autophagy deficient mutants results in accumulation of ATG8 (Agromayor et al., 2009; Phillips et al., 2008; Thompson et al., 2005; Yoshimoto et al., 2004). However, accumulation of ATG8 might result from impaired degradation of autophagosomes within the vacuole. The accumulation of

ATG8 in *amsh1-1* after nutrient starvation conditions might be a result of impaired autophagosome formation or degradation.

To inspect which step of autophagy is impaired in *amsh1-1*, a fluorescent dye, monodansylcadaverine (MDC) was used. MDC is shown in *Arabidopsis* to co-localize with ATG8 and to label selectively autophagosomes (Contento et al., 2005). I stained wild type (L*er*) and *amsh1-1* seedlings with MDC and examined the formation of autophagosomes. *atg7-2* seedlings are defective in autophagosome formation (Hofius et al., 2009) and were used as a control for MDC staining. Seedlings were grown on ½ MS medium at long day conditions for 7 days and then transferred to dark for 5 days to induce autophagy. After dark treatment seedlings were stained with MDC and root epidermal cells were observed under a confocal scanning microscope (Figure 32A). MDC positive autophagosomes were visible in Col-0, the wild type background of *atg7-2* mutants, but not in *atg7-2*. In *amsh1-1* MDC stained autophagosomes were also detected, suggesting that in these mutants the formation of autophagosomes is not impaired.

E64-d, a membrane permeable vacuolar cysteine protease inhibitor, was used to investigate whether the degradation of autophagosomes is attenuated in *amsh1-1*. E64-d inhibits the degradation of autophagic bodies within the vacuole (Inoue et al, 2006). Wild-type and *amsh1-1* seedlings were treated with E64-d and the abundance of ATG8 was analyzed. Seedlings were grown under LD conditions or were dark treated for 5 days. When wild type (L*er*) and *amsh1-1* light grown seedlings were treated with E64-d, ATG8 did not accumulate and the protein amount was comparable between L*er* and *amsh1-1* (Figure 32B). However, when the wild-type seedlings were dark-treated ATG8 accumulated after E64-d treatment (Figure 32B). In *amsh1-1* dark-treated seedlings ATG8 accumulated already prior to E64-d treatment. Treatment with E64-d caused just a slight increase in the abundance of ATG8 compared to the mock treated, indicating that the degradation of autophagosomes in *amsh1-1* is affected but not completely blocked.

Using MDC and E64-d, behaviour of autophagosomes was monitored, in order to investigate the defects in the degradation of autophagosomes. L*er* and *amsh1-1* seedlings were grown on ½ MS and kept for two days in complete darkness to induce the formation of autophagosomes, followed by 1 hour treatment with E64-d to block their degradation in the vacuole. After inhibition of the vacuolar hydrolases with E64-d, seedlings were stained with MDC and observed under a confocal fluorescent
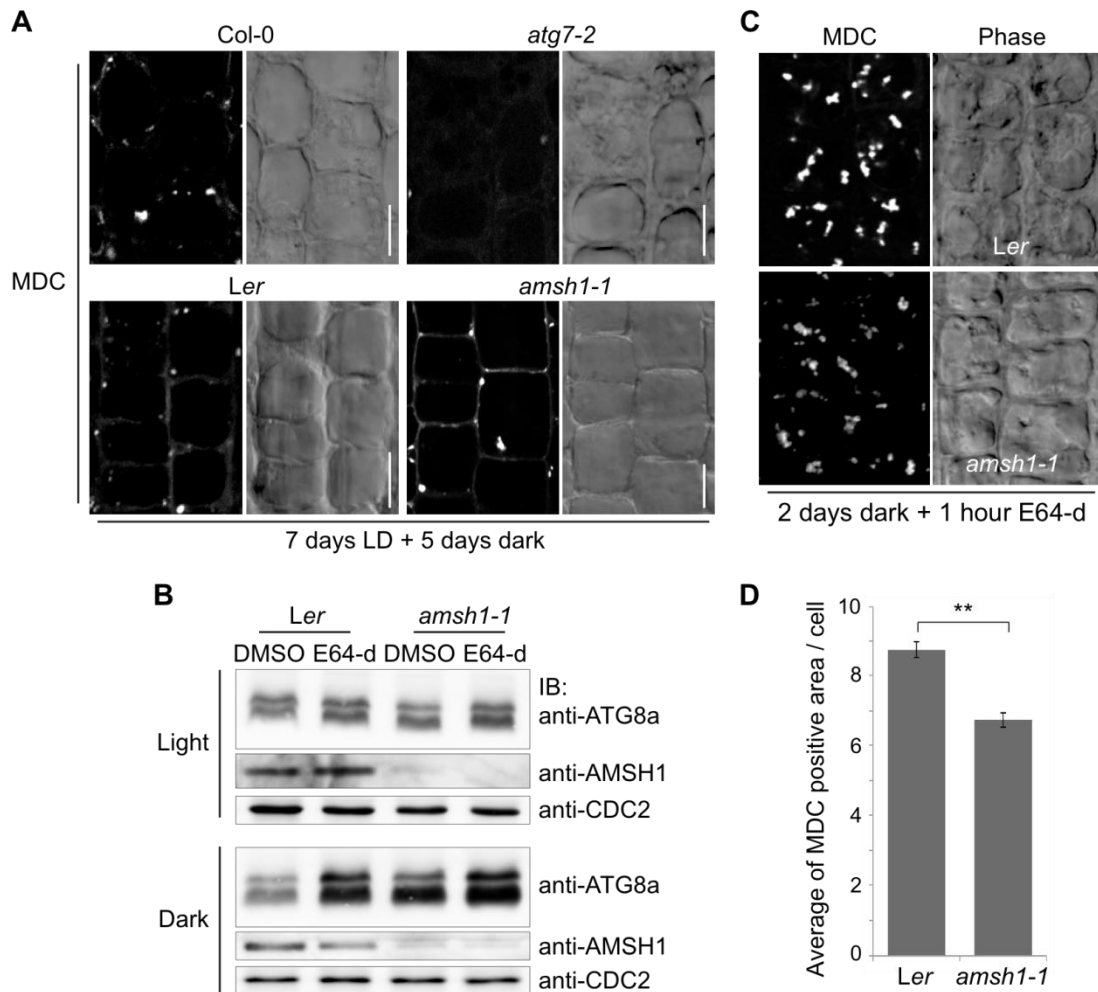
Figure 32: In *amsh1-1* fewer MDC stained autophagosomes accumulate in the vacuoles.
A) Confocal microscope images of root epidermal cells of Col-0, *atg7-2*, L*er* and *amsh1-1* seedlings, grown for 7 days under LD conditions and for 5 days in dark and stained with MDC. Scale Bars: 10 µM.
B) Total protein extracts from *Arabidopsis* seedlings grown under LD conditions (Light, upper panel) or transferred to darkness as in (A) (Dark, lower panel) and treated with DMSO (mock) or 100 µM E64-d for 18 hours, were subjected to western blot analysis with anti-ATG8 and anti-AMSH1 antibodies. CDC2 is used as loading control.
C) Confocal images of root epidermal cells of L*er* and *amsh1-1* mutant seedlings stained with MDC. Seedlings were grown for 7 days under LD conditions and then transferred to darkness for 2 days. After dark treatment seedlings were treated for 1 hour with 100 µM E64-d prior to MDC staining.
D) Statistical analysis of the area of the MDC stained autophoagic bodies within the vacuoles of each cell of L*er* and *amsh1-1* seedlings shown in (C). ** indicates significant difference (P<0,05).

microscope to visualize the autophagic bodies accumulating within the vacuole (Figure 32C). The total area of the autophagic bodies within the vacuoles of epidermal root cells was measured and compared between L*er* and *amsh1-1* (Figure 32D). While the average area of autophagic bodies within 396 cells of 20 wild-type seedlings was 8.78 µm^2 the corresponding area from 314 cells of 20 *amsh1-1* seedlings was 6.76 µm^2. There is a significant (P<0,05) reduction of 23% of autophagic bodies within the vacuoles of *amsh1-1*.

The analysis of *amsh1-1* mutants reveals that these mutants have a defective autophagy pathway under nutrient limiting conditions. Although autophagosomes are formed the amount of autophagic bodies within the vacuoles of *amsh1-1* mutant seedlings are significant fewer than in the wild-type seedlings. This indicates that fewer autophagosomes fuses with the vacuole and subsequently inadequate nutrients resources are provided for the survival of the plants. Thus, it can be speculated that AMSH1 is empoyed in the fusion of autophagosomes with the vacuolar membrane.

3.6.4 *amsh1-1* is not defective in selective autophagy

In addition to bulk, non-selective degradation of cytoplasmic content, autophagosomes can selectively sequester unwanted proteins or organelles(Mizushima, 2005; Reggiori et al., 2012).Although in bulk autophagy autophagosomes cannot recognize what they enclose, in selective autophagy ubiquitinated proteins may be recognized by specific adaptors and selectively incorporated into autophagosomes. However, bulk and selective autophagy share the same molecular core autophagic machinery(Mizushima, 2005; Reggiori et al., 2012).

To investigate wether selective autophagy is affected in *amsh1-1*, the protein abundance of the selective autophagy substrate NBR1 was tested. NBR1 functions as an autopohagic adaptor to dock proteins to autophagosomes for degradation and is degraded itself through this pathway in the vacuole (Svenning et al., 2011). An immunoblot analysis with protein extracts from *amsh1-1* and L*er* seedlings, grown as in Figure 32B, was performed using an anti-NBR1 antibody (Svenning et al., 2011). Protein extracts from *atg7-2* were used as positive control for NBR1
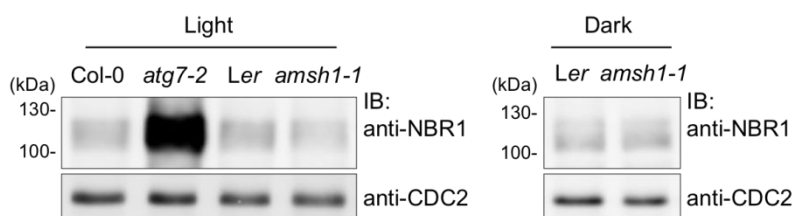
Figure 33: In *amsh1-1* selective autophagy is not impaired.
Immunoblot analysis of total protein extracts from L*er* and *amsh1-1* seedlings grown under LD conditions for 12 days (light, left panel) or for 7 days at LD and 5 days in dark (Dark, right panel), using an anti-NBR1 antibody. Total protein extract from light grown *atg7-2* mutant seedlings were used as a positive control for the accumulation of NBR1 compared to its wild type (Col-0). CDC2 is used as loading control

accumulation (Figure 33). The analysis shows that the protein levels of NBR1 were not increased in *amsh1-1* even after dark treatment, indicating that selective degradation of NBR1 is not impaired in *amsh1-1* mutants.

When seedlings are grown in light, neither ATG8 nor NBR1 accumulated in *amsh1-1*, suggesting that residual AMSH1 in *amsh1-1* is sufficient for basal autophagy (Mizushima, 2005). Autophagy is active at low levels even under normal growth conditions and is important for constitutive turnover of cytosolic components (Mizushima, 2005). However, under carbon limitation during dark, autophagy is upregulated and participates in bulk degradation, which may not require NBR1 mediated selective degradation. Under these conditions the low levels of AMSH1 probably becomes limiting for the higly induced bulk autophagy pathway, resulting in accumulation of ATG8.

3.7 ESCRT-III is implicated in autophagy

3.7.1 VPS2.1-GFP overexpressing seedlings are defective in autophagy

This study shows that AMSH1 and AMSH3 are both interacting with VPS2.1. Considering a putative role of AMSH1 and AMSH3 in autophagy, it was examined whether VPS2.1 might play also a role in this catabolic pathway. To investigate this assumption, the ability of VPS2.1-GFP overxpressing plants to survive under carbon limiting conditions was tested. GFP tag at the carboxyl terminus acts dominant on the function of VPS2.1 and plants overexpressing this construct are defective in endocytosis. To induce carbon limitation, 35S:VPS2.1-GFP seedlings, grown on ½ MS medium under LD conditions (16 hours light and 8 hours dark) for 7 days, were transferred to complete darkness for 5 days (Figure 34A). After dark treatment the 35S:VPS2.1-GFP expressing seedlings displayed accelerated senescence, confirmed by the lower chlorophyll content compared to wild type (Figure 34B). Two independent lines of VPS2.1-GFP were tested and both of them had a decreased content of chlorophyll after dark treatment. The amount of chlorophyll in wild-type seedlings was set to 100 % and the relative amount for the two VPS2.1-GFP lines was calculated. Line 7 had 39.1% of chlorophyll and line 9 32.2 %. Both lines used in this assay were hemizygous for the construct, since no homozygous lines could be
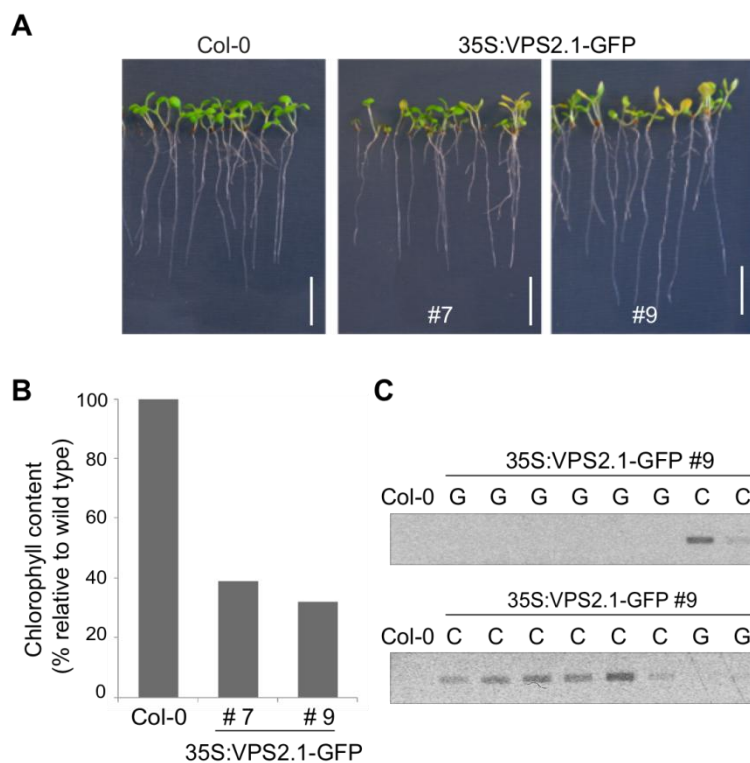
Figure 34: 35S:VPS2.1-GFP seed-lings are defective in autophagy.
A) Wild type (Col-0) and 35S:VPS2.1-GFP seedlings, from two lines (Figure 22A), were grown for 7 days under LD conditions and then transferred to dark for 5 days. Note that 35S:VPS2.1-GFP expressing seedlings exhibit starva-tion induced chlorosis. Scale Bar: 0.5 cm.
B) Chlorophyll content of seedlings shown in (A).
C) Genotypic analysis for the 35S:VPS2.1-GFP construct of the seedlings shown in (A). PCR was performed with total DNA extracted from 8 35S:VPS2.1-GFP#9 seed-lings, which were green after dark treatment (lanes:G) and from 8, which became chlorotic (lanes:C) and compared it to DNA form Col-0. Note that only those, that were chlorotic contain the construct.

obtained until now. After dark treatment not all seedlings displayed accelerated senescence. For line 9, 77% of the seedlings (n=61) became chlorotic, while only 2.5 % of wild-type seedlings (n=79). To verify that the seedlings displaying chlorosis contain the construct, 8 seedlings with or without chlorosis were genotyped for the construct (Figure 34C). Indeed only the seedlings, which were chlorotic contained the construct. Thus, VPS2.1-GFP overexpressing seedlings have impaired ability to survive under carbon limiting conditions, indicating defects in autophagy.

To continue studying putative defects of autophagy, ATG8 protein levels were investigated. An immunoblot analysis using an anti-ATG8a antibody was performed, using protein extract from dark treated seedlings and from seedlings grown under LD conditions of the same age as control (Figure 35A). ATG8 accumulated in the light grown as well as in the dark treated VPS2.1-GFP seedlings. ATG8 is accumulating under starvation and favourable conditions suggesting defects in starvation-induced autophagy and in basal constitutive autophagy.

To investigate whether also selective autophagy is impaired in the 35S:VPS2.1-GFP lines, NBR1 levels were examined. Total proteins were extracted from seedlings grown for 7 days at LD conditions and subjected to immunoblot analysis using an anti-AtNBR1 antibody (Svenning et al., 2011). I used total protein extracts from *atg7-2* mutant seedlings (Hofius et al., 2009) as a positive control for the accumulation of

NBR1 (Figure 35B). NBR1 accumulated in 35:VPS2.1-GFP lines, however, to a lesser extent than in *atg7-2*. To study further the cause for NBR1 and ATG8 accumulation, I treated 35S:VPS2.1-GFP seedlings with E64-d and analyzed the protein levels of NBR1 and ATG8 (Figure 35C). Wild type and VPS2.1-GFP overexpressing seedlings were kept for 4 days in dark to induce carbon starvation and upregulation of autophagy and then treated with E64-d to inhibit the degradation
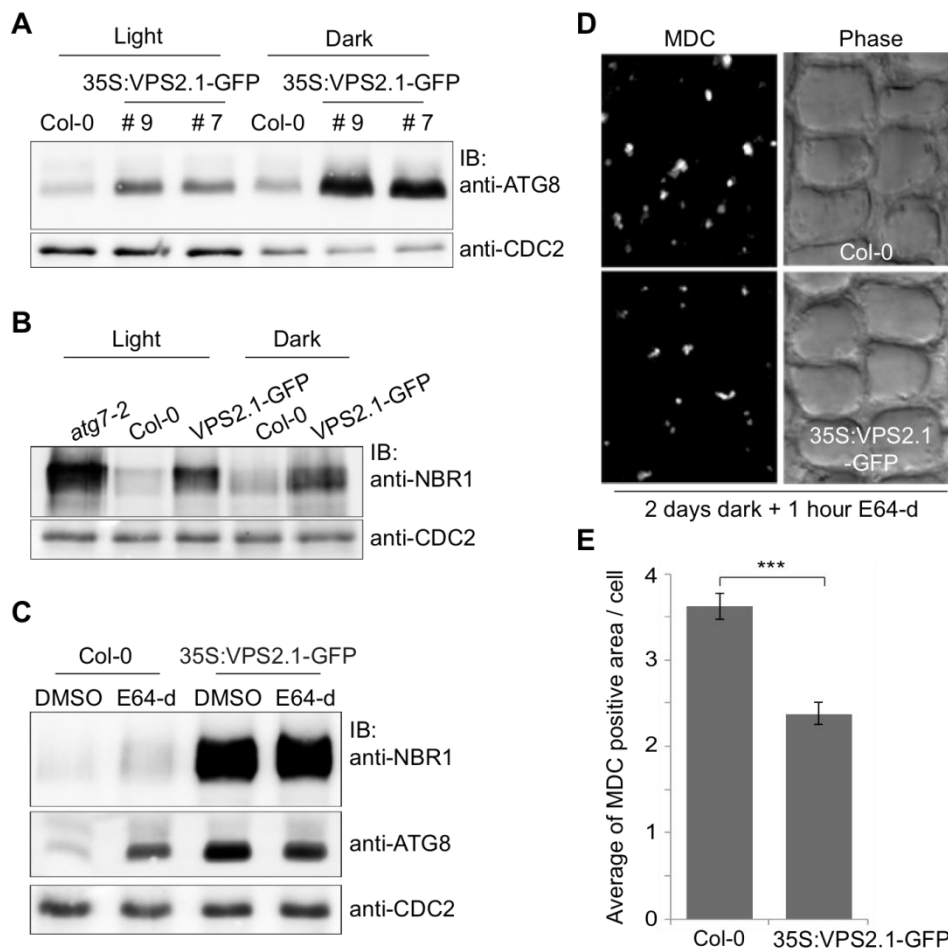
Figure 35: In 35S:VPS2.1-GFP seedlings fewer autophagosomes accumulate in the vacuoles.
A) Immunoblot analysis of protein extracts from Col-0 and 35S:VPS2.1-GFP seedlings, grown under LD conditions for 12 days (light) or for 7 days and 5 days in the dark (Dark), using an anti-ATG8 antibody. Expression of VPS2.1 was confirmed using an anti-GFP antibody. CDC2 is used as loading control.
B) Total protein extracts from Col-0 and 35S:VPS2.1-GFP seedlings grown as in (A) were analyzed on western blot with an anti-NBR1 antibody. Total protein extract from *atg7-2* mutant seedlings were used as a positive control for the accumulation of NBR1. CDC2 is used as loading control.
C) Total protein extracts from dark grown Col-0 and 35S:VPS2.1-GFP seedlings as in (A), treated with 100 µM E64-d or DMSO (mock) for 15 hours, were subjected to immunoblot analysis with anti-ATG8 and anti-NBR1 antibodies. CDC2 is used as loading control. ATG8 and NBR1 are not increased after E64-d in VPS2.1-GFP lines.
D) Confocal images of root epidermal cells of Col-0 and 35S:VPS2.1-GFP seedlings stained with MDC. Seedlings were grown for 7 days under LD conditions and then transferred to darkness for 2 days. After dark treatment seedlings were treated for 1 hour with 100 µM E64-d prior to MDC staining.
E) Statistical analysis of the area of the MDC stained autophagic bodies within the vacuoles of each cell of Col-0 and 35S:VPS2.1-GFP seedlings shown in (A). *** indicates significant difference (P<0,001).

of autophagic bodies in the vacuole. Total proteins were extracted and subjected to immunoblot analysis with an anti-NBR1 and anti-ATG8 antibody. ATG8 and NBR1 levels were increased in wild-type seedlings, while in 35S:VPS2.1-GFP the amount was constant to the mock treated seedlings. The stable levels of ATG8 and NBR1 in 35S:VPS2.1-GFP seedlings after E64-d treatment indicate that the degradation of autophagosomes within the vacuole is inhibited.

To monitor the presence of autophagosomes in the vacuoles of 35S:VPS2.1-GFP root cells, I used MDC staining combined with E64-d treatment. 35S:VPS2.1-GFP and Col-0 seedlings were grown for 7 days at LD conditions and for 2 days in dark. After dark treatment roots were treated for 1 hour with E64-d, to inhibit the degradation of the autophagic bodies in the vacuoles, and then stained with MDC (Figure 35D). The MDC positive area of autophagic bodies accumulating in the vacuoles of 547 cells of 25 wild-type and of 367 of 20 35:VPS2.1-GFP cells was measured (Figure 35D and E). The calculated average area in wild-type cells was 3.63 μm^2 and 2.39 μm^2 in 35:VPS2.1-GFP cells. There is a significant (P<0,001) 34.2% reduction of the amount of autophagic bodies accumulating in the 35:VPS2.1-GFP vacuoles.

The results obtained until this point show that the ATG8 dependent autophagy pathways, including bulk and selective autophagy, activated under favourable and starvation conditions, are attenuated in the VPS2.1-GFP lines. Fewer autophagic bodies are present in the vacuoles of these seedlings indicating defects in the fusion of autophagosomes with the vacuole, resulting in less nutrient recycling and impaired ability to survive under nutrient limiting conditions.

3.7.2 Proposed function of AMSH1, AMSH3 and VPS2.1 in autophagy

Impaired membrane fusion of autophagosomes with the vacuole in VPS2.1-GFP overexpressing seedlings, might be the result of impaired endocytosis. Proteins that are required for transport to the vacuole or for fusion of autophagosomes with the vacuole, poorly characterized in plants, are propably delivered to the vacuole via endocytosis (Figure 36). For example SNAREs, which are located at the plasma membrane or the TGN (Uemura et al., 2004) and are implicated in the fusion events of autophagosomes with the vacuole, might be delivered to the vacuole through the

endosomal trafficking system. Inhibition of endocytosis, in this case trigerred either by the expression of VPS2.1-GFP or in *amsh3* mutants, caused most likely by misfunction of ESCRT-III, results in accumulation of autophagosomes. Thus, plants in which the endosomal system is impaired are more suceptible to nutrient limiting conditions.

Taken all together, I speculate that AMSH1 and AMSH3 are playing a role in the endocytosis pathway and misfunction of the proteins results in defective endocytosis, which affects indirectly the autophagy pathway. The same is true for VPS2.1. However, it cannot be excluded that AMSH1 or AMSH3 might form a complex with VPS2.1, that acts downstream of the endosomes and the MVBs in the regulation of the activity of tethering factors, that fuse autophagosomes or even MVBs to the vacuole (Figure 36).
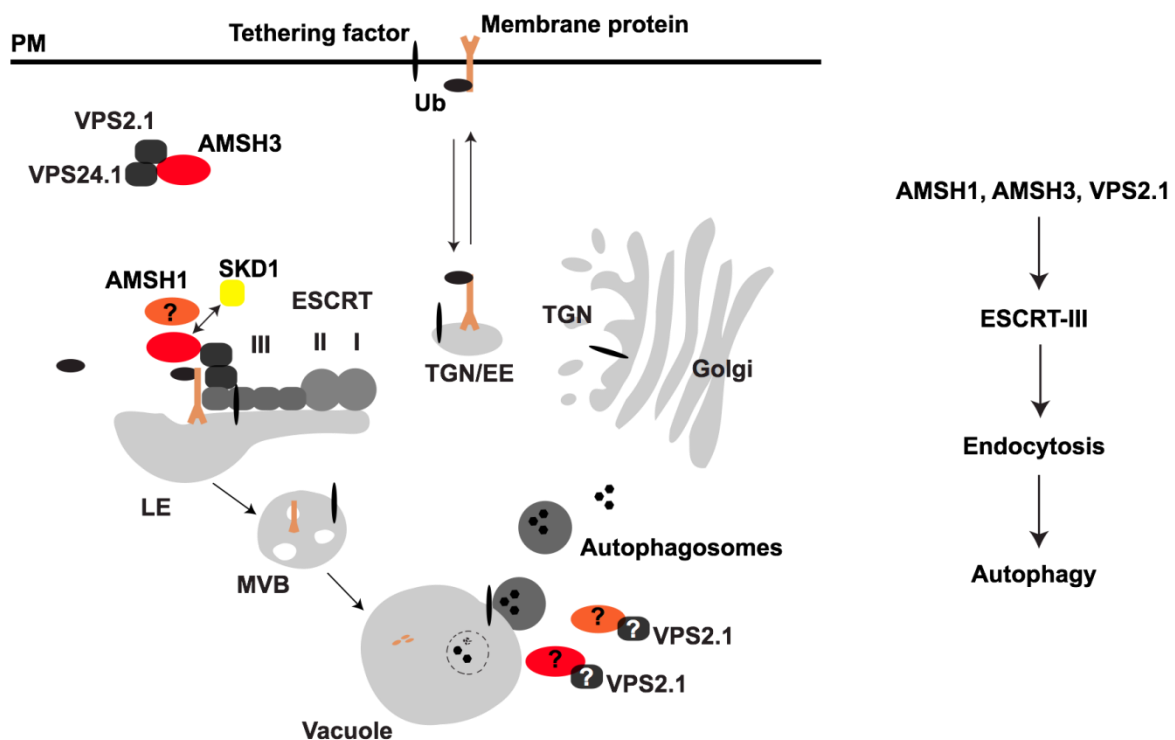
Figure 36: Endocytosis and autophagy.
AMSH1, AMSH3 and VPS2.1 contribute to the function of ESCRT-III, the last complex of the ESCRT machinery, that is important for a complete endocytosis pathway. Endocytosis promotes the autophagy pathway by delivering important tethering factors to the vacuole. These tethering factors can rely on the plasma membrane (PM) or at the trans-Golgi network (TGN) and be delivered to the vacuolar membrane through the endosomal system, in order to mediated fusion of autophagosomes with the vacuole. AMSH1, AMSH3 or VPS2.1 might play also a direct role in the fusion events of autophagosomes with the vacuole.

4. Discussion

4.1 AMSH3 interacts with ESCRT-III subunits VPS2.1 and VPS24.1 and influences the localization of these proteins

This study shows that AMSH3 interacts directly with two ESCRT-III proteins, VPS2.1 and VPS24.1. Using a dominant negative (DN) form of VPS2.1, generated by the fusion of the protein to a big carboxyl-terminal tag, the implication of VPS2.1 in endocytosis could be proved. Concurrent with these results came the publication of David Scheuring, which revealed that the expression of a dominant negative form of VPS2.1, where the MIM1 domain was depleted, inhibited the endocytosis of a reporter to the vacuole (Scheuring et al., 2011). The developmental defects upon expression of DN VPS2.1 or the embryo lethality upon loss of VPS2.1 display the severity of inhibiting endocytosis, as observed in other known *Arabidopsis*mutants of endocytosis components. *chmp1a/chmp1b* are compromised in embryo development (Spitzer et al., 2009) and expression of an inactive SKD1 mutant leads to lethality (Haas et al., 2007). To elucidate the detailed features of endocytosis in plant development, DN VPS2.1 plants will be a useful tool, since the other endocytotic mutants characterized until now are lethal. Mass spectromic analysis of the ubiquitinated conjugates, accumulating in the DN VPS2.1 plants, will be necessary to unravel new plasma membrane proteins, that are degraded in the vacuole via endocytosis.

The impaired transport of the auxin carrier PIN2 to the vacuolar like structures in *amsh3* mutants indicates the requirement of AMSH3 in endocytosis (Isono et al., 2010). Phenotypes of *amsh3* resemble effects of the expression of a dominant negative SKD1 mutant in plants (Haas et al., 2007; Shahriari et al., 2010). Constitutive overexpression of SKD1(EQ) was lethal for plants (Haas et al., 2007). Only when the expression of SKD1(EQ) was controlled by an ethanol inducible system they could observe alterations in the endomembrane system, as enlarged MVBs (Haas et al., 2007). SKD1(EQ) expressed under a trichrome specific promoter resulted in fragmented vacuoles and expression in protoplasts inhibited the transport of a soluble Carboxypeptidase S to the vacuole (Shahriari et al., 2010). The common phenotypes between AMSH3 and SKD1 in inhibition of endocytosis and vacuole fragmentation indicate that these two proteins work in the same pathway and

moreover that endocytosis might be required for proper vacuole biogenesis. Although not observed until now, it would be informative to analyze on TEM the MVBs structure in *amsh3* mutants.

Although direct association of AMSH3 with ESCRT-III is demonstrated, the precise role of AMSH3 in plant endosomal trafficking is currently unknown. The contribution of AMSH3 and its DUB activity has to be further elucidated. In *Saccharomyces cerevisiae* a specific DUB, Doa4 is shown to interact with an ESCRT-III subunit (Richter et al., 2013) and to be implicated in the endosomal trafficking system by deubiquitinating endocytosed cargos at the endosomes (Amerik et al., 2000; Richter et al., 2013). *doa4Δ* mutants exhibit cell death, caused by the limitation of free ubiquitin pool (Swaminathan et al., 1999). This is not the case for *amsh3-1* mutants, since the amount of monoubiquitin present in *amsh3* is comparable to wild-type levels (Isono et al., 2010). Binding of VPS2.1 and VPS24.1 might be required for guiding AMSH3 to its substrates, since it is not required for AMSH3 *in vitro* deubiquitination activity (Katsiarimpa et al., 2011). However, it would be informative to determine whether VPS2.1 and VPS24.1 can simultaneously bind to AMSH3 or whether they compete for AMSH3 binding, by performing a competition assay. The substrates of AMSH3 may include internalized receptors or components of the ESCRT machinery. Deubiquitination of receptors at the level of endosomes might be necessary for the proper invagination into MVBs and further degradation in the vacuole. Deubiquitination of ESCRT components might be important for their proper function.*In vivo* expression of AMSH3(ΔMIT), an AMSH3 mutant lacking the VPS2.1 and VPS24.1 binding ability, resulted in accumulation of ubiquitinated conjugates. Thus, it appears that localization of AMSH3 to certain sites, that require deubiquitination, depends on interaction with the ESCRT-III components VPS2.1 and VPS24.1. If impaired deubiquitination of the receptors or the ESCRT machinery leads to inhibition of the pathway has to be proved. This can be achieved after the characterization of AMSH3 substrates. Investigation of the endosomal system in AMSH3(ΔMIT) expressing plants, regarding cargo endocytosis, ESCRT-III assembly, MVB formation or vacuole fragmentation, will provide information about the role of AMSH3 in ESCRT-III depedent mechanisms.

While analyzing the influence of enzymatic inactive AMSH3(AXA) on the interaction with VPS2.1 and VPS24.1, stronger binding of inactive AMSH3 to VPS2.1 was detected. The AXA mutation resides in the catalytic MPN domain of the protein,

which in yeast was not required for the interaction with VPS2.1. However putative conformational changes in AMSH3, due to the mutation, might affect in a positive way the interaction. Moreover, AMSH3(AXA) sequesters specifically VPS2.1 and VPS24.1 to aberrant cytosolic compartments. This result might indicate a link between efficient enzymatic activity and release of VPS2.1 and VPS24.1. In mammalian cells an inactive version of AMSH, does not affect the localization of its interacting partner CHMP3/VPS24.1 (Kyuuma et al., 2007), suggesting that *Arabidopsis* AMSH3 might have different function than the human AMSH.

Despite the putative contribution of AMSH3 dependent deubiquitination of substrates or components of endocytosis, it can be speculated that AMSH3 contributes to the activation of VPS2.1 and VPS24.1, by releasing their autoinhibition. A study on the mammalian homologues of VPS24.1 and AMSH3 shows that AMSH can bind to the active and inactive (autoinhibited) form of CHMP3/VPS24 (Lata et al., 2008) and a model is proposed, in which AMSH is responsible for the release of the CHMP3/VPS24 autoinhibition, inducing the polymerization of the CHMP proteins and the ESCRT-III assembly (Lata et al., 2008). Release of autoinhibition is important to activate ESCRT-III proteins for membrane recruitment and complex assembly (Bajorek et al., 2009). To examine whether AMSH3 is required for the activation of VPS2.1 and VPS24.1 and the assembly of ESCRT-III, the assembly status of ESCRT-III has to be analyzed in AMSH3(ΔMIT) expressing plants or in *amsh3* mutants.

However, the partial localization of AMSH3 to class E compartments indicates that either AMSH3 disassociates from ESCRT-III after deuibiquitination or that AMSH3 interacts with additional proteins in other distinct pathways. Investigation and characterization of other interacting proteins found in the Y2H screen, that are employed in other pathways than intracellular trafficking, will provide information for the function of AMSH3 besides endocytosis and give insights into the pleiotropic effects, imposed by the disfunction of this protein.

4.2 AMSH1 interacts with VPS2.1 and VPS2.2

Besides AMSH3, this study shows that AMSH1, another *Arabidopsis* AMSH homologue, interacts in yeast also with VPS2.1. It is shown that the MIT domain of AMSH1 interacts directly with the MIM1 domain of VPS2.1 (Katsiarimpa and

Kalinowska et al., 2013). AMSH1 interacted also with VPS2.2 indicating that different residues in the MIM1 domain of VPS2.2 contribute for binding to AMSH1 than to AMSH3 or that the binding of VPS2.2 to AMSH1 is not MIT-MIM mediated. Interaction studies in yeast with different deletion constructs of VPS2.2 and AMSH1 will elucidate the binding sites.

A proteomic study of VPS2.2-GFP in *Arabidopsis* plants showed interaction with VPS2.1, SNF7.1, VPS46.1, VPS46.2 and VPS60.1, indicating incorporation of VPS2.2 in ESCRT-III (Ibl et al, 2011). Despite the ESCRT-III subunits, VPS2.2 was pulled-down with nuclear and extracellular proteins and in addition VPS2.2-GFP was located in the cytosol but also in the nucleus (Ibl et al, 2011). Due to these data and additional interaction studies in this publication they claim that diverse ESCRT-III complexes might exist in plants with different composition and roles, supporting the data obtained in this study. Although, VPS2.2 is not located to class E compartments, a role in endocytosis cannot be excluded, since it may be employed upstream of the MVB formation level. Characterization of upstream endosomal components of ESCRT-III and co-localization with VPS2.2 might reveal a functional role of VPS2.2 in intracellular trafficking.

AMSH1 might be implicated in endocytosis through interaction with VPS2.1 but also in other cellular pathways via binding to VPS2.2, which has to be further elucidated. Detailed analysis of *vps2.2* mutants as well as the behaviour of AMSH1, regarding localization or protein abundance, in *vps2.2* mutants will provide information about the role of AMSH1 dependent deubiquitination in cellular pathways despite endocytosis.

4.3 AMSH3 and AMSH1 are implicated in the autophagy pathway

This study provides evidence that AMSH3 and AMSH1 are implicated in the autophagy pathway. The impaired autophagy pathway in *amsh3* mutants (Isono et al., 2010) is also confirmed by the fact that an autophagy substrate, AGO1 is enriched in *amsh3*(Derrien et al., 2012). AGO1 is degraded upon ubiquitination through autophagy. The accumulation of AGO1 in *amsh3* suggests that autophagosomes are not degraded in this mutant. The reason of inhibition of the degradation of autophagosomes and subsequently of AGO1 can be the absent of the central vacuole with the right properties for the degradation of autophagosomes or

the impaired fusion of autophagosomes with the small vacuoles present in this mutant. In *vacuoless1* (*vcl1*), a mutant defective in vacuole formation, autophagosomes accumulate in the cytosol and do not fuse with any vacuole-like compartment formed in this mutant (Rojo et al., 2001). Thus, it can be speculated that the accumulation of autophagosomes in vacuole defective mutants like *amsh3* and *vcl1* is a consequence of the absence of vacuoles with the right properties for fusion of autophagosomes and other membrane structures, interfering in this way with nutrient supply and causing lethality. However, AMSH3 is directly implicated in this pathway, since AMSH3(AXA) are defective in autophagy but contain intact vacuoles.

In contrast to *amsh3*, *amsh1-1* does not show defects in vacuole biogenesis. In *amsh1-1* mutants minimal levels of AMSH1 might be sufficient for basal fusion of autophagosomes or other membrane structures with vacuoles. The next step would be to create a complete loss-of-function mutant of AMSH1 and analyze the autophagy and the vacuole biogenesis pathway. Moreover, it will be necessary to explore the NBR1 levels in *amsh3* mutants and investigate differences in the autophagy defects between *amsh1-1* and *amsh3*.

The data obtained in this study support the idea that AMSH1 and AMSH3 are required for autophagy, facilitating autophagosome-vacuole fusion. AMSH1 or AMSH3 might play a role in the fusion events by deubiquitinating tethering factors required for the fusion. Such tethering factors that mediate vesicular fusion events are soluble SNAREs. In yeast and mammalian cells Vam3p/Syntaxin 7 (Darsow et al., 1997; Ward et al., 2000), Vam7p/VAMP7 (Sato et al., 1998; Ward et al., 2000) Vti1p/VTI1b (Furuta et al., 2010; Ishihara et al., 2001), Ypt7p/RAB7 (Balderhaar et al., 2010; Gutierrez et al., 2004; Jager et al., 2004) participate in the docking events of autophagosomes to the vacuole/lysosome. Syntaxin 17 was recently shown in mammalian cells to be a SNARE repsonsible for fusion of autophagosomes with endosomes and lysosomes (Itakura et al., 2012). *Arabidopsis* Rab3G, the closest homologue to Ypt7p/Rab7 participates in these fusion events (Kwon et al., 2010). One of the Vti1p homologues AtVTI12, seems to be implicated in this docking, since the mutants exhibit sensitivity to nutrient limiting conditions and present defects in the fusion of autophagosomes with the vacuole (Surpin et al., 2003). *Arabidopsis* VPS45 interacts with the SNARE complex SYP41/SYP61/VTI12 and is involved in vesicle trafficking to the vacuole (Zouhar et al., 2009). *Arabidopsis* plants lacking VPS45 are

sensitive to carbon limiting conditions and through additional experiments it is claimed that breakdown of autophagosomes is impaired in these mutants (Zouhar et al., 2009). Moreover, in this study they show that loss of VPS45 results in defective vacuole formation. The fragmented vacuoles in this mutant resemble the vacuolar phenotype of *amsh3*, suggesting a connection between autophagy and vacuole biogenesis. More and more speculations are rising about the participation of autophagy in vacuole biogenesis, however, with no direct proof yet, since no vacuole formation defects have been observed until now in autophagy deficient mutants.

In *AMSH-/-* deficient mouse brains no accumulation of microtubule-associated protein 1 light chain 3 (LC3), the mammalian homologue of yeast Atg8p, positive vesicles could be detected, suggesting no accumulation of autophagosomes. However, p62 aggregates were accumulating (Suzuki et al., 2011). p62 is a selective autophagy substrate (Lamark et al., 2009). This study propose a function of mammalian AMSH in autophagosome-lysosome fusion in selective autophagy, since clearance of p62 is impaired in *AMSH-/-* deficient mouse (Suzuki et al., 2011). In contrast, in *amsh1-1* selective autophagy is not affected, since NBR1 is not increased even after nutrient limiting conditions, but autophagosomes are accumulating. Analysis of NBR1 in null *amsh1* mutants will draw conclusions about the putative role of AMSH1 in selective autophagy and unravel differences between the function of *Arabidopsis* AMSH1 and mammalian AMSH. In human AMSH deficient patients autophagosomes are accumulating (McDonell et al., 2013). Accumulation of autophagosomes in these patients was shown to be a result of increased autophagic flux, since after inhibiting the fusion of autophagosomes with the lysosome, elevated levels of LC3 amounts were observed compared to wild type (McDonell et al., 2013). In *amsh1-1* accumulation of autophagosomes is not a result of increased autophagic flux, since Atg8 transcript levels are not increased (Katsiarimpa and Kalinowska et al., 2013), as shown in *Arabidopsis* when autophagy is activated (Doelling et al., 2002; Thompson et al., 2005). Increasing evidences arises about the implication of AMSH proteins in autophagy, however, it appears that mammalian and *Arabidopsis* AMSH proteins have differential contribution to this pathway.

4.4 Endocytosis and autophagy

According to this work we are able to discuss a connection between endocytosis and autophagy. Membrane fusion defects of autophagosomes with the vacuole in DN VPS2.1 seedlings as well as in *amsh1-1* and *amsh3* mutants might be the result of impaired endocytosis, indicating that the autophagy defects in these mutants are a consequence of an ihibited endocytosis pathway. For AMSH1, characterization of the role in endocytosis as well as analysis of endocytosis in dark treated *amsh1-1* seedlings will provide information for a connection between endocytosis and autophagy.

It is shown in mammalian cells that endocytosis and autophagy are connected. A convergent point exists between the two main catabolic pathways, which result in the degradation of proteins in the vacuole. Autophagosomes can fuse with late endosomes (MVBs) and form the amphisome, which in turn fuses with the lysosome (Berg et al., 1998; Jing and Tang, 1999). Autophagy defects observed in endocytosis defective mutants, confirm the association between these two pathways. Dysfunction of ESCRT-III in mammalian cells causes accumulation of autophagosomes. Depletion of CHMP3/VPS24 causes the accumulation of p62 (Filimoneko et al., 2007). In addition overexpression of a dominant negative form of CHMP2/VPS2, where the C-terminus of the protein, containing the MIM1 domain, is depleted, results in inhibition of autophagosome degradation (Filimoneko et al., 2007; Liou et al., 1997). Moreover, the expression of VPS4(EQ) resulted also in accumulation of autophagosomes (Nara et al., 2002). Dysfunctional ESCRT-III blocks the fusion of autophagosomes with MVBs and as a result autophagic substrates are accumulated (Liou et al., 1997; Lee and Gao, 2008; Lee et al., 2007).

Co-localization studies of autophagosomal markers, like ATG8 and different endosomal markers will provide information whether in plants autophagosomes fuse with endosomes before fusing with the vacuolar membrane. TEM analysis on DN VPS2.1 plants for the structure of endosomes or autophagosomes, compared to wild type, will contribute for answering this question and will elucidate the exact defects of autophagy in these plants. Although in the confocal images of DN VPS2.1 seedlings, no aberrant defects in vacuole formation were observed, it would be useful to analyze DN VPS2.1 seedlings in more detail regarding putative vacuole defects and

discuss a putative requirement of an intact endosomal trafficking pathway for autophagy and even more for vacuole biogenesis.

References

Agromayor, M., Carlton, J.G., Phelan, J.P., Matthews, D.R., Carlin, L.M., Ameer-Beg, S., Bowers, K., Martin-Serrano, J., 2009. Essential role of hIST1 in cytokinesis. Molecular biology of the cell 20, 1374-1387.

Agromayor, M., Martin-Serrano, J., 2006. Interaction of AMSH with ESCRT-III and deubiquitination of endosomal cargo. The Journal of biological chemistry 281, 23083-23091.

Alam, S.L., Sun, J., Payne, M., Welch, B.D., Blake, B.K., Davis, D.R., Meyer, H.H., Emr, S.D., Sundquist, W.I., 2004. Ubiquitin interactions of NZF zinc fingers. The EMBO journal 23, 1411-1421.

Amerik, A.Y., Hochstrasser, M., 2004. Mechanism and function of deubiquitinating enzymes. Biochimica et biophysica acta 1695, 189-207.

Amerik, A.Y., Nowak, J., Swaminathan, S., Hochstrasser, M., 2000. The Doa4 deubiquitinating enzyme is functionally linked to the vacuolar protein-sorting and endocytic pathways. Molecular biology of the cell 11, 3365-3380.

Aoyama, T., Chua, N.H., 1997. A glucocorticoid-mediated transcriptional induction system in transgenic plants. The Plant Journal 11: 605–612

Asao, H., Sasaki, Y., Arita, T., Tanaka, N., Endo, K., Kasai, H., Takeshita, T., Endo, Y., Fujita, T., Sugamura, K., 1997. Hrs is associated with STAM, a signal-transducing adaptor molecule. Its suppressive effect on cytokine-induced cell growth. The Journal of biological chemistry 272, 32785-32791.

Azmi, I., Davies, B., Dimaano, C., Payne, J., Eckert, D., Babst, M., Katzmann, D.J., 2006. Recycling of ESCRTs by the AAA-ATPase Vps4 is regulated by a conserved VSL region in Vta1. The Journal of cell biology 172, 705-717.

Babst, M., Katzmann, D.J., Estepa-Sabal, E.J., Meerloo, T., Emr, S.D., 2002a. Escrt-III: an endosome-associated heterooligomeric protein complex required for mvb sorting. Developmental cell 3, 271-282.

Babst, M., Katzmann, D.J., Snyder, W.B., Wendland, B., Emr, S.D., 2002b. Endosome-associated complex, ESCRT-II, recruits transport machinery for protein sorting at the multivesicular body. Developmental cell 3, 283-289.

Babst, M., Sato, T.K., Banta, L.M., Emr, S.D., 1997. Endosomal transport function in yeast requires a novel AAA-type ATPase, Vps4p. The EMBO journal 16, 1820-1831.

Babst, M., Wendland, B., Estepa, E.J., Emr, S.D., 1998. The Vps4p AAA ATPase regulates membrane association of a Vps protein complex required for normal endosome function. The EMBO journal 17, 2982-2993.

Bache, K.G., Brech, A., Mehlum, A., Stenmark, H., 2003. Hrs regulates multivesicular body formation via ESCRT recruitment to endosomes. The Journal of cell biology 162, 435-442.

Bajorek, M., Schubert, H.L., McCullough, J., Langelier, C., Eckert, D.M., Stubblefield, W.M., Uter, N.T., Myszka, D.G., Hill, C.P., Sundquist, W.I., 2009. Structural basis for ESCRT-III protein autoinhibition. Nature structural & molecular biology 16, 754-762.

Balderhaar, H.J., Arlt, H., Ostrowicz, C., Brocker, C., Sundermann, F., Brandt, R., Babst, M., Ungermann, C., 2010. The Rab GTPase Ypt7 is linked to retromer-mediated receptor recycling and fusion at the yeast late endosome. Journal of cell science 123, 4085-4094.

Balut, C.M., Loch, C.M., Devor, D.C., 2011. Role of ubiquitylation and USP8-dependent deubiquitylation in the endocytosis and lysosomal targeting of plasma membrane KCa3.1. FASEB journal : official publication of the Federation of American Societies for Experimental Biology 25, 3938-3948.

Bar, M., Aharon, M., Benjamin, S., Rotblat, B., Horowitz, M., Avni, A., 2008. AtEHDs, novel Arabidopsis EH-domain-containing proteins involved in endocytosis. The Plant journal : for cell and molecular biology 55, 1025-1038.

Bar, M., Avni, A., 2009. EHD2 inhibits ligand-induced endocytosis and signaling of the leucine-rich repeat receptor-like protein LeEix2. The Plant journal : for cell and molecular biology 59, 600-611.

Barberon, M., Zelazny, E., Robert, S., Conejero, G., Curie, C., Friml, J., Vert, G., 2011. Monoubiquitin-dependent endocytosis of the iron-regulated transporter 1 (IRT1) transporter controls iron uptake in plants. Proceedings of the National Academy of Sciences of the United States of America 108, E450-458.

Bassham, D.C., 2007. Plant autophagy--more than a starvation response. Current opinion in plant biology 10, 587-593.

Bassham, D.C., 2009. Function and regulation of macroautophagy in plants. Biochimica et biophysica acta 1793, 1397-1403.

Behrends, C., Fulda, S., 2012. Receptor proteins in selective autophagy. International journal of cell biology 2012, 673290.

Bowers, K., Lottridge, J., Helliwell, S.B., Goldthwaite, L.M., Luzio, J.P., Stevens, T.H., 2004. Protein-protein interactions of ESCRT complexes in the yeast Saccharomyces cerevisiae. Traffic 5, 194-210.

Bradford M.M., 1976. A rapid and sensitive method for the quantitation of microgram quantities of protein utilizing the principle of protein-dye binding. Analytical Biochemistry 72, 248-254

Chung, T., Phillips, A.R., Vierstra, R.D., 2010. ATG8 lipidation and ATG8-mediated autophagy in Arabidopsis require ATG12 expressed from the differentially controlled ATG12A AND ATG12B loci. The Plant journal : for cell and molecular biology 62, 483-493.

Clague, M.J., Coulson, J.M., Urbe, S., 2012. Cellular functions of the DUBs. Journal of cell science 125, 277-286.

Clague, M.J., Urbe, S., 2006. Endocytosis: the DUB version. Trends in cell biology 16, 551-559.

Clough S.J., Bent A.F., 1998. Floral dip: a simplified method for Agrobacterium-mediated transformation of Arabidopsis thaliana. The Plant Journal 16, 735-743

Contento, A.L., Xiong, Y., Bassham, D.C., 2005. Visualization of autophagy in Arabidopsis using the fluorescent dye monodansylcadaverine and a GFP-AtATG8e fusion protein. The Plant journal : for cell and molecular biology 42, 598-608.

Darsow, T., Rieder, S.E., Emr, S.D., 1997. A multispecificity syntaxin homologue, Vam3p, essential for autophagic and biosynthetic protein transport to the vacuole. The Journal of cell biology 138, 517-529.

Derrien, B., Baumberger, N., Schepetilnikov, M., Viotti, C., De Cillia, J., Ziegler-Graff, V., Isono, E., Schumacher, K., Genschik, P., 2012. Degradation of the antiviral component ARGONAUTE1 by the autophagy pathway. Proceedings of the National Academy of Sciences of the United States of America 109, 15942-15946.

Dettmer, J., Hong-Hermesdorf, A., Stierhof, Y.D., Schumacher, K., 2006. Vacuolar H+-ATPase activity is required for endocytic and secretory trafficking in Arabidopsis. Plant Cell 18, 715-730.

Dikic, I., Wakatsuki, S., Walters, K.J., 2009. Ubiquitin-binding domains - from structures to functions. Nature reviews. Molecular cell biology 10, 659-671.

Doelling, J.H., Walker, J.M., Friedman, E.M., Thompson, A.R., Vierstra, R.D., 2002. The APG8/12-activating enzyme APG7 is required for proper nutrient recycling and senescence in Arabidopsis thaliana. The Journal of biological chemistry 277, 33105-33114.

Downes, B., Vierstra, R.D., 2005. Post-translational regulation in plants employing a diverse set of polypeptide tags. Biochemical Society transactions 33, 393-399.

Elsasser, S., Schmidt, M., Finley, D., 2005. Characterization of the proteasome using native gel electrophoresis. Methods in enzymology 398, 353-363.

Finley, D., Ulrich, H.D., Sommer, T., Kaiser, P., 2012. The ubiquitin-proteasome system of Saccharomyces cerevisiae. Genetics 192, 319-360.

Fujita, H., Umezuki, Y., Imamura, K., Ishikawa, D., Uchimura, S., Nara, A., Yoshimori, T., Hayashizaki, Y., Kawai, J., Ishidoh, K., Tanaka, Y., Himeno, M., 2004. Mammalian class E Vps proteins, SBP1 and mVps2/CHMP2A, interact with and regulate the function of an AAA-ATPase SKD1/Vps4B. Journal of cell science 117, 2997-3009.

Furuta, N., Fujita, N., Noda, T., Yoshimori, T., Amano, A., 2010. Combinational soluble N-ethylmaleimide-sensitive factor attachment protein receptor proteins VAMP8 and Vti1b mediate fusion

of antimicrobial and canonical autophagosomes with lysosomes. Molecular biology of the cell 21, 1001-1010.

Geetha, T., Jiang, J., Wooten, M.W., 2005. Lysine 63 polyubiquitination of the nerve growth factor receptor TrkA directs internalization and signaling. Molecular cell 20, 301-312.

Geldner, N., Denervaud-Tendon, V., Hyman, D.L., Mayer, U., Stierhof, Y.-D., Chory, J., 2009. Rapid, combinatorial analysis of membrane compartments in intact plants with a multicolor marker set. Plant J 59, 169-178.

Gusmaroli, G., Feng, S., Deng, X.W., 2004. The Arabidopsis CSN5A and CSN5B subunits are present in distinct COP9 signalosome complexes, and mutations in their JAMM domains exhibit differential dominant negative effects on development. Plant Cell 16, 2984-3001.

Gutierrez, M.G., Munafo, D.B., Beron, W., Colombo, M.I., 2004. Rab7 is required for the normal progression of the autophagic pathway in mammalian cells. Journal of cell science 117, 2687-2697.

Haas, T.J., Sliwinski, M.K., Martinez, D.E., Preuss, M., Ebine, K., Ueda, T., Nielsen, E., Odorizzi, G., Otegui, M.S., 2007. The Arabidopsis AAA ATPase SKD1 is involved in multivesicular endosome function and interacts with its positive regulator LYST-INTERACTING PROTEIN5. Plant Cell 19, 1295-1312.

Haglund, K., Dikic, I., 2012. The role of ubiquitylation in receptor endocytosis and endosomal sorting. Journal of cell science 125, 265-275.

Haglund, K., Sigismund, S., Polo, S., Szymkiewicz, I., Di Fiore, P.P., Dikic, I., 2003. Multiple monoubiquitination of RTKs is sufficient for their endocytosis and degradation. Nature cell biology 5, 461-466.

Hanaoka, H., Noda, T., Shirano, Y., Kato, T., Hayashi, H., Shibata, D., Tabata, S., Ohsumi, Y., 2002. Leaf senescence and starvation-induced chlorosis are accelerated by the disruption of an Arabidopsis autophagy gene. Plant physiology 129, 1181-1193.

Henne, W.M., Buchkovich, N.J., Emr, S.D., 2011. The ESCRT pathway. Developmental cell 21, 77-91.

Herberth, S., Shahriari, M., Bruderek, M., Hessner, F., Muller, B., Hulskamp, M., Schellmann, S., 2012. Artificial ubiquitylation is sufficient for sorting of a plasma membrane ATPase to the vacuolar lumen of Arabidopsis cells. Planta 236, 63-77.

Herrmann, J., Lerman, L.O., Lerman, A., 2007. Ubiquitin and ubiquitin-like proteins in protein regulation. Circulation research 100, 1276-1291.

Hershko, A., Ciechanover, A., 1998. The ubiquitin system. Annual review of biochemistry 67, 425-479.

Hierro, A., Sun, J., Rusnak, A.S., Kim, J., Prag, G., Emr, S.D., Hurley, J.H., 2004. Structure of the ESCRT-II endosomal trafficking complex. Nature 431, 221-225.

Hofius, D., Schultz-Larsen, T., Joensen, J., Tsitsigiannis, D.I., Petersen, N.H., Mattsson, O., Jorgensen, L.B., Jones, J.D., Mundy, J., Petersen, M., 2009. Autophagic components contribute to hypersensitive cell death in Arabidopsis. Cell 137, 773-783.

Howard, T.L., Stauffer, D.R., Degnin, C.R., Hollenberg, S.M., 2001. CHMP1 functions as a member of a newly defined family of vesicle trafficking proteins. Journal of cell science 114, 2395-2404.

Hurley, J.H., 2008. ESCRT complexes and the biogenesis of multivesicular bodies. Current opinion in cell biology 20, 4-11.

Hurley, J.H., Lee, S., Prag, G., 2006. Ubiquitin-binding domains. The Biochemical journal 399, 361-372.

Husnjak, K., Dikic, I., 2012. Ubiquitin-binding proteins: decoders of ubiquitin-mediated cellular functions. Annual review of biochemistry 81, 291-322.

Ibl, V., Csaszar, E., Schlager, N., Neubert, S., Spitzer, C., Hauser, M.T., 2012. Interactome of the plant-specific ESCRT-III component AtVPS2.2 in Arabidopsis thaliana. Journal of proteome research 11, 397-411.

Ikeda, F., Dikic, I., 2008. Atypical ubiquitin chains: new molecular signals. 'Protein Modifications: Beyond the Usual Suspects' review series. EMBO reports 9, 536-542.

Im, Y.J., Hurley, J.H., 2008. Integrated structural model and membrane targeting mechanism of the human ESCRT-II complex. Developmental cell 14, 902-913.

Im, Y.J., Wollert, T., Boura, E., Hurley, J.H., 2009. Structure and function of the ESCRT-II-III interface in multivesicular body biogenesis. Developmental cell 17, 234-243.

Inoue, Y., Suzuki, T., Hattori, M., Yoshimoto, K., Ohsumi, Y., Moriyasu, Y., 2006. AtATG genes, homologs of yeast autophagy genes, are involved in constitutive autophagy in Arabidopsis root tip cells. Plant & cell physiology 47, 1641-1652.

Ishida, H., Yoshimoto, K., 2008. Chloroplasts are partially mobilized to the vacuole by autophagy. Autophagy 4, 961-962.

Ishihara, N., Hamasaki, M., Yokota, S., Suzuki, K., Kamada, Y., Kihara, A., Yoshimori, T., Noda, T., Ohsumi, Y., 2001. Autophagosome requires specific early Sec proteins for its formation and NSF/SNARE for vacuolar fusion. Molecular biology of the cell 12, 3690-3702.

Ishii, N., Owada, Y., Yamada, M., Miura, S., Murata, K., Asao, H., Kondo, H., Sugamura, K., 2001. Loss of neurons in the hippocampus and cerebral cortex of AMSH-deficient mice. Molecular and cellular biology 21, 8626-8637.

Isono, E., Katsiarimpa, A., Muller, I.K., Anzenberger, F., Stierhof, Y.D., Geldner, N., Chory, J., Schwechheimer, C., 2010. The deubiquitinating enzyme AMSH3 is required for intracellular trafficking and vacuole biogenesis in Arabidopsis thaliana. Plant Cell 22, 1826-1837.

Itakura, E., Kishi-Itakura, C., Mizushima, N., 2012. The hairpin-type tail-anchored SNARE syntaxin 17 targets to autophagosomes for fusion with endosomes/lysosomes. Cell 151, 1256-1269.

Iwai, K., Tokunaga, F., 2009. Linear polyubiquitination: a new regulator of NF-kappaB activation. EMBO reports 10, 706-713.

Jager, S., Bucci, C., Tanida, I., Ueno, T., Kominami, E., Saftig, P., Eskelinen, E.L., 2004. Role for Rab7 in maturation of late autophagic vacuoles. Journal of cell science 117, 4837-4848.

Jou, Y., Chiang, C.P., Jauh, G.Y., Yen, H.E., 2006. Functional characterization of ice plant SKD1, an AAA-type ATPase associated with the endoplasmic reticulum-Golgi network, and its role in adaptation to salt stress. Plant physiology 141, 135-146.

Kasai, K., Takano, J., Miwa, K., Toyoda, A., Fujiwara, T., 2011. High boron-induced ubiquitination regulates vacuolar sorting of the BOR1 borate transporter in Arabidopsis thaliana. The Journal of biological chemistry 286, 6175-6183.

Kato, M., Miyazawa, K., Kitamura, N., 2000. A deubiquitinating enzyme UBPY interacts with the Src homology 3 domain of Hrs-binding protein via a novel binding motif PX(V/I)(D/N)RXXKP. The Journal of biological chemistry 275, 37481-37487.

Katsiarimpa, A., Anzenberger, F., Schlager, N., Neubert, S., Hauser, M.T., Schwechheimer, C., Isono, E., 2011. The Arabidopsis deubiquitinating enzyme AMSH3 interacts with ESCRT-III subunits and regulates their localization. Plant Cell 23, 3026-3040.

Katsiarimpa, A., Kalinowska, K., Anzenberger, F., Weis, C., Ostertag, M., Tsutsumi, C., Schwechheimer, C., Brunner, F., Huckelhoven, R., Isono, E., 2013. The Deubiquitinating Enzyme AMSH1 and the ESCRT-III Subunit VPS2.1 Are Required for Autophagic Degradation in Arabidopsis. Plant Cell.

Katzmann, D.J., Babst, M., Emr, S.D., 2001. Ubiquitin-dependent sorting into the multivesicular body pathway requires the function of a conserved endosomal protein sorting complex, ESCRT-I. Cell 106, 145-155.

Katzmann, D.J., Stefan, C.J., Babst, M., Emr, S.D., 2003. Vps27 recruits ESCRT machinery to endosomes during MVB sorting. The Journal of cell biology 162, 413-423.

Kerscher, O., Felberbaum, R., Hochstrasser, M., 2006. Modification of proteins by ubiquitin and ubiquitin-like proteins. Annual review of cell and developmental biology 22, 159-180.

Kieffer, C., Skalicky, J.J., Morita, E., De Domenico, I., Ward, D.M., Kaplan, J., Sundquist, W.I., 2008. Two distinct modes of ESCRT-III recognition are required for VPS4 functions in lysosomal protein targeting and HIV-1 budding. Developmental cell 15, 62-73.

Kikuchi, K., Ishii, N., Asao, H., Sugamura, K., 2003. Identification of AMSH-LP containing a Jab1/MPN domain metalloenzyme motif. Biochemical and biophysical research communications 306, 637-643.

Kim, J., Harter, K., Theologis, A., 1997. Protein-protein interactions among the Aux/IAA proteins. Proc Natl Acad Sci U S A 94, 11786-11791.

Kim, M.S., Kim, J.A., Song, H.K., Jeon, H., 2006. STAM-AMSH interaction facilitates the deubiquitination activity in the C-terminal AMSH. Biochemical and biophysical research communications 351, 612-618.

Kimura, Y., Tanaka, K., 2010. Regulatory mechanisms involved in the control of ubiquitin homeostasis. Journal of biochemistry 147, 793-798.

Kirisako, T., Kamei, K., Murata, S., Kato, M., Fukumoto, H., Kanie, M., Sano, S., Tokunaga, F., Tanaka, K., Iwai, K., 2006. A ubiquitin ligase complex assembles linear polyubiquitin chains. The EMBO journal 25, 4877-4887.

Kirkin, V., Lamark, T., Johansen, T., Dikic, I., 2009a. NBR1 cooperates with p62 in selective autophagy of ubiquitinated targets. Autophagy 5, 732-733.

Kirkin, V., Lamark, T., Sou, Y.S., Bjorkoy, G., Nunn, J.L., Bruun, J.A., Shvets, E., McEwan, D.G., Clausen, T.H., Wild, P., Bilusic, I., Theurillat, J.P., Overvatn, A., Ishii, T., Elazar, Z., Komatsu, M., Dikic, I., Johansen, T., 2009b. A role for NBR1 in autophagosomal degradation of ubiquitinated substrates. Molecular cell 33, 505-516.

Kirkin, V., McEwan, D.G., Novak, I., Dikic, I., 2009c. A role for ubiquitin in selective autophagy. Molecular cell 34, 259-269.

Klionsky, D.J., Emr, S.D., 2000. Autophagy as a regulated pathway of cellular degradation. Science 290, 1717-1721.

Klionsky, D.J., Ohsumi, Y., 1999. Vacuolar import of proteins and organelles from the cytoplasm. Annual review of cell and developmental biology 15, 1-32.

Koegl, M., Hoppe, T., Schlenker, S., Ulrich, H.D., Mayer, T.U., Jentsch, S., 1999. A novel ubiquitination factor, E4, is involved in multiubiquitin chain assembly. Cell 96, 635-644.

Komander, D., 2009. The emerging complexity of protein ubiquitination. Biochemical Society transactions 37, 937-953.

Komander, D., 2010. Mechanism, specificity and structure of the deubiquitinases. Sub-cellular biochemistry 54, 69-87.

Komander, D., Rape, M., 2012. The ubiquitin code. Annual review of biochemistry 81, 203-229.

Kulathu, Y., Komander, D., 2012. Atypical ubiquitylation - the unexplored world of polyubiquitin beyond Lys48 and Lys63 linkages. Nature reviews. Molecular cell biology 13, 508-523.

Kwon, S.I., Cho, H.J., Jung, J.H., Yoshimoto, K., Shirasu, K., Park, O.K., 2010. The Rab GTPase RabG3b functions in autophagy and contributes to tracheary element differentiation in Arabidopsis. The Plant journal : for cell and molecular biology 64, 151-164.

Kyuuma, M., Kikuchi, K., Kojima, K., Sugawara, Y., Sato, M., Mano, N., Goto, J., Takeshita, T., Yamamoto, A., Sugamura, K., Tanaka, N., 2007. AMSH, an ESCRT-III associated enzyme, deubiquitinates cargo on MVB/late endosomes. Cell structure and function 31, 159-172.

Lamark, T., Kirkin, V., Dikic, I., Johansen, T., 2009. NBR1 and p62 as cargo receptors for selective autophagy of ubiquitinated targets. Cell cycle 8, 1986-1990.

Lata, S., Roessle, M., Solomons, J., Jamin, M., Gottlinger, H.G., Svergun, D.I., Weissenhorn, W., 2008. Structural basis for autoinhibition of ESCRT-III CHMP3. Journal of molecular biology 378, 818-827.

Leitner, J., Petrasek, J., Tomanov, K., Retzer, K., Parezova, M., Korbei, B., Bachmair, A., Zazimalova, E., Luschnig, C., 2012. Lysine63-linked ubiquitylation of PIN2 auxin carrier protein governs hormonally controlled adaptation of Arabidopsis root growth. Proceedings of the National Academy of Sciences of the United States of America 109, 8322-8327.

Lenz, H.D., Haller, E., Melzer, E., Kober, K., Wurster, K., Stahl, M., Bassham, D.C., Vierstra, R.D., Parker, J.E., Bautor, J., Molina, A., Escudero, V., Shindo, T., van der Hoorn, R.A., Gust, A.A., Nurnberger, T., 2011. Autophagy differentially controls plant basal immunity to biotrophic and necrotrophic pathogens. The Plant journal : for cell and molecular biology 66, 818-830.

Leung, K.F., Dacks, J.B., Field, M.C., 2008. Evolution of the multivesicular body ESCRT machinery; retention across the eukaryotic lineage. Traffic 9, 1698-1716.

Levine, B., Kroemer, G., 2008. Autophagy in the pathogenesis of disease. Cell 132, 27-42.

Liu, Y., Schiff, M., Czymmek, K., Talloczy, Z., Levine, B., Dinesh-Kumar, S.P., 2005. Autophagy regulates programmed cell death during the plant innate immune response. Cell 121, 567-577.

Martin-Serrano, J., Zang, T., Bieniasz, P.D., 2003. Role of ESCRT-I in retroviral budding. Journal of virology 77, 4794-4804.

McCullough, J., Clague, M.J., Urbe, S., 2004. AMSH is an endosome-associated ubiquitin isopeptidase. The Journal of cell biology 166, 487-492.

McCullough, J., Row, P.E., Lorenzo, O., Doherty, M., Beynon, R., Clague, M.J., Urbe, S., 2006. Activation of the endosome-associated ubiquitin isopeptidase AMSH by STAM, a component of the multivesicular body-sorting machinery. Current biology : CB 16, 160-165.

McDonell, L.M., Mirzaa, G.M., Alcantara, D., Schwartzentruber, J., Carter, M.T., Lee, L.J., Clericuzio, C.L., Graham, J.M., Jr., Morris-Rosendahl, D.J., Polster, T., Acsadi, G., Townshend, S., Williams, S., Halbert, A., Isidor, B., David, A., Smyser, C.D., Paciorkowski, A.R., Willing, M., Woulfe, J., Das, S., Beaulieu, C.L., Marcadier, J., Consortium, F.C., Geraghty, M.T., Frey, B.J., Majewski, J., Bulman, D.E., Dobyns, W.B., O'Driscoll, M., Boycott, K.M., 2013. Mutations in STAMBP, encoding a deubiquitinating enzyme, cause microcephaly-capillary malformation syndrome. Nature genetics 45, 556-562.

Mevissen, T.E., Hospenthal, M.K., Geurink, P.P., Elliott, P.R., Akutsu, M., Arnaudo, N., Ekkebus, R., Kulathu, Y., Wauer, T., El Oualid, F., Freund, S.M., Ovaa, H., Komander, D., 2013. OTU deubiquitinases reveal mechanisms of linkage specificity and enable ubiquitin chain restriction analysis. Cell 154, 169-184.

Mizushima, N., 2005. The pleiotropic role of autophagy: from protein metabolism to bactericide. Cell death and differentiation 12 Suppl 2, 1535-1541.

Mizushima, N., 2007. Autophagy: process and function. Genes & development 21, 2861-2873.

Morita, E., Colf, L.A., Karren, M.A., Sandrin, V., Rodesch, C.K., Sundquist, W.I., 2010. Human ESCRT-III and VPS4 proteins are required for centrosome and spindle maintenance. Proceedings of the National Academy of Sciences of the United States of America 107, 12889-12894.

Mosesson, Y., Shtiegman, K., Katz, M., Zwang, Y., Vereb, G., Szollosi, J., Yarden, Y., 2003. Endocytosis of receptor tyrosine kinases is driven by monoubiquitylation, not polyubiquitylation. The Journal of biological chemistry 278, 21323-21326.

Mukai, A., Mizuno, E., Kobayashi, K., Matsumoto, M., Nakayama, K.I., Kitamura, N., Komada, M., 2008. Dynamic regulation of ubiquitylation and deubiquitylation at the central spindle during cytokinesis. Journal of cell science 121, 1325-1333.

Nakagawa, T., Kurose, T., Hino, T., Tanaka, K., Kawamukai, M., Niwa, Y., Toyooka, K., Matsuoka, K., Jinbo, T., Kimura, T., 2007. Development of series of gateway binary vectors, pGWBs, for realizing efficient construction of fusion genes for plant transformation. J Biosci Bioeng 104, 34-41.

Nakamura, M., Tanaka, N., Kitamura, N., Komada, M., 2006. Clathrin anchors deubiquitinating enzymes, AMSH and AMSH-like protein, on early endosomes. Genes to cells : devoted to molecular & cellular mechanisms 11, 593-606.

Nickerson, D.P., West, M., Odorizzi, G., 2006. Did2 coordinates Vps4-mediated dissociation of ESCRT-III from endosomes. The Journal of cell biology 175, 715-720.

Nijman, S.M., Luna-Vargas, M.P., Velds, A., Brummelkamp, T.R., Dirac, A.M., Sixma, T.K., Bernards, R., 2005. A genomic and functional inventory of deubiquitinating enzymes. Cell 123, 773-786.

Nikko, E., Andre, B., 2007. Evidence for a direct role of the Doa4 deubiquitinating enzyme in protein sorting into the MVB pathway. Traffic 8, 566-581.

Obita, T., Saksena, S., Ghazi-Tabatabai, S., Gill, D.J., Perisic, O., Emr, S.D., Williams, R.L., 2007. Structural basis for selective recognition of ESCRT-III by the AAA ATPase Vps4. Nature 449, 735-739.

Ohsumi, Y., 2001. Molecular dissection of autophagy: two ubiquitin-like systems. Nature reviews. Molecular cell biology 2, 211-216.

Otegui, M.S., Spitzer, C., 2008. Endosomal functions in plants. Traffic 9, 1589-1598.

Papa, F.R., Amerik, A.Y., Hochstrasser, M., 1999. Interaction of the Doa4 deubiquitinating enzyme with the yeast 26S proteasome. Molecular biology of the cell 10, 741-756.

Papa, F.R., Hochstrasser, M., 1993. The yeast DOA4 gene encodes a deubiquitinating enzyme related to a product of the human tre-2 oncogene. Nature 366, 313-319.

Phillips, A.R., Suttangkakul, A., Vierstra, R.D., 2008. The ATG12-conjugating enzyme ATG10 Is essential for autophagic vesicle formation in Arabidopsis thaliana. Genetics 178, 1339-1353.

Piper, R.C., Cooper, A.A., Yang, H., Stevens, T.H., 1995. VPS27 controls vacuolar and endocytic traffic through a prevacuolar compartment in Saccharomyces cerevisiae. The Journal of cell biology 131, 603-617.

Piper, R.C., Katzmann, D.J., 2007. Biogenesis and function of multivesicular bodies. Annual review of cell and developmental biology 23, 519-547.

Porra, R.J., Urzinger, M., Winkler, J., Bubenzer, C., Scheer, H., 1998. Biosynthesis of the 3-acetyl and 13(1)-oxo groups of bacteriochlorophyll a in the facultative aerobic bacterium, Rhodovulum sulfidophilum--the presence of both oxygenase and hydratase pathways for isocyclic ring formation. Eur J Biochem 257, 185-191.

Pourcel, L., Irani, N.G., Lu, Y., Riedl, K., Schwartz, S., Grotewold, E., 2010. The formation of Anthocyanic Vacuolar Inclusions in Arabidopsis thaliana and implications for the sequestration of anthocyanin pigments. Molecular plant 3, 78-90.

Prag, G., Watson, H., Kim, Y.C., Beach, B.M., Ghirlando, R., Hummer, G., Bonifacino, J.S., Hurley, J.H., 2007. The Vps27/Hse1 complex is a GAT domain-based scaffold for ubiquitin-dependent sorting. Developmental cell 12, 973-986.

Rahighi, S., Dikic, I., 2012. Selectivity of the ubiquitin-binding modules. FEBS letters 586, 2705-2710.

Raymond, C.K., Howald-Stevenson, I., Vater, C.A., Stevens, T.H., 1992. Morphological classification of the yeast vacuolar protein sorting mutants: evidence for a prevacuolar compartment in class E vps mutants. Molecular biology of the cell 3, 1389-1402.

Reggiori, F., Komatsu, M., Finley, K., Simonsen, A., 2012. Autophagy: more than a nonselective pathway. International journal of cell biology 2012, 219625.

Reyes-Ibarra, A.P., Garcia-Regalado, A., Ramirez-Rangel, I., Esparza-Silva, A.L., Valadez-Sanchez, M., Vazquez-Prado, J., Reyes-Cruz, G., 2007. Calcium-sensing receptor endocytosis links extracellular calcium signaling to parathyroid hormone-related peptide secretion via a Rab11a-dependent and AMSH-sensitive mechanism. Molecular endocrinology 21, 1394-1407.

Reyes-Turcu, F.E., Ventii, K.H., Wilkinson, K.D., 2009. Regulation and cellular roles of ubiquitin-specific deubiquitinating enzymes. Annual review of biochemistry 78, 363-397.

Richardson, L.G., Howard, A.S., Khuu, N., Gidda, S.K., McCartney, A., Morphy, B.J., Mullen, R.T., 2011. Protein-Protein Interaction Network and Subcellular Localization of the Arabidopsis Thaliana ESCRT Machinery. Frontiers in plant science 2, 20.

Richardson, L.G., Mullen, R.T., 2011. Meta-analysis of the expression profiles of the Arabidopsis ESCRT machinery. Plant signaling & behavior 6, 1897-1903.

Richter, C.M., West, M., Odorizzi, G., 2013. Doa4 function in ILV budding is restricted through its interaction with the Vps20 subunit of ESCRT-III. Journal of cell science 126, 1881-1890.

Rieder, S.E., Banta, L.M., Kohrer, K., McCaffery, J.M., Emr, S.D., 1996. Multilamellar endosome-like compartment accumulates in the yeast vps28 vacuolar protein sorting mutant. Molecular biology of the cell 7, 985-999.

Robinson, D.G., Jiang, L., Schumacher, K., 2008. The endosomal system of plants: charting new and familiar territories. Plant physiology 147, 1482-1492.

Rojo, E., Gillmor, C.S., Kovaleva, V., Somerville, C.R., Raikhel, N.V., 2001. VACUOLELESS1 is an essential gene required for vacuole formation and morphogenesis in Arabidopsis. Developmental cell 1, 303-310.

Row, P.E., Liu, H., Hayes, S., Welchman, R., Charalabous, P., Hofmann, K., Clague, M.J., Sanderson, C.M., Urbe, S., 2007. The MIT domain of UBPY constitutes a CHMP binding and endosomal localization signal required for efficient epidermal growth factor receptor degradation. The Journal of biological chemistry 282, 30929-30937.

Row, P.E., Prior, I.A., McCullough, J., Clague, M.J., Urbe, S., 2006. The ubiquitin isopeptidase UBPY regulates endosomal ubiquitin dynamics and is essential for receptor down-regulation. The Journal of biological chemistry 281, 12618-12624.

Roxrud, I., Stenmark, H., Malerod, L., 2010. ESCRT & Co. Biology of the cell / under the auspices of the European Cell Biology Organization 102, 293-318.

Saksena, S., Wahlman, J., Teis, D., Johnson, A.E., Emr, S.D., 2009. Functional reconstitution of ESCRT-III assembly and disassembly. Cell 136, 97-109.

Sato, T.K., Darsow, T., Emr, S.D., 1998. Vam7p, a SNAP-25-like molecule, and Vam3p, a syntaxin homolog, function together in yeast vacuolar protein trafficking. Molecular and cellular biology 18, 5308-5319.

Schandel, K.A., Jenness, D.D., 1994. Direct evidence for ligand-induced internalization of the yeast alpha-factor pheromone receptor. Molecular and cellular biology 14, 7245-7255.

Scheuring, D., Viotti, C., Kruger, F., Kunzl, F., Sturm, S., Bubeck, J., Hillmer, S., Frigerio, L., Robinson, D.G., Pimpl, P., Schumacher, K., 2011. Multivesicular bodies mature from the trans-Golgi network/early endosome in Arabidopsis. Plant Cell 23, 3463-3481.

Schmidt, O., Teis, D., 2012. The ESCRT machinery. Current biology : CB 22, R116-120.

Shields, S.B., Piper, R.C., 2011. How ubiquitin functions with ESCRTs. Traffic 12, 1306-1317.

Schwechheimer C., Deng X.W., 2002. Studying protein-protein interactions with the yeast two-hybrid system. . *In* PM Gilmartin, C Bowler, eds, Molecular Plant Biology: A Practical Approach. Oxford University Press., Oxford, UK, pp 173–198

Scott, A., Gaspar, J., Stuchell-Brereton, M.D., Alam, S.L., Skalicky, J.J., Sundquist, W.I., 2005. Structure and ESCRT-III protein interactions of the MIT domain of human VPS4A. Proceedings of the National Academy of Sciences of the United States of America 102, 13813-13818.

Seki, T., Gong, L., Williams, A.J., Sakai, N., Todi, S.V., Paulson, H.L., 2013. JosD1, a membrane-targeted deubiquitinating enzyme, is activated by ubiquitination and regulates membrane dynamics, cell motility, and endocytosis. The Journal of biological chemistry 288, 17145-17155.

Shahriari, M., Keshavaiah, C., Scheuring, D., Sabovljevic, A., Pimpl, P., Hausler, R.E., Hulskamp, M., Schellmann, S., 2010. The AAA-type ATPase AtSKD1 contributes to vacuolar maintenance of Arabidopsis thaliana. The Plant journal : for cell and molecular biology 64, 71-85.

Shaid, S., Brandts, C.H., Serve, H., Dikic, I., 2013. Ubiquitination and selective autophagy. Cell death and differentiation 20, 21-30.

Shen, B., Li, C., Min, Z., Meeley, R.B., Tarczynski, M.C., Olsen, O.A., 2003. sal1 determines the number of aleurone cell layers in maize endosperm and encodes a class E vacuolar sorting protein. Proceedings of the National Academy of Sciences of the United States of America 100, 6552-6557.

Shields, S.B., Oestreich, A.J., Winistorfer, S., Nguyen, D., Payne, J.A., Katzmann, D.J., Piper, R., 2009. ESCRT ubiquitin-binding domains function cooperatively during MVB cargo sorting. The Journal of cell biology 185, 213-224.

Shim, S., Kimpler, L.A., Hanson, P.I., 2007. Structure/function analysis of four core ESCRT-III proteins reveals common regulatory role for extreme C-terminal domain. Traffic 8, 1068-1079.

Sierra, M.I., Wright, M.H., Nash, P.D., 2010. AMSH interacts with ESCRT-0 to regulate the stability and trafficking of CXCR4. The Journal of biological chemistry 285, 13990-14004.

Spitzer, C., Reyes, F.C., Buono, R., Sliwinski, M.K., Haas, T.J., Otegui, M.S., 2009. The ESCRT-related CHMP1A and B proteins mediate multivesicular body sorting of auxin carriers in Arabidopsis and are required for plant development. Plant Cell 21, 749-766.

Spitzer, C., Schellmann, S., Sabovljevic, A., Shahriari, M., Keshavaiah, C., Bechtold, N., Herzog, M., Muller, S., Hanisch, F.G., Hulskamp, M., 2006. The Arabidopsis elch mutant reveals functions of an ESCRT component in cytokinesis. Development 133, 4679-4689.

Surpin, M., Zheng, H., Morita, M.T., Saito, C., Avila, E., Blakeslee, J.J., Bandyopadhyay, A., Kovaleva, V., Carter, D., Murphy, A., Tasaka, M., Raikhel, N., 2003. The VTI family of SNARE proteins is necessary for plant viability and mediates different protein transport pathways. Plant Cell 15, 2885-2899.

Suttangkakul, A., Li, F., Chung, T., Vierstra, R.D., 2011. The ATG1/ATG13 protein kinase complex is both a regulator and a target of autophagic recycling in Arabidopsis. Plant Cell 23, 3761-3779.

Suzuki, K., Ohsumi, Y., 2007. Molecular machinery of autophagosome formation in yeast, Saccharomyces cerevisiae. FEBS letters 581, 2156-2161.

Suzuki, S., Tamai, K., Watanabe, M., Kyuuma, M., Ono, M., Sugamura, K., Tanaka, N., 2011. AMSH is required to degrade ubiquitinated proteins in the central nervous system. Biochemical and biophysical research communications 408, 582-588.

Svenning, S., Lamark, T., Krause, K., Johansen, T., 2011. Plant NBR1 is a selective autophagy substrate and a functional hybrid of the mammalian autophagic adapters NBR1 and p62/SQSTM1. Autophagy 7, 993-1010.

Swaminathan, S., Amerik, A.Y., Hochstrasser, M., 1999. The Doa4 deubiquitinating enzyme is required for ubiquitin homeostasis in yeast. Molecular biology of the cell 10, 2583-2594.

Tanaka, N., Kaneko, K., Asao, H., Kasai, H., Endo, Y., Fujita, T., Takeshita, T., Sugamura, K., 1999. Possible involvement of a novel STAM-associated molecule "AMSH" in intracellular signal transduction mediated by cytokines. The Journal of biological chemistry 274, 19129-19135.

Tanchak, M.A., Fowke, L.C., 1987. The morphology of multivesicular bodies in soybean protoplasts and their role in endocytosis. Protoplasma, 138:173–182.

Teis, D., Saksena, S., Emr, S.D., 2008. Ordered assembly of the ESCRT-III complex on endosomes is required to sequester cargo during MVB formation. Developmental cell 15, 578-589.

Thompson, A.R., Doelling, J.H., Suttangkakul, A., Vierstra, R.D., 2005. Autophagic nutrient recycling in Arabidopsis directed by the ATG8 and ATG12 conjugation pathways. Plant physiology 138, 2097-2110.

Thompson, A.R., Vierstra, R.D., 2005. Autophagic recycling: lessons from yeast help define the process in plants. Current opinion in plant biology 8, 165-173.

Thrower, J.S., Hoffman, L., Rechsteiner, M., Pickart, C.M., 2000. Recognition of the polyubiquitin proteolytic signal. The EMBO journal 19, 94-102.

Toyooka, K., Moriyasu, Y., Goto, Y., Takeuchi, M., Fukuda, H., Matsuoka, K., 2006. Protein aggregates are transported to vacuoles by a macroautophagic mechanism in nutrient-starved plant cells. Autophagy 2, 96-106.

Tsang, H.T., Connell, J.W., Brown, S.E., Thompson, A., Reid, E., Sanderson, C.M., 2006. A systematic analysis of human CHMP protein interactions: additional MIT domain-containing proteins bind to multiple components of the human ESCRT III complex. Genomics 88, 333-346.

Tse, Y.C., Mo, B., Hillmer, S., Zhao, M., Lo, S.W., Robinson, D.G., Jiang, L., 2004. Identification of multivesicular bodies as prevacuolar compartments in Nicotiana tabacum BY-2 cells. The Plant cell 16, 672-693.

Uemura, T., Ueda, T., Ohniwa, R.L., Nakano, A., Takeyasu, K., Sato, M.H., 2004. Systematic analysis of SNARE molecules in Arabidopsis: dissection of the post-Golgi network in plant cells. Cell structure and function 29, 49-65.

van der Veen, A.G., Ploegh, H.L., 2012. Ubiquitin-like proteins. Annual review of biochemistry 81, 323-357.

Verma, R., Aravind, L., Oania, R., McDonald, W.H., Yates, J.R., 3rd, Koonin, E.V., Deshaies, R.J., 2002. Role of Rpn11 metalloprotease in deubiquitination and degradation by the 26S proteasome. Science 298, 611-615.

Vierstra, R.D., 2009. The ubiquitin-26S proteasome system at the nexus of plant biology. Nature reviews. Molecular cell biology 10, 385-397.

Vierstra, R.D., 2012. The expanding universe of ubiquitin and ubiquitin-like modifiers. Plant physiology 160, 2-14.

Viotti, C., Bubeck, J., Stierhof, Y.D., Krebs, M., Langhans, M., van den Berg, W., van Dongen, W., Richter, S., Geldner, N., Takano, J., Jurgens, G., de Vries, S.C., Robinson, D.G., Schumacher, K., 2010. Endocytic and secretory traffic in Arabidopsis merge in the trans-Golgi network/early endosome, an independent and highly dynamic organelle. Plant Cell 22, 1344-1357.

Wang, F., Deng, X.W., 2011. Plant ubiquitin-proteasome pathway and its role in gibberellin signaling. Cell research 21, 1286-1294.

Wang, T., Liu, N.S., Seet, L.F., Hong, W., 2010. The emerging role of VHS domain-containing Tom1, Tom1L1 and Tom1L2 in membrane trafficking. Traffic 11, 1119-1128.

Ward, D.M., Pevsner, J., Scullion, M.A., Vaughn, M., Kaplan, J., 2000. Syntaxin 7 and VAMP-7 are soluble N-ethylmaleimide-sensitive factor attachment protein receptors required for late endosome-lysosome and homotypic lysosome fusion in alveolar macrophages. Molecular biology of the cell 11, 2327-2333.

Ward, D.M., Vaughn, M.B., Shiflett, S.L., White, P.L., Pollock, A.L., Hill, J., Schnegelberger, R., Sundquist, W.I., Kaplan, J., 2005. The role of LIP5 and CHMP5 in multivesicular body formation and HIV-1 budding in mammalian cells. The Journal of biological chemistry 280, 10548-10555.

Waters, S., Marchbank, K., Solomon, E., Whitehouse, C., Gautel, M., 2009. Interactions with LC3 and polyubiquitin chains link nbr1 to autophagic protein turnover. FEBS letters 583, 1846-1852.

Wemmer, M., Azmi, I., West, M., Davies, B., Katzmann, D., Odorizzi, G., 2011. Bro1 binding to Snf7 regulates ESCRT-III membrane scission activity in yeast. The Journal of cell biology 192, 295-306.

Wilkinson, K.D., 2009. DUBs at a glance. Journal of cell science 122, 2325-2329.

Willige, B.C., Isono, E., Richter, R., Zourelidou, M., Schwechheimer, C., 2011. Gibberellin regulates PIN-FORMED abundance and is required for auxin transport-dependent growth and development in Arabidopsis thaliana. Plant Cell 23, 2184-2195.

Winter, V., Hauser, M.T., 2006. Exploring the ESCRTing machinery in eukaryotes. Trends in plant science 11, 115-123.

Xie, Z., Klionsky, D.J., 2007. Autophagosome formation: core machinery and adaptations. Nature cell biology 9, 1102-1109.

Xiong, Y., Contento, A.L., Bassham, D.C., 2005. AtATG18a is required for the formation of autophagosomes during nutrient stress and senescence in Arabidopsis thaliana. The Plant journal : for cell and molecular biology 42, 535-546.

Xiong, Y., Contento, A.L., Bassham, D.C., 2007a. Disruption of autophagy results in constitutive oxidative stress in Arabidopsis. Autophagy 3, 257-258.

Xiong, Y., Contento, A.L., Nguyen, P.Q., Bassham, D.C., 2007b. Degradation of oxidized proteins by autophagy during oxidative stress in Arabidopsis. Plant physiology 143, 291-299.

Xu, P., Duong, D.M., Seyfried, N.T., Cheng, D., Xie, Y., Robert, J., Rush, J., Hochstrasser, M., Finley, D., Peng, J., 2009. Quantitative proteomics reveals the function of unconventional ubiquitin chains in proteasomal degradation. Cell 137, 133-145.

Yang, K.S., Jin, U.H., Kim, J., Song, K., Kim, S.J., Hwang, I., Lim, Y.P., Pai, H.S., 2004. Molecular characterization of NbCHMP1 encoding a homolog of human CHMP1 in Nicotiana benthamiana. Molecules and cells 17, 255-261.

Ye, Y., Rape, M., 2009. Building ubiquitin chains: E2 enzymes at work. Nature reviews. Molecular cell biology 10, 755-764.

Yeo, S.C., Xu, L., Ren, J., Boulton, V.J., Wagle, M.D., Liu, C., Ren, G., Wong, P., Zahn, R., Sasajala, P., Yang, H., Piper, R.C., Munn, A.L., 2003. Vps20p and Vta1p interact with Vps4p and function in multivesicular body sorting and endosomal transport in Saccharomyces cerevisiae. Journal of cell science 116, 3957-3970.

Yoshimoto, K., Hanaoka, H., Sato, S., Kato, T., Tabata, S., Noda, T., Ohsumi, Y., 2004. Processing of ATG8s, ubiquitin-like proteins, and their deconjugation by ATG4s are essential for plant autophagy. Plant Cell 16, 2967-2983.

Yoshimoto, K., Jikumaru, Y., Kamiya, Y., Kusano, M., Consonni, C., Panstruga, R., Ohsumi, Y., Shirasu, K., 2009. Autophagy negatively regulates cell death by controlling NPR1-dependent salicylic acid signaling during senescence and the innate immune response in Arabidopsis. Plant Cell 21, 2914-2927.

Zamborlini, A., Usami, Y., Radoshitzky, S.R., Popova, E., Palu, G., Gottlinger, H., 2006. Release of autoinhibition converts ESCRT-III components into potent inhibitors of HIV-1 budding. Proceedings of the National Academy of Sciences of the United States of America 103, 19140-19145.

Zhang, X.Q., Hou, P., Zhu, H.T., Li, G.D., Liu, X.G., Xie, X.M., 2013. Knockout of the VPS22 component of the ESCRT-II complex in rice (Oryza sativa L.) causes chalky endosperm and early seedling lethality. Molecular biology reports 40, 3475-3481.

Zhou, J., Wang, J., Cheng, Y., Chi, Y.J., Fan, B., Yu, J.Q., Chen, Z., 2013. NBR1-mediated selective autophagy targets insoluble ubiquitinated protein aggregates in plant stress responses. PLoS genetics 9, e1003196.

Zientara-Rytter, K., Lukomska, J., Moniuszko, G., Gwozdecki, R., Surowiecki, P., Lewandowska, M., Liszewska, F., Wawrzynska, A., Sirko, A., 2011. Identification and functional analysis of Joka2, a tobacco member of the family of selective autophagy cargo receptors. Autophagy 7, 1145-1158.

Zouhar, J., Rojo, E., Bassham, D.C., 2009. AtVPS45 is a positive regulator of the SYP41/SYP61/VTI12 SNARE complex involved in trafficking of vacuolar cargo. Plant physiology 149, 1668-1678.

Appendix

Table 9: Positive candidates found in the yeast two-hybrid screen.

Gene	Characterization
AT1G04410	CYTOSOLIC-NAD-DEPENDENT MALATE DEHYDROGENASE
AT1G09340	CHLOROPLAST RNA BINDING
AT1G11910	ASPARTIC PROTEINASE A1
AT1G20620	CATALASE 3/SENESCENCE 2
AT1G20910	ARID/BRIGHT DNA-binding domain-CONTAINING PROTEIN
AT1G27090	glycine-rich protein
AT1G28520	VASCULAR PLANT ONE ZINC FINGER PROTEIN
AT1G29990	PREFOLDIN 6
AT1G30230	ELONGATION FACTOR 1-beta
AT1G34370	SENSITIVE TO PROTON RHIZOTOXICITY 1
AT1G35620	DISULFIDE ISOMERASE 8
AT1G35625	RING/U-box superfamily protein
AT1G37130	CHLORATE RESISTANT 3
AT1G47128	RESPONSIVE TO DEHYDRATION 21
AT1G50480	10-FORMYLTETRAHYDROFOLATE SYNTHETASE
AT1G54100	ALDEHYDE DEHYDROGENASE 7B4
AT1G56070	LOW EXPRESSION OF OSMOTICALLY RESPONSIVE GENES 1
AT1G59900	PYRUVATE DEHYDROGENASE COMPLEX E1 ALPHA SUBUNIT
AT1G61660	basic helix-loop-helix (bHLH) DNA-binding superfamily protein
AT1G62380	ACC OXIDASE 2
AT1G66280	BETA-GLUCOSIDASE 22
AT1G67070	PHOSPHOMANNOSE ISOMERASE 1
AT1G68670	myb-like family transcription factor
AT1G72370	40S RIBOSOMAL PROTEIN SA
AT1G77330	similar to 1-aminocyclopropane-1-carboxylate oxidase
AT1G79010	ALPHA-HELICAL FERREDOXIN
AT2G04700	ferredoxin thioredoxin reductase catalytic beta chain family p
AT2G06530	VACUOLAR PROTEIN SORTING 2.1
AT2G18510	EMBRYO DEFECTIVE
AT2G21170	PLASTID ISOFORM TRIOSE PHOSPHATE ISOMERASE
AT2G27100	SERRATE
AT2G33150	PEROXISOMAL 3-KETOACYL-COA THIOLASE 3
AT2G36320	A20/AN1-like zinc finger family protein
AT2G36460	FRUCTOSE-BISPHOSPHATE ALDOLASE 6
AT2G37130	Peroxidase superfamily protein

AT2G42610	LIGHT SENSITIVE HYPOCOTYLS 10
AT2G44650	CHLOROPLAST CHAPERONIN 10
AT3G02080	Ribosomal protein S19e family protein
AT3G05560	Ribosomal L22e protein family
AT3G09260	LONG ER BODY
AT3G15950	NAI2
AT3G16770	ETHYLENE RESPONSE FACTOR 72
AT3G17820	GLUTAMINE SYNTHETASE 1.3
AT3G18780	ACTIN 2
AT3G19390	Granulin repeat cysteine protease family protein
AT3G22960	PLASTIDIAL PYRUVATE KINASE 1
AT3G25230	FK506 BINDING PROTEIN 62
AT3G27090	Development and Cell Death domain protein
AT3G27960	KINESIN LIGHT CHAIN-RELATED 2
AT3G44600	CYCLOPHILIN71
AT3G47000	Glycosyl hydrolase family protein
AT3G52930	FRUCTOSE-BISPHOSPHATE ALDOLASE 8
AT3G27960	KINESIN LIGHT CHAIN-RELATED 2
AT3G44600	CYCLOPHILIN71
AT3G63210	MEDIATOR OF ABA-REGULATED DORMANCY 1
AT4G05520	EPS15 HOMOLOGY DOMAIN 2, EHD2
AT4G09650	ATP SYNTHASE DELTA-SUBUNIT GENE
AT4G13660	PINORESINOL REDUCTASE 2
AT4G15080	DHHC-type zinc finger family protein
AT4G15960	alpha/beta-hydrolases superfamily protein
AT4G25840	GLYCEROL-3-PHOSPHATASE 1
AT4G27320	UNIVERSAL STRESS PROTEIN FAMILY PROTEIN 34
AT4G32260	PIGMENT DEFECTIVE 334
AT4G32410	CELLULOSE SYNTHASE 1
AT4G35090	CATALASE 2
AT5G02160	unkown protein
AT5G11650	alpha/beta-hydrolases superfamily protein
AT5G14740	BETA CARBONIC ANHYDRASE 2
AT5G19990	REGULATORY PARTICLE TRIPLE-A ATPASE 6A
AT5G21170	AKINbeta1
AT5G22510	ALKALINE/NEUTRAL INVERTASE E
AT5G23080	TOUGH
AT5G23120	HIGH CHLOROPHYLL FLUORESCENCE 136
AT5G23450	LONG-CHAIN BASE (LCB) KINASE 1
AT5G23860	TUBULIN BETA 8
AT5G26260	TRAF-like family protein

AT5G28840	GDP-D-MANNOSE3,5.EPIMERASE
AT5G40200	DEGP PROTEASE 9
AT5G42050	Development and cell death domain protein
AT5G42850	Thioredoxin superfamily protein
AT5G47010	LOW-LEVEL BETA-AMYLASE 1
AT5G47840	ADENOSINE MONOPHOSPHATE KINASE
AT5G51970	SORBITOL DEHYDROGENASE
AT5G54430	UNIVERSAL STRESS PROTEIN FAMILY PROTEIN 32
AT5G60390	GTP binding elongation factor TU family protein
AT5G62690	TUBULIN BETA CHAIN 2
AT5G66570	OXYGEN EVOLVING POLYPEPTIDE 1
ATCG00480	ATP SYNTHASE SUBUNIT BETA

Table 10: **Embryo analysis of wild type (Col-0) and *VPS2.1+/-* plants.**

Parent plant	Walcking stick	Torpedo / Heart	n
Col-0	98 %	2 %	0 %
VPS2.1+/-	85 %	15 %	7,2 %

Table 11: All primers used for this thesis project.

Name	Description	Sequences 5´- 3´
AKA	GW adaptor fw	GGGGACAAGTTTGTACAAAAAAGCAGGCT
AKB	GW adaptor rv	GGGGACCACTTTGTACAAGAAAGCTGGGT
AK0	AMSH3 fw BamHI	TCGGGGATCCGTATGAAGATTGATCTGAAC
AK1	VPS2.1 fw XhoI	AAGGCTCGAGATGATGAATTCAATCTTCGG
AK2	VPS2.1 rv SalI	AAGGGTCGACTCACATTTTTCTAAGGTTAT
AK3	VPS2.3 fw EcoRI	AAGGGAATTCATGAACATCTTCACTAAG
AK4	VPS2.3 rv SalI	AAGGGTCGACCTATCTAAGCGCCGCCAA
AK7	EHD2 fw BamHI	AAGGGGATCCATATGGAGACTTCATCG
AK8	EHD2 rv XhoI	AAGGCTCGAGTTAATTATCATAAGG
AK9	EPSIN1 fw EcoRI	AAGGGAATTCATGGATTTCATGAAG
AK10	EPSIN1 rv XhoI	AAGGCTCGAGTCACTGCTTAAAGCC
AK11	RD21 fw E.coRI	AAGGGAATTCATGGGGTTCCTTAAGCC
AK12	RD21 rv BamHI	AAGGGGATCCTTAGGCAATGTTCTTTC
AK13	EHD1 fw SfiI	CAGGCCGTCAAGGCCTATGGAGATCGAATCCGTCG
AK14	EHD1 rv NotI	CAGCGGCCGCTTAATCATAAGGGTTTTTG
AK15	EHD2 fw SfiI	CAGGCCGTCAAGGCCTATGGAGACTTCATCG
AK16	EHD2 rv NotI	CAGCGGCCGCTTAATTATCATAAGG
AK17	EPSIN1 fw SfiI	CAGGCCGTCAAGGCCTATGGATTTCATGAAG
AK18	EPSIN1 rv NotI	CAGCGGCCGCTCACTGCTTAAAGCC
AK19	RD21 fw SfiI	CAGGCCGTCAAGGCCTATGGGGTTCCTTAAGCC
AK20	RD21 rv NotI	CAGCGGCCGCTTAGGCAATGTTCTTTC
AK21	VPS2.1 fw SfiI	CAGGCCGTCAAGGCCTATGATGAATTCAATC
AK22	VPS2.1 rv NotI	CAGCGGCCGGCTCACATTTTTCTAAG
AK23	PATL1 fw BamHI	TTGGGGATCCATATGGCTCAAGAGGAAG
AK24	PATL1 rv SalI	TTGGGTCGACTTATTGAGTTTTGAACCT
AK25	PATL2 fw BamHI	TTGGGGATCCATATGGCTCAAGAAGAG
AK26	PATL2 rv XhoI	TTGGCTCGAGTTATGCTTGGGTTTTGG
AK27	PATL6 fw BamHI	TTGGGGATCCATATGGATGCTTCATTG
AK28	PATL6 rv SalI	TTGGGTCGACTTAGACGGTTGTAGTAG
AK32	VPS2.1 GW fw 1	AAAAAGCAGGCTCCATGATGAATTCAATCTTCGG
AK33	VPS2.1 GW rv 1	AGAAAGCTGGGTATCAGAATCTTACGTGGCAGCT
AK34	VPS2.1 GW fw	AAAAAGCAGGCTCCATGATGAATTCAATCTTCGG
AK35	VPS2.1 GW rv (-STOP)	AGAAAGCTGGGTACATTTTTCTAAGGTTATCCAAC
AK36	VPS2.1-ter fw	AAGGGCATGCAGCCTTTCCTGTTTCTGTATC
AK37	VPS2.1-ter rv	AAGGACTAGTGAATCTTACGTGGCAGCTTC
AK38	pVPS2.1 XhoI	AAGGCTCGAGGATTCAATACCGAAAAGGTG
AK39	pVPS2.1prom AscI	AAGGGGCGCGCCATGATTTTACGGTCTTGGCG
AK40	pVPS2.1prom SalI	AAGGGTCGACATGATTTTACGGTCTTGGCG
AK41	pVPS2.1prom Asc 2	AAGGGGCGCGCCACGTTGTTGTCGGGAAAATATG

AK42	pVPS2.1prom Asc 3	AAGGGGCGCGCCCCATCCAAATGGTCCAATTAAG
AK43	pVPS2.1prom Asc4	AAGGGGCGCGCCTGATCCATCTGGATGGAGAAAC
AK44	VPS2.1 D212N fw	ACAGTGGAGGTATAAACAGTGACCTTCAAGC
AK45	VPS2.1 D212N rv	GCTTGAAGGTCACTGTTTATACCTCCACTGT
AK46	VPS2.1 MIM1 fw	AAGGGGATCCGGAGGTATAGATAGTGAC
AK47	VPS2.3 I199D fw	TTGGCAGTTCTGGAGATGATGAACTGGAGAA
AK48	VPS2.3 I199D rv	TTCTCCAGTTCATCATCTCCAGAACTGCCAA
AK49	AMSH3(MIT) fw BamHI	AAGGGGATCCAATCGTATTCCTCTCCGT
AK50	AMSH3(MIT) rv SalI (-STOP)	AAGGGTCGACCAGCTTATCCACTAGCTG
AK51	AMSH3(MIT) rv SalI	AAGGGTCGACTAACAGCTTATCCACTAG
AK52	SKD1 fw BamHI	AAGGGGATCCATGTACAGCAATTTCAAGG
AK53	SKD1 rv XhoI	AAGGCTCGAGACCTTCTTCTCCAAACTCC
AK54	pVPS2.1 SalI	AAGGGTCGACATGACGTTGTTGTCGGGAAAATATG
AK55	pAMSH1 1kb fw NotI	AAGGGCGGCCGCTTTTGTATGATACTGGTAAT
AK56	pAMSH1 rv BamHI	AAGGGGATCCAGTTGCTCCGATCAAAAGCA
AK57	YFP rv (+STOP) EcoRI	AGGAATTCTTACTTGTACAGCTCGTCCA
AK58	AMSH1 (genomic) fw EcoRI	AGGAATTCATGGGGTCGTCTTTTGAGAC
AK59	AMSH1 (genomic) rv KpnI	AGGGTACCACGTAGGTTTGAATAGATGG
AK60	EHD2 1194b fw BamHI	AAGGGGATCCATAAACCCATAAACGAAG
AK61	AMSH1 (genomic-800b) fw	GAATGGTAAGTGAACATAATATC
AK62	AMSH1 (genomic-1690b) fw	CAAGGTTAGATCATCTAGCTGC
AK63	AMSH1 (genomic-2600b) rv	CTAGTGAACCGGCAAGAATAC
AK64	VPS2.1(mut) GW rv (+STOP)	AGAAAGCTGGGTATCACATTTTTCTAAGGTTATCC
AK65	YFP rv EcoRI	AGGAATTCCTTGTACAGCTCGTCCATGC
AK66	VPS24.1 fw BamHI	AAGGGGATCCATGGAGAGAGTGATGAAC
AK67	VPS24.1 rv SalI	TTGGGTCGACTTAGGATCTAACTTTAGC
AK68	VPS60.1 fw BamHI	AAGGGAATCCATGAGGAGAGTTTTCGG
AK69	VPS60.1 rv SalI	TTGGGTCGACTTAACCCCGGAGAGAAG
AK70	AMSH3(MIT) fw BamHI	AAGGGGATCCAGAATCGTATTCCTCTCCGT
AK75	AMSH1 rv (-STOP) EcoRI	AGGAATTCTCTGAGATCAATGACATCAA
AK76	YFP fw EcoRI	AGGAATTCGTGAGCAAGGGCGAGGAGC
AK77	VPS2.2 fw EcoRI	AGGAATTCATATGAACATTTTCAAGAAG
AK78	VPS2.2 rv SalI	AGGTCGACTCAGATTCGTCGTAGCGA
AK79	EHD2 GW fw	AAAAAGCAGGCTCCATGGAGACTTCATCGACGAT
AK80	EHD2 (-STOP) GW rv	AGAAAGCTGGGTAATTATCATAAGGATTTCTGA
AK81	EHD2 (1194b) GW fw CGW	AAAAAGCAGGCTCCATGATAAACCCATAAACGAAG
AK82	PYK10 fw NdeI	AAGGCATATGATGGCCCAAAAGGTGGAAG
AK83	PYK10 rv SalI	AAGGGTCGACTCAGTTGGATAAAGGACGA
AK84	VPS2.1(ΔMIM) (621b) rv SpeI	AAGGACTAGTTCAGTCCTCAGCTCCGGTCG
AK85	VPS2.1 rv SpeI	AAGGACTAGTTCACATTTTTCTAAGGTTAT
AK86	AMSH3(MIT) fw XhoI	AAGGCTCGAGATGAATCGTATTCCTCTCCGT

AK87	AMSH3(MIT) (+STOP) rv SpeI	AAGGACTAGTTAACAGCTTATCCACTAG
AK88	AMSH3(ΔMIT) fw XhoI	AAGGCTCGAGATGAGGATGAATCCCGTCAGG
AK89	AMSH3 rv SpeI	AAGGACTAGTTTAGCGGAGATCGAGGAC
AK90	VPS24.1 GW fw	AAAAAGCAGGCTCCATGGAGAGAGTGATGAAC
AK91	VPS24.1 GW rv (+STOP)	AGAAAGCTGGGTATTAGGATCTAACTTTAGCGAG
AK92	VPS24.1 GW rv (-STOP)	AGAAAGCTGGGTAGGATCTAACTTTAGCGAGCC
AK93	VPS60.1 GW fw	AAAAAGCAGGCTCCATGAGGAGAGTTTTCGGCGC
AK94	VPS60.1 GW (+STOP) rv	AGAAAGCTGGGTATTAACCCCGGAGAGAAGCTC
AK95	VPS60.1 GW (-STOP) rv	AGAAAGCTGGGTAACCCCGGAGAGAAGCTCGTG
AK96	AMSH3(501b) rv (+STOP) SalI	AAGGGTCGACTTACTGTGTACGATTTGATG
AK97	AMSH3(-N154) rv SalI	AAGGGTCGAGTTACGTCCAGGATGGTTGAG
AK98	AMSH3 (-N165) rv (+STOP) SalI	AAGGGTCGACTTACGGGAGATCACTTCCAT
AK99	F2-2 VPS2.1	GTATGCTTTATTTTTACCAAG
AK100	F2-3 VPS2.1	TGGATACTTTCTCTCACAGGG
AK101	VPS2.1 (genomic) rv	TTGAAAAGTGATCAGCCTCAG
AK102	VPS2.1 (genomic) rv2	TATCCAACCTTGCTTGAAGGT
AK103	AMSH3(ΔMIT, 321) GW fw	AAAAAGCAGGCTCCATGGATGAATCCCGTCAGGAT
AK104	AMSH3(ΔMIT) fw XhoI	AAGGCTCGAGATGGATGAATCCCGTCAGGAT
AK105	pRPS5a (end) fw	CTCACGCTCTGTTTCTCACC
AK106	pVPS2.1 (end) fw	TCACCTTTTTCGGTATTGAATC
AK107	VPS2.1 (genomic) rv	GTAGGCCTTGTCTCTCCCTCTC
AK108	pRPS5a fw 1	GCAGAGTATCTGTTATTCCC
AK109	pRPS5a fw 2	CGGTTCTGGACTTCTGCTAG
AK110	AK89 rv1	CGGATCCCCCGGGCTGCAGG
AK111	AK89 rv2	GTATAATTGCGGGACTCTAATCAT
AK112	SAG12 fw	GCCGGTTTCTGTTGACTGGA
AK113	SAG12 rv	CTAACCGGTTGGTGTGCCAC
AK114	SEN1 fw	CTCGTCCCACTTCAGGAAACA
AK115	SEN1 rv	TGTCCTAAACCGGATAACGGC
AK116	YFP rv SalI	AAGGGTCGACTTACTTGTACAGCTCGTCCA
AK117	ATG5 fw	ATGGCGAAGGAAGCGGTCAA
AK118	ATG5 rv	TCACCTTTGAGGAGCTTTCAC
AK119	ATG6 fw	ATGAGGAAAGAGGAGATTCC
AK120	ATG6 rv	GATTGCATCTCTCTCTTCCTG
AK121	ATG8c fw	ATGACAGGACAAATGGCAACA
AK122	ATG8c rv	TTAAACCAAACCAAAGGTGTTC
AK124	SNF7.1 GW fw	AAAAAGCAGGCTCCATGATGAATCGGCTATTCGG
AK125	SNF7.1 GW rv	AGAAAGCTGGGTATTAGAGGGCCATCTCAGCCTG
AK126	ATG8e fw XhoI	AAGGCTCGAGATGAATAAAGGAAGCATC

AK127	ATG8e rv NotI	AAGGGCGGCCGCTTAGATTGAAGAAGCACC
AK128	ATG8f fw XhoI	AAGGCTCGAGATGGCAAAAAGCTCGTTC
AK129	ATG8f rv NotI	AAGGGCGGCCGCTTATGGAGATCCAAATCC
AK130	eGFP rv XhoI	AAGGCTCGAGCTTGTACAGCTCGTCCAT
AK131	ATG8e fw GW	AAAAAGCAGGCTCCATGAATAAAGGAAGCATCT
AK132	ATG8e rv GW	AGAAAGCTGGGTATTAGATTGAAGAAGCACCG
AK133	ATG8f fw GW	AAAAAGCAGGCTCCATGGCAAAAAGCTCGTTCAAG
AK134	ATG8f rv GW	AGAAAGCTGGGTATTATGGAGATCCAAATCCAAA
AK135	VPS2.1 (-STOP)rv NotI	AAGGGCGGCCGCCATTTTTCTAAGGTTATCC
AK136	YFP fw NotI	AAGGGCGGCCGCGTGAGCAAGGGCGAGGAGC
AK137	YFP (+STOP) rv SalI	AGGTCGACTTACTTGTACAGCTCGTCCA

Table 12: All plasmids generated during this thesis project.

Name	Description	Vector
AK7	TAC:GST-VPS2.1	pGEX-6P1
AK8	TAC:GST-VPS2.2	pGEX-6P1
AK9	TAC:GST-VPS2.3	pGEX-6P1
AK10	PATL1	Topo2.1
AK11	ADH1:BD-PATL1	pGBKT7
AK12	ADH1:BD-RD21	pGBKT7
AK13	ADH1:BD-EpsinI N95S	pGBKT7
AK14	EPSIN1	Topo2.1
AK15	ADH1:BD-EPSIN1	pGBKT7
AK17	AMSH3	Topo2.1
AK18	ADH1:AD-AMSH3	pGADT7
AK19	VPS2.1	pUNI51
AK20	AMSH3axa	Topo2.1
AK21	PATL2	Topo2.1
AK22	ADH1:BD-PATL2	pGBKT7
AK23	ADH1:AD-AMSH3axa	pGADT7
AK24	ADH1:AD-RD21	pGADT7
AK25	EHD2 Y2H clone	Topo2.1
AK26	ADH1:BD-EHD2	pGBKT7
AK27	ADH1:BD-PATL6	pGBKT7
AK28	UBQ10:YFP-VPS2.1	pNIGEL07
AK29	UBQ10:mCherry-VPS2.1	pNIGEL17
AK30	VPS2.1 (-STOP)	pDONR207
AK31	VPS2.1+terminator	pDONR207
AK32	35S:VPS2.1-RFP	p0229-RFP
AK33	TAC:GST-VPS2.1(mut)	pGEX-6P1
AK34	VPS2.2	pUNI51
AK35	TAC:GST-VPS2.3(mut)	pGEX-6P1
AK36	TAC:GST-VPS2.1(MIM1)	pGEX-6P1
AK37	TAC:GST-AMSH(MIT)	pGEX-6P1
AK38	UBQ10:YFP-VPS2.2	pNIGEL07
AK39	UBQ10:mCherry-VPS2.2	pNIGEL17
AK40	pVPS2.1 (1,9 kB)	Topo 2.1
AK41	VPS2.1:YFP-VPS2.1(genomic)	pExtag-YFP-GW
AK42	VPS2.1:VPS2.1-RFP	pExtag-YFP-GW
AK43	VPS2.1:VPS2.1-RFP-VPS2.1term	pExtag-YFP-GW
AK44	35S:VPS2.1-Flag	pEarly-GW302
AK45	35S:3xHA-VPS2.1(genomic)	pJawohl-3xHA-GW
AK46	2x35S:VPS2.1-3xHA	p35s-intron-GW-HA

AK47	2x35S:VPS2.1(genomic)	p35s-intron-GW-HA
AK48	ADH1:BD-VPS46.2	pGBKT7
AK49	35S:VPS2.1-GFP	35S-GW-GFP
AK50	ADH1:AD-VPS2.3	pGADT7
AK51	AMSH1(1 kb):YFP-AMSH1(genomic)	pGreenII
AK52	35S:YFP-VPS2.3	pExtag-YFP-GW
AK53	ADH1:BD-EHD2(1194-1641b)	pGBKT7
AK54	ADH1:AD-AMSH3((MIT)16-102)	pGADT7
AK55	TAC:GST-VPS24.1	pGEX-6P1
AK56	TAC:GST-VPS60.1	pGEX-6P1
AK57	AMSH3:AMSH1	pGreenII
AK58	AMSH1:AMSH1-YFP	pGreenII
AK59	AMSH3:YFP-AMSH1	pGreenII
AK60	AMSH3:AMSH1-YFP	pGreenII
AK61	ADH1:BD-JAL4	pGBKT7
AK62	ADH1:BD-BGLU21	pGBKT7
AK63	ADH1:AD-EHD2	pGADT7
AK64	ADH1:AD-AMSH3(MIT) 1-102)	pGADT7
AK65	DEX-35S:VPS2.1(mut)	pTA 7002
AK66	DEX-35S:VPS2.1(ΔMIM)	pTA 7002
AK67	DEX-35S:AMSH3(ΔMIT)	pTA 7002
AK68	DEX-35S:AMSH3((MIT) 1-102)	pTA 7002
AK69	VPS60.1	pDONR207
AK70	35S:3xHA-VPS60.1	pJawohl-3xHA-GW
AK71	35S:YFP-VPS60.1	pExtag-YFP-GW
AK72	VPS24.1 (-STOP)	pDONR207
AK73	35S:VPS24.1-GFP	35S-GW-GFP
AK74	35S:VPS24.1-HA	35S-intron-HA
AK75	VPS60.1 (-STOP)	pDONR207
AK76	VPS24.1	pDONR207
AK77	35S:YFP-VPS24.1	pExtag-YFP-GW
AK78	35S:3xHA-VPS24.1	pJawohl-3xHA-GW
AK79	35S:VPS60.1-GFP	35S-GW-GFP
AK80	AMSH3:AMSH3(genomic)-CFP-termAMSH3	FA15
AK81	ADH1:AD-AMSH3 (N118)	pGAD
AK82	ADH1:AD-AMSH3 (N154)	pGAD
AK83	ADH1:AD-AMSH3 (N167)	pGAD
AK84	6xHis-SKD1	pDEST17
AK85	ADH1:AD-AMSH3 (N1000)	pGADT7
AK86	VPS2.1(mut)	pDONR207
AK87	35S:YFP-VPS2.1(mut)	pExtag-YFP-GW
AK88	ADH1:AD-AMSH3(MPN)	pGADT7

AK89	RPS5a:VPS2.1	pGreenII Basta RPS5
AK90	pVPS2.1	pGreenII
AK91	VPS2.1:YFP-VPS2.1(genomic)	AK90
AK92	AMSH3(ΔMIT)	pDONR207
AK93	35S:YFP:AMSH3ΔMIT	pExtag-YFP-GW
AK94	DEX-35:-AMSH3(ΔMIT)	pTA 7002
AK95	DEX-35S:AMSH3(ΔMIT)(AXA)	pTA 7002
AK97	AMSH3(2kb):YFP-AMSH1	FA88 + AK59
AK98	35S:YFP-AMSH3ΔMPN	pUC18 (DD1)
AK99	TAC:GST-AMSH3ΔMIT(WT)	pGEX-6P1
AK100	TAC:GST-AMSH3ΔMIT(AXA)	pGEX-6P1
AK101	35S:VPS24.1(+STOP)-HA	35S-intron-HA
AK102	VPS2.1(mut)	Topo 2.1
AK103	YFP-VPS2.1	Topo 2.1
AK104	RPS5a:YFP-VPS2.1	pGreenII Basta RPS5
AK105	6xHis-VPS24.1	pDEST17
AK106	35S:VPS24.1-RFP	pGWB560
AK107	35S:RFP-SKD1	pGWB561
AK108	RPS5a:VPS2.1(mut)	pGreenII Basta RPS5
AK109	RPS5a:VPS2.1-GFP	pGreenII Basta RPS5
AK110	35S:RFP-VPS24.1	pGWB561
AK111	35S:RFP-AMSH1	pGWB561
AK112	SNF7.1	pDONR207
AK113	35S:SNF7.1(+STOP)-HA	35S-intron-HA
AK114	ATG8f	pDONR207
AK115	UBQ10:GFP-Atg8f	pUBN-GFP-DEST
AK116	UBQ10:CFP-Atg8f	pUBN-CFP-DEST
AK117	35S:VPS2.1-mCherry	pGWB560
AK118	AMSH1:AMSH1	AK51
AK119	ATG8e	pDONR207
AK120	UBQ10:GFP-Atg8e	pUBN-GFP-DEST
AK121	UBQ10:CFP-Atg8e	pUBN-CFP-DEST

The *Arabidopsis* Deubiquitinating Enzyme AMSH3 Interacts with ESCRT-III Subunits and Regulates Their Localization [C][W]

Anthi Katsiarimpa,[a] Franziska Anzenberger,[a] Nicole Schlager,[b] Susanne Neubert,[b] Marie-Theres Hauser,[b] Claus Schwechheimer,[a,c] and Erika Isono[a,c,1]

[a] Department of Plant Systems Biology, Technische Universität München, 85354 Freising, Germany
[b] Department of Applied Genetics and Cell Biology, BOKU, University of Natural Resources and Life Sciences, 1190 Vienna, Austria
[c] Department of Developmental Genetics, Center for Plant Molecular Biology, Tübingen University, 72076 Tuebingen, Germany

Ubiquitination and deubiquitination regulate various cellular processes. We have recently shown that the deubiquitinating enzyme Associated Molecule with the SH3 domain of STAM3 (AMSH3) is involved in vacuole biogenesis and intracellular trafficking in *Arabidopsis thaliana*. However, little is known about the identity of its interaction partners and deubiquitination substrates. Here, we provide evidence that AMSH3 interacts with ESCRT-III subunits VPS2.1 and VPS24.1. The interaction of ESCRT-III subunits with AMSH3 is mediated by the MIM1 domain and depends on the MIT domain of AMSH3. We further show that AMSH3, VPS2.1, and VPS24.1 localize to class E compartments when ESCRT-III disassembly is inhibited by coexpression of inactive Suppressor of K+ transport Defect 1 (SKD1), an AAA-ATPase involved in the disassembly of ESCRT-III. We also provide evidence that AMSH3 and SKD1 compete for binding to VPS2.1. Furthermore, we show that the loss of AMSH3 enzymatic activity leads to the formation of cellular compartments that contain AMSH3, VPS2.1, and VPS24.1. Taken together, our study presents evidence that AMSH3 interacts with classical core ESCRT-III components and thereby provides a molecular framework for the function of AMSH3 in plants.

INTRODUCTION

Ubiquitination and deubiquitination are functionally reciprocal processes that regulate a broad range of cellular events. Deubiquitinating enzymes (DUBs) and ubiquitinating enzymes play active roles in the regulation of substrate stability, activity, and cellular behavior (reviewed in Clague and Urbé, 2006; Reyes-Turcu et al., 2009). DUBs are also essential for ubiquitin precursor processing and the recycling of ubiquitin molecules, and they thereby contribute to the maintenance of the free ubiquitin pool. Recent studies have shown that DUB function is also required for various aspects of plant development (Yan et al., 2000; Doelling et al., 2001, 2007; Sridhar et al., 2007; Liu et al., 2008; Luo et al., 2008; Schmitz et al., 2009).

MPR1, PAD1 N-terminal+ (MPN+) domain metalloproteases comprise one class of eukaryotic DUBs in addition to four families of Cys proteases, the ubiquitin-specific proteases, ubiquitin C-terminal hydrolases, ovarian tumor proteins, and Machado Joseph disease domain proteins (Komander et al., 2009). Associated Molecule with the SH3 domain of STAM (AMSH) proteins are MPN+ domain DUBs that are widely conserved (Maytal-Kivity et al., 2002). *Arabidopsis thaliana* has three AMSH homologs,

named AMSH1, AMSH2, and AMSH3, that were identified by the homology of their catalytic MPN+ domain to the MPN+ domain of the human AMSH (Maytal-Kivity et al., 2002; Isono et al., 2010). We recently showed that AMSH3 is an active DUB that hydrolyzes both K48- and K63-linked ubiquitin chains (Isono et al., 2010). *amsh3* null mutants are seedling lethal and show vacuole biogenesis and intracellular trafficking defects.

Endosomal sorting complex required for transport (ESCRT) -0, I, II, and III are involved in intracellular trafficking and are important for the proper sorting of ubiquitinated membrane proteins to the intraluminal vesicles of the multivesicular bodies (MVBs) (reviewed in Williams and Urbé, 2007; Raiborg and Stenmark, 2009; Hurley and Hanson, 2010). This process is crucial for the proper delivery of the cargo for degradation in the vacuole/lysosome. The endocytosis of transmembrane proteins is triggered by ubiquitination. ESCRT-0, I, and II subunits recruit the ubiquitinated cargos on endosomal membranes via their ubiquitin binding motifs. ESCRT-III then sorts the cargos into the intraluminal vesicles of the MVB by exerting membrane bending, scission, and fusion.

ESCRT-III is best studied in yeast and consists of a core complex comprised of four subunits: vacuolar protein sorting 2 (Vps2p)/charged MVB proteins or chromatin modifying protein 2 (CHMP2), Vps20p/CHMP6, Vps24p/CHMP3, and Sucrose Non-Fermenting 7 (Snf7p)/VPS32/CHMP4. There are further ESCRT-III–associated proteins like Vps46p/CHMP1/Doa4-independent degradation 2 (Did2p) and Vps60p/CHMP5 that were shown to function together with the ESCRT-III core complex (Babst et al., 2002). Vps20p is a membrane-anchored subunit that recruits Snf7p to the endosomal membrane, which then oligomerizes on

the membrane. The binding of Vps24p to the Snf7p filament stops the oligomerization. Vps2p binds to Vps24p and together with Vps46p and Vps60p then recruits the AAA-ATPase Vps4p/ suppressor of K+ transport growth defect 1 (SKD1) to ESCRT-III (Teis et al., 2008; Saksena et al., 2009). Vps4p/SKD1 forms an oligomeric complex that disassembles ESCRT-III upon binding. The disassembly of ESCRT-III is essential for the completion of the sorting of cargos to the intraluminal vesicles of MVBs (Babst et al., 1998; Ghazi-Tabatabai et al., 2008; Lata et al., 2008). The regulated assembly and disassembly of ESCRT-III is a prereq-uisite for proper MVB formation, and in a yeast *vps4* mutant, ESCRT-III components aggregate in so-called class E compart-ments while cargo sorting is blocked (Babst et al., 1997).

ESCRT-III subunits are highly conserved in eukaryotes, and homologs of all ESCRT components, except those of ESCRT-0, can be detected in the *Arabidopsis* genome (Winter and Hauser, 2006; Schellmann and Pimpl, 2009). Although as yet poorly understood, accumulating evidence suggests that *Arabidopsis* ESCRT proteins also constitute an important part of the MVB sorting pathway and contribute to proper plant development. A recent study of *Arabidopsis* CHMP1A/B or VPS46 has shown that they are required for the delivery of PIN1, PIN2, and AUX1 to the vacuole (Spitzer et al., 2009). It was also shown that an ESCRT-I subunit ELCH/VPS23 is involved in cytokinesis (Spitzer et al., 2006), and the characterization of SKD1 indicated that it is involved in MVB formation and vacuole maintenance (Haas et al., 2007). In contrast with yeast and cultured mammalian cells, *SKD1* is an essential gene in *Arabidopsis* (Haas et al., 2007). Despite their presumed central role in endocytosis, the analysis of *Arabidopsis* ESCRT proteins at the biochemical and cell biological level has just started.

Human AMSH was originally identified as an interactor of the signal transducing adaptor molecule (STAM) that is one of the ESCRT-0 proteins (Tanaka et al., 1999) and is implicated in intracellular trafficking. Further studies have revealed the interac-tion of human AMSH with multiple ESCRT-0 and ESCRT-III com-ponents. A *Xenopus laevis* AMSH protein was shown to interact with an ESCRT-III binding protein, apoptosis-linked gene 2 inter-acting protein X/Bro1p (McCullough et al., 2004, 2006; Agromayor and Martin-Serrano, 2006; Tsang et al., 2006; Kyuuma et al., 2007; Ma et al., 2007). It was also shown that the binding of STAM enhances the DUB activity of human AMSH in vitro (McCullough et al., 2006). The interaction of human AMSH with the ESCRT proteins suggests two possibilities for AMSH function at different steps in endocytosis. First, human AMSH may deubiquitinate endocytosed cargo through the interaction with ESCRT-0 and thereby promote recycling of the cargo to the plasma membrane. Second, human AMSH may serve to recycle ubiquitin molecules from cargos prior sorting into the MVB. However, despite intensive studies, whether and how AMSH regulates ESCRT assembly and disassembly and whether AMSH3 DUB activity is required for proper ESCRT-III formation have not been resolved.

Although the catalytic MPN+ domain is conserved in *Arabi-dopsis* AMSH3, the N terminus of the protein has only low homology to human AMSH (Isono et al., 2010). While the human AMSH possesses three characterized protein interaction do-mains, the microtubule interacting and trafficking (MIT), clathrin binding, and STAM binding domains (Tanaka et al., 1999;

McCullough et al., 2006; Nakamura et al., 2006; Tsang et al., 2006), *Arabidopsis* AMSH3 has only the MIT domain. Together with the fact that apparent ESCRT-0 homologs are absent in *Arabidopsis*, this suggests that *Arabidopsis* AMSH3 may have different interacting partners than its mammalian homolog.

To date, no direct interactors of *Arabidopsis* AMSH3 have been identified. In this study, we therefore aimed at identifying interacting proteins of AMSH3 to understand the role and mode of AMSH3 function. Here, we report that AMSH3 interacts with ESCRT-III subunits VPS2.1 and VPS24.1 in vitro and that they colocalize and interact in class E compartments when the disassembly of ESCRT-III is inhibited by the overexpression of an inactive SKD1. In addition, two MIT domain–containing pro-teins, AMSH3 and SKD1, compete for binding to VPS2.1. We also show that the loss of AMSH3 DUB activity causes the formation of class E–like compartments that contain VPS2.1 and VPS24.1 and thereby provide the molecular framework for AMSH3 and ESCRT-III interaction in plants.

RESULTS

AMSH3 Interacts with Subunits of ESCRT-III

We recently showed that the *Arabidopsis* DUB AMSH3 is involved in vacuole biogenesis and intracellular trafficking (Isono et al., 2010). To further understand the molecular function of AMSH3, we wanted to identify interacting proteins of AMSH3, and conducted a yeast two-hybrid (Y2H) screen with a GAL4 DNA binding domain (GBD) fused to an enzymatically inactive AMSH3(AXA) variant (Isono et al., 2010) and an *Arabidopsis* cDNA library (Kim et al., 1997). We chose the GBD-AMSH3(AXA) fusion as bait, as the wild-type GBD-AMSH3 showed autoactivation in our Y2H assay. Since AMSH3 is implicated in vacuole biogenesis and intracellular trafficking, we decided to focus on interactor candidates with known function in intracellular trafficking and found gene frag-ments coding for *VPS2.1*, which is a homolog of yeast *VPS2* (Winter and Hauser, 2006). When the full-length open reading frame (ORF) of *Arabidopsis VPS2.1* was cloned and tested for interaction with AMSH3 in a Y2H assay, the interaction was confirmed (Figure 1A; see Supplemental Figure 1A online).

In mammals and yeast, Vps2p/CHMP2 is one of the core components of ESCRT-III. Since VPS2 proteins in other organisms are part of the multiprotein complex ESCRT-III, we next tested whether other predicted *Arabidopsis* ESCRT-III subunits also interact with AMSH3. ESCRT-III consists of a so-called core complex and ESCRT-III–associated or –related proteins (Babst et al., 2002). We therefore conducted a directed Y2H analysis of AMSH3 with *Arabidopsis* ESCRT-III core subunit homologs (VPS20.1, VPS24.1, and SNF7.1) and ESCRT-III–related protein homologs (VPS46.2/CHMP1B and VPS60.1) (Winter and Hauser, 2006). Among the tested components, two additional ESCRT-III proteins, VPS24.1 and VPS60.1, showed interaction with AMSH3, regardless of its DUB activity, since the enzymatically inactive AMSH3(AXA) also showed interaction (Figure 1B; see Supple-mental Figure 1B online).

To test whether the interactions between AMSH3 and ESCRT-III components are direct, we next performed an in vitro
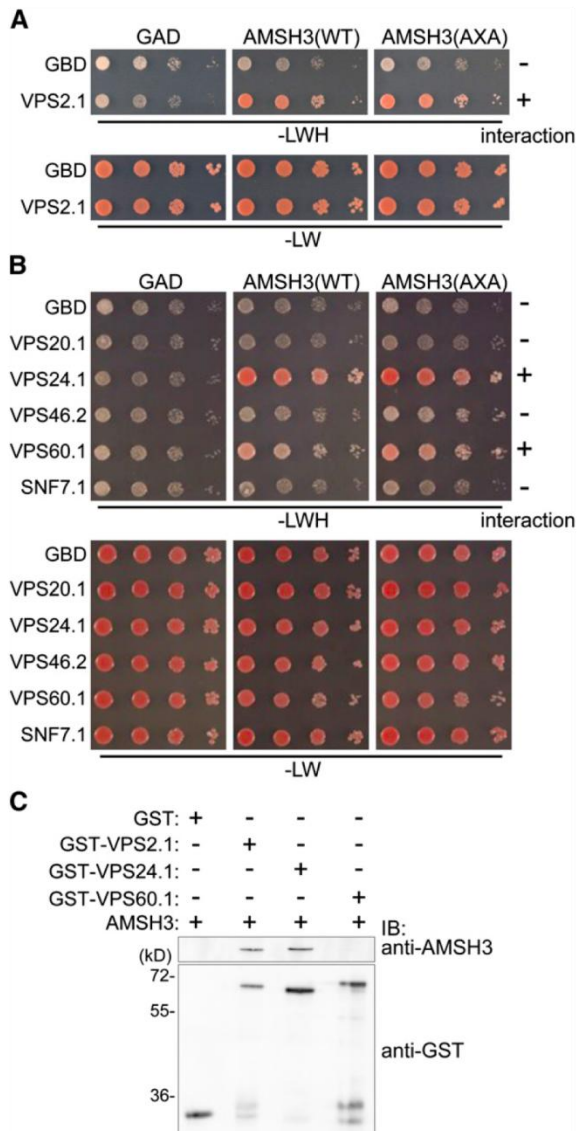
Figure 1. AMSH3 Interacts with ESCRT-III Homologs VPS2.1, VPS24.1, and VPS60.1.

(A) and **(B)** Y2H analysis of GAD-AMSH3(WT) and GAD-AMSH3(AXA) with GBD-VPS2.1 **(A)** and GBD-fused ESCRT-III components VPS20.1, VPS24.1, VPS46.2, VPS60.1, or SNF7.1 **(B)**. Transformants were grown in liquid culture and diluted to $A_{600} = 1$, and 10-fold serial dilutions were spotted on SC-LW or SC-LWH plates to test their auxotrophic growth. The presence or absence of the interaction is indicated on the right of each panel. The expression of all fusion proteins was verified by immunoblotting (see Supplemental Figures 1A and 1B online).
(C) In vitro binding assay using purified GST, GST-VPS2.1, GST-VPS24.1, and GST-VPS60.1 with AMSH3. After the GST pull-down, bead-bound materials were analyzed by immunoblotting with anti-AMSH3 and anti-GST antibodies.
[See online article for color version of this figure.]

glutathione *S*-transferase (GST) pull-down assay. For this assay, AMSH3, GST fusion proteins of VPS2.1, VPS24.1, VPS60.1, and the GST moiety alone were expressed and purified from *Escherichia coli*. AMSH3 was pulled down when incubated together with GST-VPS2.1 or GST-VPS24.1, but not with GST or GST-VPS60.1 (Figure 1C), indicating that VPS2.1 and VPS24.1, but not VPS60.1, directly interact with AMSH3. This result suggests that AMSH3 and the ESCRT-III interaction is mediated by at least two different subunits.

VPS2.1 but Not VPS2.2 or VPS2.3 Interact with AMSH3

Most of the ESCRT-III subunits have multiple sequence homologs in *Arabidopsis*. There are three VPS2 homologs and two VPS24 homologs (Winter and Hauser, 2006) (see Supplemental Figures 2 and 3 online). Among the three *Arabidopsis* VPS2 proteins, VPS2.1, VPS2.2, and VPS2.3, VPS2.1 is more closely related to the yeast, *Drosophila melanogaster*, mouse, and human VPS2 proteins than to the VPS2.2 and VPS2.3 proteins (Figure 2A; see Supplemental Data Set 1 and Supplemental Figure 2 online).

The observation that the three *Arabidopsis* VPS2 proteins belong to different clusters raised the question as to whether the three proteins have distinct functions. To investigate this possibility, we first wanted to know whether VPS2.2 and VPS2.3 can also interact with AMSH3 and performed a Y2H assay. While VPS2.1 interacted with AMSH3, neither VPS2.2 nor VPS2.3 did (Figure 2B; see Supplemental Figure 1C online). To further examine this interaction, we next performed an in vitro binding assay with purified AMSH3 and GST-fused VPS2.1, VPS2.2, and VPS2.3 using GST as a negative control (Figure 2C). GST-VPS2 proteins migrate higher than the calculated molecular mass ($\sim$50 kD) (Figure 2C) like their yeast homolog (Babst et al., 2002), probably owing to the protein properties. While GST-VPS2.1 directly interacted with AMSH3, only 19.8 and 22.6% of the amount of AMSH3 bound to GST-VPS2.1 was bound to GST-VPS2.2 and GST-VPS2.3, respectively (Figure 2D), indicating that VPS2.1, VPS2.2, and VPS2.3 have indeed differential binding affinities for AMSH3.

VPS2.1 Interacts with AMSH3 through Its MIM1 Domain

To further examine the molecular cause for the differential interaction of the *Arabidopsis* VPS2 proteins with AMSH3, we analyzed the amino acid sequence of VPS2.1, VPS2.2, and VPS2.3 more closely. VPS2 is conserved from yeast to humans, and all VPS2/CHMP2 proteins have a Microtubule Interacting and Transport (MIT)-Interacting Motif (MIM) at their C terminus (Figure 3A; see Supplemental Figure 2 online). The MIM domain is defined by its interaction with the MIT domain (Obita et al., 2007; Stuchell-Brereton et al., 2007), and two variations of the MIM domain have been identified in different ESCRT-III components from yeast: MIM1 in VPS2 and VPS24, and MIM2 in VPS20 and SNF7 (Obita et al., 2007; Shim et al., 2007; Stuchell-Brereton et al., 2007; Kieffer et al., 2008).

Since AMSH3 has a MIT domain at its N terminus, we speculated that VPS2.1 and AMSH3 interact through their MIM1 and MIT domains, respectively. Amino acid sequence comparisons of
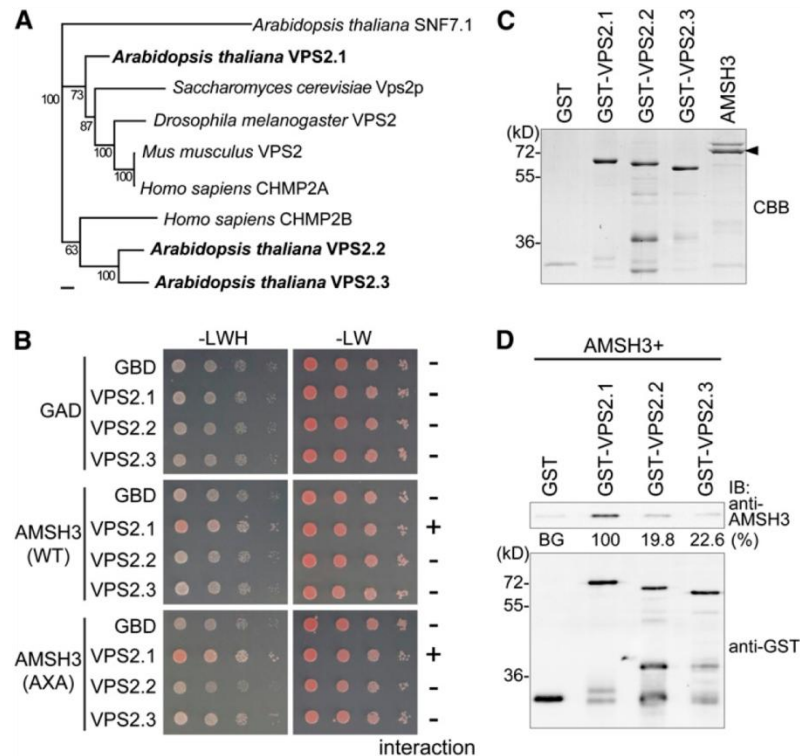
Figure 2. VPS2.1, but Not VPS2.2 and VPS2.3, Interacts with AMSH3.

(A) Phylogenetic analysis of *Arabidopsis* VPS2.1, VPS2.2, and VPS2.3, budding yeast Vps2p, fruit fly VPS2, mouse CHMP2, and human CHMP2A and CHMP2B using the Geneious Tree Builder. The accession numbers are provided in Methods. AtSNF7.1 was used as an outgroup. Bootstrap values are indicated beside each branch. Bar = 0.1 amino acid substitutions per site.

(B) Y2H analysis of GAD-AMSH3(WT) or GAD-AMSH3(AXA) and GBD, GBD-VPS2.1, GBD-VPS2.2, or GBD-VPS2.3. Transformants were tested for growth on SC-LWH medium as in Figures 1A and 1B. The presence or absence of the interaction is indicated on the right of each panel. Note that only VPS2.1 interacts with AMSH3. The expression of all fusion proteins was verified by immunoblotting (see Supplemental Figure 1C online).

(C) Purified GST, GST-VPS2.1, GST-VPS2.2, GST-VPS2.3, and AMSH3 were resolved by SDS-PAGE and stained by Coomassie blue to show equal loading. The arrowhead indicates AMSH3.

(D) In vitro binding assay of AMSH3 with GST-fused *Arabidopsis* VPS2 proteins. After GST pull down, bead-bound proteins were analyzed by immunoblotting using anti-AMSH3 and anti-GST antibodies. The efficiency of the GST pull-down assay was assessed as a percentage of the bound AMSH3 after subtraction of signal intensity of the GST alone sample (BG, background) using Multi Gauge software. The average value of three independent experiments is shown. The percentage of the VPS2.1 sample was set to 100%.

[See online article for color version of this figure.]

VPS2.1, VPS2.2, and VPS2.3 showed that the conserved residues in MIM1 [(D/E)XXLXXRLXXL(K/R)] are present in all three *Arabidopsis* VPS2 proteins. We noted, however, that the spacing between two acidic amino acids (Asp-212 and Asp-214 in VPS2.1) is altered in the MIM1 of VPS2.2 and VPS2.3 (Figure 3A). To test whether the amino acid sequence of the MIM1 is important for the interaction of VPS2 proteins and AMSH3, we constructed mutant variants of VPS2.1 and VPS2.3. In VPS2.1(mut), Asp-212 was mutated to an Asn, and in VPS2.3(mut), an additional Asp was inserted after the conserved D200 (Figure 3B). The wild-type and mutant VPS2.1 and VPS2.3 proteins were then expressed as GST fusion proteins in *E. coli*, and purified proteins were tested in an in vitro binding assay (Figure 3C). While the wild-type VPS2.1 interacted with AMSH3, the mutation in VSP2.1 [VPS2.1(mut)] led to a much weaker interaction with AMSH3 (34.9% of the GST-VPS2.1), suggesting that the Asp-212 residue is required for

the interaction of these two proteins (Figure 3D). In turn, to investigate whether an additional amino acid after Asp-200 in VPS2.3 is necessary for the interaction, wild-type and mutant VPS2.3 proteins were tested for their binding to AMSH3. Interestingly, while the wild-type VPS2.3 interacted only weakly with AMSH3, VPS2.3(mut) could strongly interact with AMSH3 (Figure 3E), suggesting that the spacing between the two conserved acidic amino acids in MIM1 is indeed important for the interaction of VPS2 proteins with AMSH3.

The AMSH3 MIT Domain Is Necessary for the Interaction with ESCRT-III Subunits

We next wanted to know whether the interactions of VPS2.1 and VPS24.1 with AMSH3 are dependent on the MIT domain of AMSH3. To examine this, we created truncated versions of
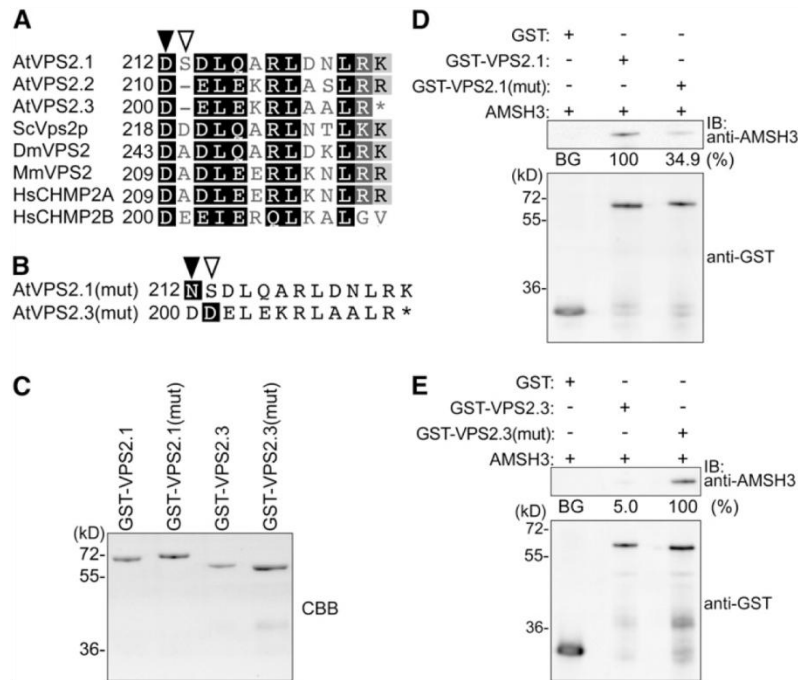
Figure 3. Differences in the MIM1 Sequence Account for the Differential Interaction of VPS2 Proteins and AMSH3.

(A) MIM1 sequence alignment of At VPS2.1, VPS2.2, and VPS2.3 and their budding yeast (Sc), fruit fly (Dm), mouse (Mm), and human (Hs) homologs. The filled arrowhead indicates the position of the conserved Asp, and the open arrowhead indicates the gap present in *Arabidopsis* VPS2.2 and VPS2.3 MIM1.

(B) Mutations introduced to create *Arabidopsis* VPS2.1(mut) and VPS2.3(mut). For AtVPS2.1(mut), the Asp (D212) (filled arrow, Figure 3A) was mutated to an Asn, and for AtVPS2.3 (mut), the gap between D200 and D201 (open arrow, Figure 3A) was filled with an Asp.

(C) Purified GST-VPS2.1, GST-VPS2.1(mut), GST-VPS2.3, and GST-VPS2.3(mut) were subjected to SDS-PAGE and stained with Coomassie blue to show equal loading.

(D) In vitro binding assays of GST, GST-VPS2.1, and GST-VPS2.1(mut) with AMSH3. The binding assay was performed as in Figure 2D. Note that GST-VPS2.1(mut) interacts more weakly with AMSH3 than does the wild-type GST-VPS2.1. The efficiency of the GST pull-down assay was assessed as in Figure 2D. The average values of three independent experiments are shown.

(E) In vitro binding assays of GST, GST-VPS2.3, and GST-VPS2.3 (mut) with AMSH3 were performed as in Figure 2D. Note that GST-VPS2.3(mut) interacts much stronger with AMSH3 than GST-VPS2.3. The efficiency of the GST pull-down assay was assessed as a percentage of the bound AMSH3 after subtraction of signal intensity of the GST alone sample (BG, background) using Multi Gauge software. The average percentage value of three independent experiments is shown. The percentage of VPS2.3(mut) was set to 100%.

AMSH3 (ΔMIT, ΔMPN, MIT, N102, and N154) and tested their interaction with VPS2.1 and VPS24.1 by Y2H (Figure 4A). Supporting the notion that AMSH3 and the ESCRT-III subunits interact via the MIT domain of AMSH3, both VPS2.1 and VPS24.1 lost their interaction with AMSH3 when the N-terminal MIT domain was deleted (Figure 4B; see Supplemental Figure 1D online). In turn, we found that the isolated MIT domain (MIT) was not sufficient for the interaction with VPS2.1 or VPS24.1. However, when the N-terminal 16 amino acids were added to the MIT domain of AMSH3 (N102), VPS24.1 interacted with this variant (Figure 4B; see Supplemental Figure 1D online), showing that this extended MIT domain of AMSH3 is sufficient for the interaction with VPS24.1. By contrast, VPS2.1 required a much longer N-terminal region (ΔMPN) for the interaction with AMSH3 (Figure 4B; see Supplemental Figure 1D online), suggesting that the two ESCRT-III subunit homologs may have different interaction surfaces on AMSH3.

VPS2.1 but Not VPS2.2 and VPS2.3 Localize to SKD1 (EQ)-Induced Class E Compartments

Another MIT domain containing protein in the ESCRT pathway is SKD1/VPS4 (Obita et al., 2007) (see Supplemental Figure 4 online). SKD1 is an AAA-ATPase that interacts with ESCRT-III subunits via its MIT domain and whose ATPase activity is required for ESCRT-III disassembly (Babst et al., 1998). It was previously shown that the expression of an enzymatically inactive SKD1 leads to the formation of so-called class E compartments in yeast and *Arabidopsis* (Babst et al., 1997, 1998; Haas et al., 2007). Class E compartments are aberrant endosomal structures, and in yeast, it was shown that ESCRT-III subunits accumulate on these structures in *vps4* mutant cells (Babst et al., 1998).

We thus reasoned that if VPS2.1 was a bona fide *Arabidopsis* ESCRT-III subunit and if the VPS2.1-containing ESCRT-III
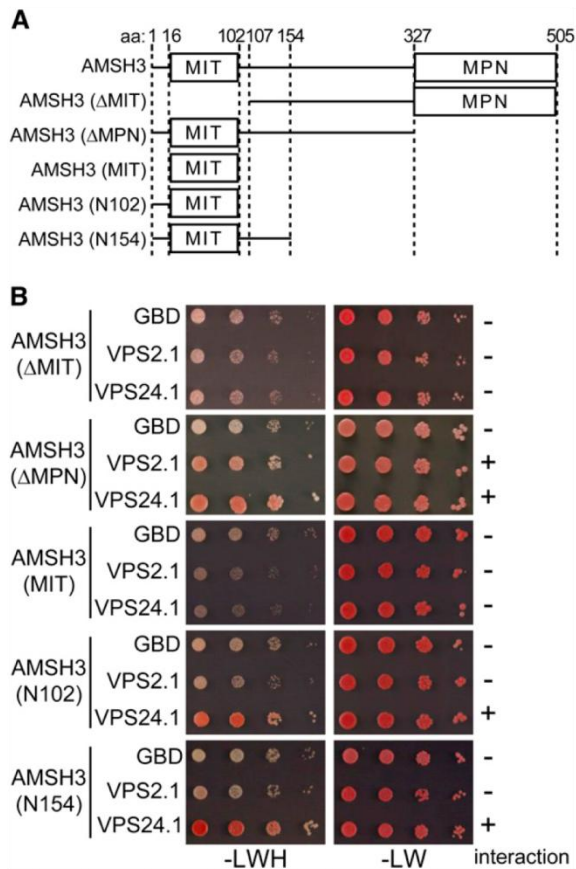
Figure 4. The MIT Domain of AMSH3 Is Necessary for the Interaction of AMSH3 and Putative ESCRT-III Subunits.

(A) Schematic presentation of the AMSH3 truncation constructs used in the Y2H analysis.

(B) Y2H analysis with truncation constructs of AMSH3 with VPS2.1 or VPS24.1. Yeast cells were transformed with the indicated truncation constructs of GAD-AMSH3 and GBD-, GBD-VPS2.1–, or GBD-VSP24.1– containing plasmids. Transformants were tested for their auxotrophic growth on SC-LW and SC-LWH media as in Figures 1A and 1B. The presence or absence of the interaction is indicated on the right of each panel. The expression of the Y2H constructs was verified by immunoblotting (see Supplemental Figure 1D online).

[See online article for color version of this figure.]

complex disassembly was dependent on SKD1, then VPS2.1 should accumulate in class E compartments upon ATPase-defective SKD1(EQ) coexpression. Since the overexpression of SKD1(EQ) had been shown to be toxic to plants (Haas et al., 2007), we had to examine its effect in *Arabidopsis* cell culture–derived protoplasts. To test our hypothesis, we generated a wild-type SKD1 [SKD1(WT)], and a SKD1(EQ) mutant variant fused to an HA-tag. Upon overexpression of SKD1(EQ) but not SKD1(WT), yellow fluorescent protein (YFP)-VPS2.1 relocated from the cytosol to large punctate structures (Figures 5A to 5C). Since the endocytosis tracer dye FM4-64 also accumulated in these structures (Figure 5D) and since VPS24.1-GFP (green fluorescent protein) and mCherry-VPS2.1 colocalized in these

structures specifically upon SKD1(EQ) overexpression (Figure 5E; see Supplemental Figure 5A online), we concluded that these structures are class E compartments that were induced by SKD1(EQ) expression. The localization and relocation observed upon SKD1(EQ) coexpression are not due to the overexpression of VPS2.1 since VPS2.1 expressed under its own promoter showed similar cytosolic localization and reactivity toward SKD1(EQ) overexpression (see Supplemental Figures 6A and 6B online). Furthermore, since VPS2.1 and VPS24.1 colocalized in class E compartments, we concluded that these two proteins are bona fide ESCRT-III subunits that are integrated into the membrane-bound ESCRT-III like their animal and yeast homologs.

Among the three *Arabidopsis* VPS2 homologs, only VPS2.1 showed in vitro and Y2H interaction with AMSH3, probably owing to differences in the MIM1 sequence. Since SKD1 has a MIT domain, we speculated that these differences in MIM1 could also lead to differential interactions of the VPS2 proteins with SKD1 and, thus, to differential reactivity toward SKD1(EQ) overexpression. Indeed, in contrast with YFP-VPS2.1, where 95% (n = 47) of all cells accumulate the fusion protein on class E compartments upon coexpression of SKD1(EQ), only 18% (n = 40) and 26% (n = 59) of cells accumulated YFP-VPS2.2 and YFP-VPS2.3 in class E compartments after SKD1(EQ) overexpression (Figures 5F to 5H). Upon SKD1(WT) overexpression or without SKD1 coexpression, VPS2 fusion proteins showed cytosolic localization (Figure 5A; see Supplemental Figures 5B and 5C online). Since only VPS2.1 shows interaction with AMSH3, and only VPS2.1 reacts toward the overexpression of dominant-negative SKD1, VPS2.1 may be the only true ESCRT-III subunit among the *Arabidopsis* VPS2 proteins. It can thus be speculated that VPS2.2 and VPS2.3 may function in a different context outside of the classical ESCRT-III that is not dependent on SKD1 activity.

vps2.1 Homozygous Mutants Are Embryo Lethal

To date, mutant analysis of the ESCRT-III core complex subunits has not been reported in *Arabidopsis*. We therefore obtained and examined a T-DNA insertion mutant of *VPS2.1*, in which the T-DNA is inserted in the fourth exon (Figure 6A). Since we could not detect any *vps2.1* homozygous seedlings among the progeny of a self-pollinated *VPS2.1/vps2.1* heterozygous plant, we hypothesized that the homozygous *vps2.1* is embryo lethal. Indeed, among the seeds of a *VPS2.1/vps2.1* heterozygous plant (total n = 416), we found that 13.7% did not germinate and 7.2% were aborted within the silique (Table 1). Since we found fewer ungerminated seeds (3.3%, n = 183) in a self-pollinated wild-type plant (Table 1), this result suggests that *vps2.1* homozygous mutants arrest growth during embryogenesis. To confirm this, we genotyped embryos dissected from ungerminated seeds together with wild-type embryos and a *VPS2.1/vps2.1* heterozygous seedlings. Since the DNA yield from individual ungerminated embryos was very low, we analyzed them in pools of four embryos. This experiment revealed that the ungerminated seeds indeed contain *vps2.1/vps2.1* homozygous mutant embryos (Figures 6B and 6C). Phenotypic analysis of the dissected mutant embryos showed that these are smaller than those of the wild
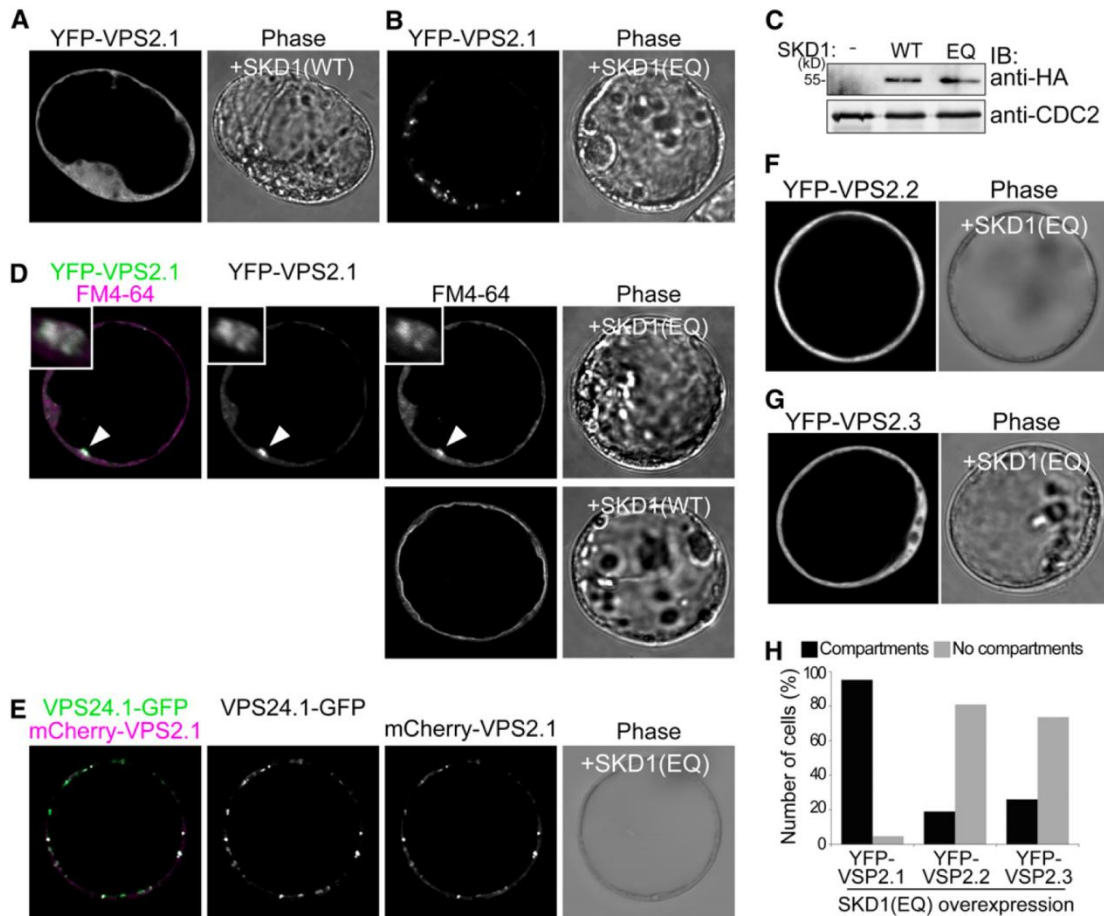
Figure 5. VPS2.1, but Not VPS2.2 and VPS2.3, Localize to SKD1(EQ)-Induced Class E Compartments.

(A) and **(B)** UBQ10pro:YFP-VPS2.1 was coexpressed with 35Spro:HA-SKD1(WT) **(A)** and 35Spro:HA-SKD1(EQ) **(B)** in *Arabidopsis* protoplasts and analyzed using a confocal laser scanning microscope. Note that instead of the cytosolic localization observed in **(A)**, YFP is localized to intracellular structures in **(B)**.

(C) Expression of HA-SKD1(WT) and HA-SKD1(EQ) was verified by immunoblotting with an anti-HA antibody on total extracts of transformed protoplasts. An anti-CDC2 antibody was used as a loading control.

(D) UBQ10pro:YFP-VPS2.1 was coexpressed with 35Spro:HA-SKD1(EQ), and protoplasts were stained with FM4-64 2 h prior to observation by confocal microscopy (top panel). Arrowheads indicate the class E compartment where YFP-VPS2.1 and FM4-64 signals colocalize. Insets are magnifications of a class E compartment. Note that FM4-64 reaches the tonoplast membrane after 3 h of incubation in a cell overexpressing SKD1(WT) (bottom panel).

(E) Coexpression of 35Spro:VPS24.1-GFP, UBQ10pro:mCherry-VPS2.1, and 35Spro:HA-SKD1(EQ) in *Arabidopsis* protoplasts. Upon overexpression of SKD1(EQ), VPS24.1-GFP and mCherry-VPS2.1 colocalize in class E compartments.

(F) and **(G)** UBQ10pro:YFP-VPS2.2 **(F)** and 35Spro:YFP-VPS2.3 **(G)** were coexpressed in *Arabidopsis* protoplasts with 35Spro:HA-SKD1(EQ). Note that in contrast with YFP-VPS2.1, the cytosolic localization of YFP-VPS2.2 and YFP-VPS2.3 does not change upon SKD1(EQ) overexpression.

(H) Number of cells (percentage) with YFP-VPS2.1 (*n* = 47), YFP-VPS2.2 (*n* = 40), and YFP-VPS2.3 (*n* = 59) positive class E compartments after SKD1(EQ) overexpression. Black bars, cells with class E compartments; gray bars: cells without class E compartments.

type and that they arrest development at the walking-stick stage of embryogenesis (Figure 6B). Furthermore, 15% of the embryos (*n* = 225) of a *VPS2.1/vps2.1* self-pollinated plant showed developmental delay in the heart or torpedo stage, suggesting that the loss of VPS2.1 function already has consequences at an early stage of embryogenesis (Figure 6D; see Supplemental Table 1 online). The *VPS2.1pro:YFP-VPS2.1* (genomic) construct could partially rescue the developmental arrest of *vps2.1* mutant em-

bryos, whereas a Ribosomal Protein S5 (RPS5a):VPS2.1 (cDNA) construct could also rescue the germination defects of *vps2.1* homozygous mutants (see Supplemental Figures 7A to 7D and Supplemental Tables 1 and 2 online). These results indicate that the observed *vps2.1* phenotypes are indeed due to the misregulation of *VPS2.1*.

To find out whether the underrepresentation of the homozygous mutants is due to a defect in female or male gametes, we
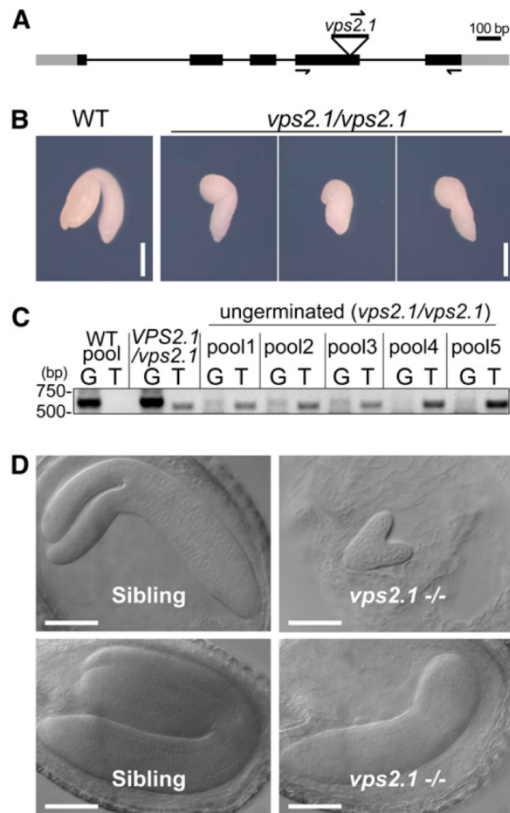
Figure 6. *vps2.1* Homozygous Mutants Are Embryo Lethal.

(A) T-DNA insertion and primer binding site in *VPS2.1*. Lines indicate introns and boxes indicate exons (black boxes, coding region; gray boxes, untranslated regions). The position of the T-DNA in the *vps2.1* mutant is shown.

(B) Photographs of wild-type (WT) and *vps2.1* homozygous embryos dissected from dry seeds. Bars = 0.2 mm.

(C) PCR analysis of wild-type and *vps2.1* homozygous mutant embryos. Twenty embryos were dissected from the ungerminated seeds of a *VPS2.1/vps2.1* self-pollinated plant, and total DNA was extracted from pools of four embryos. DNA extracted from a pool of four wild-type embryos, and DNA from a *VPS2.1/vps2.1* heterozygous plant was used as control. PCR was performed with either gene-specific forward and reverse primers (G lanes) or a T-DNA left border primer in combination with the gene-specific reverse primer (T lanes). Note that all ungerminated seeds contain embryos homozygous for the T-DNA insertion. The primers used for genotyping and their sequences are presented in Methods and Supplemental Table 3 online.

(D) *vps2.1* homozygous mutant embryos (right panels) are delayed in embryogenesis in comparison to their wild-type-looking siblings (left panels). Bars = 100 μm.

[See online article for color version of this figure.]

performed reciprocal crosses between a *VPS2.1/vps2.1* and a wild-type plant (Table 2). The progeny of the two types of crosses was genotyped. When *VPS2.1/vps2.1* was used as the female partner, the ratio of heterozygous to wild-type progeny was with 42.1:57.9%, which is not significantly different from the expected 50:50% ratio. However, when *VPS2.1/vps2.1* was used as the

male parent, the ratio of heterozygous to wild-type progeny was 29.5:70.5%, which deviates significantly from the expected 50:50% ratio, indicating that *vps2.1* pollen are less fertile than the wild type. Together, these results suggest that VPS2.1 is already required during gametogenesis and is necessary for proper embryogenesis. Moreover, the observation that a *vps2.1* single mutant develops a severe phenotype indicates that VPS2.1 function is not redundant with that of VPS2.2 and VPS2.3, both of whose homozygous T-DNA insertion mutants show only mild growth defects but not embryo lethality (see Supplemental Figures 8A to 8C online).

AMSH3 and ESCRT-III Components Colocalize in Class E Compartments

We next wanted to examine whether AMSH3 functions together with the ESCRT-III subunits in vivo. For this aim, we first tried to coimmunoprecipitate AMSH3 and VPS2.1. However, VPS2.1 turned out to be a very unstable protein, and we could not detect YFP-VPS2.1 with an anti-GFP or with a generated specific anti-VPS2.1 antibody (see Supplemental Figures 9A and 9B online) in the total extract precleared for immunoprecipitation (see Supplemental Figure 9C online). Therefore, we decided to examine the colocalization of AMSH3 and VPS2.1. Both AMSH3 and VPS2.1 fusion proteins showed an apparent cytoplasmic localization in *Arabidopsis* cell culture–derived protoplasts (Figure 7A) as well as in the root epidermal cells of transgenic *Arabidopsis* seedlings (see Supplemental Figure 5E online). The localization of both AMSH3 and VPS2.1 was not affected by treatments of the commonly used endocytosis inhibitors Brefeldin A or Wortmannin A (see Supplemental Figure 5E online), suggesting that both proteins are not stably associated with endosomes or organelles that are sensitive to these treatments.

If AMSH3 interacts with ESCRT-III in vivo, its localization should also be affected by SKD1(EQ) overexpression. Indeed, when cotransformed with SKD1(EQ), 31% of YFP-AMSH3 expressing cells (n = 45) had YFP signals in class E compartments (Figure 7B), while cotransformation with wild-type SKD1 did not yield such signals (see Supplemental Figure 5D online). Moreover, YFP-AMSH3 colocalized in these compartments with mCherry-VPS2.1 upon SKD1(EQ) expression (Figure 7C), suggesting that AMSH3 and ESCRT-III closely localize in vivo. The SKD1(EQ)-dependent colocalization of mCherry-VPS2.1 and YFP-AMSH3 was also observed when both fusion proteins were expressed under their native promoter (see Supplemental Figure 6C online). Notably, even after SKD1(EQ) overexpression, part of YFP-AMSH3 remained cytosolic, suggesting that either only a small fraction of AMSH3 interacts with ESCRT-III or that the interaction between AMSH3 and ESCRT-III is transient.

Table 1. Progeny Analysis of Wild-Type and *VPS2.1/vps2.1* Heterozygous Plants

Genotype of the Parent Plant	Germinated	Ungerminated	Aborted	n
VPS2.1/VPS2.1	96.7%	3.3%	0%	183
VPS2.1/vps2.1	79.1%	13.7%	7.2%	416

Table 2. Analysis of Genetic Transmission of *VPS2.1/vps2.1*

Genotype (Female × Male)	VPS2.1/VPS2.1	VPS2.1/vps2.1	n	χ^2 P
VPS2.1/vps2.1 × Col-0	57.9%	42.1%	38	0.11410
Col-0 × *VPS2.1/vps2.1*	70.4%	29.5%	54	0.00005

To address the question of whether AMSH3 and VPS2.1 interact in class E compartments, we further analyzed Förster resonance energy transfer (FRET) efficiency in YFP-AMSH3, mCherry-VPS2.1, and HA-SKD(EQ) cotransformed cells. An increase in energy transfer efficiency was expected if AMSH3 and VPS2.1 interact in vivo. Indeed, YFP-AMSH3 and mCherry-VPS2.1 showed an average FRET efficiency of 33.5% in class E compartments, while the FRET efficiency in the cytosol was only 6.7% (Figure 7D), indicating that these proteins interact in vivo specifically on these compartments.

ESCRT-III Does Not Directly Regulate AMSH3 DUB Activity

The binding of an ESCRT-0 component STAM to human AMSH was shown to promote the AMSH DUB activity in vitro (Kim et al., 2006; McCullough et al., 2006). To see whether ESCRT-III subunits can affect the enzyme activity of AMSH3, we tested the DUB activity of AMSH3 in an in vitro DUB assay in the presence of GST-VPS2.1 and GST-VPS24.1. In our assay, AMSH3 typically hydrolyzed K48 ubiquitin chains to monoubi-

quitins after 20 min. This tendency was not affected when AMSH3 was preincubated with either GST-VPS2.1 or GST-VPS24.1 for 20 min prior to the DUB assay (Figure 8A; see Supplemental Figure 10 online), indicating that neither VPS2.1 nor VPS24.1 directly regulate AMSH3 DUB activity in vitro.

AMSH3 DUB Activity Is Required for Proper ESCRT-III Localization

Finally, we wanted to know whether AMSH3 dysfunction in turn can affect ESCRT-III localization. To investigate this possibility, we coexpressed the enzymatically inactive AMSH3(AXA) with YFP-VPS2.1 and VPS24.1-GFP. Interestingly, the cytosolic localization of both YFP-VPS2.1 and VPS24.1-GFP was affected by the coexpression of HA-AMSH3(AXA) (Figure 8B). G/YFP signals accumulated in the intracellular compartments of 79.4% (*n* = 34) and 66.7% (*n* = 30) of the VPS24.1-GFP– and YFP-VPS2.1–expressing cells, respectively. By contrast, only 25.7% (*n* = 35) and 6.25% (*n* = 16) of cells showed G/YFP signals, respectively, in compartments with coexpression of wild-type AMSH3 (Figure 8D). mCherry-VPS2.1 and VPS24.1-GFP colocalized on these AMSH(AXA)-induced compartments (Figure 8C). Furthermore, in contrast with YFP-AMSH3(WT), YFP-AMSH3(AXA) itself was relocated to these compartments and colocalized with mCherry-VPS2.1 (cf. Figures 8E and 7A). If these compartments are class E–like compartments, VPS2.3, which is resistant to SKD1(EQ) overexpression, should also be resistant to AMSH3(AXA) overexpression. Indeed, when YFP-VPS2.3,
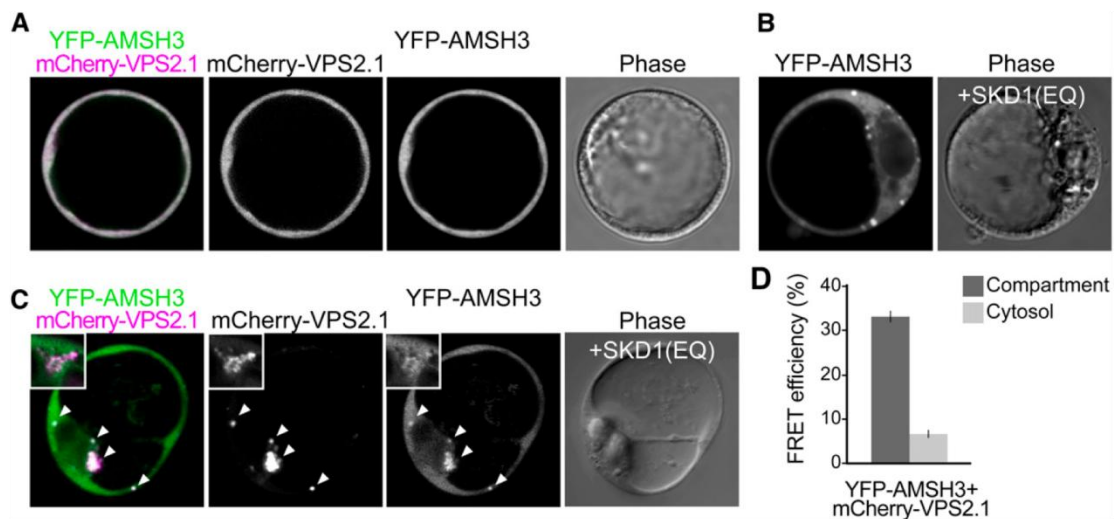
Figure 7. AMSH3 and VPS2.1 Colocalize and Interact in Class E Compartments.

(A) AMSH3pro:YFP-AMSH3 was cotransformed with UBQ10pro:mCherry-VPS2.1 in *Arabidopsis* protoplasts. Both fusion proteins show cytoplasmic localization in *Arabidopsis* cell culture–derived protoplasts.
(B) YFP-AMSH3 localizes to class E compartments upon SKD1(EQ) coexpression.
(C) Coexpression of AMSH3pro:YFP-AMSH3 and UBQ10pro:mCherry-VPS2.1 with 35Spro:HA-SKD1(EQ) in *Arabidopsis* cell culture–derived protoplasts. Note that a fraction of YFP-AMSH3 colocalizes with mCherry-VPS2.1 in class E compartments is shown in the inset. Arrowheads indicate class E compartments.
(D) FRET analysis by the sensitized emission method between YFP-AMSH3 and mCherry-VPS2.1. *Arabidopsis* cell culture–derived protoplasts were cotransformed with 35Spro:HA-SKD1(EQ), AMSH3pro:YFP-AMSH3, and UBQ10pro:mCherry-VPS2.1, and the mean FRET efficiency in either the compartments or the cytosol was measured in a total of 16 cells. Dark-gray bar, compartment; light-gray bar, cytosol. Error bars indicate SE.
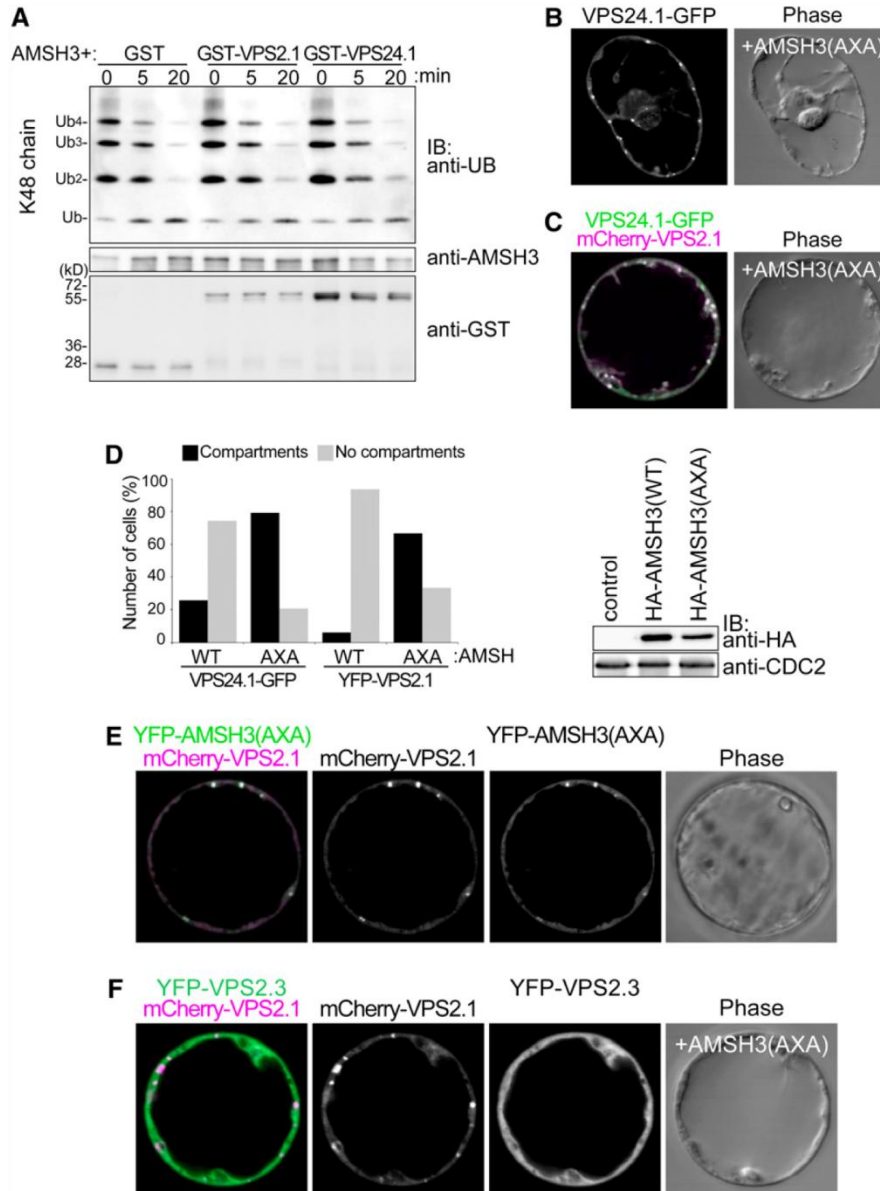
Figure 8. AMSH3 Enzymatic Activity Affects VPS2.1 and VPS24.1 Intracellular Localization.

(A) AMSH3 DUB assay with purified GST, GST-VPS2.1, or GST-VPS24.1 using K48-linked ubiquitin chains. AMSH3 was preincubated with GST fusion proteins prior the addition of ubiquitin chains to the reaction mixture. Reactions were stopped after 0, 5, and 20 min and subjected to immunoblots using the indicated antibodies.

(B) and **(C)** Coexpression of 35Spro:HA-AMSH3(AXA) with 35Spro:VPS24.1-GFP **(B)** or UBQ10pro:YFP-VPS2.1 and 35Spro:VPS24.1-GFP **(C)**. Upon expression of AMSH3(AXA), both VPS2.1 and VSP24.1 fusion proteins partially mislocalize on compartments.

(D) Quantification of the effect of 35Spro:HA-AMSH3(WT) and 35Spro:HA-AMSH3(AXA) coexpression on ESCRT-III localization (left panel). Solid bars, cells with compartments; gray bars, cells without compartments. $n = 35$ and 34 for 35Spro:VPS24.1-GFP expressed with 35Spro:HA-AMSH3(WT) and 35Spro:HA-AMSH3(AXA), respectively, and $n = 16$ and 30 for UBQ10pro:YFP-VPS2.1 expressed with 35Spro:HA-AMSH3(WT) and 35Spro:HA-AMSH3 (AXA), respectively. Expression of HA-AMSH3(WT) and HA-AMSH3(AXA) was verified by immunoblotting with an anti-HA antibody (right panel). An anti-CDC2 antibody was used to show equal loading.

(E) mCherry-VPS2.1 and YFP-AMSH3(AXA) colocalized on the AMSH3(AXA)-induced compartments.

(F) mCherry-VPS2.1, but not YFP-VPS2.3, localizes on AMSH3(AXA)-induced cellular compartments.

mCherry-VPS2.1, and HA-AMSH3(AXA) were coexpressed, only mCherry-VPS2.1 localized on the AMSH3(AXA)-induced compartments, whereas YFP-VPS2.3 remained cytosolic (Figure 8F). These results suggest that the DUB activity of AMSH3 is required for proper localization of AMSH3 as well as of ESCRT-III.

SKD1 and AMSH3 Compete for ESCRT-III Binding

AMSH3 and SKD1 both possess a MIT domain that can serve as an interaction surface for ESCRT-III components. The fact that AMSH3(AXA) overexpression causes a strong mislocalization of ESCRT-III subunits to class E–like compartments suggests that the binding of AMSH3 to ESCRT-III, especially when it is inactive, may partially block the access of SKD1 to ESCRT-III. If this was true, SKD1 and AMSH3 should compete for the binding to ESCRT-III. To test this hypothesis, we first wanted to establish whether SKD1 could interact with VPS2.1 and VPS24.1, two ESCRT-III subunits that interact with AMSH3, since SKD1 and VPS2.1 interaction was not reported in previous interaction studies using *Arabidopsis* ESCRT proteins (Shahriari et al., 2010). We therefore conducted an in vitro binding assay of SKD1 with VPS2.1 and VPS24.1 and found that VPS2.1 interacts with SKD1 (Figure 9A).

We next performed a competition assay with purified His-SKD1, AMSH3, GST-VPS2.1, and GST-VPS24.1. While His-SKD1 did not affect the binding of AMSH3 to VPS24.1, we found that an increasing amount of SKD1 in the binding assay lead to a reduction of AMSH3 binding to GST-VPS2.1 (Figure 9B), suggesting that AMSH3 and SKD1 compete for the binding to VPS2.1. In an assay without AMSH3, SKD1 bound to VPS2.1 in a dosage-dependent manner (Figure 9B). Taken together, our results indicate that SKD1 competes with AMSH3 for binding to VPS2.1 and that AMSH3 activity is probably required for the efficient disassociation of AMSH3 from ESCRT-III and, hence, the recruitment of SKD1 to the complex (Figure 9C).

DISCUSSION

In this study, we identified two ESCRT-III core subunit homologs, VPS2.1 and VPS24.1, as interactors of the DUB AMSH3 in *Arabidopsis*. Human AMSH was shown to strongly interact with VPS24/CHMP3, VPS46/CHMP1, and SNF7/CHMP4 (Agromayor and Martin-Serrano, 2006; Tsang et al., 2006), indicating a partially different interaction pattern between the human and plant AMSH proteins and the ESCRT-III subunits. This may be due to the difference in the region surrounding the MIT domain of the human and *Arabidopsis* AMSH proteins. Although bioinformatic analyses have shown that the ESCRT components are conserved in *Arabidopsis* (Winter and Hauser, 2006), little is known about the ESCRT-III function in plants. Through coexpression studies using SKD1(EQ), we could show that VPS2.1 and VPS24.1 behave like bona fide ESCRT-III subunits and that they interact directly with AMSH3 and colocalize with AMSH3 in class E compartments.

Interestingly, we found that the three VPS2 homologs from *Arabidopsis* have different characteristics. First, in contrast with
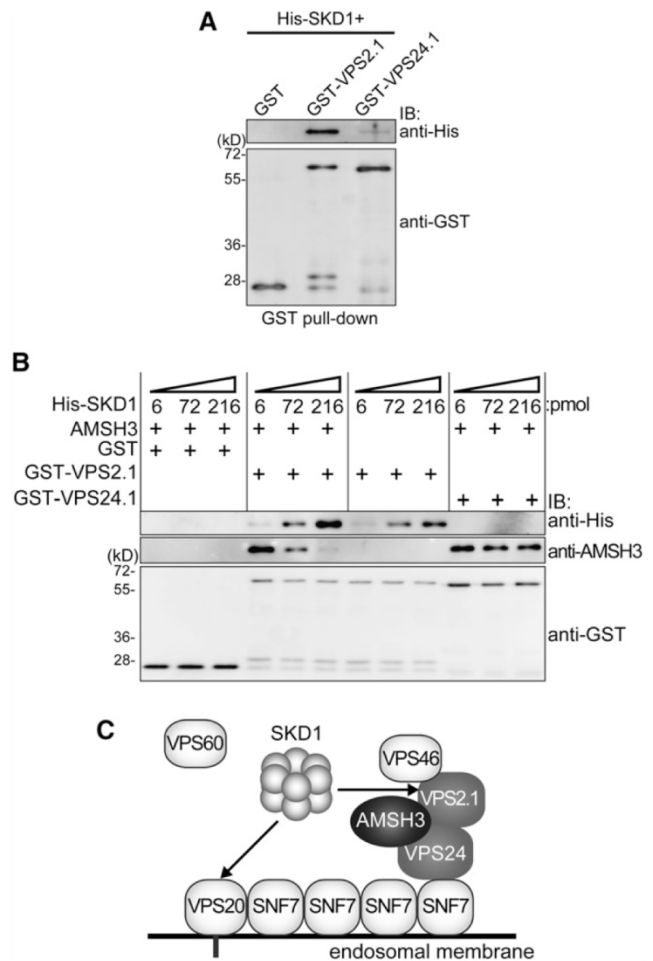

Figure 9. AMSH3 Competes with SKD1 for VPS2.1 Binding.

(A) SKD1 in vitro binding assay. GST, GST-VPS2.1, and GST-VPS24.1 loaded on GST Sepharose 4B beads were incubated with His-SKD1. After extensive washing, the bead-bound materials were analyzed by immunoblotting using anti-His and anti-GST antibodies.

(B) SKD1 competition assay. Binding assay of GST-2.1 or GST-24.1 with 6 pmol of AMSH3 was performed as in Figure 1C in the presence of 6, 72, and 216 pmol of His-SKD1. Note that AMSH3 binding becomes weaker in the presence of an excess amount of SKD1.

(C) Predicted model for the AMSH3–ESCRT-III interaction. AMSH3 associates with ESCRT-III through its binding to VPS2.1 and VPS24.1. AMSH3 competes with SKD1 for the binding to VPS2.1 MIM1, but probably not to VPS20. The timely disassociation of AMSH3 may be necessary for SKD1 to be able to bind efficiently and disassemble ESCRT-III.

VPS2.1, which is the closest *Arabidopsis* homolog of yeast Vps2p, VPS2.2 and VPS2.3 did not show MIM1-dependent interaction with AMSH3. Second, VPS2.1, but not VSP2.2 and VPS2.3, accumulate in class E compartments induced by the overexpression of the dominant-negative SKD1 and VPS2.3 also did not accumulate in the AMSH3(AXA)-induced compartments. Third, the *vps2.1* single homozygous mutant is embryo lethal, implicating the nonredundancy of *VPS2.1*. VPS2.1, VPS2.2, and VPS2.3 may therefore be integrated into different ESCRT-III

complexes that are differently regulated by SKD1. Alternatively, VPS2.2 and VPS2.3 may function independently of the classical ESCRT-III and are therefore not regulated by SKD1. A recent article by Shahriari et al. (2011) describes the investigation of the interaction network of ESCRT proteins by Y2H and bimolecular fluorescence complementation. They propose that VPS2.3 is the VPS2 protein of *Arabidopsis* that is integrated into ESCRT-III. However, at the same time we noticed that in their system only VPS2.1 shows interaction with VPS24.1. Since yeast *vps24Δ* mutant analysis has shown that the binding of Vps2p, but of no other ESCRT-III core subunit, is dependent on Vps24p, these subunits probably function closely with each other (Teis et al., 2008). Moreover, since we found VPS2.1 and VPS24.1 to colocalize on SKD1(EQ)-induced class E compartments, we suggest that VPS2.1 is part of ESCRT-III in *Arabidopsis*. This differential function of the three different *Arabidopsis* VPS2 homologs will be the theme of future investigations.

In contrast with the binding of STAM, which was reported to promote human AMSH DUB activity (Kim et al., 2006; McCullough et al., 2006), the binding of ESCRT-III subunits to AMSH3 did not regulate its DUB activity directly. We therefore speculate that ESCRT-III may serve as a platform for AMSH3 to deubiquitinate ubiquitinated MVB cargos at the ESCRT-III positive endosomes. Alternatively, AMSH3 may deubiquitinate proteins of the endocytosis machinery itself that are localized in the proximity to ESCRT-III.

Interestingly, the previously reported SKD1(EQ) overexpression phenotype (Shahriari et al., 2010) and the *amsh3* mutant (Isono et al., 2010) phenotype have several features in common. First, both have defects in soluble cargo transport to the vacuole, and second, both have defects in vacuole biogenesis or maintenance. These resemblances indicate that the loss of AMSH3 or AMSH3 activity may have the same impact on cellular events as the dominant-negative SKD1. In line with this notion, our results showed that VPS2.1 and VPS24.1 mislocalize upon overexpression of the enzymatically inactive AMSH3(AXA).

In contrast with the wild-type AMSH fusion protein, YFP-AMSH3 (AXA) localized on intracellular compartments. The inhibition of AMSH3 activity may therefore prevent the dissociation of AMSH3 from ESCRT-III or the ESCRT-III–containing endosomes, where its substrates reside. The inhibition of AMSH3 DUB activity is predicted to prevent its disassociation from the ubiquitinated substrates (Isono et al., 2010). This, in turn, may mask the SKD1 interaction sites on ESCRT-III and causes incomplete or inefficient disassembly of the complex. Alternatively, the disassociation of AMSH3 from ESCRT-III after the completion of deubiquitination may be required for the efficient binding of the ESCRT-III–associated proteins, such as VPS46/CHMP1/Did2p, which was shown to be involved in SKD1 recruitment (Nickerson et al., 2006). Future studies should seek to identify the major substrates of AMSH3 and determine how AMSH3 deubiquitination contributes to the ESCRT-mediated MVB pathway.

METHODS

Biological Material

All experiments were performed with *Arabidopsis thaliana* (Columbia-0 [Col-0] background). The T-DNA insertion line of *VPS2.1* was obtained from the GABI-Kat collection (GABI_670D06) (Rosso et al., 2003). The T-DNA insertion mutant of *VPS2.2* (SALK_059274) and *VPS2.3* (SALK_127119) was obtained from the Nottingham Arabidopsis Stock Centre. Genotyping-PCR, RT-PCR, and analysis of the mutants are described in Supplemental Methods online.

Plant transformations were performed using the floral dip method (Clough and Bent, 1998). Seedlings were grown in continuous light on standard Murashige and Skoog growth medium (Duchefa Biochemie) supplemented with 1% Suc, and adult plants were grown in soil.

Cloning Procedures

All of the primers used for cloning are listed in Supplemental Table 3 online.

For the Y2H constructs, the ORFs of VPS2.1, VPS2.3, and VPS24.1 were PCR amplified, and the resulting fragments were cloned into the *Nde*I and *Sma*I (VPS2.1), *Nde*I and *Eco*RI (VPS2.3), and the *Nde*I and *Bam*HI (VPS24.1) sites of pGBKT7 vector (Clontech). The amplified ORFs of VPS2.2, VPS20.1, VPS46.1, VPS46.2, VPS60.1, and SNF7.1 were cloned into the *Eco*RI and *Bam*HI sites of pGBKT7 vector. To yield AD-AMSH3, GAD-AMSH3(AXA) and GBD-AMSH3(AXA), the wild-type and mutant AMSH3 were amplified with primers AK0 and EI14 using G67772 clone (ABRC) and GST:AMSH3(AXA) (Isono et al., 2010) as template, respectively, and cloned into the *Bam*HI-*Sal*I sites of pGADT7 (Clontech) and pGBKT7 vector, respectively. The truncated constructs of AMSH3, GAD-AMSH3-ΔMPN, -MIT, -N102, and -N154 were constructed with fragments amplified with AK0 and At AMSH3 rv, AK70 and AK51, AK0 and AK51, and AK0 and AK97, respectively, and ligated into the *Bam*HI-*Sal*I sites of the pGADT7 vector. The AMSH3-ΔMIT was amplified with AK88 and EI14 and cloned into the *Xho*I site of pGADT7.

GST-AMSH3 was described previously (Isono et al., 2010). For GST-VPS2.1, GST-2.3, GST-24.1, and GST-60.1, the corresponding ORFs were PCR amplified using primers AK1 and AK2, AK3 and AK4, AK66 and AK67, and AK68 and AK69, respectively, and the resulting fragments were cloned between the *Xho*I and *Sal*I sites (VPS2.1), *Eco*RI and *Sal*I sites (VPS2.3), and the *Bam*HI and *Sal*I sites (VPS24.1 and VPS60.1) of pGEX-6P-1 (GE Healthcare). GST-VPS2.2 was obtained by subcloning the *VPS2.2* gene from the Y2H construct into the pGEX-6P-1 vector between the *Eco*RI and *Sal*I sites. For GST-VPS2.1(mut) and GST-VPS2.3 (mut) constructs, the mutations were introduced with primers AK44 and AK45 and AK47 and AK48, respectively, using *Dpn*I-based site-directed mutagenesis (Stratagene).

UBQ10pro:YFP-VPS2.1, UBQ10pro:YFP-VPS2.2, and UBQ10pro: mCherry-VPS2.1 were generated with Cre/Lox recombination (NEB) using pUNI-VPS2.1 and pUNI-VPS2.2 for the recombination with pNIGEL7 and pNIGEL17 (Geldner et al., 2009) for YFP and mCherry fusion, respectively. To yield pUNI-VPS2.1 and pUNI-VPS2.2, the ORFs were PCR amplified using primers AK21 and AK22 and AK77 and AK78, respectively, and cloned between the *Sfi*I and *Not*I (VPS2.1) and *Eco*RI and *Sal*I (VPS2.3) sites of the pUNI51 vector (ABRC). 35Spro:VPS24.1-GFP was generated in 35S-GW-GFP (J. Parker, Cologne, Germany) by Gateway cloning (Invitrogen) with fragments amplified with AK90 and AK92 and Gateway adaptor primers. For the 35Spro:YFP-VPS2.3 construct, the *VPS2.3* coding sequence was transferred by recombination from the G13604 (ABRC) clone to the pExtag-YFP-GW (J. Parker). To generate a VPS2.1pro:YFP-VPS2.1 construct, a *VPS2.1* genomic fragments including 195 bp of the teminator region was amplified with AK32 and AK33 as well as Gateway adaptor primers and cloned by Gateway technology into pExtag-YFP-GW (J. Parker). YFP-VPS2.1 was then cut out and subcloned into the *Xho*I-*Not*I site of pGreen0229. A 1940-bp promoter region of *VPS2.1* was amplified with AK38 and AK41 and first cloned into pCR 2.1-TOPO TA (Invitrogen) to be subcloned into the *Kpn*I-*Xho*I site of pGreen0229 to obtain VPS2.1pro:YFP-VPS2.1. To generate RPS5apro: VPS2.1, the ORF of *VPS2.1* was amplified with primers AK1 and AK2

and cloned into the XhoI site of pGreenII BAR RPS5a-tNOS (D. Weijers, Wageningen, The Netherlands).

For the SKD1 constructs, the ORF of *SKD1* was amplified using primers EI189 and EI190 as well as Gateway adaptor primers and first cloned into the Gateway entry vector pDONR207 (Invitrogen). The EQ mutation was introduced using primers EI193 and EI194, and the wild type and EQ mutant ORFs were cloned into pJaWohl 2B HA (J. Parker) and pDEST17 (Invitrogen) to yield 35Spro:HA-SKD1 and His-SKD1, respectively. 35Spro:HA-AMSH3(AXA) (pJaWohl 2B HA) and 35Spro:YFP-AMSH3 (AXA) (pExTag YFP) were created using a previously described Gateway entry clone (Isono et al., 2010). UBQ10pro:mCherry-AMSH3 was created by Cre recombinase-based cloning into the pNIGEL17 vector (Geldner et al., 2009). For AMSH3pro:YFP-AMSH3, the *AMSH3* promoter and coding region were amplified using primers EI180 and EI181 and EI182 and EI141, respectively, and YFP was inserted between the promoter and the coding region.

Y2H Assays

A Y2H screen was performed as described previously (Schwechheimer and Deng, 2002). An *Arabidopsis* full-length cDNA library (Kim et al., 1997) was transformed into the yeast strain Y190 containing the pGBKT7-AMSH3(AXA) plasmid. Approximately 2×10^6 transformants were screened on synthetic complete (SC) medium lacking Leu (L), Trp (W), and His (H) and supplemented with 10 mM 3-amino-1,2,4-triazole. The prey plasmids were extracted, transformed into the XL1Blue *Escherichia coli* strain, and retransformed together with pGBKT7 or pGBKT7-AMSH3(AXA) into Y190 yeast cells for testing the growth and β-galactosidase activity. The positive candidates were sequenced with the GAL4-AD and ACT-rv primers.

pGBKT7 plasmids containing the ESCRT-III subunits VPS2.1, VPS2.2, VPS2.3, VPS20.1, VPS24.1, VPS46.1, VPS46.2, VPS60.1, and SNF7.1 were cotransformed with pGADT7-AMSH3 or pGADT7-AMSH3(AXA) plasmids into the yeast strain Y190. In addition, the truncated versions of AMSH3, GAD-AMSH3-ΔMIT, -ΔMPN, -MIT, -N102, and -N154 were cotransformed with pGBKT7, -VPS2.1, and -VPS24.1. Transformants were selected after 3 d on SC medium lacking Leu and Trp (-LW) at 30°C. To examine Y2H interactions, the transformants were grown in liquid culture to the late log phase, diluted to $A_{600} = 1$, and 10-fold serial dilutions were grown on solid SC medium lacking Leu and Trp (SC-LW) or Leu, Trp, and His (-LWH) with 5 mM 3-amino-1,2,4-triazole for 2 d at 30°C.

Protein Extraction, Immunoblotting, and Antibodies

Yeast total proteins were extracted as described previously (Kushnirov, 2000). SDS-PAGE, Coomassie Brilliant Blue staining, and immunoblotting were performed according to the standard protocol. Antibodies used for immunoblotting were anti-AMSH3 (Isono et al., 2010), anti-GST (GE Healthcare), anti-GAL4BD (Santa-Cruz), anti-CDC2(PSTAIRE) (Santa-Cruz), horseradish peroxidase–conjugated anti-HA (Sigma-Aldrich), and anti-His (Sigma-Aldrich).

Protein Purification, in Vitro Binding Assays, and DUB Assays

GST and GST-VPS2.1, GST-VPS2.2, GST-VPS2.3, and His-SKD1 were expressed in the *E. coli* Rosetta (DE3) strain (Merck Chemicals) and purified with Glutathione-Sepharose 4B beads (GE Healthcare). Proteins were eluted with 0.2 M reduced glutathione. His-SKD1 was purified using Ni Sepharose High Performance beads (GE Healthcare) and eluted with 250 mM imidazole. Eluted proteins were dialyzed against buffer A (50 mM Tris-HCl, 100 mM NaCl, and 10% glycerol, pH 7.5). The purification of AMSH3 has been previously described (Isono et al., 2010). Protein concentration was determined after SDS-PAGE and Coomassie Brilliant Blue staining using the Benchmark Protein Ladder (Invitrogen) as a

standard and a LAS-4000 mini (FUJI Film) and the Multi Gauge (FUJI Film) software.

For the in vitro binding assay, Glutathione-Sepharose 4B beads (GE Healthcare) were saturated with GST or GST fusion proteins. Glutathione-Sepharose 4B beads with 1.5 μg of bound GST, GST-VPS2.1, GST-VPS2.2, or GST-VPS2.3 were then incubated with 6 pmol AMSH3 in 100 μL cold buffer A containing 0.2% Triton X-100 for 30 min at 4°C. The beads were then washed three times with cold buffer A containing 0.3% Triton X-100 and 1 mM dithiothreitol and three times more with cold buffer A. Bead-bound proteins were analyzed by immunoblotting. For the competition of SKD1 and AMSH3, the in vitro binding assay was performed with the addition of 6, 72, or 216 pmol of His-SKD1 to each reaction. DUB assays were performed as described previously (Isono et al., 2010), with 250 μg K48-linked UB chains (Biomol) and 1 pmol of AMSH3 preincubated with 2 pmol of GST, GST-VPS2.1, or GST-VPS24.1.

Protoplast Transformation

Protoplasts were isolated from *Arabidopsis* suspension-cultured cells (Col-0) 3 to 4 d after subculturing by incubation of 2 g of cell culture with 1% Cellulase R-10 (Yakult Pharmaceutical) and 0.25% Macerozyme R-10 (Yakult Pharmaceutical). Typically, 20 μg of plasmid DNA was transformed by polyethylene glycol–mediated transformation to the protoplasts and analyzed after 16 to 20 h of incubation.

Microscopy and FRET Measurements

GFP-, YFP-, and mCherry-fused proteins were analyzed with an FV-1000/IX81 confocal laser scanning microscope (Olympus) using a UPlanSApo ×60/1.20 (Olympus) objective. GFP, YFP, and mCherry were excited using the 488-, 515-, and 559-nm laser line, respectively. Images were obtained using the Fluoview software (Olympus) and processed using Photoshop CS3 (Adobe). FRET efficiency measurement between YFP-AMSH3 and mCherry-VPS2.1 was performed by the sensitized emission method and analyzed using the Fluoview software (Olympus). Acceptor spectral bleed-through and donor spectral bleed-through were determined by capturing images of cells expressing only YFP-AMSH3 or mCherry-VPS2.1. Average FRET efficiency was calculated for 86 regions (compartments) and 57 regions (cytosol) in a total of 16 cells.

Accession Numbers

Sequence data from this article can be found in the Arabidopsis Genome Initiative database under the following accession numbers: AMSH3 (AT4G16144), CDC2 (AT3G48750), SKD1 (AT2G27600), SNF7.1 (AT4G29160), VPS2.1 (AT2G06530), VPS2.2 (AT5G44560), VPS2.3 (AT1G03950), VPS20.1 (AT5G63880) VPS24.1 (AT5G22950), VPS24.2 (AT3G45000), VPS46.2 (AT1G73030), VPS60.1 (AT3G10640), ScVPS2p (P36108-1), DmVPS2 (Q8SXB1-1), MmVPS2 (Q9DB34-1), CHMP2A (O43633-1), CHMP2B (Q9UQN3-1), HsVPS4A (Q9UN37), HsVPS4B (O75351), MmVPS4A (Q8VEJ9), MmVPS4B (P46467), DmVPS4 (Q9Y162), ScVPS4p (P52917), and AtSKD1(At2g27600).

Supplemental Data

The following materials are available in the online version of this article.

Supplemental Figure 1. Verification of Y2H Construct Expression.

Supplemental Figure 2. Alignment of VPS2.1, VPS2.2, and VPS2.3 with Their Counterparts from Human, Mouse, Fruit Fly, and Yeast.

Supplemental Figure 3. Alignment of VPS24.1 and VPS24.2 with Their Counterparts from Human, Mouse, Fruit Fly, and Yeast.

ACKNOWLEDGMENTS

AUTHOR CONTRIBUTIONS

A.K., M.-T.H., C.S., and E.I designed and analyzed the experiments. A.K., F.A., N.S., S.N., and E.I. performed the experiments. A.K. and E.I. wrote the article.

REFERENCES

Agromayor, M., and Martin-Serrano, J. (2006). Interaction of AMSH with ESCRT-III and deubiquitination of endosomal cargo. J. Biol. Chem. **281:** 23083–23091.

Babst, M., Katzmann, D.J., Estepa-Sabal, E.J., Meerloo, T., and Emr, S.D. (2002). Escrt-III: An endosome-associated heterooligomeric protein complex required for mvb sorting. Dev. Cell **3:** 271–282.

Babst, M., Sato, T.K., Banta, L.M., and Emr, S.D. (1997). Endosomal transport function in yeast requires a novel AAA-type ATPase, Vps4p. EMBO J. **16:** 1820–1831.

Babst, M., Wendland, B., Estepa, E.J., and Emr, S.D. (1998). The Vps4p AAA ATPase regulates membrane association of a Vps protein complex required for normal endosome function. EMBO J. **17:** 2982–2993.

Clague, M.J., and Urbé, S. (2006). Endocytosis: The DUB version. Trends Cell Biol. **16:** 551–559.

Clough, S.J., and Bent, A.F. (1998). Floral dip: A simplified method for Agrobacterium-mediated transformation of *Arabidopsis thaliana*. Plant J. **16:** 735–743.

Doelling, J.H., Phillips, A.R., Soyler-Ogretim, G., Wise, J., Chandler, J., Callis, J., Otegui, M.S., and Vierstra, R.D. (2007). The ubiquitin-specific protease subfamily UBP3/UBP4 is essential for pollen development and transmission in Arabidopsis. Plant Physiol. **145:** 801–813.

Doelling, J.H., Yan, N., Kurepa, J., Walker, J., and Vierstra, R.D. (2001). The ubiquitin-specific protease UBP14 is essential for early embryo development in *Arabidopsis thaliana*. Plant J. **27:** 393–405.

Geldner, N., Dénervaud-Tendon, V., Hyman, D.L., Mayer, U., Stierhof, Y.-D., and Chory, J. (2009). Rapid, combinatorial analysis of membrane compartments in intact plants with a multicolor marker set. Plant J. **59:** 169–178.

Ghazi-Tabatabai, S., Saksena, S., Short, J.M., Pobbati, A.V., Veprintsev, D.B., Crowther, R.A., Emr, S.D., Egelman, E.H., and Williams, R.L. (2008). Structure and disassembly of filaments formed by the ESCRT-III subunit Vps24. Structure **16:** 1345–1356.

Haas, T.J., Sliwinski, M.K., Martínez, D.E., Preuss, M., Ebine, K., Ueda, T., Nielsen, E., Odorizzi, G., and Otegui, M.S. (2007). The *Arabidopsis* AAA ATPase SKD1 is involved in multivesicular endosome function and interacts with its positive regulator LYST-INTERACTING PROTEIN5. Plant Cell **19:** 1295–1312.

Hurley, J.H., and Hanson, P.I. (2010). Membrane budding and scission by the ESCRT machinery: It's all in the neck. Nat. Rev. Mol. Cell Biol. **11:** 556–566.

Isono, E., Katsiarimpa, A., Müller, I.K., Anzenberger, F., Stierhof, Y. D., Geldner, N., Chory, J., and Schwechheimer, C. (2010). The deubiquitinating enzyme AMSH3 is required for intracellular trafficking and vacuole biogenesis in *Arabidopsis thaliana*. Plant Cell **22:** 1826–1837.

Kieffer, C., Skalicky, J.J., Morita, E., De Domenico, I., Ward, D.M., Kaplan, J., and Sundquist, W.I. (2008). Two distinct modes of ESCRT-III recognition are required for VPS4 functions in lysosomal protein targeting and HIV-1 budding. Dev. Cell **15:** 62–73.

Kim, J., Harter, K., and Theologis, A. (1997). Protein-protein interactions among the Aux/IAA proteins. Proc. Natl. Acad. Sci. USA **94:** 11786–11791.

Kim, M.S., Kim, J.A., Song, H.K., and Jeon, H. (2006). STAM-AMSH interaction facilitates the deubiquitination activity in the C-terminal AMSH. Biochem. Biophys. Res. Commun. **351:** 612–618.

Komander, D., Clague, M.J., and Urbé, S. (2009). Breaking the chains: Structure and function of the deubiquitinases. Nat. Rev. Mol. Cell Biol. **10:** 550–563.

Kushnirov, V.V. (2000). Rapid and reliable protein extraction from yeast. Yeast **16:** 857–860.

Kyuuma, M., Kikuchi, K., Kojima, K., Sugawara, Y., Sato, M., Mano, N., Goto, J., Takeshita, T., Yamamoto, A., Sugamura, K., and Tanaka, N. (2007). AMSH, an ESCRT-III associated enzyme, deubiquitinates cargo on MVB/late endosomes. Cell Struct. Funct. **31:** 159–172.

Lata, S., Schoehn, G., Jain, A., Pires, R., Piehler, J., Gottlinger, H.G., and Weissenhorn, W. (2008). Helical structures of ESCRT-III are disassembled by VPS4. Science **321:** 1354–1357.

Liu, Y., Wang, F., Zhang, H., He, H., Ma, L., and Deng, X.W. (2008). Functional characterization of the Arabidopsis ubiquitin-specific protease gene family reveals specific role and redundancy of individual members in development. Plant J. **55:** 844–856.

Luo, M., Luo, M.Z., Buzas, D., Finnegan, J., Helliwell, C., Dennis, E.S., Peacock, W.J., and Chaudhury, A. (2008). UBIQUITIN-SPECIFIC PROTEASE 26 is required for seed development and the repression of PHERES1 in Arabidopsis. Genetics **180:** 229–236.

Ma, Y.M., Boucrot, E., Villén, J., Affar, B., Gygi, S.P., Göttlinger, H.G., and Kirchhausen, T. (2007). Targeting of AMSH to endosomes is required for epidermal growth factor receptor degradation. J. Biol. Chem. **282:** 9805–9812.

Maytal-Kivity, V., Reis, N., Hofmann, K., and Glickman, M.H. (2002). MPN+, a putative catalytic motif found in a subset of MPN domain proteins from eukaryotes and prokaryotes, is critical for Rpn11 function. BMC Biochem. **3:** 28.

McCullough, J., Clague, M.J., and Urbé, S. (2004). AMSH is an endosome-associated ubiquitin isopeptidase. J. Cell Biol. **166:** 487–492.

McCullough, J., Row, P.E., Lorenzo, O., Doherty, M., Beynon, R., Clague, M.J., and Urbé, S. (2006). Activation of the endosome-associated ubiquitin isopeptidase AMSH by STAM, a component of the multivesicular body-sorting machinery. Curr. Biol. **16:** 160–165.

Nakamura, M., Tanaka, N., Kitamura, N., and Komada, M. (2006). Clathrin anchors deubiquitinating enzymes, AMSH and AMSH-like protein, on early endosomes. Genes Cells **11:** 593–606.

Nickerson, D.P., West, M., and Odorizzi, G. (2006). Did2 coordinates Vps4-mediated dissociation of ESCRT-III from endosomes. J. Cell Biol. **175:** 715–720.

Obita, T., Saksena, S., Ghazi-Tabatabai, S., Gill, D.J., Perisic, O., Emr, S.D., and Williams, R.L. (2007). Structural basis for selective recognition of ESCRT-III by the AAA ATPase Vps4. Nature **449:** 735–739.

Raiborg, C., and Stenmark, H. (2009). The ESCRT machinery in endosomal sorting of ubiquitylated membrane proteins. Nature **458:** 445–452.

Reyes-Turcu, F.E., Ventii, K.H., and Wilkinson, K.D. (2009). Regulation and cellular roles of ubiquitin-specific deubiquitinating enzymes. Annu. Rev. Biochem. **78:** 363–397.

Rosso, M.G., Li, Y., Strizhov, N., Reiss, B., Dekker, K., and Weisshaar, B. (2003). An Arabidopsis thaliana T-DNA mutagenized population (GABI-Kat) for flanking sequence tag-based reverse genetics. Plant Mol. Biol. **53:** 247–259.

Saksena, S., Wahlman, J., Teis, D., Johnson, A.E., and Emr, S.D. (2009). Functional reconstitution of ESCRT-III assembly and disassembly. Cell **136:** 97–109.

Schellmann, S., and Pimpl, P. (2009). Coats of endosomal protein sorting: Retromer and ESCRT. Curr. Opin. Plant Biol. **12:** 670–676.

Schmitz, R.J., Tamada, Y., Doyle, M.R., Zhang, X., and Amasino, R.M. (2009). Histone H2B deubiquitination is required for transcriptional activation of FLOWERING LOCUS C and for proper control of flowering in Arabidopsis. Plant Physiol. **149:** 1196–1204.

Schwechheimer, C., and Deng, X.W. (2002). Studying protein-protein interactions with the yeast two-hybid system. In Molecular Plant Biology: A Practical Approach, P.M. Gilmartin and C. Bowler, eds (Oxford, UK: Oxford University Press.), pp. 173–198.

Shahriari, M., Keshavaiah, C., Scheuring, D., Sabovljevic, A., Pimpl, P., Häusler, R.E., Hülskamp, M., and Schellmann, S. (2010). The AAA-type ATPase AtSKD1 contributes to vacuolar maintenance of Arabidopsis thaliana. Plant J. **64:** 71–85.

Shahriari, M., Richter, K., Keshavaiah, C., Sabovljevic, A., Huelskamp, M., and Schellmann, S. (2011). The Arabidopsis ESCRT protein-protein interaction network. Plant Mol. Biol. **76:** 85–96.

Shim, S., Kimpler, L.A., and Hanson, P.I. (2007). Structure/function analysis of four core ESCRT-III proteins reveals common regulatory role for extreme C-terminal domain. Traffic **8:** 1068–1079.

Spitzer, C., Reyes, F.C., Buono, R., Sliwinski, M.K., Haas, T.J., and Otegui, M.S. (2009). The ESCRT-related CHMP1A and B proteins mediate multivesicular body sorting of auxin carriers in Arabidopsis and are required for plant development. Plant Cell **21:** 749–766.

Spitzer, C., Schellmann, S., Sabovljevic, A., Shahriari, M., Keshavaiah, C., Bechtold, N., Herzog, M., Müller, S., Hanisch, F.G., and Hülskamp, M. (2006). The Arabidopsis elch mutant reveals functions of an ESCRT component in cytokinesis. Development **133:** 4679–4689.

Sridhar, V.V., Kapoor, A., Zhang, K., Zhu, J., Zhou, T., Hasegawa, P.M., Bressan, R.A., and Zhu, J.K. (2007). Control of DNA methylation and heterochromatic silencing by histone H2B deubiquitination. Nature **447:** 735–738.

Stuchell-Brereton, M.D., Skalicky, J.J., Kieffer, C., Karren, M.A., Ghaffarian, S., and Sundquist, W.I. (2007). ESCRT-III recognition by VPS4 ATPases. Nature **449:** 740–744.

Tanaka, N., Kaneko, K., Asao, H., Kasai, H., Endo, Y., Fujita, T., Takeshita, T., and Sugamura, K. (1999). Possible involvement of a novel STAM-associated molecule "AMSH" in intracellular signal transduction mediated by cytokines. J. Biol. Chem. **274:** 19129–19135.

Teis, D., Saksena, S., and Emr, S.D. (2008). Ordered assembly of the ESCRT-III complex on endosomes is required to sequester cargo during MVB formation. Dev. Cell **15:** 578–589.

Tsang, H.T., Connell, J.W., Brown, S.E., Thompson, A., Reid, E., and Sanderson, C.M. (2006). A systematic analysis of human CHMP protein interactions: Additional MIT domain-containing proteins bind to multiple components of the human ESCRT III complex. Genomics **88:** 333–346.

Williams, R.L., and Urbé, S. (2007). The emerging shape of the ESCRT machinery. Nat. Rev. Mol. Cell Biol. **8:** 355–368.

Winter, V., and Hauser, M.T. (2006). Exploring the ESCRTing machinery in eukaryotes. Trends Plant Sci. **11:** 115–123.

Yan, N., Doelling, J.H., Falbel, T.G., Durski, A.M., and Vierstra, R.D. (2000). The ubiquitin-specific protease family from Arabidopsis. AtUBP1 and 2 are required for the resistance to the amino acid analog canavanine. Plant Physiol. **124:** 1828–1843.

The Deubiquitinating Enzyme AMSH1 and the ESCRT-III Subunit VPS2.1 Are Required for Autophagic Degradation in *Arabidopsis*[C][W][OPEN]

Anthi Katsiarimpa,[a,1] Kamila Kalinowska,[a,1] Franziska Anzenberger,[a] Corina Weis,[b] Maya Ostertag,[b] Chie Tsutsumi,[c] Claus Schwechheimer,[a] Frédéric Brunner,[d] Ralph Hückelhoven,[b] and Erika Isono[a,2]

[a] Department of Plant Systems Biology, Technische Universität München, 85354 Freising, Germany
[b] Department of Phytopathology, Technische Universität München, 85354 Freising, Germany
[c] Department of Botany, National Museum of Nature and Science, Tsukuba 305-0005, Japan
[d] Department of Plant Biochemistry, Center for Plant Molecular Biology, Tübingen University, 72076 Tuebingen, Germany

In eukaryotes, posttranslational modification by ubiquitin regulates the activity and stability of many proteins and thus influences a variety of developmental processes as well as environmental responses. Ubiquitination also plays a critical role in intracellular trafficking by serving as a signal for endocytosis. We have previously shown that the *Arabidopsis thaliana* ASSOCIATED MOLECULE WITH THE SH3 DOMAIN OF STAM3 (AMSH3) is a deubiquitinating enzyme (DUB) that interacts with ENDOSOMAL COMPLEX REQUIRED FOR TRANSPORT-III (ESCRT-III) and is essential for intracellular transport and vacuole biogenesis. However, physiological functions of AMSH3 in the context of its ESCRT-III interaction are not well understood due to the severe seedling lethal phenotype of its null mutant. In this article, we show that *Arabidopsis* AMSH1, an AMSH3-related DUB, interacts with the ESCRT-III subunit VACUOLAR PROTEIN SORTING2.1 (VPS2.1) and that impairment of both AMSH1 and VPS2.1 causes early senescence and hypersensitivity to artificial carbon starvation in the dark similar to previously reported autophagy mutants. Consistent with this, both mutants accumulate autophagosome markers and accumulate less autophagic bodies in the vacuole. Taken together, our results demonstrate that AMSH1 and the ESCRT-III-subunit VPS2.1 are important for autophagic degradation and autophagy-mediated physiological processes.

INTRODUCTION

Reversible posttranslational modification by the small modifier protein ubiquitin is a critical step for regulating protein activities and abundance in many plant signaling pathways and cellular processes (reviewed in Vierstra, 2009). Thus, ubiquitinating as well as deubiquitinating enzymes (DUBs) play key roles in diverse cellular functions. Whereas soluble proteins can be degraded by the 26S proteasome upon polyubiquitination, plasma membrane–bound proteins are degraded by vacuolar proteases following ubiquitin-dependent endocytosis (reviewed in Zelazny et al., 2011). In plants, the auxin efflux facilitator PIN-FORMED2 (PIN2), the flagellin receptor FLAGELLIN-SENSITIVE2, the water channel PLASMA MEMBRANE INTRINSIC PROTEIN2, the iron transporter IRON-REGULATED TRANSPORTER1, and the boron transporter REQUIRES HIGH BORON1 have been shown to be ubiquitinated prior to endocytosis (Abas et al., 2006; Göhre et al., 2008; Lee et al., 2009; Barberon et al., 2011; Kasai et al.,

2011). Furthermore, translational fusion of monoubiquitin to PLASMA MEMBRANE PROTON ATPASE (PMA) was shown to be sufficient for triggering endocytosis and vacuolar transport via multivesicular bodies (MVBs) (Herberth et al., 2012). However, how exactly ubiquitin-dependent endocytosis is regulated at the molecular level in plants and contributes to different physiological processes remains to be elucidated.

We have recently shown that the *Arabidopsis thaliana* DUB, ASSOCIATED MOLECULE WITH THE SH3 DOMAIN OF STAM3 (AMSH3), interacts with the endocytosis machinery and is essential for plant development (Isono et al., 2010; Katsiarimpa et al., 2011). AMSH3 is closely related to the human DUBs AMSH and AMSH-LP, which belong to the class of eukaryotic DUBs and metalloproteases with an MPR1, PAD1 N-terminal+ (MPN+) domain (Tanaka et al., 1999; Maytal-Kivity et al., 2002; Komander et al., 2009). Two MPN+ domain proteins, namely, REGULATORY PARTICLE NON-ATPASE11 (RPN11) (Glickman et al., 1998; Verma et al., 2002) and COP9 SIGNALOSOME5 (CSN5) (Chamovitz et al., 1996; Cope et al., 2002), are subunits of stable multiprotein complexes. By contrast, *Arabidopsis* AMSH3 is not part of a stable higher molecular weight complex (Isono et al., 2010), and, in contrast with RPN11 and CSN5, AMSH proteins are active as monomers (McCullough et al., 2004). AMSH proteins have essential functions in the development of animals and plants, since AMSH-deficient mice die postnatum with loss of neurons in the hippocampus (Ishii et al., 2001), and *Arabidopsis amsh3* null mutations are seedling lethal and cause a number of intracellular trafficking defects (Isono et al., 2010).

[C] Some figures in this article are displayed in color online but in black and white in the print edition.
[W] Online version contains Web-only data.
[OPEN] Articles can be viewed online without a subscription.
www.plantcell.org/cgi/doi/10.1105/tpc.113.113399

Autophagy (macroautophagy) is another vacuolar degradation pathway, by which cytosolic components or organelles are selectively or nonselectively transported to the vacuole/lysosome for degradation (reviewed in Klionsky and Ohsumi, 1999). Since the discovery of *AUTOPHAGY-RELATED* (*ATG*) genes from yeast in the 1990s, intensive genetic and molecular analyses have identified over 30 autophagy-related genes. Autophagy is also implicated in a diverse array of physiological and pathological effects in mammals (reviewed in Mizushima and Levine, 2010). *ATG* genes are highly conserved also in plants, and mutant analyses have shown them to have central functions in nutrient remobilization during starvation and senescence (Doelling et al., 2002; Yoshimoto et al., 2004, 2009; Sláviková et al., 2005; Thompson et al., 2005; Inoue et al., 2006; Phillips et al., 2008; Chung et al., 2009).

The individual steps of autophagosome formation have been revealed by ultrastructural and biochemical studies (reviewed in Klionsky and Ohsumi, 1999). First, isolation membranes or phagophores are formed, probably from the endoplasmic reticulum, which will then engulf parts of the cytosol in autophagosomes with characteristic double-membrane structures. Autophagosomes are then targeted to vacuoles or lysosomes in which their contents are degraded by resident proteases. Alternatively, depending on organism and cell type, autophagosomes may undergo fusion with late endosomes or MVBs to form amphisomes. Amphisomes can then fuse to vacuoles/lysosomes to become autolysosomes, in which the autophagosomal contents are degraded. In mammals and flies, several studies have reported that intact MVBs as well as a functional ENDOSOMAL COMPLEX REQUIRED FOR TRANSPORT-III (ESCRT-III), a core complex in MVB sorting, are necessary for proper autophagosomal degradation (Filimonenko et al., 2007; Lee et al., 2007; Rusten et al., 2007; Han et al., 2012). However, a role for ESCRT-III in the plant autophagy pathway has not been demonstrated yet.

We have previously shown that *Arabidopsis* AMSH3 interacts with the ESCRT-III subunits VACUOLAR PROTEIN SORTING2.1 (VPS2.1) and VPS24.1 (Katsiarimpa et al., 2011). The embryo- and seedling-lethal phenotypes of *vps2.1* and *amsh3* mutations, respectively, have prevented us so far from analyzing the physiological functions of VPS2.1 and AMSH3. In this study, we characterize the *Arabidopsis amsh1-1* mutant, which has reduced levels of the *AMSH3*-related gene, *AMSH1*.

Unlike the *amsh3* null mutants, the *amsh1-1* knockdown mutant does not have an apparent growth defect. However, *amsh1-1* accumulates ubiquitinated proteins and shows chlorosis when transferred to the dark, a phenotype reminiscent of autophagy mutants. Furthermore, *amsh1-1* accumulates ATG8 in the dark and accumulates less autophagic bodies in the vacuole. AMSH1, like AMSH3, directly interacts with the ESCRT-III subunit VPS2.1. Plants that overexpress a dominant-negative form of *VPS2.1* are deficient in endocytosis, accumulate ATG8, and show hypersensitivity to dark treatment. Similar to previously identified autophagy-defective *atg* mutants from *Arabidopsis*, *amsh1-1* shows also altered susceptibility toward pathogen infection. Together, the results presented here demonstrate the importance of AMSH1 and VPS2.1 in autophagic degradation and in the physiological processes related to it.

RESULTS

Arabidopsis AMSH Genes Are Evolutionary Conserved and Belong to Independent Clades within the *AMSH* Gene Family

AMSH proteins are widely conserved in eukaryotes. In the *Arabidopsis* genome, three *AMSH* genes can be found according to sequence similarity in the catalytic domain (Maytal-Kivity et al., 2002; Isono et al., 2010). To understand the evolutionary origin of the three *Arabidopsis AMSH* genes, we identified sequences related to *Arabidopsis AMSHs* in the genomes of 10 fully sequenced plant species (*Physcomitrella patens*, *Selaginella moellendorffii*, maize [*Zea mays*], sorghum [*Sorghum bicolor*], rice [*Oryza sativa*], *Populus trichocarpa*, castor bean [*Ricinus communis*], soybean [*Glycine max*], grape [*Vitis vinifera*], and *Arabidopsis lyrata*). Phylogenic analysis based on nucleotide sequences of the resulting 37 genes showed that each of the three *Arabidopsis AMSH* genes is part of an independent clade with other eudicot homologs, suggesting an evolutionary conservation of the three genes in eudicot species (Figure 1; see Supplemental Data Set 1 online).

The monophyly of *AMSH2* with high support allowed us to infer that the hitherto uncharacterized *AMSH2* genes have been conserved at least from ancestral angiosperms. By contrast, *AMSH1* and *AMSH3* may have originated from a eudicot-specific gene duplication event after the separation from monocots. Alternatively, *AMSH1* and *AMSH3* may have already been present before the separation of monocots and eudicots, and monocots may have lost their copy of the *AMSH1* gene and gone through an independent gene duplication event in the course of evolution.

AMSH1 and *AMSH3* Show Synergistic Interaction

We next wanted to establish whether the three *Arabidopsis AMSH* genes have redundant functions. We previously identified two *amsh3* mutant null alleles (Isono et al., 2010) and now investigated additional T-DNA insertion lines of *AMSH1* and *AMSH2*. For *AMSH1*, we identified one T-DNA insertion line, which we named *amsh1-1*, with reduced *AMSH1* transcript level. *amsh1-1* carried an insertion in the 5′-untranslated region of the gene (Figure 2A), and the transcript level of *AMSH1* was reduced more than 10-fold compared with the wild type (see Supplemental Figure 1A online). AMSH1 protein levels were also strongly decreased in this mutant (Figure 2F). Since *AMSH1* transcripts were still detectable, and since immunoblotting with the anti-AMSH1 antibody showed a weak band in *amsh1-1*, it is likely that *amsh1-1* is not a complete loss-of-function mutant but rather a weak mutant allele with compromised AMSH1 function. By contrast, we found that the available T-DNA insertion line of *AMSH2* did not have significantly reduced *AMSH2* transcript levels (data not shown).

When grown in continuous light, homozygous *amsh1-1* plants did not show obvious developmental phenotypes (Figure 2B). However, when we introduced the *amsh3-2* allele into *amsh1-1*, the resulting *amsh1-1/amsh1-1 AMSH3/amsh3-2* mutant (*a1/a1 A3/a3*) showed severe growth defects and early senescence (Figures 2B to 2D), indicating a synergistic interaction between *AMSH1* and *AMSH3*.

AMSH1 is an active enzyme and its catalytic MPN+ domain possesses DUB activity toward K63-linked, but not K48-linked, ubiquitin chains. The activity of the AMSH1 MPN+ domain was
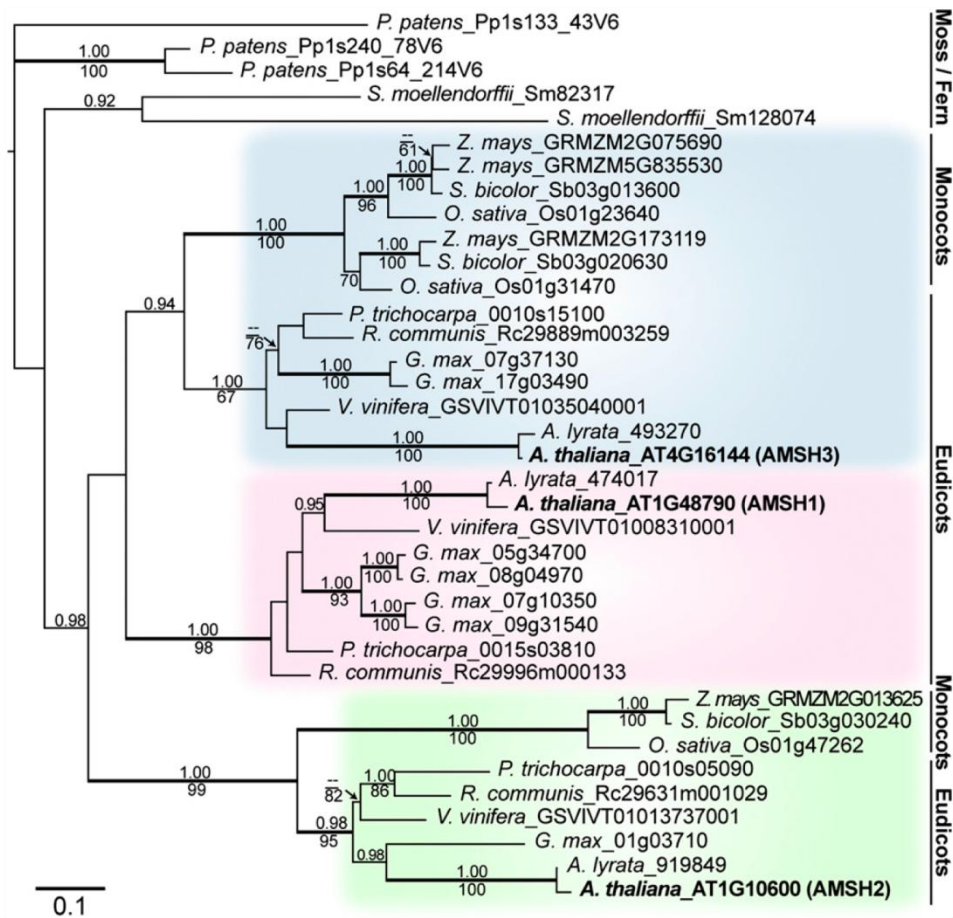
Figure 1. AMSH1, AMSH2, and AMSH3 Belong to Independent Clades.

Phylogenetic analysis of AMSH genes from *P. patens*, *S. moellendorffii*, maize, sorghum, rice, *P. trichocarpa*, castor bean, soybean, grape, *A. lyrata*, and *Arabidopsis* using P. patens_Pp133_43V6 as an outgroup. A maximum likelihood tree (-ln L = 9462.34) based on the region surrounding the MPN+ domain (549 bp) is shown. The alignment used for generating the phylogenic tree is available as Supplemental Data Set 1 online. Values above branches indicate posterior probabilities (>0.9) calculated by Bayesian analysis, and those below branches indicate maximum parsimony bootstrap values (>60). Thick branches are highly supported (posterior probabilities P > 0.95 and bootstrap values >90). Bar = 0.1 amino acid substitutions per site. [See online article for color version of this figure.]

inhibited by the metalloprotease inhibitor 1,10-phenanthroline (Figure 2E), indicating that like other MPN+ domain proteins, AMSH1 activity is also dependent on metal ions coordinated in the MPN+ domain. Molecular analysis showed that the *amsh1-1* homozygous mutants, in spite of their normal growth, accumulated ubiquitinated proteins at a higher level than the wild type, and *amsh1-1/amsh1-1 AMSH3/amsh3-2* accumulated ubiquitin conjugates at an even higher level (Figure 2F). Interestingly, *amsh1-1* did not show obvious decreases in its monoubiquitin levels (see Supplemental Figure 1B online), suggesting that the depletion of free ubiquitin molecules is probably not the cause of its phenotype, in contrast with the yeast DUB mutant *doa4* (Swaminathan et al., 1999).

AMSH1 and AMSH3 Have Distinct Expression Patterns

To test whether *AMSH1* and *AMSH3* are expressed in the same tissues, we generated promoter–β-glucuronidase (GUS) fusions for

both genes and analyzed the expression patterns. During seedling development, the expression of both *AMSH1* and *AMSH3* could be observed in leaves and hypocotyls as well as in roots, though their expression patterns overlapped only partially (Figures 3A to 3F). Furthermore, *AMSH3* was strongly expressed in emerging lateral roots, whereas *AMSH1* expression seemed to be excluded from this region (Figures 3G to 3L). The largely differential expression pattern of *AMSH1* and *AMSH3* implies that the two genes might be under different spatio-temporal regulation and that AMSH1 and AMSH3 functions are not interdependent.

amsh1-1 Shows Hypersensitivity to Dark Treatment

The senescence phenotype of *amsh1/amsh1 AMSH3/amsh3* caught our attention since we observed that *amsh1-1* also showed early senescence when grown under short-day conditions with 8 h light (110 to 120 μmol m^{-2} s^{-1} light) and 16 h
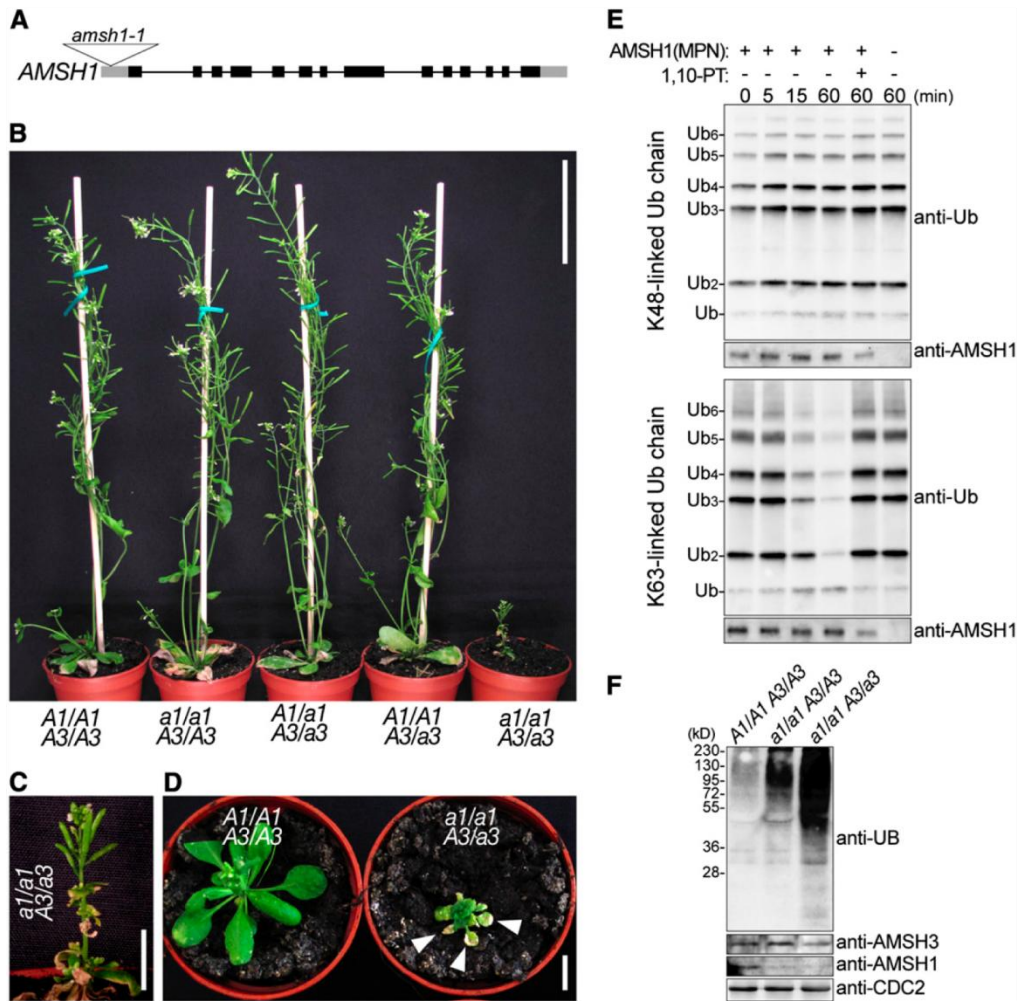
Figure 2. *amsh1/amsh1 AMSH3/amsh3* Is Dwarf and Accumulates Ubiquitinated Proteins.

(A) T-DNA insertion site of *amsh1-1*. Lines indicate introns and boxes indicate exons (black boxes, coding region; gray boxes, untranslated regions). The triangle indicates the site of T-DNA insertion.

(B) Phenotypes of progeny from an *amsh1-1 amsh3-2* double heterozygous (*A1/a1 A3/a3*) plant. The *amsh1-1* homozygous mutant in an *amsh3-2* heterozygous background (*a1/a1 A3/a3*) shows dwarfism. Bar = 6 cm.

(C) Magnification of the *a1/a1 A3/a3* plant shown in **(B)**. Bar = 1 cm.

(D) Photographs of an *a1/a1 A3/a3* plant in comparison with a wild-type (*A1/A1 A3/A3*) plant of the same age. Note that the *a1/a1 A3/a3* mutant plant exhibits early senescence, indicated by arrowheads. Bar = 1 cm.

(E) DUB assay with K48- or K63-linked ubiquitin chains. The MPN+ domain of AMSH1 was incubated with or without the metalloprotease inhibitor 1,10-phenanthroline (1,10-PT). The reactions were terminated at the indicated time points, and hydrolysis of ubiquitin chains was detected by immuno-blotting using an anti-UB antibody. The amount of AMSH1 (MPN+) in each reaction was verified by immunoblotting with an anti-AMSH1 antibody.

(F) Immunoblots with anti-UB, anti-AMSH3, and anti-AMSH1 antibodies on total protein extracts from the wild type (*A1/A1 A3/A3*), homozygous *amsh1-1* (*a1/a1 A3/A3*), and *a1/a1 A3/a3*. CDC2 is used as a loading control.

dark. This phenotype was not apparent in *amsh1-1* plants that had been grown in 10 h light/14 h dark (see Supplemental Figure 1E online), indicating that daylength has a critical effect on the physiology of *amsh1-1*.

Early senescence is, among others, a hallmark of autophagy mutants (Doelling et al., 2002; Thompson et al., 2005; Xiong et al., 2005; Yoshimoto et al., 2009). Since autophagy is also associated with intracellular trafficking and protein degradation

(Rojo et al., 2001; Surpin et al., 2003; Zouhar et al., 2009), a function associated with AMSH3 (Isono et al., 2010; Katsiarimpa et al., 2011), we examined the autophagy pathway in *amsh1-1* in more detail.

We first analyzed the response of *amsh1-1* to artificial carbon starvation upon transfer to the dark. Wild-type seedlings nor-mally survive the prolonged dark treatment, probably due to a functional autophagic nutrient recycling pathway, whereas
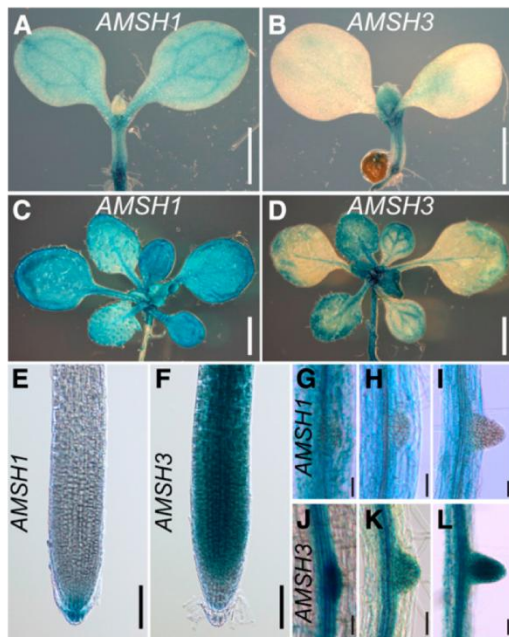
Figure 3. *AMSH1* and *AMSH3* Are Differentially Expressed during Plant Development.

Histochemical assay showing expression patterns of *AMSH1pro*:GUS (**[A]**, **[C]**, **[E]**, and **[G]** to **[I]**) and *AMSH3pro:AMSH3-GUS* (**[B]**, **[D]**, **[F]**, and **[J]** to **[L]**).
(A) and **(B)** Seven-day-old seedlings. Bars = 0.5 mm.
(C) and **(D)** Fourteen-day-old seedlings. Bars = 1 mm.
(E) and **(F)** Root tips of 7-d-old seedlings. Bars = 0.1 mm.
(G) to **(L)** Emerging lateral roots of 14-d-old seedlings.

mutants of autophagic components show chlorosis upon prolonged dark treatment (Doelling et al., 2002; Thompson et al., 2005; Xiong et al., 2005; Phillips et al., 2008; Yoshimoto et al., 2009; Chung et al., 2010). To investigate whether *amsh1-1* also has altered response to dark treatment, we transferred wild-type and *amsh1-1* seedlings for 5 d to the dark. Indeed, while wild-type seedlings were still green after 5 d of dark treatment, *amsh1-1* seedlings became yellowish and had reduced chlorophyll content (51.7% in comparison with the wild type) (Figures 4A and 4B). This result suggests that *amsh1-1*, like previously reported *atg* mutants, may have also defects in the autophagic pathway. The dark-induced chlorosis and the accumulation of ubiquitinated proteins in *amsh1-1* could be complemented by a genomic fragment of *AMSH1*, indicating that the downregulation of *AMSH1* in *amsh1-1* is indeed the cause of these phenotypes (see Supplemental Figures 1C and 1D online).

amsh1-1 Is Defective in Autophagic Degradation

To further assess the autophagy pathway in *amsh1-1*, we monitored the abundance of ATG8, which is a structural component of autophagosomes (Yoshimoto et al., 2004). ATG8 can be used as an autophagy marker, since its accumulation implies defect in the autophagy pathway. ATG8 accumulates either upon inhibition of degradation by the application of protease

inhibitors like E-64d (Inoue et al., 2006) or in mutants defective in autophagosome formation (Yoshimoto et al., 2004; Thompson et al., 2005; Phillips et al., 2008; Chung et al., 2010). Indeed, when wild-type and *atg7-2* (Hofius et al., 2009) seedlings were incubated with E-64d, E64d–induced accumulation of ATG8 was observed in the wild type, while *atg7-2* accumulated ATG8 without E-64d (see Supplemental Figure 2C online).

The amount of ATG8 was comparable in light-grown wild type and *amsh1-1* (Figure 4C, top panel). However, when the seedlings were grown in the dark for 5 d to induce autophagy, high amounts of ATG8 accumulated in *amsh1-1* in comparison with the wild type (Figure 4C, bottom panel), suggesting that *amsh1-1* is less efficient in autophagic degradation. The accumulation of ATG8 was enhanced in both genotypes upon E-64d treatment, indicating that even in *amsh1-1*, autophagic degradation was not completely inhibited. Transcript levels of all *ATG8* isoforms in *amsh1-1* were comparable to the wild type under this condition (see Supplemental Figure 2E online), inferring that the accumulation of ATG8 is not a consequence of transcriptional misregulation in *amsh1-1*.

We next wanted to examine whether selective autophagy is also impaired in *amsh1-1*. As opposed to bulk autophagy, during selective autophagy, specific cargo proteins are recognized by cargo adaptors and degraded via the autophagy pathway. NEIGHBOR of BRCA1 GENE1 (NBR1) is a cargo receptor and substrate of selective autophagy (Svenning et al., 2011). NBR1 accumulated in *atg7-2* as previously reported, but not in *amsh1-1* (Figure 4D; see Supplemental Figure 2D online), suggesting that NBR1-mediated selective autophagy is not defective in *amsh1-1*. The fact that *amsh1-1* does not show bulk and selective autophagic degradation defects in light suggests that residual AMSH1 in *amsh1-1* is sufficient for both processes in light. However, the low amount of AMSH1 probably becomes limiting in the dark, where bulk autophagy, but not NBR1-mediated selective autophagy, is highly activated.

To distinguish between the defects in autophagic protein degradation and autophagosome formation, we made use of the dye monodansylcadaverine (MDC), which stains autophagic bodies (Contento et al., 2005) upon treatment with the vacuolar protease inhibitor E-64d. E-64d inhibits the degradation of autophagic bodies in the vacuole and thus causes accumulation of MDC-stained autophagic bodies in the vacuoles stained with 2′,7′-bis-(2-carboxyethyl)-5-(and 6)carboxyfluorescein acetoxymethyl ester (BCECF-AM) (Figure 4E). The accumulation of MDC-positive aggregates was not detected in *atg7-2* (see Supplemental Figure 2A online), indicating that although it accumulates ATG8, the formation of autophagosomes is not visible in this mutant. Furthermore, E-64d–induced MDC-positive vacuolar aggregates colocalized with the autophagosome marker GFP-ATG8e (Contento et al., 2005) (Figure 4F), but not with the late-endosome marker YFP-ARA7 (Geldner et al., 2009) (see Supplemental Figure 2B online), corroborating the specificity of MDC staining under our experimental conditions.

amsh1-1, in contrast with *atg7-2*, is not impaired in the formation of autophagosomes, since MDC-stained compartments were visible in *amsh1-1*. However, accumulation of E-64d–induced aggregates was less apparent in *amsh1-1* compared with the wild type when maximal projection images of z-stacks obtained
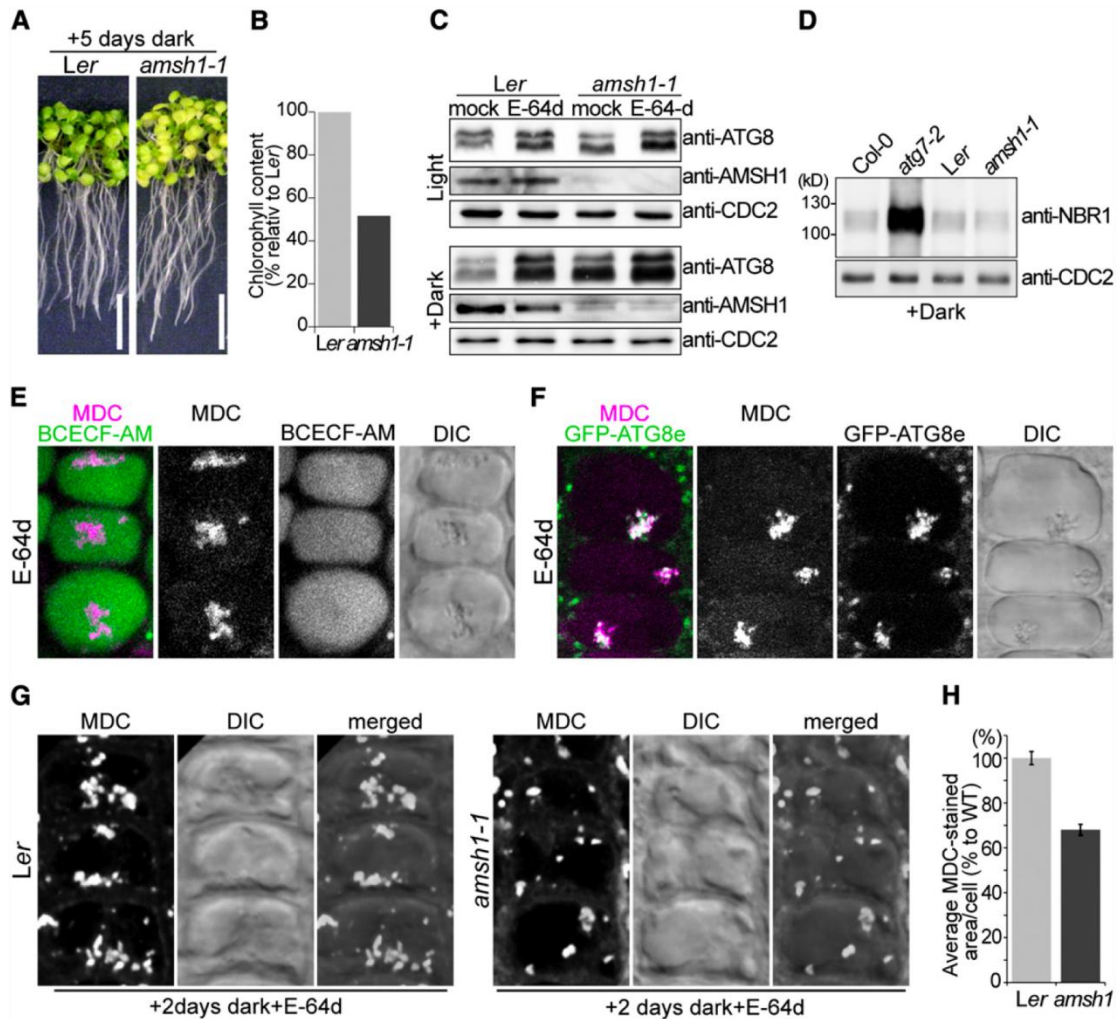
Figure 4. *amsh1-1* Is Deficient in Autophagic Degradation.

(A) Photographs of wild-type (L*er*) and *amsh1-1* seedlings after 5 d in the dark (left panel). Seedlings were grown 7 d on half-strength MS under long-day conditions before transfer to dark. Note that starvation-induced chlorosis is enhanced in *amsh1-1* compared with the wild type. Bars = 1 cm.

(B) Total chlorophyll content of seedlings in **(A)**. Value of the wild type was set to 100%.

(C) Immunoblot with an anti-ATG8 antibody. Total proteins were extracted from seedlings grown in light for 12 d (Light, top panel) or as in **(A)** (Dark, bottom panel) before treatment with either DMSO (mock) or E-64d.

(D) Total proteins were extracted from seedlings grown as in **(A)** and subjected to immunoblot with an anti-NBR1 antibody. *atg7-2* is used as a positive control and CDC2 is used as loading control.

(E) Confocal images of MDC-stained wild-type root epidermal cells. BCECF-AM was used to visualize the vacuoles. Seedlings were grown as in **(A)** and treated with E-64d for 1 h before staining with MDC. Note that upon E-64d treatment, MDC positive autophagic bodies accumulate in the BCECF-AM–stained vacuole.

(F) Confocal images of MDC-stained GFP-ATG8e–expressing root epidermal cells. Seedlings were grown as in **(A)** and treated 6 h with E-64d before staining with MDC.

(G) Wild-type (L*er*) and *amsh1-1* seedlings were grown as in **(A)**. Seedlings were subsequently treated with E-64d for 1 h and stained with MDC. Confocal images (maximal projection) of MDC-stained root epidermal cells of the wild type (L*er*, left panel) and *amsh1-1* (right panel) are shown.

(H) Quantification of MDC-staining positive area per cell in the wild type (L*er*) and *amsh1-1* (*n* = 831 for L*er* and *n* = 749 for *amsh1-1*). Photographs taken in **(G)** were analyzed by the FluoView software, and the values of the wild type were set to 100%. Error bars indicate sᴇ.

by confocal microscopy were analyzed (Figure 4G). Subsequent quantification of the thus imaged MDC-positive signal area in individual cells ($n = 831$ for the wild type, and $n = 749$ for *amsh1-1*) showed that *amsh1-1* had reduced accumulation of autophagic bodies in the vacuole when compared with the wild type (68% of average MDC-stained area per cell compared with the wild type) (Figure 4H). This result indicates that autophagosomes are less efficiently targeted to the vacuole in *amsh1-1*.

AMSH1 Interacts with the ESCRT-III Subunit VPS2.1 through Its MIT Domain

We next investigated whether the inhibition of bulk autophagic degradation in *amsh1-1* is a consequence of altered intracellular trafficking. For this purpose, we examined the interaction of AMSH1 with the endocytosis machinery. AMSH1, like AMSH3, contains an N-terminal microtubule interacting and trafficking (MIT) domain, which we had previously shown to be important for the interaction with the MIT interacting motif (MIM) present in ESCRT-III subunits (Katsiarimpa et al., 2011). We therefore tested in a directed yeast two-hybrid (Y2H) assay whether AMSH1 can also interact with the ESCRT-III core subunits VPS2.1, VPS20.1, VPS24.1, and SUCROSE NON-FERMENTING7.1 (SNF7.1) (Winter and Hauser, 2006; Richardson et al., 2011; Shahriari et al., 2011). Among the four tested subunits, AMSH1 interacted only with VPS2.1 (Figure 5A; see Supplemental Figure 3A online).

The MIT domain is necessary for the interaction of AMSH1 with VPS2.1 since deletion of this domain led to loss of interaction (Figure 5B; see Supplemental Figure 3B online). Moreover, AMSH1 and VPS2.1 interact directly through the 154–amino acid MIT and 17–amino acid MIM region, respectively, as shown by an in vitro binding assay (Figure 5C). Altogether, these data indicate that AMSH1, like AMSH3, may play a role in ESCRT-III–mediated intracellular trafficking pathway by interacting with VPS2.1.

Overexpression of VPS2.1-GFP Causes Inhibition of Endocytosis

To investigate whether VPS2.1 is also involved in the same physiological pathway as AMSH1, we generated transgenic plants that express VPS2.1 as a C-terminal fusion with green fluorescent protein (*35Spro:VPS2.1-GFP*). C-terminal fusions of ESCRT-III subunits, including VPS2.1, with large proteins, such as GFP, have been shown to disturb ESCRT-III function in other organisms due to their aggregation in class-E compartments (Howard et al., 2001; Teis et al., 2008; Teis et al., 2010). Indeed, we found that *35Spro:VPS2.1-GFP* plants occasionally showed abnormal growth already at the seedling stage (see Supplemental Figure 4A online) and that part of the overexpressed VPS2.1-GFP localized to large aggregates in the cytosol that may represent class-E compartments (see Supplemental Figure 4B online). After transfer to soil, adult *35Spro:VPS2.1-GFP* plants, similarly to *amsh1-1/amsh1-1 amsh3-2/AMSH3* plants, showed early leaf senescence and a severe dwarf phenotype (Figure 6A) and were mostly sterile (data not shown).

We then tested whether the expression of *VPS2.1-GFP* has an inhibitory effect on endocytosis of plasma membrane cargo. For
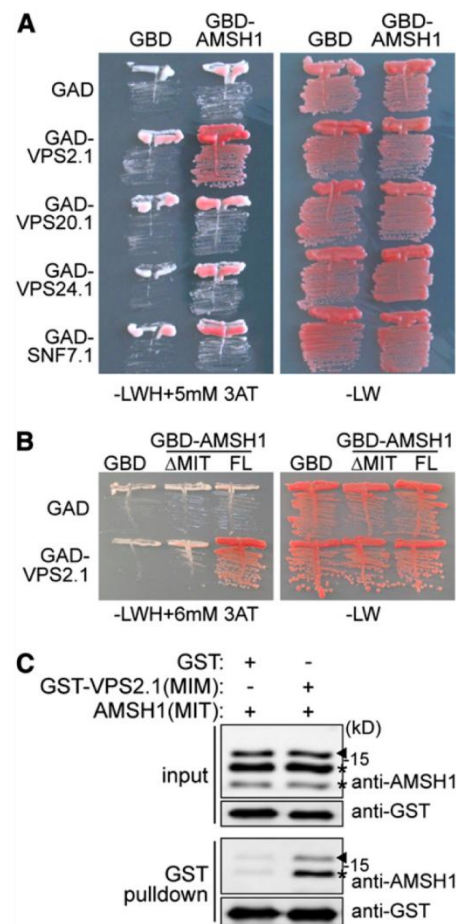

Figure 5. AMSH1 Interacts with ESCRT-III Subunit VPS2.1 through the MIT Domain.

(A) Y2H analysis of GBD-AMSH1 with GAD-fused ESCRT-III subunits VPS2.1, VPS20.1, VPS24.1, and SNF7.1. Transformants were plated on medium lacking Leu, Trp, and His (-LWH) supplemented with 5 mM 3-Amino-1,2,4-triazole (3-AT) (left panel) to test for their auxotrophic growth or on medium lacking Leu and Trp (-LW) (right panel).
(B) Y2H analysis of GBD-AMSH1 (FL; full-length) and GBD-AMSH1(ΔMIT) with GAD-VPS2.1. Transformants were grown on –LWH+6 mM 3-AT (left panel) or -LW (right panel) medium to test for their auxotrophic growth.
(C) In vitro binding assay of the MIT domain of AMSH1 with GST or GST-fused MIM domain of VPS2.1. After GST pulldown, bead-bound proteins were analyzed by immunoblotting using anti-AMSH1 and anti-GST antibodies. Arrowheads indicate the positions of AMSH1(MIT), and asterisks indicate degradation products.
[See online article for color version of this figure.]

this purpose, we examined the endocytosis of an artificial MVB cargo PMA-GFP-UB (Herberth et al., 2012) upon coexpression with *35Spro:VPS2.1-TagRFP*, a construct expressing *VPS2.1* with a C-terminal *TagRFP* in *Arabidopsis* cell culture–derived protoplasts. Fusion of monoubiquitin to PMA-GFP alters the intracellular distribution of this normally plasma membrane–localized protein, which then becomes visible in vesicles and in the vacuolar lumen (Figure 6B). SKD1/Vps4p is an AAA-ATPase required for the disassembly of ESCRT-III (Babst et al., 1997). As

previously reported, coexpression of an inactive SKD1(EQ), but not that of wild-type SKD1(WT), results in the inhibition of vacuolar targeting of PMA-GFP-UB (Figure 6C). Similarly, we found PMA-GFP-UB signals to be excluded from the vacuolar lumen upon coexpression with *35Spro:VPS2.1-TagRFP*, suggesting that the C-terminal fluorophore fusion of VPS2.1 has an inhibitory effect similar to SKD1(EQ) (Figure 6C).

We next analyzed the vacuolar degradation of the auxin efflux facilitator PIN2, a well-characterized cargo of the MVB pathway (Abas et al., 2006; Spitzer et al., 2009). While no apparent accumulation of PIN2 was observed in *amsh1-1* (see Supplemental Figure 4C online), ubiquitinated proteins as well as PIN2 accumulated in *35Spro:VPS2.1-GFP* seedlings at a higher level compared with wild-type seedlings (Figures 6D and 6E). Since the transcript levels of *PIN2* were not consistently and strongly upregulated in *35Spro:VPS2.1-GFP* seedlings (see Supplemental Figure 4D online), accumulation of PIN2 is probably a consequence of a posttranscriptional mechanism. Together, these results indicate

that the overexpression of the dominant-negative *VPS2.1-GFP* has an inhibitory effect on the degradation of (ubiquitinated) MVB cargo, probably due to impaired ESCRT-III and MVB function.

VPS2.1-GFP–Overexpressing Plants Are Defective in Autophagic Degradation

Since our studies had implicated the VPS2.1-interactor AMSH1 in autophagy, we examined the response of *VPS2.1-GFP*–overexpressing plants to dark treatment. After 5 d in the dark, *35Spro:VPS2.1-GFP* seedlings, like *amsh1-1* seedlings, showed strong chlorosis and reduction in chlorophyll content (39 and 32% compared with the wild type) (Figures 7A and 7B).

When we analyzed ATG8 protein abundance in *35Spro: VPS2.1-GFP* seedlings, more ATG8 was detected even under normal growth conditions and a further increase was observed after transfer to the dark (Figure 7C). Expression of *ATG8a-i* was not increased in these lines, indicating that the accumulation of
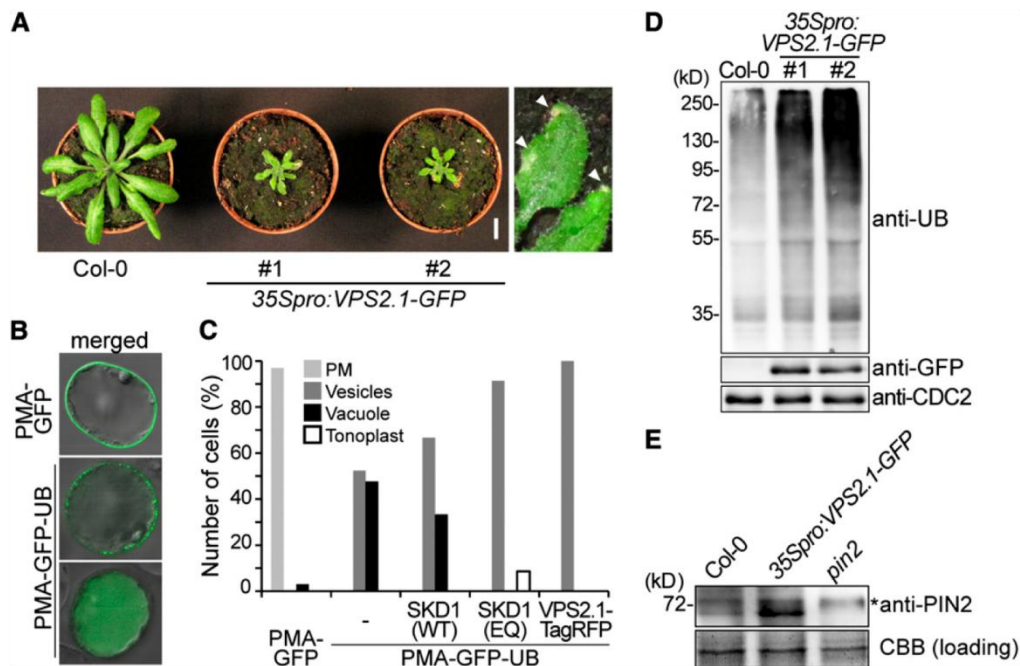

Figure 6. *VPS2.1-GFP*–Overexpressing Seedlings Are Deficient in Endocytosis and Accumulate PIN2.

(A) *VPS2.1-GFP*–overexpressing plants are dwarf and exhibit an early senescence phenotype. Plants of two independent transgenic lines (#1 and #2) are shown together with a wild-type plant (Col-0) of the same age. Magnification of senescing leaves (arrowheads) is shown on the far right. Bar = 1cm.
(B) Analysis of the differential intracellular distribution of PMA-GFP and PMA-GFP-UB. PMA-GFP shows predominantly plasma membrane localization (top panel), while PMA-GFP-UB signals are found in vesicles and the vacuolar lumen (middle and bottom panels, respectively). Photographs are merged with differential interference contrast pictures of the corresponding cell.
(C) Localization of PMA-GFP and PMA-GFP-UB upon coexpression with *SKD1* and *VSP2.1* constructs. Cell culture–derived protoplasts expressing *PMA-GFP* alone (n = 33), *PMA-GFP-UB* (n = 128) alone or with *35Spro:HA-SKD1(WT)* (n = 21), *35Spro:HA-SKD1(EQ)* (n = 116), and *35Spro:VPS2.1-TagRFP* (n = 40) were analyzed by confocal microscopy. Relative number of cells showing each localization was scored. Light-gray bars, plasma membrane; dark-gray bars, vesicles; solid bars, vacuole lumen; and open bars, tonoplast.
(D) *VPS2.1-GFP*–overexpressing plants accumulate ubiquitinated proteins. Total extract of wild-type (Col-0) and *35Spro:VPS2.1-GFP* seedlings were subjected to immunoblotting using anti-UB, anti-GFP, and anti-CDC2 antibodies. CDC2 was used as a loading control.
(E) *35Spro:VPS2.1-GFP* seedlings accumulate PIN2. Membrane protein extract from the roots of wild-type (Col-0), *35Spro:VPS2.1-GFP*, and *pin2* seedlings were subjected to immunoblotting using an anti-PIN2 antibody. A representative immunoblot is shown. Coomassie blue (CBB)–stained protein bands were used as a loading control. The asterisk indicates an unspecific band.

ATG8 is not a consequence of transcriptional misregulation of *ATG8* genes (see Supplemental Figure 4F online).

Next, we examined the protein level of NBR1 in *VPS2.1-GFP*–overexpressing plants. In contrast with *amsh1-1*, in which NBR1 accumulation was not observed, NBR1 accumulated at high levels in *35Spro:VPS2.1-GFP* plants (Figure 7D), while its transcript level remained unchanged (see Supplemental Figure 4E online). In

contrast with ATG8, however, the amount of accumulated NBR1 remained unaltered after dark treatment, suggesting that NBR1-dependent selective autophagy is not dark induced. Treatment with E-64d did not enhance the accumulation of either NBR1 or ATG8 (Figure 7E), indicating that *35Spro:VPS2.1-GFP* is severely impaired in autophagic degradation. Since, in contrast with *amsh1-1*, *35Spro:VPS2.1-GFP* plants are incapable of dealing
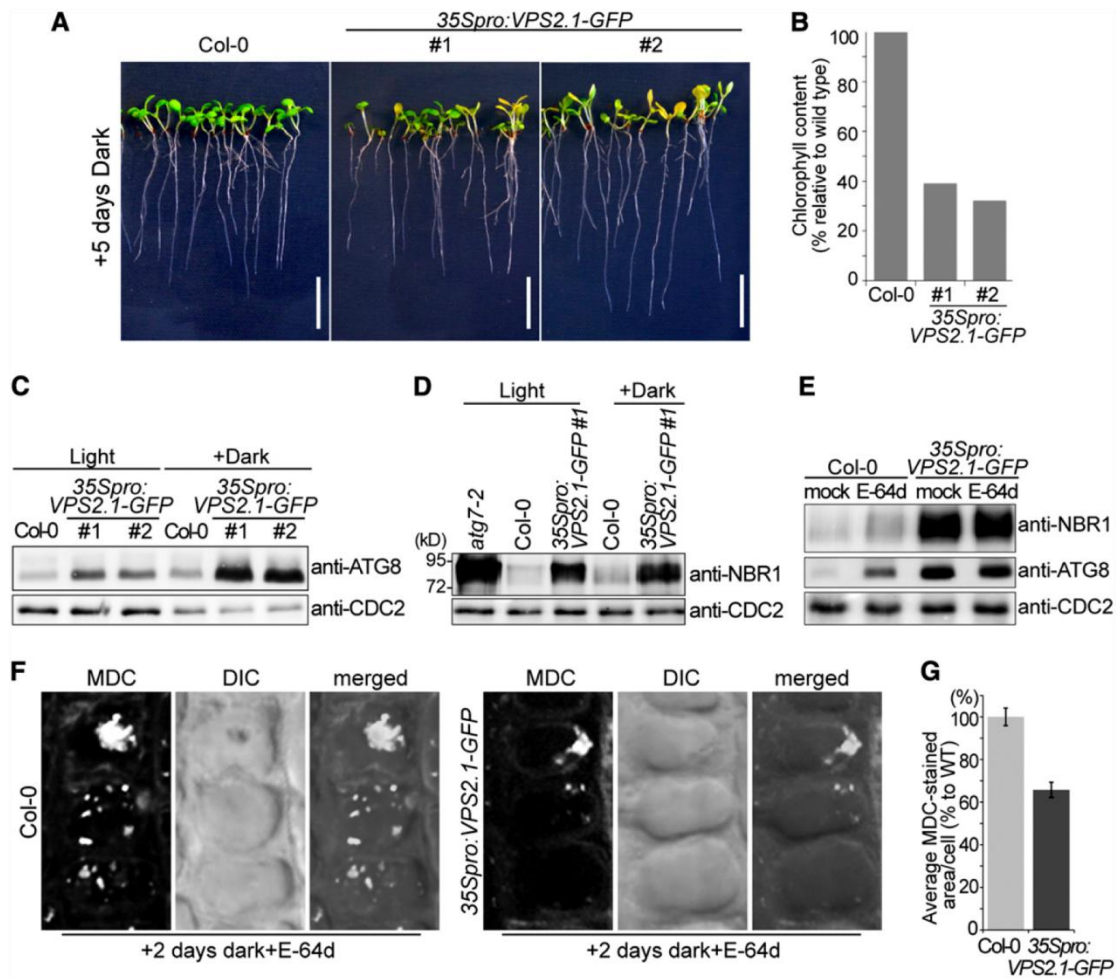

Figure 7. *VPS2.1-GFP*–Overexpressing Seedlings Have Defects in Both Nonselective and Selective Autophagy.

(A) *35Spro:VPS2.1-GFP* seedlings exhibit starvation-induced chlorosis after dark treatment. Long-day-grown wild-type (Col-0) and *35Spro:VPS2.1-GFP* seedlings were transferred to the dark for 5 d. Note that the *35Spro:VPS2.1-GFP* lines segregate for the transgene. Bars = 1 cm.
(B) Chlorophyll content of seedlings shown in **(A)**.
(C) *35Spro:VPS2.1-GFP* seedlings accumulate ATG8. Immunoblot using an anti-ATG8 antibody on total protein extract from wild-type (Col-0) and *35Spro:VPS2.1-GFP* seedlings grown under long-day conditions for 12 d (Light) or transferred to dark after 7 d for 5 d (Dark). CDC2 was used as loading control.
(D) NBR1 accumulates in *35Spro:VPS2.1-GFP* seedlings. Total protein extracts of *atg7-2*, the wild type (Col-0), and *35Spro:VPS2.1-GFP* grown as in **(C)** were analyzed by immunoblotting using an anti-NBR1 antibody. CDC2 was used as loading control.
(E) E-64d does not enhance the accumulation of NBR1 and ATG8 in *35Spro:VPS2.1-GFP*. Seedlings grown in the dark for 5 d were treated with E-64d for 6 h, and total extracts were submitted to immunoblotting with anti-NBR1 and anti-ATG8 antibodies. CDC2 was used as loading control. Note that E-64d enhances the accumulation of NBR1 and ATG8 only in the wild type (Col-0).
(F) Wild-type (Col-0) and *35Spro:VPS2.1-GFP* seedlings were grown for 7 d in long days and subsequently 2 d in the dark. Seedlings were then treated with E-64d for 1 h and stained with MDC. Confocal images (maximal projection) of MDC-stained root epidermal cells of the wild type (Col-0, left panel) and *35Spro:VPS2.1-GFP* (right panel) are shown. DIC, differential interference contrast.
(G) Quantification of MDC-stained area per cell in the wild type (WT; Col-0) and *35Spro:VPS2.1-GFP* (*n* = 547 for Col-0, and *n* = 376 for *35Spro:VPS2.1-GFP*). Photographs taken in **(F)** were analyzed by the FluoView software and the value of wild type was set to 100%. Error bars indicate SE.
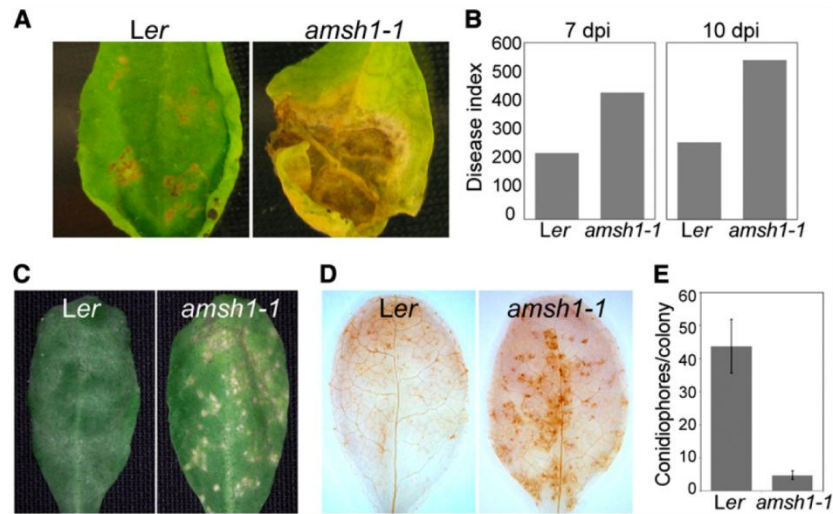
Figure 8. *amsh1-1* Displays Altered Susceptibility to Mildew Infection.

(A) Wild-type (L*er*) and *amsh1-1* plants were grown under short-day conditions (10 h light/14 h dark). Rosetta leaves of 5.5-week-old plants were drop-inoculated with 10^6 spores/mL *A. brassicicola*, and a representative leaf was photographed after 11 d of inoculation.

(B) Disease indices from experiments shown in **(A)** were calculated 7 d (7 dpi) and 10 d (10 dpi) after inoculation with *A. brassicicola* spores.

(C) Disease symptoms of wild-type (L*er*) and *amsh1-1* plants upon infection with *E. cruciferarum* spores. Plants were grown as in **(A)**, and 6-week-old plants were inoculated with *E. cruciferarum* spores. A representative leaf was photographed 7 d after inoculation.

(D) *amsh1-1* plants accumulate hydrogen peroxide. Leaves of wild-type (L*er*) and *amsh1-1* plants 2 d after infection with *E. cruciferarum* spores were stained with DAB for hydrogen peroxide accumulation, which is indicated by brown stain.

(E) Quantification of conidiophores per spore. Leaves were stained with trypan blue 6 d after inoculation with *E. cruciferarum* spores, and the number of conidiophores per colony was counted. Error bars indicate SE.

with basal levels of bulk and selective autophagic degradation in the light, we can conclude that overexpression of *VPS2.1-GFP* has a much stronger inhibitory effect on autophagic degradation than does the knockdown of *AMSH1*.

A report on *Caenorhabditis elegans* ESCRT-III RNAi mutants suggests that the accumulation of autophagosomes in ESCRT-III mutants is a consequence of the activation of autophagy due to a protective mechanism (Djeddi et al., 2012). In *Arabidopsis*, activation of autophagy, for example, after dark treatment, was shown to be coupled with transcriptional upregulation of *ATG8* (Doelling et al., 2002; Thompson et al., 2005). Thus, the comparable transcript levels of *ATG8* isoforms in *amsh1-1* and *35Spro:VPS2.1-GFP* with their corresponding wild types imply that autophagic flux is not increased in these mutants.

To examine the behavior of autophagosomes in dark-treated *35Spro:VPS2.1-GFP*, we stained E-64d–treated seedlings with MDC. We reasoned that if VPS2.1 function is necessary for the autophagic degradation, cells should accumulate less MDC-stained autophagic bodies in the vacuoles of *35Spro:VPS2.1-GFP*. MDC-stained vacuolar aggregates were observed in *35Spro:VPS2.1-GFP*, indicating that autophagosomes formation is not inhibited (Figure 7F). Further quantification showed that the area of MDC-stained autophagic bodies per cell was smaller in *35Spro:VPS2.1-GFP* cells (65.8% of average MDC-stained area per cell compared with the wild type; $n = 547$ for the wild type and $n = 376$ for *35Spro:VPS2.1-GFP*) (Figure 7G), implying that *VPS2.1-GFP* overexpression and the partial loss of AMSH1 function lead to similar defects in autophagic degradation.

amsh1-1 Displays Altered Pathogen Susceptibility

Recent studies on *atg* mutants showed the involvement of autophagy in plant innate immunity and pathogen defense (Liu et al., 2005; Patel and Dinesh-Kumar, 2008; Hofius et al., 2009; Yoshimoto et al., 2009; Lai et al., 2011; Lenz et al., 2011; Wang
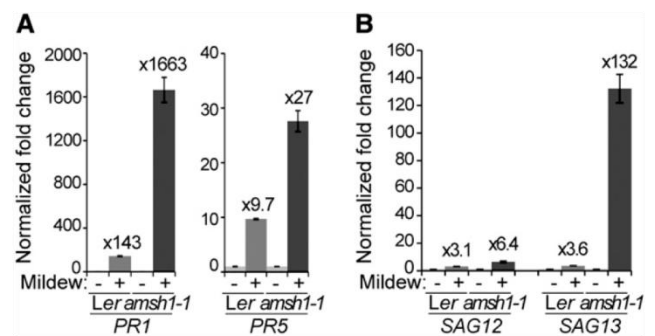

Figure 9. Transcript Levels of Pathogen- and Senescence-Related Genes Are Highly Upregulated in *amsh1-1* after Mildew Infection.

(A) and **(B)** Relative gene expression of pathogen-related genes *PR1* and *PR5* **(A)** and senescence-related genes *SAG12* and *SAG13* **(B)** in wild-type (L*er*) and *amsh1-1* plants uninfected or infected with *E. cruciferarum* spores. Total RNA was extracted from plants 2 d after infection. Expression levels were normalized to the reference gene *ACT8* and the expression levels in mock-treated L*er* and *amsh1-1* plants were set to 1 in each experiment. Error bars indicate SE.
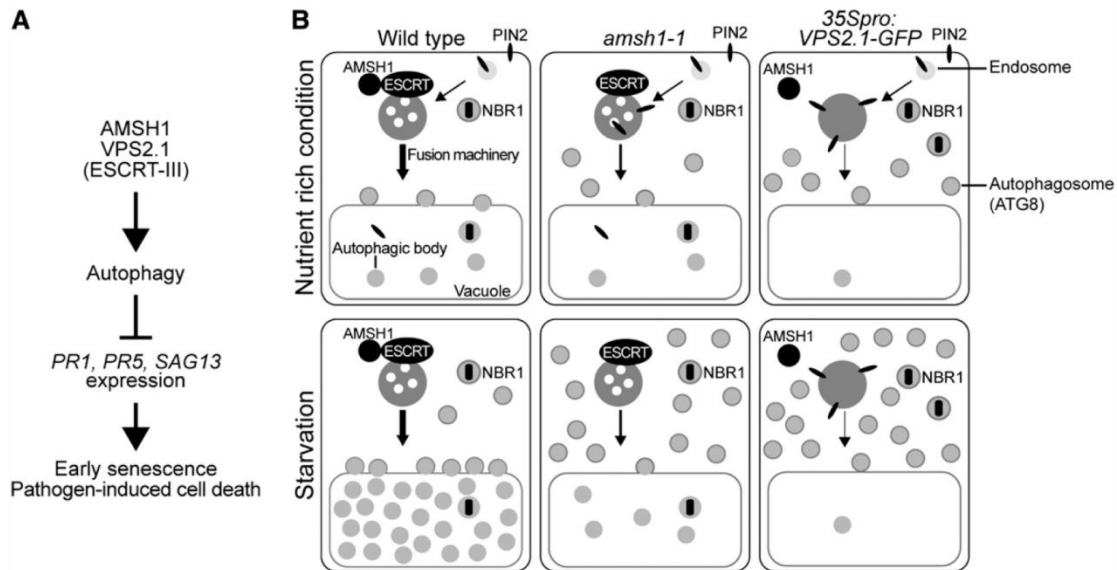
Figure 10. AMSH1 and ESCRT-III Are Important for Autophagy and Autophagy-Mediated Physiological Responses in Plants.

(A) AMSH1 and VPS2.1 functions are important for autophagic degradation. As previously reported, functional autophagy represses *PR* and *SAG* gene expression, induction of which causes early senescence and pathogen-induced cell death.

(B) *amsh1-1* and *35Spro:VPS2.1-GFP* are impaired in the degradation of autophagosomes to different extents. In wild-type cells, plasma membrane–localized PIN2 is endocytosed via the MVB pathway. The selective autophagy cargo receptor and substrate NBR1 is delivered to the vacuole via autophagosomes. Autophagosomes fuse with the vacuole in order to degrade its contents. Factors required for the recognition and fusion of autophagosomes with the vacuolar membrane as well as proteases responsible for the degradation of autophagic bodies may be transported via an MVB-dependent pathway. Upon carbon deprivation in the dark, autophagic recycling is highly upregulated. The weak *amsh1-1* knockdown mutant is still capable of endocytic and autophagic degradation under optimal growth condition. However, when bulk autophagy is highly activated upon dark-induced carbon starvation, *amsh1-1* accumulates ATG8 and shows less autophagic bodies in the vacuole, indicative for impaired autophagic degradation. When ESCRT-III function is disturbed by overexpressing *VPS2.1-GFP*, both endocytosis and autophagic recycling is strongly inhibited even under optimal growth conditions, leading to the accumulation of ATG8, NBR1, and PIN2. Accumulation of ATG8 increases when bulk autophagy is activated in the dark. Taken together, intact AMSH1 and ESCRT-III (VPS2.1) are essential for proper autophagic degradation.

et al., 2011). As *amsh1-1* and *35Spro:VPS2.1-GFP* showed impaired autophagic degradation, we hypothesized that these mutants may also exhibit altered pathogen response. Since *VPS2.1-GFP*–overexpressing plants were dwarf and had altered leaf size and morphology, we decided to conduct the pathogen assays only with *amsh1-1*. We used 5- to 6-week-old *amsh1-1* plants grown under 10-h-light/14-h-dark conditions because under this condition *amsh1-1* did not show early senescence (see Supplemental Figure 1E online).

Wild-type and *amsh1-1* plants were inoculated with the *Arabidopsis* pathogens *Alternaria brassicicola* or *Erysiphe cruciferarum*. *A. brassicicola* is a necrotrophic fungus that induces cell death upon infection. In comparison with the wild type, in which cell lesion was restricted to the inoculation spots, *amsh1-1* showed increased susceptibility, visible by the complete wilting and spreading necrosis along the entire leaf 10 to 11 d after infection (Figures 8A and 8B). Thus, similarly to previously characterized *atg* mutants, *amsh1-1* is also hypersensitive to *A. brassicicola* infection.

E. cruciferarum is an obligate biotroph that requires living cells for growth. In the wild type, *E. cruciferarum* infection did not cause visible cell lesions on leaves 5 d after infection (Figure 8C, left panel). However, at the same stage, *amsh1-1* showed spontaneous cell death on leaves (Figure 8C, right panel). This

pathogen-induced cell death in *amsh1-1* was accompanied by an increased production of reactive oxygen species (Figure 8D). We also counted fewer conidiophores per spores on *amsh1-1* leaves when compared with the wild type (Figure 8E; see Supplemental Figures 5A to 5C online), indicating that *amsh1-1* is more resistant against *E. cruciferarum* as an indirect consequence of programmed cell death, which is triggered in the mutant.

Transcriptional Upregulation of Defense-Related Genes May Be Responsible for the Early Senescence of *amsh1-1* and 35Spro:VPS2.1-GFP

To further investigate the molecular mechanism underlying the *amsh1-1* pathogen response phenotype, we examined the expression of defense-related genes in wild-type and *amsh1-1* plants after infection with *E. cruciferarum*. Upon pathogen infection, basal immune responses, which are dependent on salicylic acid (SA), are upregulated and the expression of typical SA marker genes, such as *PATHOGENE-RELATED GENE1* (*PR1*) and *PR5* (Ward et al., 1991) as well as *SENESCENCE ASSOCIATED GENE12* (*SAG12*) and *SAG13* (Morris et al., 2000; Brodersen et al., 2002), is induced (reviewed in Wiermer et al., 2005).

Two days after infection with *E. cruciferarum* spores, a strong induction of *PR1*, *PR5*, *SAG12*, and *SAG13* was detected both in the wild type and in *amsh1-1* (Figures 9A and 9B). However, the induction of *PR1*, *PR5*, and *SAG13* was much stronger in *amsh1-1* (Figures 9A and 9B), suggesting that the SA signaling pathway is hyperactivated in *amsh1-1*. High *PR* gene transcript accumulation in association with programmed cell death may be the cause for the enhanced resistance phenotype toward *E. cruciferarum* while conferring enhanced susceptibility to a necrotrophic pathogen such as *A. brassicicola*.

We then tested the possibility that the early senescence phenotype of *amsh1-1* under short-day conditions (8 h light/16 h dark) is also a consequence of the upregulation of SA-induced genes. Indeed, a strong upregulation of *PR1*, *PR5*, and *SAG13* was observed in 8-week-old *amsh1-1*, specifically when grown under 8 h light/16 h dark, but not under 10 h light/14 h dark (see Supplemental Figures 6A and 6B online). This suggests a correlation of the photoperiod-dependent early senescence phenotype (see Supplemental Figure 1D online) with the hyperactivated SA signaling in *amsh1-1*. Similar transcriptional upregulation of *PR* genes and *SAG13* was also found in the *35Spro:VPS2.1-GFP* seedlings (see Supplemental Figure 6C online).

Altogether, these results suggest that AMSH1 and VPS2.1 are necessary for proper autophagy in plants and, thus, for physiological processes depending on an intact autophagy pathway (Figures 10A and 10B).

DISCUSSION

In this study, we showed that AMSH1, an AMSH3-related DUB, interacts with the endocytosis machinery through the ESCRT-III subunit VPS2.1. AMSH1 and AMSH3 possess an N-terminal MIT domain and a C-terminal MPN domain (Isono et al., 2010) but share only 47% overall amino acid identity, suggesting that the two proteins might have similar biochemical properties but also specific physiological functions. The fact that *AMSH1* and *AMSH3* are not products of a recent duplication event in *Arabidopsis*, that they show in part mutually exclusive expression patterns, and that in contrast with AMSH3, AMSH1 does not interact with VPS24.1 in Y2H interaction studies might further support this hypothesis.

Mutant analyses showed that AMSH1 and VPS2.1 are part of the autophagic degradation pathway and are important for plant survival in the dark, regulation of senescence, and pathogen defense. Phenotypes of *amsh1-1* and *35Spro:VPS2.1-GFP* include early senescence and chlorosis in the dark. At the molecular level, they both accumulate ubiquitinated proteins, and though to different degrees, both accumulate ATG8 and show defects in autophagosome delivery to the vacuole, indicating the involvement of AMSH1 and VPS2.1 in autophagic degradation. However, in contrast with *35Spro:VPS2.1-GFP*, *amsh1-1* does not show accumulation of PIN2. This might be due to the nature of the *amsh1-1* allele, which allows a residual amount of AMSH1 to still exist. It is a future challenge to investigate whether AMSH1 directly targets ubiquitinated MVB cargos or rather components of the trafficking machinery. Taken together, our results imply that an intact MVB pathway with its associated DUB AMSH1 is also essential for autophagy in plants and, hence, for autophagy-mediated physiological processes.

Although there is a strong indication that SA-dependent basal immunity and cell death are indirectly deregulated in *amsh1-1*, we cannot exclude the possibility that AMSH1 and also VPS2.1 may directly affect plant defense. Receptor-mediated endocytosis and exocytosis are known to play important roles in plant immune response, and many specific and general players involved in this pathway have been identified. For example, PENETRATION1 (PEN1)/SYNTAXIN OF PLANTS121 (SYP121) is a SNARE protein that contributes to the delivery of antimicrobial compounds to the infection site (Collins et al., 2003). PEN1 and multiple other components of the intracellular trafficking pathway, including VAMP72 proteins, GNOM, an ESCRT-I subunit VPS28, and MVBs, have been shown to relocate to pathogen infection sites (Assaad et al., 2004; An et al., 2006; Kwon et al., 2008; Lu et al., 2012; Nielsen et al., 2012).

In contrast with *syp122*, *syp42/syp43*, which is defective in *trans*-Golgi dependent intracellular trafficking, shows increased susceptibility to the obligate biotroph *Golovinomyces orontii* (Zhang et al., 2007; Uemura et al., 2012). Similarly, ESCRT-I mutants are also more susceptible to infection with the obligate biotrophic oomycete *Hyaloperonospora arabidopsidis* (Lu et al., 2012), in contrast with *amsh1-1*, which is more resistant to the obligate biotroph *E. cruciferarum*. These apparently conflicting results might reflect the complexity of regulatory mechanisms with a different outcome depending on the mutant-pathogen combination.

Dysfunction of AMSH1 and VPS2.1 may inhibit trafficking of autophagosomes to the vacuole. The process of heterotypic membrane fusion by which autophagosome membranes are combined with other membranes is not yet well understood. One group of proteins important for proper and efficient fusion between membranes is the SNAREs, which reside on membranes and form heteromeric complexes. A recent article reported the identification of human Syntaxin 7 as an autophagosomal SNARE, essential for autophagosome fusion to endosomes and lysosomes (Itakura et al., 2012). Similar fusion mechanisms involving SNAREs might also take place in plants. A family of Rab GTPases, Ypt7p/Rab7/RAB7, was also shown to affect fusion of autophagosomes with endosomes and vacuoles in yeast (Balderhaar et al., 2010), human cell culture (Gutierrez et al., 2004; Jäger et al., 2004), and plants (Kwon et al., 2010). In *amsh1-1* and *VPS2.1-GFP*–overexpressing plants, proteins required for docking and/or fusion between autophagosomes and the target membrane might be mistargeted or reduced, leading to fusion defects. Alternatively, the ESCRT machinery and AMSH1 may be directly involved in the heterotypic fusion event. Future experiments are needed to identify and reveal the identity of the factors involved in this process and elucidate the molecular mechanism of their regulation.

METHODS

Biological Material

All experiments were performed with *Arabidopsis thaliana* (Columbia-0 [Col-0] or Landsberg *erecta* [L*er*] background). T-DNA insertion lines of *AMSH1*, designated *amsh1-1* (CSHL_ET8678; L*er* ecotype) and *AMSH2* (CSHL_ET4018; L*er* ecotype) were obtained from the Martienssen Lab (Cold Spring Harbor Laboratory). The T-DNA insertion site of *amsh1-1* was identified using the specific T-DNA primer DS3.1 in combination with

the gene-specific AMSH1 reverse primer and the wild type with the combination of AMSH1 forward and AMSH1 reverse primers. T-DNA insertion mutants *atg7-2* (Hofius et al., 2009) and *pin2* (Willige et al., 2011) in the Col-0 background were described previously.

Plant transformations were performed using the floral dip method (Clough and Bent, 1998). Seedlings were grown in continuous light, long-day (16 h light and 8 h dark), or short-day (8 h light and 16 h dark or 10 h light and 14 h dark) conditions, as indicated for each experiment, at 110 to 120 µmol m^{-2} s^{-1} light intensity. Standard Murashige and Skoog (MS) growth medium (Duchefa Biochemie) supplemented with 1% Suc or half-strength MS (2.15 g/L MS and 2.3 mM MES, pH 5.7) was used to grow seedlings, and adult plants were grown in soil.

For exposure to artificial starvation or carbon deprivation, 7-d-old seedlings grown on half-strength MS or 3-week-old plants grown on soil under long-day (16 h daylight/8 h dark) conditions were transferred to the dark for 2 or 5 d as indicated for each experiment.

Cloning Procedures

All primers used for cloning and subcloning are listed in Supplemental Table 1 online. Detailed cloning procedures are described in Supplemental Methods 1 online.

Molecular Phylogeny

The nucleotide sequences from various species were identified in Phytozome (http://www.phytozome.net) according to their similarity to *Arabidopsis* AMSH genes, aligned with ClustalX (Thompson et al., 1997), and then improved manually. Phylogenetic analyses were performed by maximum likelihood with PAUP using the sequence from *Physcomitrella patens* (Pp1s133_43V6) as an outgroup. All characters were equally weighted, and gaps were treated as missing data. The nucleotide substitution model was set as GTR + I + G by MrModeltest 2.2 (Nylander, 2004), and a heuristic search was implemented with 100 random addition sequence replicates involving TBR branch swapping.

To estimate clade credibility, bootstrap values by maximum parsimony method, and posterior probabilities by Bayesian analysis were calculated. Bootstrap values were calculated from 1000 pseudo-replicates, each with 100 random additions. For posterior probabilities, the Bayesian search was conducted by MCMC with two independent sets of four chains, each run for 10 million generations, sampling every 100 generations by MrBayes 3.1.2 (Ronquist and Huelsenbeck, 2003). The nucleotide substitution model was set as GTR + I + G. The program Tracer (Tracer v1.4; available from http://beast.bio.ed.ac.uk/Tracer) was used to check the runs had reached stationarity and effective sample size of all the parameters was high (>100). The first 2.5 million generations before sufficient stationary generations were discarded as burn-in periods and the rest of trees were used to calculate posterior probabilities.

GUS Assay

Excised mature embryos from seeds as well as 7- and 14-d-old seedlings were treated with heptan (Roth) for 15 min. After removing heptan, the embryos and seedlings were incubated in GUS substrate solution (50 mM sodium phosphate, pH 7, 10 mM EDTA, 0.5 mM K$_4$[Fe(CN)$_6$], 0.5 mM K$_3$[Fe(CN)$_6$], 0.5 mM X-Gluc, and 0.02% Silvett) at 37°C. Tissues were cleared with an ethanol:acetic acid solution (6:1) at 37°C for 1 h and subsequently with a series of decreasing percentage of ethanol. Photographs were taken using a MZ16 (Leica) or BX61 (Olympus) microscope equipped with a charge-coupled device camera.

Chlorophyll Content Measurement

Twenty seedlings were weighed and immediately incubated in 1 mL *N,N*-dimethylformamide at 4°C under agitation in dark. After 48 h, the absorbance of the supernatant was measured at 664 and 647 nm. Subsequently, total chlorophyll content was determined according to total chlorophyll = [(OD664*7.04) + (OD647*20.27)]/fresh weight (Porra et al., 1998).

Quantitative RT-PCR

All primers used for quantitative RT-PCR are listed in Supplemental Table 2 online. Total RNA was extracted with a NucleoSpin RNA plant kit (Machery-Nagel), and 1 µg of total RNA was reverse transcribed with an oligo(dT) primer and M-MulV reverse transcriptase (Fermentas) following the manufacturer's instructions. Quantitative real-time PCR was performed using iQ SYBR Green Supermix (Bio-Rad) in a CFX96 real-time system cycler (Bio-Rad). A 45-cycle two-step amplification protocol (10 s at 95°C, 25 s at 60°C) was used for all measurements.

Protein Extraction, Immunoblotting, and Antibodies

Yeast total proteins were extracted as described previously (Kushnirov, 2000). SDS-PAGE and immunoblotting were performed according to standard methods.

Total protein extracts were prepared in extraction buffer (50 mM Tris-HCl, pH 7.5, 150 mM NaCl, 0.5% Triton X-100, and protease inhibitor cocktail [Roche]). For PIN2 immunoblot analysis, roots of 10-d-old seedlings were homogenized in extraction buffer. Extracts were centrifuged for 20 min at 9000*g*, and the supernatant was further centrifuged for 1 h at 100,000*g* in a Sorvall MTX 500 benchtop centrifuge (Thermo-Scientific), and the P100 fraction was subjected to immunoblotting.

An anti-AMSH1 antibody was raised against the full-length protein 6xHis-AMSH1 expressed and purified from *Escherichia coli* Rosetta(DE3) strain (Novagen). Six hundred micrograms of purified protein was used to raise antibodies in rabbits (Eurogentec). The serum was used at a 1:1000 dilution. The specificity of the antibody was verified using total extracts from *amsh1-1*.

Additional antibodies used were as follows: anti-AMSH3 (Isono et al., 2010), anti-ATG8 (Thompson et al., 2005), anti-GFP (Invitrogen), anti-CDC2 (Santa Cruz), anti-GAL4BD (Santa Cruz), anti-PIN2 (Agrisera), anti-NBR1 (Svenning et al., 2011), anti-UB(P4D1) (Santa Cruz), and horseradish peroxidase–conjugated anti-HA (Sigma-Aldrich).

In Vitro DUB Assay, Glutathione *S*-Transferase Pulldown, and Y2H Analysis

Glutathione *S*-transferase (GST), GST-VPS2.1(MIM), GST-AMSH1(MPN), and GST-AMSH1(MIT) were expressed in *E. coli* Rosetta(DE3) cells (Merck) and purified with Glutathione Sepharose 4B (GE Healthcare). After purification, the GST moiety of GST-AMSH1(MPN) and GST-AMSH1(MIT) was removed by digestion with PreScission Protease (GE Healthcare). DUB assays and GST pull-down assays were performed as described previously (Isono et al., 2010; Katsiarimpa et al., 2011). Y2H analysis was performed as described previously (Katsiarimpa et al., 2011).

MDC and BCECF-AM Staining and E-64d Treatment

Arabidopsis seedlings were stained with 50 µM MDC (Sigma-Aldrich) in PBS for 10 min at room temperature to visualize autophagosomes. Subsequently, the seedlings were washed twice with PBS to remove excess stain. To visualize the vacuole, seedlings were incubated with 5 µM BCECF-AM (Molecular Probes) for 1 h. To inhibit vacuolar proteases, seedlings were incubated with 100 µM E-64d (Santa Cruz) for 1, 6, or 12 h as indicated for each experiment.

Microscopy

GFP-fused proteins, BCECF staining and MDC staining were analyzed with an FV-1000/IX81 confocal laser scanning microscope (Olympus) with

a UPlanSApo ×60/1.20 (Olympus) objective using the 488- and 405-nm laser line, respectively. For maximal projection images of MDC-stained root cells, sequential Z-stack images were collected with 0.48-μm plane distance. Images were subsequently processed using FluoView (Olympus) and Photoshop CS6 (Adobe).

Pathogen Assays

For *Alternaria brassicicola* infection, 5.5-week-old plants grown under short-day conditions (10 h light/14 h dark) were drop inoculated with 10^6 spores/mL of *A. brassicicola*. Disease indices were calculated 7 and 10 d after inoculation according to Epple et al. (1997).

For the *Erysiphe cruciferarum* assay, 6-week-old plants grown under short-day conditions (10 h light/14 h dark) were inoculated with a density of 3 to 5 spores per mm². Susceptibility of plants to mildew was scored by visual examination after 5 and 7 d of inoculation. To quantify fungal growth, the number of hyphae and of conidiophores per spore was counted under the microscope 5 and 7 d after inoculation, respectively, after staining the leaves with trypan blue (Pelikan).

Accession Numbers

Sequence data from this article can be found in the Arabidopsis Genome Initiative database under the following accession numbers: *AMSH1* (AT1G48790), *AMSH2* (AT1G10600), *AMSH3* (AT4G16144), *CDC2* (AT3G48750), *SKD1* (AT2G27600), *VPS2*.1 (AT2G06530), *VPS20.1* (AT5G63880), *VPS24.1* (AT5G22950), *SNF7.1* (AT4G29160), *ATG8a* (AT4G21980), *ATG8b* (AT4G04620), *ATG8c* (AT1G62040), *ATG8d* (AT2G05630), *ATG8e* (AT2G45170), *ATG8f* (AT4G16520), *ATG8g* (AT3G60640), *ATG8h* (AT3G06420), *ATG8i* (AT3G15580), *PR1* (AT2G14610), *PR5* (AT1G75040), *SAG12* (AT5G45890), *SAG13* (AT2G29350), *ACT8* (AT1G49240), *PIN2* (AT5G57090), and *NBR1* (AT4G24690). Sequence accession numbers (Phytozome) for *AMSH* homologs are as follows: *P. patens* (Pp1s133_43V6, Pp1s240_78V6, and Pp1s64_214V6), *Selaginella moellendorffii* (Sm82317 and Sm128074), *Zea mays* (GRMZM2g075690, GRMZM5g835530, and GRMZM2g173119), *Sorghum bicolor* (Sb13g013600 and Sb3g020630), *Oryza sativa* (Os1g23640 and Os1g31470), *Populus trichocarpa* (0010s15100, 0015s03810, and 0010s05090), *Ricinus communis* (Rc29889m003259, Rc29996m000133, and Rc29631m001029), *Glycine max* (07g37130, 17g03490, 05g34700, 08g04970, 07g10350, 09g31540, and 01g03710), *Vitis vinifera* (GSVIVT01035040001, GSVIVT010083100001, and GSVIVT01013737001), and *Arabidopsis lyrata* (493270, 474017, and 919849).

Supplemental Data

The following materials are available in the online version of this article.

Supplemental Figure 1. *amsh1-1* Shows Early Senescence under 8-h Daylight Short-Day Conditions.

Supplemental Figure 2. Autophagosomes Accumulate in Wild-Type Plants after Dark Treatment.

Supplemental Figure 3. Expression of Y2H Constructs.

Supplemental Figure 4. Phenotypes of *VPS2.1-GFP*–Overexpressing Plants.

Supplemental Figure 5. *E. cruciferarum* Growth Is Restricted in *amsh1-1* Plants.

Supplemental Figure 6. *PR1*, *PR5*, and *SAG13* Are Upregulated in *35Spro:VPS2.1-GFP* Plants under 8-h Daylight Conditions in *amsh1-1* Plants.

Supplemental Table 1. List of Primers Used for Cloning.

Supplemental Table 2. List of Primers Used for qRT-PCR.

Supplemental Data Set 1. Nucleotide Sequence Alignment of *Arabidopsis AMSH1*, *AMSH2*, and *AMSH3* with Their Counterparts from Other Plant Species.

Supplemental Methods 1. Cloning Procedure.

AUTHOR CONTRIBUTIONS

A.K., K.K., C.S., F.B., R.H., and E.I. designed the experiments. A.K., K.K., F.A., C.W., M.O., C.T., F.B., and E.I. performed the experiments. A.K., K.K., C.T., F.B., R.H., and E.I. analyzed the experiments. E.I. wrote the article.

REFERENCES

Abas, L., Benjamins, R., Malenica, N., Paciorek, T., Wiśniewska, J., Moulinier-Anzola, J.C., Sieberer, T., Friml, J., and Luschnig, C. (2006). Intracellular trafficking and proteolysis of the *Arabidopsis* auxin-efflux facilitator PIN2 are involved in root gravitropism. Nat. Cell Biol. **8:** 249–256. Erratum. Nat. Cell Biol. **8:** 424.

An, Q., Ehlers, K., Kogel, K.H., van Bel, A.J., and Hückelhoven, R. (2006). Multivesicular compartments proliferate in susceptible and resistant MLA12-barley leaves in response to infection by the biotrophic powdery mildew fungus. New Phytol. **172:** 563–576.

Assaad, F.F., Qiu, J.L., Youngs, H., Ehrhardt, D., Zimmerli, L., Kalde, M., Wanner, G., Peck, S.C., Edwards, H., Ramonell, K., Somerville, C.R., and Thordal-Christensen, H. (2004). The PEN1 syntaxin defines a novel cellular compartment upon fungal attack and is required for the timely assembly of papillae. Mol. Biol. Cell **15:** 5118–5129.

Babst, M., Sato, T.K., Banta, L.M., and Emr, S.D. (1997). Endosomal transport function in yeast requires a novel AAA-type ATPase, Vps4p. EMBO J. **16:** 1820–1831.

Balderhaar, H.J., Arlt, H., Ostrowicz, C., Bröcker, C., Sündermann, F., Brandt, R., Babst, M., and Ungermann, C. (2010). The Rab GTPase Ypt7 is linked to retromer-mediated receptor recycling and fusion at the yeast late endosome. J. Cell Sci. **123:** 4085–4094.

Barberon, M., Zelazny, E., Robert, S., Conéjéro, G., Curie, C., Friml, J., and Vert, G. (2011). Monoubiquitin-dependent endocytosis of the

iron-regulated transporter 1 (IRT1) transporter controls iron uptake in plants. Proc. Natl. Acad. Sci. USA **108:** E450–E458.

Brodersen, P., Petersen, M., Pike, H.M., Olszak, B., Skov, S., Odum, N., Jørgensen, L.B., Brown, R.E., and Mundy, J. (2002). Knockout of *Arabidopsis* accelerated-cell-death11 encoding a sphingosine transfer protein causes activation of programmed cell death and defense. Genes Dev. **16:** 490–502.

Chamovitz, D.A., Wei, N., Osterlund, M.T., von Arnim, A.G., Staub, J.M., Matsui, M., and Deng, X.W. (1996). The COP9 complex, a novel multisubunit nuclear regulator involved in light control of a plant developmental switch. Cell **86:** 115–121.

Chung, T., Phillips, A.R., and Vierstra, R.D. (2010). ATG8 lipidation and ATG8-mediated autophagy in *Arabidopsis* require ATG12 expressed from the differentially controlled ATG12A AND ATG12B loci. Plant J. **62:** 483–493.

Chung, T., Suttangkakul, A., and Vierstra, R.D. (2009). The ATG autophagic conjugation system in maize: ATG transcripts and abundance of the ATG8-lipid adduct are regulated by development and nutrient availability. Plant Physiol. **149:** 220–234.

Clough, S.J., and Bent, A.F. (1998). Floral dip: A simplified method for Agrobacterium-mediated transformation of *Arabidopsis thaliana*. Plant J. **16:** 735–743.

Collins, N.C., Thordal-Christensen, H., Lipka, V., Bau, S., Kombrink, E., Qiu, J.L., Hückelhoven, R., Stein, M., Freialdenhoven, A., Somerville, S.C., and Schulze-Lefert, P. (2003). SNARE-protein-mediated disease resistance at the plant cell wall. Nature **425:** 973–977.

Contento, A.L., Xiong, Y., and Bassham, D.C. (2005). Visualization of autophagy in *Arabidopsis* using the fluorescent dye monodansylcadaverine and a GFP-AtATG8e fusion protein. Plant J. **42:** 598–608.

Cope, G.A., Suh, G.S., Aravind, L., Schwarz, S.E., Zipursky, S.L., Koonin, E.V., and Deshaies, R.J. (2002). Role of predicted metalloprotease motif of Jab1/Csn5 in cleavage of Nedd8 from Cul1. Science **298:** 608–611.

Djeddi, A., Michelet, X., Culetto, E., Alberti, A., Barois, N., and Legouis, R. (2012). Induction of autophagy in ESCRT mutants is an adaptive response for cell survival in *C. elegans*. J. Cell Sci. **125:** 685–694.

Doelling, J.H., Walker, J.M., Friedman, E.M., Thompson, A.R., and Vierstra, R.D. (2002). The APG8/12-activating enzyme APG7 is required for proper nutrient recycling and senescence in *Arabidopsis thaliana*. J. Biol. Chem. **277:** 33105–33114.

Epple, P., Apel, K., and Bohlmann, H. (1997). Overexpression of an endogenous thionin enhances resistance of *Arabidopsis* against *Fusarium oxysporum*. Plant Cell **9:** 509–520.

Filimonenko, M., Stuffers, S., Raiborg, C., Yamamoto, A., Malerød, L., Fisher, E.M., Isaacs, A., Brech, A., Stenmark, H., and Simonsen, A. (2007). Functional multivesicular bodies are required for autophagic clearance of protein aggregates associated with neurodegenerative disease. J. Cell Biol. **179:** 485–500.

Geldner, N., Dénervaud-Tendon, V., Hyman, D.L., Mayer, U., Stierhof, Y.-D., and Chory, J. (2009). Rapid, combinatorial analysis of membrane compartments in intact plants with a multicolor marker set. Plant J. **59:** 169–178.

Glickman, M.H., Rubin, D.M., Coux, O., Wefes, I., Pfeifer, G., Cjeka, Z., Baumeister, W., Fried, V.A., and Finley, D. (1998). A subcomplex of the proteasome regulatory particle required for ubiquitin-conjugate degradation and related to the COP9-signalosome and eIF3. Cell **94:** 615–623.

Göhre, V., Spallek, T., Häweker, H., Mersmann, S., Mentzel, T., Boller, T., de Torres, M., Mansfield, J.W., and Robatzek, S. (2008). Plant pattern-recognition receptor FLS2 is directed for degradation by the bacterial ubiquitin ligase AvrPtoB. Curr. Biol. **18:** 1824–1832.

Gutierrez, M.G., Munafó, D.B., Berón, W., and Colombo, M.I. (2004). Rab7 is required for the normal progression of the autophagic pathway in mammalian cells. J. Cell Sci. **117:** 2687–2697.

Han, J.H., Ryu, H.H., Jun, M.H., Jang, D.J., and Lee, J.A. (2012). The functional analysis of the CHMP2B missense mutation associated with neurodegenerative diseases in the endo-lysosomal pathway. Biochem. Biophys. Res. Commun. **421:** 544–549.

Herberth, S., Shahriari, M., Bruderek, M., Hessner, F., Müller, B., Hülskamp, M., and Schellmann, S. (2012). Artificial ubiquitylation is sufficient for sorting of a plasma membrane ATPase to the vacuolar lumen of *Arabidopsis* cells. Planta **236:** 63–77.

Hofius, D., Schultz-Larsen, T., Joensen, J., Tsitsigiannis, D.I., Petersen, N.H., Mattsson, O., Jørgensen, L.B., Jones, J.D., Mundy, J., and Petersen, M. (2009). Autophagic components contribute to hypersensitive cell death in *Arabidopsis*. Cell **137:** 773–783.

Howard, T.L., Stauffer, D.R., Degnin, C.R., and Hollenberg, S.M. (2001). CHMP1 functions as a member of a newly defined family of vesicle trafficking proteins. J. Cell Sci. **114:** 2395–2404.

Inoue, Y., Suzuki, T., Hattori, M., Yoshimoto, K., Ohsumi, Y., and Moriyasu, Y. (2006). AtATG genes, homologs of yeast autophagy genes, are involved in constitutive autophagy in *Arabidopsis* root tip cells. Plant Cell Physiol. **47:** 1641–1652.

Ishii, N., Owada, Y., Yamada, M., Miura, S., Murata, K., Asao, H., Kondo, H., and Sugamura, K. (2001). Loss of neurons in the hippocampus and cerebral cortex of AMSH-deficient mice. Mol. Cell. Biol. **21:** 8626–8637.

Isono, E., Katsiarimpa, A., Müller, I.K., Anzenberger, F., Stierhof, Y.D., Geldner, N., Chory, J., and Schwechheimer, C. (2010). The deubiquitinating enzyme AMSH3 is required for intracellular trafficking and vacuole biogenesis in *Arabidopsis thaliana*. Plant Cell **22:** 1826–1837.

Itakura, E., Kishi-Itakura, C., and Mizushima, N. (2012). The hairpin-type tail-anchored SNARE syntaxin 17 targets to autophagosomes for fusion with endosomes/lysosomes. Cell **151:** 1256–1269.

Jäger, S., Bucci, C., Tanida, I., Ueno, T., Kominami, E., Saftig, P., and Eskelinen, E.L. (2004). Role for Rab7 in maturation of late autophagic vacuoles. J. Cell Sci. **117:** 4837–4848.

Kasai, K., Takano, J., Miwa, K., Toyoda, A., and Fujiwara, T. (2011). High boron-induced ubiquitination regulates vacuolar sorting of the BOR1 borate transporter in *Arabidopsis thaliana*. J. Biol. Chem. **286:** 6175–6183.

Katsiarimpa, A., Anzenberger, F., Schlager, N., Neubert, S., Hauser, M.T., Schwechheimer, C., and Isono, E. (2011). The *Arabidopsis* deubiquitinating enzyme AMSH3 interacts with ESCRT-III subunits and regulates their localization. Plant Cell **23:** 3026–3040.

Klionsky, D.J., and Ohsumi, Y. (1999). Vacuolar import of proteins and organelles from the cytoplasm. Annu. Rev. Cell Dev. Biol. **15:** 1–32.

Komander, D., Clague, M.J., and Urbé, S. (2009). Breaking the chains: Structure and function of the deubiquitinases. Nat. Rev. Mol. Cell Biol. **10:** 550–563.

Kushnirov, V.V. (2000). Rapid and reliable protein extraction from yeast. Yeast **16:** 857–860.

Kwon, C., et al. (2008). Co-option of a default secretory pathway for plant immune responses. Nature **451:** 835–840.

Kwon, S.I., Cho, H.J., Jung, J.H., Yoshimoto, K., Shirasu, K., and Park, O.K. (2010). The Rab GTPase RabG3b functions in autophagy and contributes to tracheary element differentiation in *Arabidopsis*. Plant J. **64:** 151–164.

Lai, Z., Wang, F., Zheng, Z., Fan, B., and Chen, Z. (2011). A critical role of autophagy in plant resistance to necrotrophic fungal pathogens. Plant J. **66:** 953–968.

Lee, H.K., Cho, S.K., Son, O., Xu, Z., Hwang, I., and Kim, W.T. (2009). Drought stress-induced Rma1H1, a RING membrane-anchor

E3 ubiquitin ligase homolog, regulates aquaporin levels via ubiquitination in transgenic *Arabidopsis* plants. Plant Cell **21:** 622–641.

Lee, J.A., Beigneux, A., Ahmad, S.T., Young, S.G., and Gao, F.B. (2007). ESCRT-III dysfunction causes autophagosome accumulation and neurodegeneration. Curr. Biol. **17:** 1561–1567.

Lenz, H.D., et al. (2011). Autophagy differentially controls plant basal immunity to biotrophic and necrotrophic pathogens. Plant J. **66:** 818–830.

Liu, Y., Schiff, M., Czymmek, K., Tallóczy, Z., Levine, B., and Dinesh-Kumar, S.P. (2005). Autophagy regulates programmed cell death during the plant innate immune response. Cell **121:** 567–577.

Lu, Y.J., Schornack, S., Spallek, T., Geldner, N., Chory, J., Schellmann, S., Schumacher, K., Kamoun, S., and Robatzek, S. (2012). Patterns of plant subcellular responses to successful oomycete infections reveal differences in host cell reprogramming and endocytic trafficking. Cell. Microbiol. **14:** 682–697.

Maytal-Kivity, V., Reis, N., Hofmann, K., and Glickman, M.H. (2002). MPN+, a putative catalytic motif found in a subset of MPN domain proteins from eukaryotes and prokaryotes, is critical for Rpn11 function. BMC Biochem. **3:** 28.

McCullough, J., Clague, M.J., and Urbé, S. (2004). AMSH is an endosome-associated ubiquitin isopeptidase. J. Cell Biol. **166:** 487–492.

Mizushima, N., and Levine, B. (2010). Autophagy in mammalian development and differentiation. Nat. Cell Biol. **12:** 823–830.

Morris, K., MacKerness, S.A., Page, T., John, C.F., Murphy, A.M., Carr, J.P., and Buchanan-Wollaston, V. (2000). Salicylic acid has a role in regulating gene expression during leaf senescence. Plant J. **23:** 677–685.

Nielsen, M.E., Feechan, A., Böhlenius, H., Ueda, T., and Thordal-Christensen, H. (2012). *Arabidopsis* ARF-GTP exchange factor, GNOM, mediates transport required for innate immunity and focal accumulation of syntaxin PEN1. Proc. Natl. Acad. Sci. USA **109:** 11443–11448.

Nylander, J.A. (2004). MrModeltest 2.0. (Uppsala, Sweden: Uppsala University).

Patel, S., and Dinesh-Kumar, S.P. (2008). *Arabidopsis* ATG6 is required to limit the pathogen-associated cell death response. Autophagy **4:** 20–27.

Phillips, A.R., Suttangkakul, A., and Vierstra, R.D. (2008). The ATG12-conjugating enzyme ATG10 Is essential for autophagic vesicle formation in *Arabidopsis thaliana*. Genetics **178:** 1339–1353.

Porra, R.J., Urzinger, M., Winkler, J., Bubenzer, C., and Scheer, H. (1998). Biosynthesis of the 3-acetyl and 13(1)-oxo groups of bacteriochlorophyll a in the facultative aerobic bacterium, *Rhodovulum sulfidophilum*—The presence of both oxygenase and hydratase pathways for isocyclic ring formation. Eur. J. Biochem. **257:** 185–191.

Richardson, L.G., Howard, A.S., Khuu, N., Gidda, S.K., McCartney, A., Morphy, B.J., and Mullen, R.T. (2011). Protein-protein interaction network and subcellular localization of the *Arabidopsis thaliana* ESCRT machinery. Front. Plant Sci. **2:** 20.

Rojo, E., Gillmor, C.S., Kovaleva, V., Somerville, C.R., and Raikhel, N.V. (2001). VACUOLELESS1 is an essential gene required for vacuole formation and morphogenesis in *Arabidopsis*. Dev. Cell **1:** 303–310.

Ronquist, F., and Huelsenbeck, J.P. (2003). MrBayes 3: Bayesian phylogenetic inference under mixed models. Bioinformatics **19:** 1572–1574.

Rusten, T.E., Vaccari, T., Lindmo, K., Rodahl, L.M., Nezis, I.P., Sem-Jacobsen, C., Wendler, F., Vincent, J.P., Brech, A., Bilder, D., and Stenmark, H. (2007). ESCRTs and Fab1 regulate distinct steps of autophagy. Curr. Biol. **17:** 1817–1825.

Shahriari, M., Richter, K., Keshavaiah, C., Sabovljevic, A., Huelskamp, M., and Schellmann, S. (2011). The *Arabidopsis* ESCRT protein-protein interaction network. Plant Mol. Biol. **76:** 85–96.

Sláviková, S., Shy, G., Yao, Y., Glozman, R., Levanony, H., Pietrokovski, S., Elazar, Z., and Galili, G. (2005). The autophagy-associated Atg8 gene family operates both under favourable growth conditions and under starvation stresses in *Arabidopsis* plants. J. Exp. Bot. **56:** 2839–2849.

Spitzer, C., Reyes, F.C., Buono, R., Sliwinski, M.K., Haas, T.J., and Otegui, M.S. (2009). The ESCRT-related CHMP1A and B proteins mediate multivesicular body sorting of auxin carriers in *Arabidopsis* and are required for plant development. Plant Cell **21:** 749–766.

Surpin, M., Zheng, H., Morita, M.T., Saito, C., Avila, E., Blakeslee, J.J., Bandyopadhyay, A., Kovaleva, V., Carter, D., Murphy, A., Tasaka, M., and Raikhel, N. (2003). The VTI family of SNARE proteins is necessary for plant viability and mediates different protein transport pathways. Plant Cell **15:** 2885–2899.

Svenning, S., Lamark, T., Krause, K., and Johansen, T. (2011). Plant NBR1 is a selective autophagy substrate and a functional hybrid of the mammalian autophagic adapters NBR1 and p62/SQSTM1. Autophagy **7:** 993–1010.

Swaminathan, S., Amerik, A.Y., and Hochstrasser, M. (1999). The Doa4 deubiquitinating enzyme is required for ubiquitin homeostasis in yeast. Mol. Biol. Cell **10:** 2583–2594.

Tanaka, N., Kaneko, K., Asao, H., Kasai, H., Endo, Y., Fujita, T., Takeshita, T., and Sugamura, K. (1999). Possible involvement of a novel STAM-associated molecule "AMSH" in intracellular signal transduction mediated by cytokines. J. Biol. Chem. **274:** 19129–19135.

Teis, D., Saksena, S., and Emr, S.D. (2008). Ordered assembly of the ESCRT-III complex on endosomes is required to sequester cargo during MVB formation. Dev. Cell **15:** 578–589.

Teis, D., Saksena, S., Judson, B.L., and Emr, S.D. (2010). ESCRT-II coordinates the assembly of ESCRT-III filaments for cargo sorting and multivesicular body vesicle formation. EMBO J. **29:** 871–883.

Thompson, A.R., Doelling, J.H., Suttangkakul, A., and Vierstra, R.D. (2005). Autophagic nutrient recycling in *Arabidopsis* directed by the ATG8 and ATG12 conjugation pathways. Plant Physiol. **138:** 2097–2110.

Thompson, J.D., Gibson, T.J., Plewniak, F., Jeanmougin, F., and Higgins, D.G. (1997). The CLUSTAL_X windows interface: Flexible strategies for multiple sequence alignment aided by quality analysis tools. Nucleic Acids Res. **25:** 4876–4882.

Uemura, T., Kim, H., Saito, C., Ebine, K., Ueda, T., Schulze-Lefert, P., and Nakano, A. (2012). Qa-SNAREs localized to the trans-Golgi network regulate multiple transport pathways and extracellular disease resistance in plants. Proc. Natl. Acad. Sci. USA **109:** 1784–1789.

Verma, R., Aravind, L., Oania, R., McDonald, W.H., Yates, J.R., III., Koonin, E.V., and Deshaies, R.J. (2002). Role of Rpn11 metalloprotease in deubiquitination and degradation by the 26S proteasome. Science **298:** 611–615.

Vierstra, R.D. (2009). The ubiquitin-26S proteasome system at the nexus of plant biology. Nat. Rev. Mol. Cell Biol. **10:** 385–397.

Wang, Y., Nishimura, M.T., Zhao, T., and Tang, D. (2011). ATG2, an autophagy-related protein, negatively affects powdery mildew resistance and mildew-induced cell death in *Arabidopsis*. Plant J. **68:** 74–87.

Ward, E.R., Uknes, S.J., Williams, S.C., Dincher, S.S., Wiederhold, D.L., Alexander, D.C., Ahl-Goy, P., Metraux, J.P., and Ryals, J.A. (1991). Coordinate gene activity in response to agents that induce systemic acquired resistance. Plant Cell **3:** 1085–1094.

Wiermer, M., Feys, B.J., and Parker, J.E. (2005). Plant immunity: The EDS1 regulatory node. Curr. Opin. Plant Biol. **8:** 383–389.

Willige, B.C., Isono, E., Richter, R., Zourelidou, M., and Schwechheimer, C. (2011). Gibberellin regulates PIN-FORMED abundance and is required for auxin transport-dependent growth and development in *Arabidopsis thaliana*. Plant Cell **23:** 2184–2195.

Winter, V., and Hauser, M.T. (2006). Exploring the ESCRTing machinery in eukaryotes. Trends Plant Sci. **11:** 115–123.

Xiong, Y., Contento, A.L., and Bassham, D.C. (2005). AtATG18a is required for the formation of autophagosomes during nutrient stress and senescence in *Arabidopsis thaliana*. Plant J. **42:** 535–546.

Yoshimoto, K., Hanaoka, H., Sato, S., Kato, T., Tabata, S., Noda, T., and Ohsumi, Y. (2004). Processing of ATG8s, ubiquitin-like proteins, and their deconjugation by ATG4s are essential for plant autophagy. Plant Cell **16:** 2967–2983.

Yoshimoto, K., Jikumaru, Y., Kamiya, Y., Kusano, M., Consonni, C., Panstruga, R., Ohsumi, Y., and Shirasu, K. (2009). Autophagy negatively regulates cell death by controlling NPR1-dependent salicylic acid signaling during senescence and the innate immune response in *Arabidopsis*. Plant Cell **21:** 2914–2927.

Zelazny, E., Barberon, M., Curie, C., and Vert, G. (2011). Ubiquitination of transporters at the forefront of plant nutrition. Plant Signal. Behav. **6:** 1597–1599.

Zhang, Z., Feechan, A., Pedersen, C., Newman, M.A., Qiu, J.L., Olesen, K.L., and Thordal-Christensen, H. (2007). A SNARE-protein has opposing functions in penetration resistance and defence signalling pathways. Plant J. **49:** 302–312.

Zouhar, J., Rojo, E., and Bassham, D.C. (2009). AtVPS45 is a positive regulator of the SYP41/SYP61/VTI12 SNARE complex involved in trafficking of vacuolar cargo. Plant Physiol. **149:** 1668–1678.

Lebenslauf

Persönliche Angaben

Adresse	Reichstr. 12, 90408 Nürnberg
Geburtsdatum	17 Dezember, 1984
Geburtsort	Nürnberg, Deutschland
Nationalität	griechisch
Familienstand	ledig, keine Kinder

Ausbildung

06/2009 bis 06/2013	Doktorarbeit, Systembiologie der Pflanzen Technische Universität München, Deutschland Titel der Dissertation: „Interaction of *Arabidopsis* AMSH proteins with ESCRT-III and their role in intracellular membrane trafficking"
05/2008 bis 05/2009	**Wissenschaftliche Mitarbeiterin,** Universität Tübingen (ZMBP), Deutschland Entwicklungsbiologie der Pflanzen
4/2008	**Abschluss alsDiplom-Biochemiker und Biotechnologe** Universität von Thessalien, Griechenland
10/2003 bis 4/2008	**Studium der Biochemie und Biotechnologie** Universität von Thessalien, Griechenland
03/2007 bis 05/2007	**Diplomarbeit** Universität Tübingen (ZMBP), Deutschland Entwicklungsbiologie der Pflanzen Titel der Diplomarbeit: *„AMHS2 is a deubiquitinating enzyme"*
9/2003	**Abitur** Griechisches Lyzeum Nürnberg, Deutschland
7/2000	**Qualifizierender Hauptschulabschluss** Griechische Volksschule Nürnberg, Deutschland

Publikationen

Katsiarimpa, A.*, Kalinowska, K.*, Anzenberger, F., Weis, C., Ostertag, M., Tsutsumi, C., Schwechheimer, C., Brunner, F., Huckelhoven, R., Isono, E., 2013. The deubiquitinating enzyme AMSH1 and the ESCRT-III subunit VPS2.1 are required for autophagic degradation in Arabidopsis. The Plant cell 25, 2236-2252. * equal contribution

Katsiarimpa, A., Anzenberger, F., Schlager, N., Neubert, S., Hauser, M.T., Schwechheimer, C., Isono, E., 2011. The Arabidopsis deubiquitinating enzyme AMSH3 interacts with ESCRT-III subunits and regulates their localization. The Plant cell 23, 3026-3040.

Hakenjos, J.P., Richter, R., Dohmann, E.M., **Katsiarimpa, A.**, Isono, E., Schwechheimer, C., 2011. MLN4924 is an efficient inhibitor of NEDD8 conjugation in plants. Plant physiology 156, 527-536.

Isono, E., **Katsiarimpa, A.**, Muller, I.K., Anzenberger, F., Stierhof, Y.D., Geldner, N., Chory, J., Schwechheimer, C., 2010. The deubiquitinating enzyme AMSH3 is required for intracellular trafficking and vacuole biogenesis in Arabidopsis thaliana. The Plant cell 22, 1826-1837.

Sprachen

Griechisch	Muttersprache
Deutsch	Verhandlungssicher (Grosses Deutsches Sprachdiplom)
Englisch	Verhandlungssicher (First Certificate in English)